Enabling Utility-Scale Electrical Energy Storage through Underground Hydrogen-Natural Gas Co-Storage

by

Dan Peng

A thesis
presented to the University of Waterloo
in fulfillment of the
thesis requirement for the degree of
Master of Applied Science
in
Chemical Engineering

Waterloo, Ontario, Canada, 2013

AUTHOR'S DECLARATION

I hereby declare that I am the sole author of this thesis. This is a true copy of the thesis, including any required final revisions, as accepted by my examiners.

I understand that my thesis may be made electronically available to the public.

Abstract

Energy storage technology is needed for the storage of surplus baseload generation and the storage of intermittent wind power, because it can increase the flexibility of power grid operations. Underground storage of hydrogen with natural gas (UHNG) is proposed as a new energy storage technology, to be considered for utility-scale energy storage applications. UHNG is a composite technology: using electrolyzers to convert electrical energy to chemical energy in the form of hydrogen. The latter is then injected along with natural gas into existing gas distribution and storage facilities. The energy stored as hydrogen is recovered as needed; as hydrogen for industrial and transportation applications, as electricity to serve power demand, or as hydrogen-enriched natural gas to serve gas demand. The storage of electrical energy in gaseous form is also termed “Power to Gas”. Such large scale electrical energy storage is desirable to baseload generators operators, renewable energy-based generator operators, independent system operators, and natural gas distribution utilities. Due to the low density of hydrogen, the hydrogen-natural gas mixture thus formed has lower volumetric energy content than conventional natural gas. But, compared to the combustion of conventional natural gas, to provide the same amount of energy, the hydrogen-enriched mixture emits less carbon dioxide.

This thesis investigates the dynamic behaviour, financial and environmental performance of UHNG through scenario-based simulation. A proposed energy hub embodying the UHNG principle, located in Southwestern Ontario, is modeled in the MATLAB/Simulink environment. Then, the performance of UHNG for four different scenarios are assessed: injection of hydrogen for long term energy storage, surplus baseload generation load shifting, wind power integration and supplying large hydrogen demand. For each scenario, the configuration of the energy hub, its scale of operation and operating strategy are selected to match the application involved. All four scenarios are compared to the base case scenario, which simulates the operations of a conventional underground gas storage facility.

For all scenarios in which hydrogen production and storage is not prioritized, the concentration of hydrogen in the storage reservoir is shown to remain lower than 7% for the first three years of operation. The simulation results also suggest that, of the five scenarios, hydrogen injection followed by recovery of hydrogen-enriched natural gas is the most likely energy recovery pathway in the near future. For this particular scenario, it was also found that it is not profitable to sell the hydrogen-

enriched natural gas at the same price as regular natural gas. For the range of scenarios evaluated, a list of benchmark parameters has been established for the UHNG technology. With a roundtrip efficiency of 39%, rated capacity ranging from 25,000 MWh to 582,000 MWh and rated power from 1 to 100 MW, UHNG is an energy storage technology suitable for large storage capacity, low to medium power rating storage applications.

Acknowledgements

The research included in this thesis could not have been performed if not for the assistance, patience, and support of many individuals.

First and foremost, I would like to thank my supervisors, Prof. Ali Elkamel and Prof. Michael Fowler for mentoring me over the course of this two year journey. Their insights are at the origin of this project, and they have been great sources of academic and professional inspirations.

My gratitude is also extended to past and present members of my research group: much of my work is based on the previous ground covered by my colleagues Yaser Maniyali, Faraz Syed and Abduslam Mohamed Sharif, and I am very thankful of Lisa Tong, Andreas Mertes, Ivan Kantor and Leila Ahmadi for your good company.

I would like to thank my parents and my friends, whose patient company and encouragement helped me progress when I most needed it, especially Tianyu for offering to read my manuscript.

Finally, my appreciation is extended to the Natural Sciences and Engineering Research Council of Canada and to University of Waterloo for their sponsorship throughout this program.

Dedication

I dedicate this thesis to my grandfather, Baozhang He, the first chemical engineer in my family. He had taught me important lessons in perseverance and kindness. May he rest in peace.

Table of Contents

List of Figures

List of Tables

List of Acronyms

CAES	Compressed Air Energy Storage
CCGT	Combined Cycle Gas Turbine
EIA	Energy Information Agency
FIT	Feed-In Tariff
HENG	Hydrogen-Enriched Natural Gas
IESO	Independent Electricity System Operator
NPV	Net Present Value
PtoG	Power to Gas
PSA	Pressure Swing Adsorption
RE	Renewable Energy
SBG	Surplus Baseload Generation
SMR	Steam-Methane Reforming
UGS	Underground Gas Storage
UHNG	Underground Hydrogen storage with Natural Gas

Chapter 1
Introduction

Since its foundation in the late 19th century, the electricity grid has operated along one key directive: the constant matching of power supply and demand across the grid [1]. More than one hundred years later, the management of today's power grid, a critical infrastructure for modern society, is encountering new challenges which have led to the study of energy storage technologies.

Underground storage of hydrogen with natural gas (UHNG) is a novel compound technology which is proposed to provide utility-scale energy storage capacity. This technology revolves around the use of electrolyzers to convert electrical energy to chemical energy in the form of hydrogen. Hydrogen is then injected in to natural gas distribution system and natural gas underground storage facilities, along with the natural gas. This has technological and economic advantages since this technology makes use of existing natural facilities. Finally, depending on the particular application, the energy stored as hydrogen can be recovered in different forms: as hydrogen for industrial and transportation applications, as electricity to serve power demand, or as hydrogen-enriched natural gas to serve gas demand. UHNG is of special interest for Southwestern Ontario, where there exists extensive infrastructure for natural gas storage and distribution. The generation of hydrogen from surplus power and injection of this hydrogen into the natural gas system is generally termed as 'Power to Gas' (PtoG).

Building on the published concept of "energy hub", a framework which allows for the study of integrated energy systems, a modeling and simulation study is proposed to better characterize the UHNG technology. The objective of this thesis is to contribute to a better understanding of the technology of underground storage of hydrogen with natural gas. This will be accomplished by investigating its dynamic behaviour, financial and environmental performance through scenario-based simulation. Results from this research project may be used to inform further research and investment decisions by technology developers and relevant policy makers.

In the following introduction, the motivation and objective of this study of UHNG is described, and the scope of the project is defined. In Chapter 2, literature on the topics of energy storage, energy hub,

and key component technologies involved in underground storage of hydrogen with natural gas (UHNG) is reviewed. Chapter 3 specifies the main input, output and exogenous variables used for modeling. Model development, which relates the detailed structure of the models constructed for this project, is presented in Chapter 4 through Chapter 6. In Chapter 7, possible sets of input variables are combined to form scenarios, which yield the results presented in Chapter 8 after simulation. Finally, the implications of the results are discussed in Chapter 9; key findings and recommendations are summarized in Chapter 10.

1.1 Research Motivation

Traditionally, power is generated in centralized locations, and then transmitted through great distances to reach the end users who use electric power to perform various services – mechanical work, lighting, refrigeration or heating. In order to manage the flow of energy on the grid, grid operators dispatched orders to the generators, informing them of the action required to balance supply with demand. Increasingly, grid operators have also engaged in demand management programs, in which power end-users agree to modify their energy consumption pattern as needed.

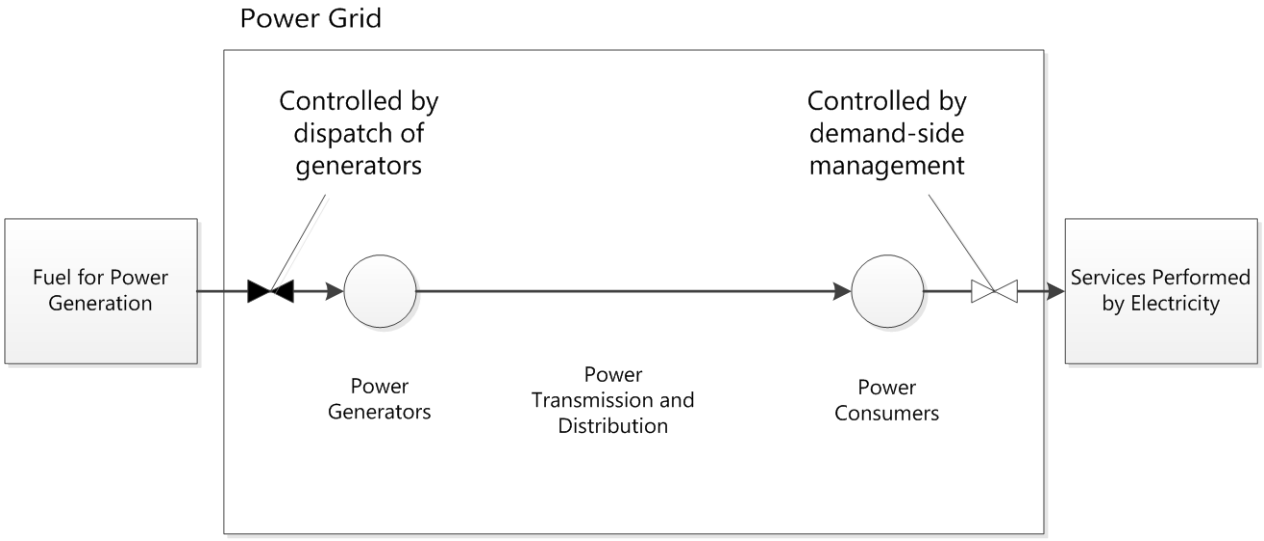

Figure 1.1Traditional paradigm for power grid management

Since the 1970s, many nuclear power plants came online and grew to become the dominant baseload power supplier in several jurisdictions, of which Ontario is an example. In 2011, nuclear power plants supplied 57% of all electricity generated in the province [2]. Compared to conventional thermal

generators, nuclear generators have limited capability to adjust their power output and require long lead times to change power output; therefore stable operating conditions are preferred. Sometimes, Ontario's electricity production from baseload facilities – mostly nuclear, but also including run-of-the-river hydro and wind – is greater than the provincial demand unless managed. Consequently, during such periods, electricity produced in Ontario is sometimes exported at a negative price to neighbouring jurisdictions, or, the baseload facilities are curtailed. It is possible to reduce the power output from nuclear power plants by manipulating their condenser steam discharge valves, but it is not the purpose for which such valves have been designed. Such maneuvers increase the risk of equipment failure, the costs associated with inspections and repairs, while impacting the temperature of water discharged by the power plant [3]. The Independent Electricity System Operator (IESO) of Ontario currently forecasts surplus baseload generation (SBG) for a 10 day period to facilitate coordination between market participants. In its 18-month outlook for the period 2013-2014, the IESO forecasts a median weekly SBG of 116 to 4608 MW [4].

Concurrently, collective efforts to decrease global carbon emissions and to embrace sustainable energy resulted in the growth of renewable energy (RE) generators such as wind and solar among the supply mix. In Ontario, the Feed-in-Tariff (FIT) program has contracted 4,600 MW of non-hydro renewable energy projects since its inception in 2009. It is on track to increase RE generation to 10,700 MW by 2015 [5]. The inherent intermittency of renewable energy, specifically for wind and solar, is another cause of concern for grid operators, because renewable energy generators cannot be dispatched as conventional thermal generators. It is impossible to increase production when the weather conditions are unfavourable. And, although curtailment is possible during periods of surplus, the fixed FIT contracts with RE generators make it economically unfavourable to do so. Such loss in supply flexibility will be felt more acutely as renewable energy generators gain higher penetration in the grid.

Utility-scale energy storage is seen as a promising solution to address the emerging problems – surplus baseload generation and increasing intermittency from the deployment of RE generators – faced by the electric power supply chain, because, energy storage technologies can facilitate grid operations by providing energy buffering capacity, a new method to regulate the flow of energy through the power grid.

Energy storage facility operators can respond to both generation and demand management dispatches. Furthermore, they provide a mechanism to capture and store intermittent renewable energy and to condition its output (Figure 1.2).

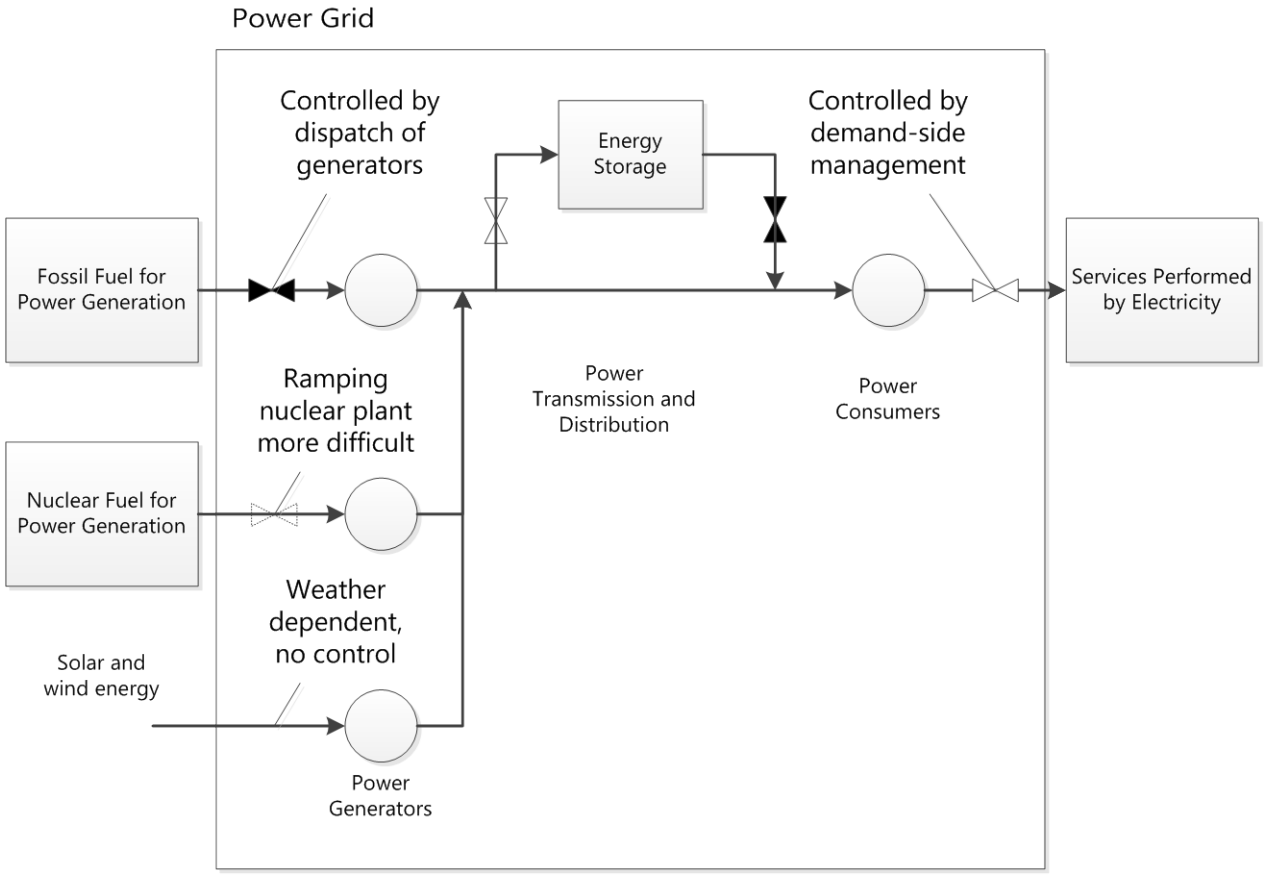

Figure 1.2 Proposed new paradigm for power grid management with energy storage facilities

There are many specific applications for energy storage technologies, depending on its position within the electric power supply chain: close to the generators, close to the end-users or at critical points of the transmission and distribution network. Different applications require storage technologies with different profiles in terms of energy storage capacity, rated input and output. Therefore, many energy storage technologies have been proposed and studied. The different technologies differ by the mechanism in which they convert electrical energy to a storable form. The technologies typically proposed for grid energy storage are batteries, compressed air energy storage

(CAES), pumped hydro energy storage, advanced capacitors, flywheel energy storage, superconducting magnetic energy storage, and energy storage through hydrogen [6-11].

Energy storage through the underground storage of hydrogen with natural gas (UHNG) is one of the new technologies proposed. To store energy using UHNG, electrical energy from the power grid or other sources is converted to hydrogen via electrolysis. Then, the hydrogen gas is blended with incoming natural gas to be stored underground; it can also be sent send directly to end users through the gas distribution system, thus making use of existing natural gas storage and distribution facilities. If stored, to recover the energy stored, the gas mixture stored underground is retrieved and routed to one of the three pathways below:

1) Power to Gas: the hydrogen-enriched natural gas is delivered as-is to end-users through the existing distribution network, performing duties originally performed by natural gas;
2) Power to Power: the gas mixture is sent directly to a combined cycle gas turbine hosted on-site to generate electricity, which is delivered to the electrical grid or to local demand;
3) Power to Hydrogen: after distribution in the natural gas system or stored with natural gas, the gas mixture is separated into its components, hydrogen and natural gas, then used-up by distributed end-users and delivered to end-user via existing pipelines, respectively. Direct production of hydrogen followed by immediate use, bypassing underground storage, is also a possibility.

Compared to older technologies, pumped hydro storage or battery storage, for example, UHNG is significantly different, in that:

1) UHNG is a conceptually new composite technology, consisting of technically mature components;
2) As a composite technology, the performance of UHNG is dependent upon its constituent technologies, which makes it a more complex physical system than traditional energy storage technologies;
3) Unlike the more common energy storage technologies, which store and release energy in reversible pathways, there exist multiple energy recovery pathways for UNHG, in the form of different energy vectors (i.e.: as hydrogen, electricity and hydrogen enriched natural gas).

Thus, UHNG is a potentially innovative technology, which has yet to prove itself. Its use of multiple energy vectors deviates from conventional forms of energy storage, and its overall performance is contingent upon the exact configuration of its constituents.

1.2 Research Objective and Approach

The objective of this simulation study is chosen after a comprehensive literature review, considering resources available to complete the study. The overarching objective is to contribute to a better understanding of the technology of underground storage of hydrogen with natural gas. This is accomplished by investigating its dynamic behaviour, financial and environmental performance through scenario-based simulation. This simulation project will also pave the way for future optimization projects based on the same system. The following milestones have been identified to ensure the success of the project:

1. Locate the key decision variables in system operations;
2. Locate and specify the physical constraints (energy and material balances, subsidiary relationships, technology specifications) of the overall technology through physical modeling;
3. Compile the value of a list of predetermined parameters (round-trip efficiency, rated storage capacity, rated power input/output, storage time scale, durability and capital costs), for they are used in conventional benchmarking studies for energy storage technologies;
4. Develop a set of physical, financial and environmental indicators which can be used to evaluate the performance of the system;
5. Formulate possible simulation scenarios by setting up meaningful sets of key decision variables;
6. Assess simulation trials for different scenarios using the performance indicators developed, and make recommendations concerning applications of technology.

The milestones listed above are to be achieved sequentially, for output from the completion of one milestone becomes the input to the next milestone (Figure 1.3).

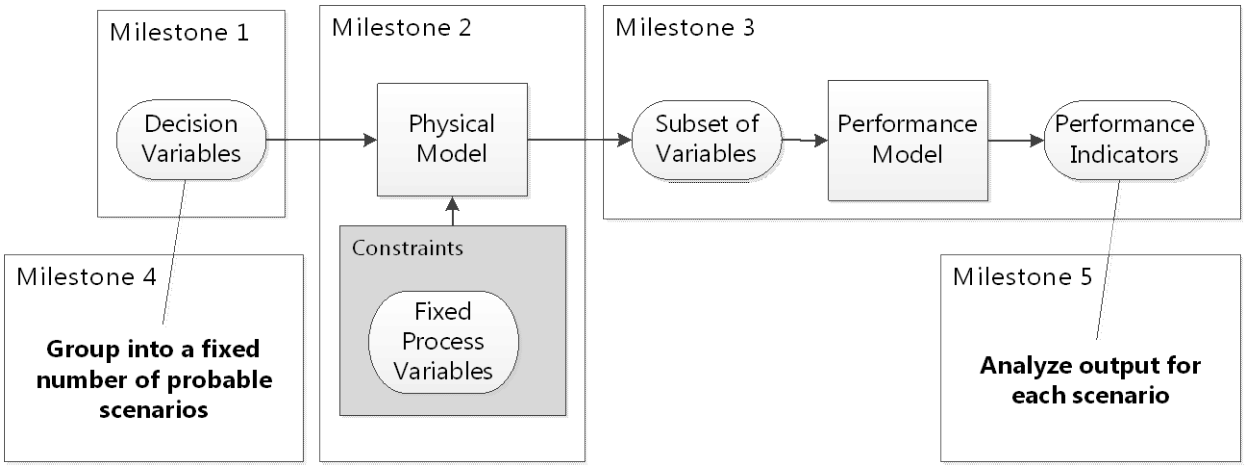

Figure 1.3 Milestones of simulation project

1.3 Thesis Scope

The scope of the simulations to be carried out in this is limited by the content of the model: the components that are represented in the model and their interconnections. In this section, the boundary of the physical and performance models are outlined.

1.3.1 Physical Model

Figure 1.4 illustrates the interface of the system under consideration, also referred to as the 'energy hub', with its environment. The components of the energy hub and their interactions are modeled extensively in this project, whereas the environment (power grid, natural gas grid, hydrogen need and mixture need) are taken to be exogenous parameters. They are described but not modeled dynamically.

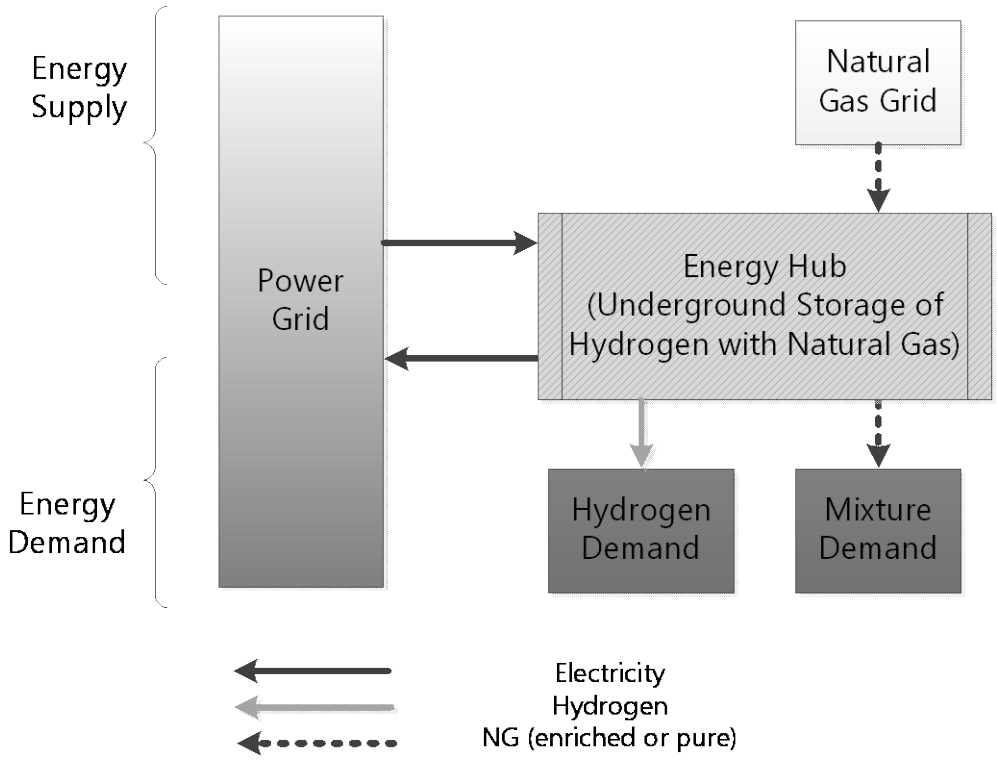

Figure 1.4 Project scope for the physical model

1.3.2 Performance Model

The performance model uses some process variables from the physical model and additional model parameters to evaluate the financial and environmental performance of the energy hub. These two aspects are evaluated by two separate sub-models: the financial model and the environmental model. In the end, three types of performance indicators are reported: physical, financial and environmental (Figure 1.5).

Financially, the performance model evaluates the expected annual cash flow from the operation of the energy hub, consisting of contribution from the amortized capital cost, fixed and variable operating and maintenance cost, energy purchases and sales, as well as change in the value of storage inventory (if applicable). These items are compiled so that the net present value of the energy hub can be calculated. For simplicity, the performance model assesses the environmental impact of the energy hub through the accounting of annual carbon dioxide emissions associated with the operation of the energy hub.

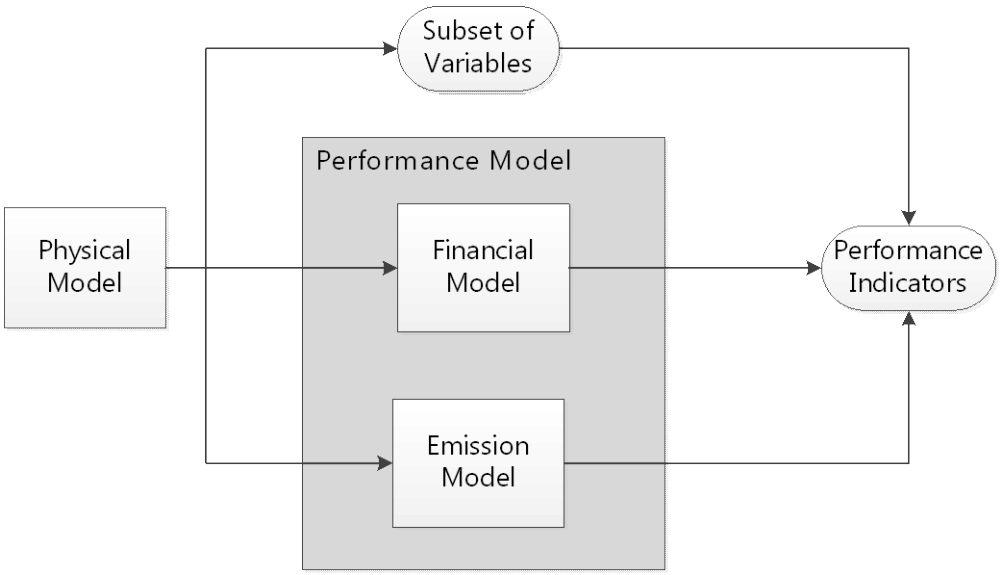

Figure 1.5 Structure of the performance model

The name of the financial model is chosen with care, since there is common confusion between "economic analysis" and "financial analysis". The main difference between the two types of analysis is the scope of analysis, in other words, the boundary of the system under consideration. In an economic analysis of the energy hub operations, the system to be analyzed would be the energy

system of Ontario, in which all provincial suppliers, importers, consumers and exporters of electricity, natural gas and hydrogen are included. The costs and benefits calculated amount to the total benefits or costs experienced by the whole province. Meanwhile, a financial analysis is smaller in scope. It focuses on the costs and benefits for one group of stakeholders – in this project, the operators of the energy hub – disregarding the benefits and costs experienced by other stakeholders.

The two analysis are complementary: the wider-scoped economic analysis evaluate the overall benefits of the project to the population involved; whereas the narrower-scoped financial analysis evaluate whether the incentive of specific stakeholders is adequate for the solvency and longer-term sustainability of the project. When a project is economically beneficial, but not financially beneficial to the operators of the project, it is unlikely that the project can be operated sustainably. On the other hand, if a project is financially beneficial to certain key stakeholders, but costly in the economic analysis, then the project must be re-examined with care, as it may reveal that some financial benefits are but transfers between stakeholders.

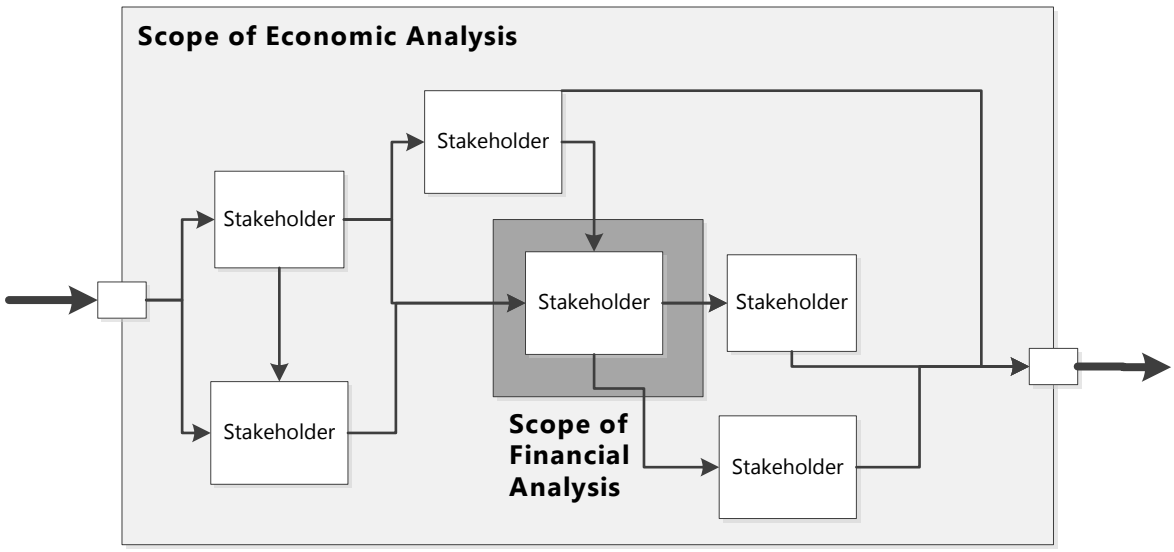

Figure 1.6 Comparison of economic and financial analysis

Chapter 2
Literature Review

This literature review surveys the applications that are commonly attributed to energy storage technologies and the portfolio of technologies that is currently under research. Then, the features of the Ontario energy system that are of interest to energy storage are reviewed. Finally, “energy hub”, a modeling frame work for integrated energy systems is introduced, followed by descriptions of the key technological components of the UHNG concept.

2.1 Energy Storage

Energy storage is not a specific material or a product. It is a service that is performed to facilitate the delivery of energy from upstream suppliers to downstream end-users, by providing buffering capacity. Thus, the suppliers and the end-users do not need to complete their transactions *simultaneously*. Overall, the bulk of the energy harvested by human society for specific services comes from a few primary sources, of which fossil fuels constitute the largest part at 80.9% [12]. Since the primary energy resources typically occur in a location different from that of the energy demands, we often need to transport them to their final destination, where they are consumed. Except for cases of continuous transportation through pipelines, the primary energy resources often need to be stored prior to and after transportation in batches. Then, once distributed to their points of use, energy resources are also frequently stockpiled, awaiting the time of use.

An energy vector is a form of energy that can be readily transported and stored. Out of all primary energy sources, only the fossil fuels and biomass can be considered to be energy vectors. Electricity, a secondary form of energy, is also a transportable energy vector. Since its commercial implementation in the late 19^{th} century, a wide range of appliances and services has been designed to depend on it. Thus, as shown in Figure 2.1, a non-negligible portion of fossil fuels and biomass is converted to electricity.

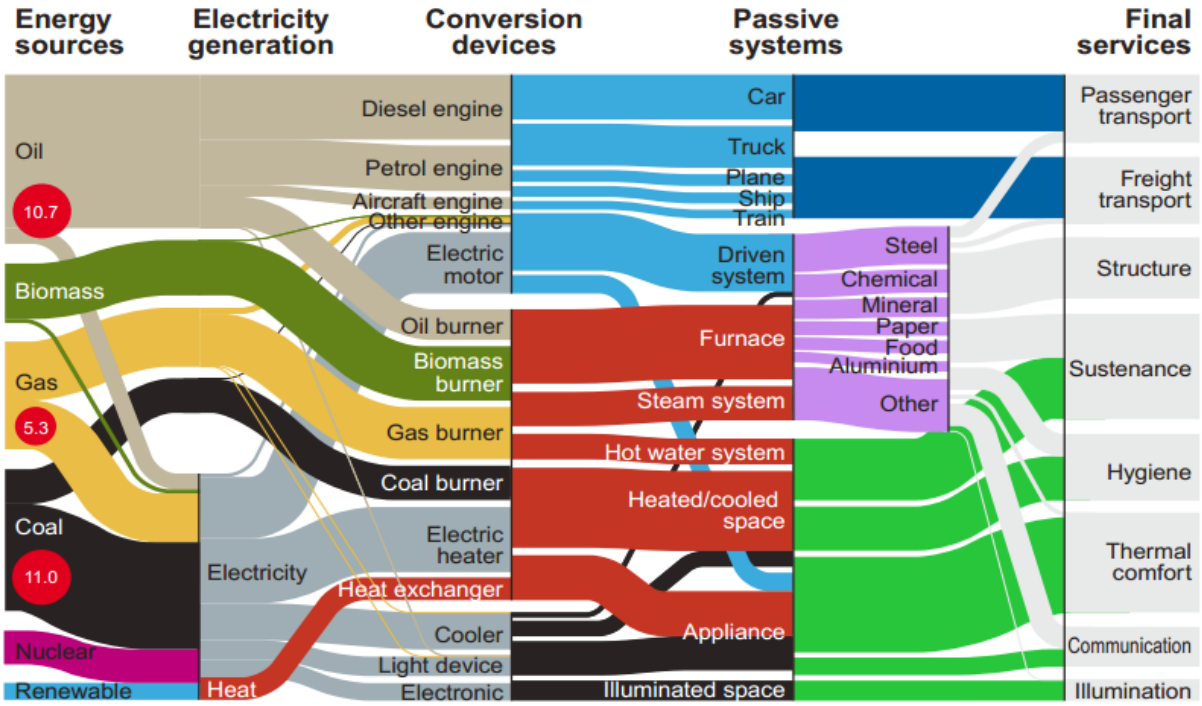

Figure 2.1 Global energy flow for societies [13]

In recent years, electricity is also generated from non-vector primary energy sources such as uranium (nuclear fission), solar, wind, tidal and geothermal energy. Unlike fossil fuels and biomass, these non-vector sources cannot be directly used by end-users and are hard to transport. They rely upon conversion to electricity for transportation and the provision of services, unless distribution of heat is also feasible.

In a way, electricity is an imperfect energy vector, for, unlike coal or oil, it cannot be readily stored. The storage of electricity is inherently more complex and less convenient. Typically, electrical energy cannot be stored directly, requiring conversion to another storable form of energy, the exception being the case of capacitors. Therefore, historically, the electrical power system was built around one central tenet: “Electricity must be produced when it is needed and used once it is produced” [1]. The prevailing operational strategy to maintain electricity supply-demand equilibrium is to reduce demand through deferrable loads and to adjust supply through dispatchable generators.

In the past years, energy storage has attracted increasing academic, industrial and governmental attention. To understand this new wave of interest, it is necessary to acquire a thorough understanding of the existing electrical power supply industry, following which the cases of applications of energy storage could be established.

2.1.1 Electricity Supply Chain

The electric power industry is technically complex. The variety of physical and socio-economic legacy in which it is grounded led to the development of a variety of forms of ownership, operation and control. In this section, the various members that participate in the supply chain of electrical power supply are outlined.

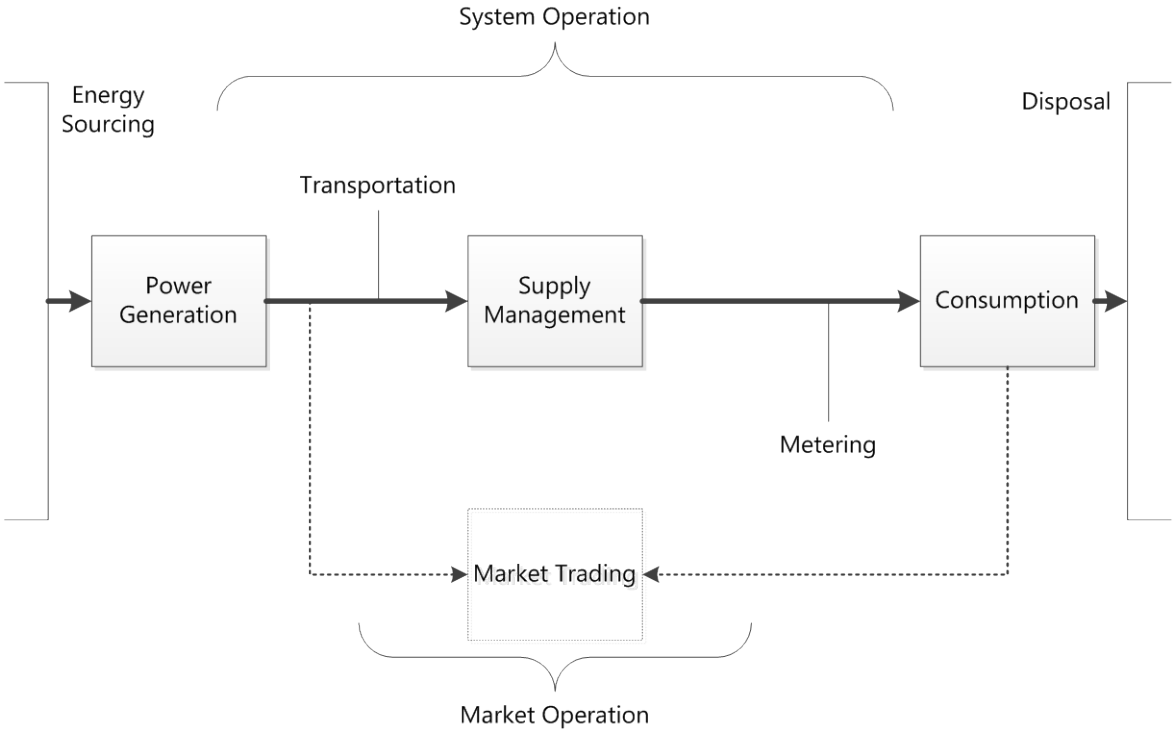

Figure 2.2 Stages in the electricity supply chain

The thick black line in Figure 2.2 represents the flow of electricity. The physical flow is initiated with energy sourcing, followed by power generation, transportation, supply management (also known as distribution), metering, consumption, and ends with disposal. Since the consumption of electricity is relatively clean, generating no waste products, the environment concerns typically associated with product disposal are not directly applicable. Instead, more attention is paid to the environmental

impact of power generation, the stage during which there are significant combustion emissions when fossil fuels are used.

Market trading is represented by a box by dashed lines, because the market transactions are made using information about the availability of supply and demand. In Ontario, operators of facilities connected to the high voltage lines are obligated to participate in the wholesale market: generators, transmitters, distributors and large loads. Embedded loads, which are not directly connected to the high voltage lines, are eligible to participate in the wholesale market if their consumption exceeds 250,000 kWh per year. Also, it is possible to participate in market trading without having physical facilities to generate or consumer electricity: wholesalers, retailers and financial market participants. The Independent Electricity System Operator (IESO) oversees and coordinates the physical operations of the system and the financial transactions on the market in real time.

Table 2.1 Typical life cycle of electricity and its participants

Lifecycle Stage	Description	Participants
Energy Sourcing	Harvest energy resource and deliver to the power station	Gas suppliers, uranium suppliers, wind/solar farm operators, hydro-electricity project operators
Power Generation	Convert *in situ* energy supply to electricity, then deliver to transportation infrastructure	Generator operators
Transportation	Transmit electricity	Transmission network owners
Market Operation	Arrange and coordinate energy trading transactions	Independent system operators
System Operation	Manage the grid to match supply and demand	Independent system operators
Market Trading	Trade electricity in the competitive market	Market participants
Supply Management	Sell electricity as a ‘bundled’ product to consumers	Energy retailers, local distributors
Metering	Meter the amount of energy consumed and/or traded	Market: all market participants; Residential: local distribution

Consumption	Consume energy	Loads, retail consumers
Disposal and Environmental Impact	Impact predominantly incurred during power generation	Generator operators, regulators

As previously mentioned, currently, electricity is produced as it is needed, at all moments. The key facilitator in the electricity supply chain, who performs the essential coordination between electricity consumers and suppliers, is the system operator. The system operator has the duties of forecasting the varying demand for electricity, considering the seasonal and daily factors, and scheduling a large number of power plants to meet that demand. Based on their economics and dynamic behaviour, power plants can be divided into three categories:

1. Baseload power plants, which are typically nuclear or coal-fired plants that operate near full opacity year round; they supply the power that is always needed. In Ontario, baseload power amounts to about 11,000 MW, supplied mostly by nuclear power generators.
2. Load following power plants, which are intermediate plants used to meet most of the day-to-day variation in demand. In Ontario, this is supplied by hydro and coal (the latter is to be phased out by 2014);
3. Peaking power plants, which typically operate only a few hundred hours per year, during the time of highest demand, often in summer, such as any generation required above 20,000 MW in Ontario (not visible from figure attached).

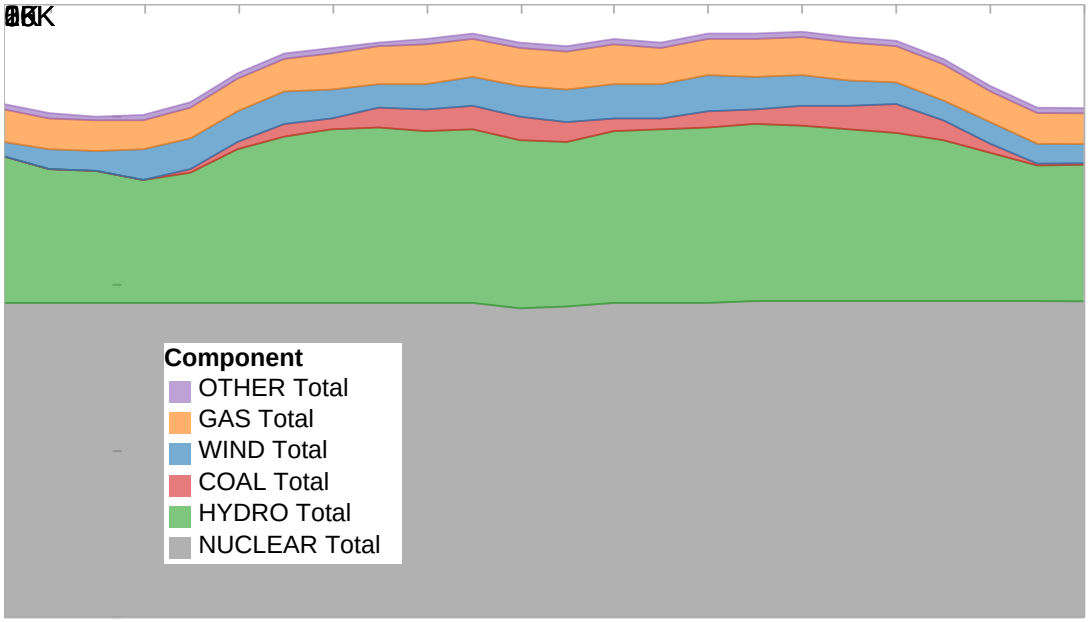

Figure 2.3 Ontario power generation by type for June 30th, 2013 [14]

In the case that adequate service cannot be provided by the regular generators, additional power plants under special contracts are brought on-line to restore reliable power supply. The generators on call to replace normal supply in case of equipment failures or emergencies are known as the operating reserve. Operating reserve generators are contracted for their ability to supply power on demand; they receive payment even when actual energy service is not invoked. They can be either spinning or supplemental; spinning reserves are units that are partially loaded or highly responsive. Generators which can be restarted without outside source of power (black-start capability), generators which vary their output automatically, within seconds or minutes, in response to signals sent by the IESO (regulation service), and generators that are able to adsorb and generate reactive power (reactive support and voltage control) are known as ancillary services, which are contracted by the system operator to ensure system reliability for all users of the grid.

Energy storage is considered to be one of the methods that can be used to match supply with demand; the others include traditional load following, spinning reserve plants and demand-side management.

Whether energy storage is deployed, depends on its economics compared to other alternatives to provide grid balancing services.

2.1.2 Applications of Storage in the Existing Grid

It is believed that in historical studies, the economic benefits of energy storage have not been properly accounted for. This is due to the simplistic assessment method used and the difficulty to quantify the various values streams generated by energy storage. In this section, the various applications of energy storage are grouped according to the location of the energy storage facility in the existing electricity supply chain. The location of the energy storage facility has implications on its ownership and operating philosophy. The stage of resources extraction is absent, because by then, energy is still in a pre-electricity form (fossil fuels, uranium, heat, wind, etc.), therefore beyond the scope of electrical energy storage.

2.1.2.1 Located Near and Operated by Power Generators

For baseload generators, such as nuclear power plants, changes in power output according to dispatches are possible but undesirable, because plant equilibrium takes a long time to establish or other operational requirements limit such adjustments. The economics of such plants typically improve with the higher power plant utilization factor; therefore, they are used to provide more or less constant power near their generation capacity throughout the year. Occasionally, during off-peak hours, the output from baseload power plants exceeds the demand on the grid and causes negative electricity pricing.

Generation shifting for baseload power is the practice of charging an energy storage device using the low cost baseload power during off-peak hours, saving it for dispatch when market demand is higher. Here, it is assumed that the storage technology is operated by the baseload power supplier. From this perspective, an energy storage project will be economically attractive if the decreased O&M costs due to higher capacity utilization and increased revenue from shifting time of transaction are higher than the costs of implementation.

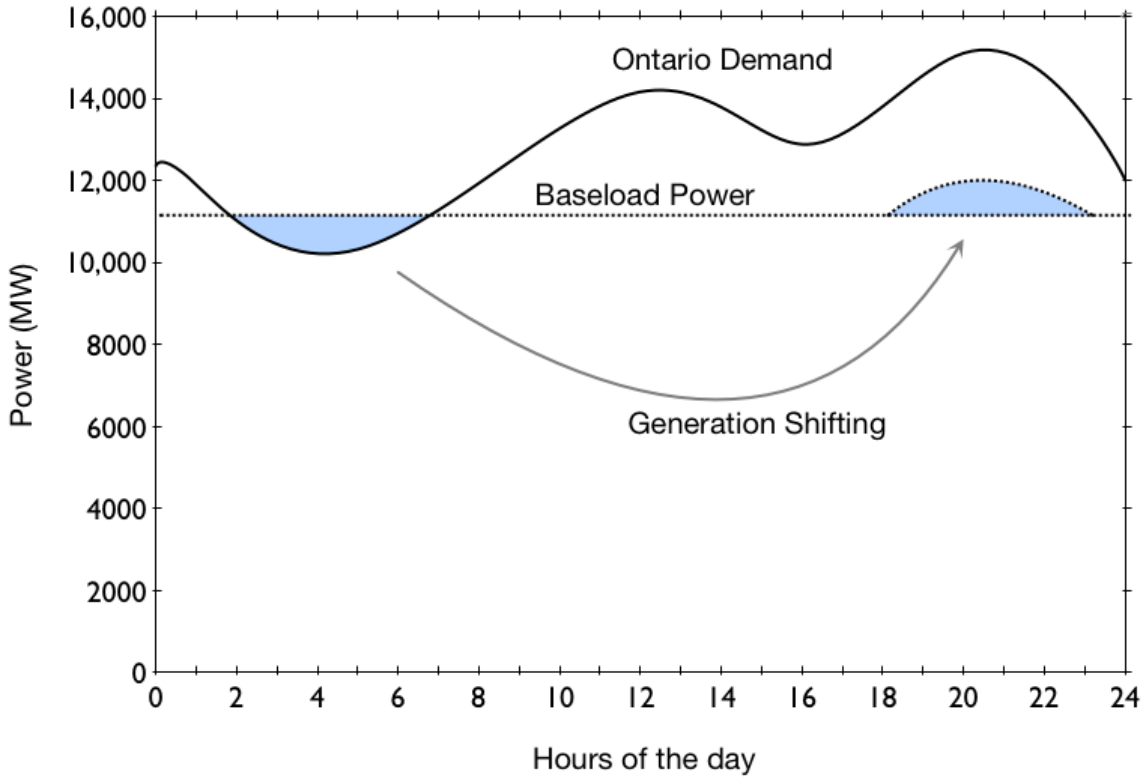

Figure 2.4 Conceptual diagram for baseload power generation shifting

In additional to the aforementioned benefits, from the system operator's perspective, generation shifting may decreases the cost of power that must be produced to meet demand during on-peak hours, given that lower-cost power from baseload generators are moved to replace some of the output from load-following and peaking power plants. If the power output provided by energy storage facilities is large enough, it may even be able to defer the construction of more load-following and peaking plants. A more comprehensive economic analysis would compare the economic costs and benefits of the case with and without energy storage, for the scope indicated in Figure 2.5. The price-setting mechanism within the wholesale electricity market will need to be included in the analysis, if the power drawn and delivered by the energy storage facility is deemed large enough to influence the market-clearing price.

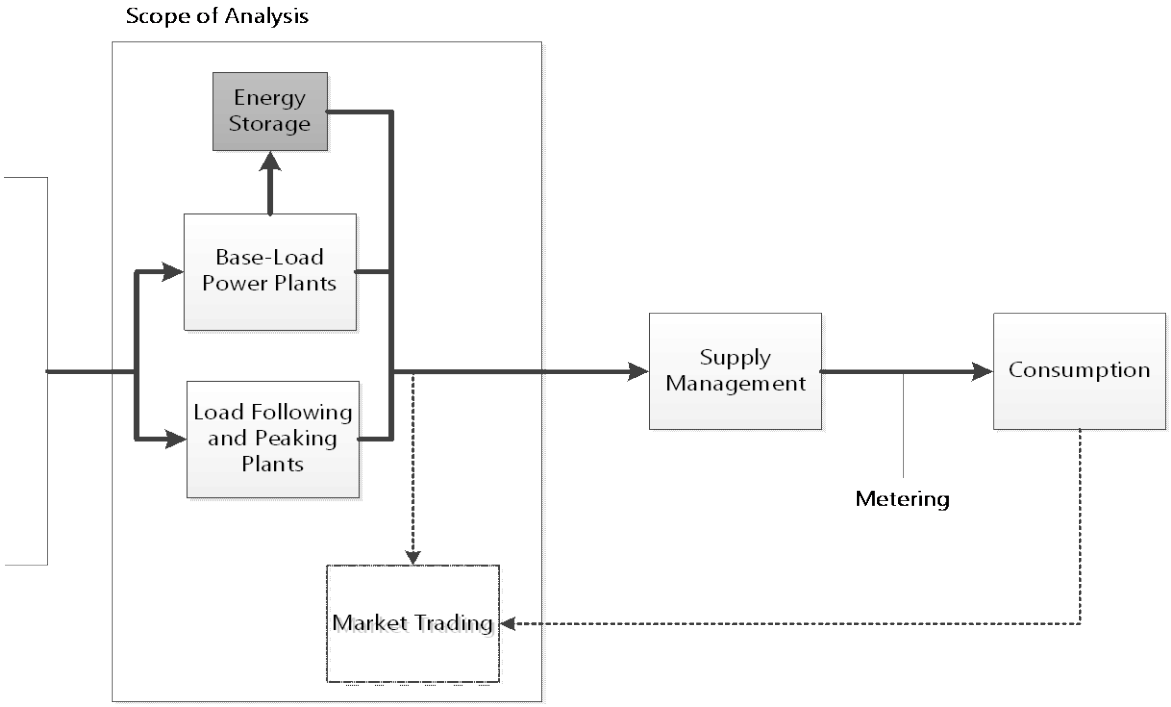

Figure 2.5 Scope of analysis for generation shifting

2.1.2.2 Located Near Transmission Network and Independently Operated

Currently, the transmission and distribution facilities of a power system are built to serve the peak demand, so the lines must be expanded at the same rate as the peak demand, regardless of under-usage during off-peak hours. In Ontario, the high capital costs of the under-used T&D network are borne by all market participants via the payment of Wholesale Transmission Charges. Given that grid demands are now met instantaneously with transmitted supply, it has been impossible to justify transmission networks which are sized below the peak demand.

In this context, energy storage can be used to relief network congestion, decreasing the need for expansion in transmission capabilities, and allowing the grid to operate with transmission lines which are sized below peak demand. It achieves this by allowing charging and discharging of power independent of transmission network congestion.

Located downstream of points of grid congestion, the energy storage facility can proceed to charging when the lines are not congested, then deliver that energy downstream during periods of congestion. Figure 2.6 is only a much simplified version of the real scope of analysis; a complete analysis for this type of application must take into account the geographically disaggregated nature of power transmission lines, power generators and power loads. An energy storage facility would be preferred if it successfully alleviates grid congestion with costs lower than that of alternatives (expansion and construction of new power lines).

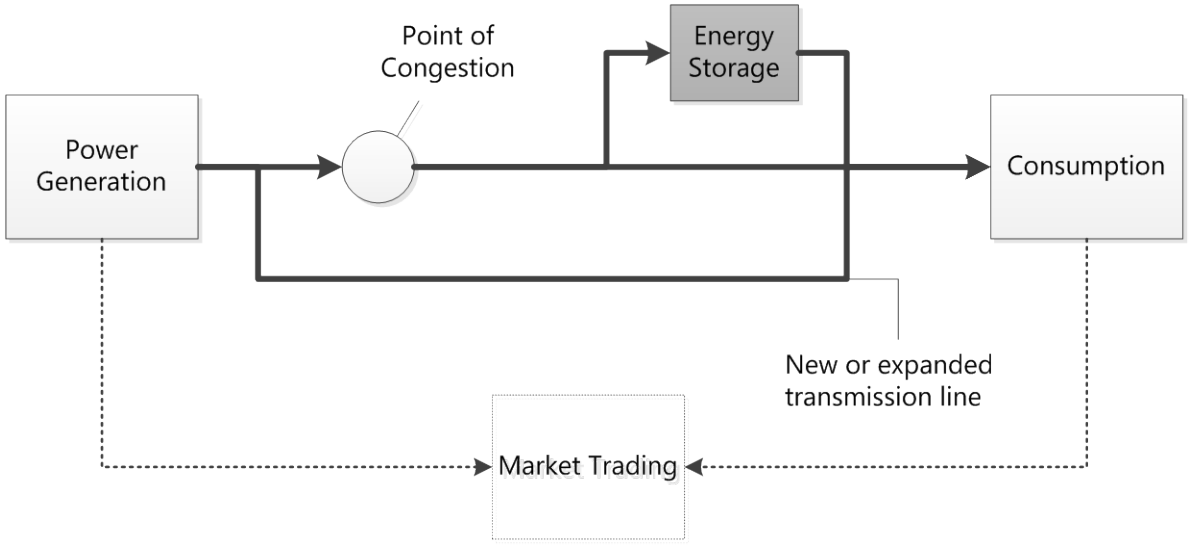

Figure 2.6 Scope of analysis for grid congestion relief

2.1.2.3 Other Applications for Independently Operated Storage

The restructuring of the electricity wholesale market has also created a market for ancillary services that energy storage facility operators can participate in. In Ontario, the ancillary services that the IESO contracts on the procurement market are certified black start facilities[1], regulation service[2],

[1] Certified Black Start Facilities are able to restart their generation facility with no outside source of power.
[2] Regulation Service corrects variation sin power system frequency by responding to IESO signals with response times ranging from tens of seconds to a few minutes.

reactive support and voltage control service[3]. Operating reserve contracts, requiring response of generators within 10 to 30 minutes of activation, are also available.

2.1.2.4 Located Near and Operated by Energy End-Users

Energy end-users can sometimes use energy storage for energy cost reduction. Currently, many utilities have implemented a power tariff that varies based on the time of use. In this case, energy storage could be used to shift demand from periods with high prices to those with lower prices. This is comparable to generation-shifting by power suppliers. There exists the difference that the small volume power end-user makes charging and discharging decisions based on energy retail price, whereas power suppliers base their decisions on energy wholesale market price. Some industrial and commercial customers, which are large volume end-users, pay a demand factor-based tariff which varies with the time of use and the amount of power used. In other words, they also participate in the energy wholesale market. Energy storage can help them spread out their peak demand over a longer period of time, thus reducing the costs of energy.

If the end-users have devices or equipment highly sensitive to voltage or frequency deviation, they will benefit from energy storage for improved reliability. Energy storage facilities will buffer imbalances between the local demand and the supply from the grid, keeping frequency and voltage at the nominal value. Energy storage is equally beneficial to customers who are concerned with power supply disruption. Near the end of the supply chain, the flow of power tends to be smaller, and the scope of the cost and benefits study, also smaller.

[3] Reactive Support and Voltage Control Service are reimbursement to dispatchable generating facilities which incurred additional costs to provide reactive support/voltage control services.

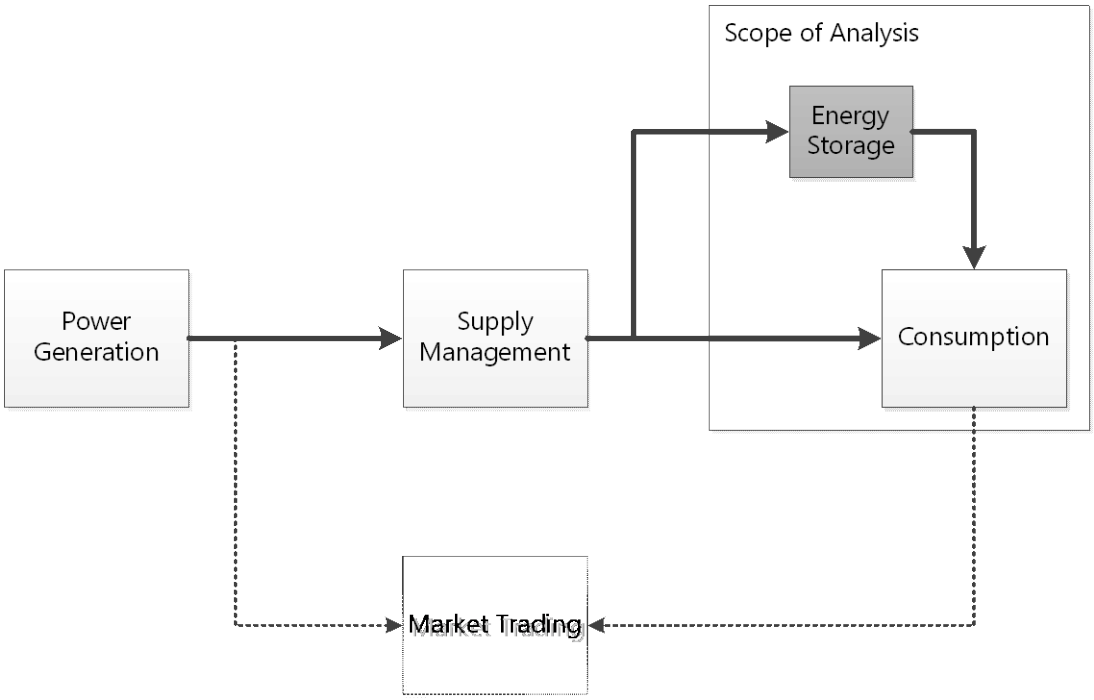

Figure 2.7 Scope of analysis for end-use energy reliability and cost reduction

2.1.3 Applications of Storage in the Future Grid

For intermittent power generators, such as wind turbines and run-of-the-river hydro generators, their source of energy can at best be forecasted, let alone varying their output at will. From a RE generator operator's perspective, the viability of RE projects, is hindered by their lack of control over the time of power generation once governmental subventions are removed. Power from renewable sources must be sent to the grid as it is produced, without consideration of market supply and demand.

Energy storage technology could improve RE projects profitability by making their intermittent power output predictable and dispatchable. Operated by *RE project operators* (Various commercial firms in Ontario), energy storage will enable RE generators to compete on an equal basis as conventional, often fossil-fuel-based dispatchable generators. Depending on the scale of storage, part or all of the fluctuating power generated could be consolidated and dispatched according to the instructions of the system operator, as power is needed. This is expected to increase the revenues of RE project operators.

Once the penetration of RE projects has crossed a critical threshold, beyond which significant power variability control is required. Figure 2.8 shows how, with a high wind penetration (>20%), currently small fluctuations in power output could be amplified and place even more requirement on conventional generators used for load following. By 2018, the non-hydro renewable energy generating capacity is expected to expand to 10,700 [15]. In the year 2012, most of the non-hydro renewable energy generating capacity in Ontario comes from wind power. It would need to be increased by seven times, if the Supply Mix Directive of the Ontario Ministry of Energy were to be followed. A hypothetical scenario in which the wind power levels in Ontario increases by ten-fold is shown in Figure 2.8.

From a system operator's point of view, the intermittency and unpredictability in their power output will become increasingly problematic, as the percentage of renewable energy (RE) generators in a grid's supply mix increases. The increasing fluctuations will need to be countered by the installation of more dispatchable generators (i.e. gas-fired generators). This problem is believed to be significant once RE penetration exceeds 20% of the total supply mix [16]. For lower penetration, the variability in wind power output is smoothed by the aggregation of multiple geographically-dispersed sources.

By that time, in order to ensure the reliability of the grid, supply variability from *individual power supplier* might be discouraged with penalty charges (which do not exist as of now). They may then choose to operate an energy storage technology of appropriate scale to release power in a controlled manner. The *system operator* could also manage supply variability caused by RE project centrally, by adopting a larger-scale energy storage technology capable of smoothing the aggregated supply from multiple RE generators.

On the side of supply, because some of the RE resources are found in remote locations, new transmission lines and expansion of existing lines are often needed to connect them to the point of use. The sizing of those new transmission and expansion projects reveals a dilemma: the lines could be sized to accommodate the peaks in RE production, remaining under-used during off-peak hours. They could also be sized for the typical flow throughout the day, cutting off the supply of RE power once the lines have reached full-capacity during peak hours. The first approach has high capital costs, which are eventually borne by *all ratepayers* as delivery fees; the second approach result in

constrained-on and constrained-off payments which are charged as overheads to *the participants of the real-time wholesale electricity market.*

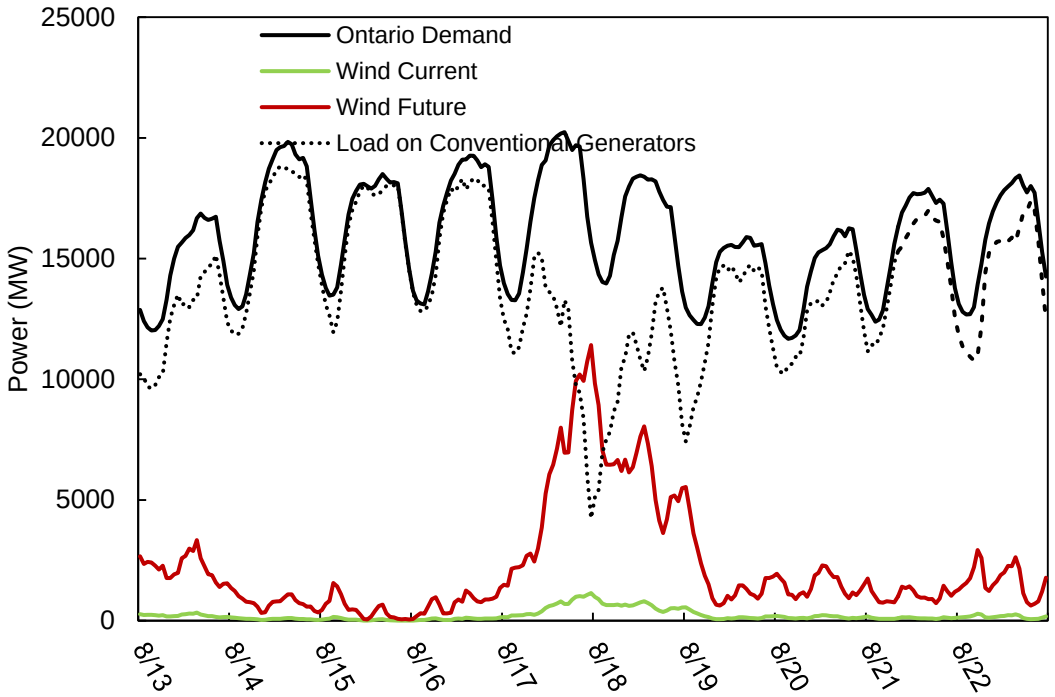

Figure 2.8 Hypothetical weekly grid supply scenario with high wind power penetration

2.1.4 Conventional Energy Storage Technologies

The applications that a given energy storage facility can perform is dependent on the amount of energy that it can store, its response time and the rate at which the energy can be released or stored. The Electric Power Research Institute has published their findings on the scale of energy storage system required for different applications (Figure 2.10). It can be seen that, despite of some small overlaps in between applications, most applications are not simultaneously compatible. Those interested in a particular application of energy storage need to select an energy storage technology that is able to perform within the ranges prescribed by the given application.

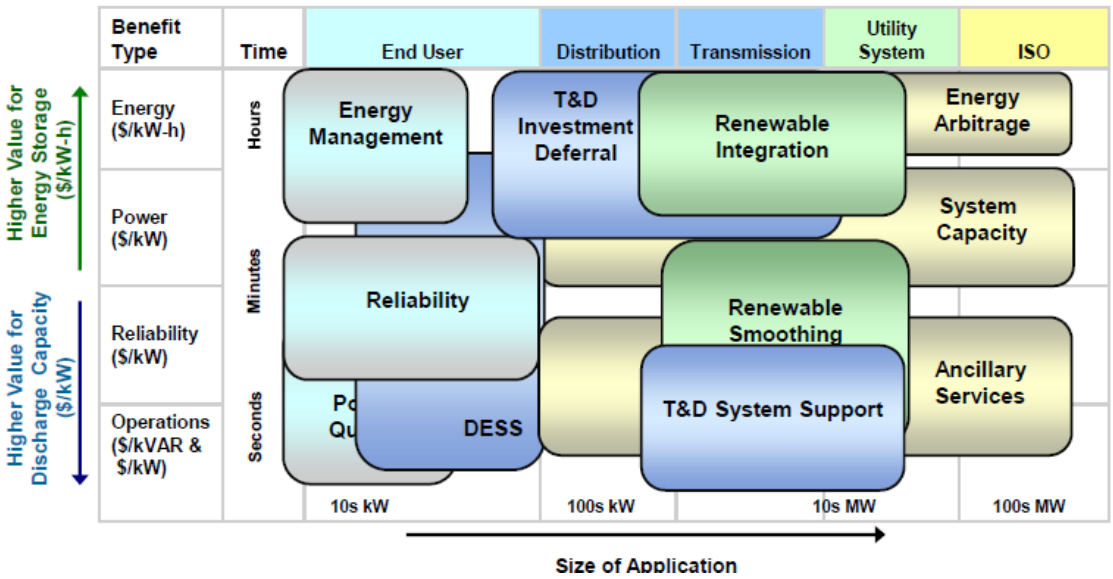

Figure 2.9 Operational benefits monetizing the value of energy storage [10]

The following section provides a survey of the different methods of bulk energy storage currently available or under active development. The technologies typically proposed for grid energy storage are batteries, compressed air energy storage (CAES), pumped hydro energy storage, advanced capacitors, flywheel energy storage, superconducting magnetic energy storage, and energy storage through hydrogen [6-11]. Because energy storage through hydrogen is still at a conceptual stage and will be the main focus of this project, it is discussed in an independent section following the literature review.

Vehicle-to-grid (V2G), a system in which electric vehicles act as distributed energy storage devices has also been proposed [11]. However, the deployment of V2G at utility scale requires the participation of individual consumers, through the purchase and use of plug-in hybrid electric vehicles (PHEVs). This is subject to many socio-technological impediments[17]. Therefore, the V2G concept is not addressed as part of this literature review.

When describing each energy storage system, the fundamental principle of its operation, the system components, and its stage of development are outlined. Then, in order to achieve meaningful comparison, a fixed set of properties is introduced for each alternative and compared whenever possible. The selected properties are:

Round trip efficiency, defined here as the percentage of electricity sent for storage which can be recovered as electricity. The technology with the highest round trip efficiency is more favorable, because low efficiency, implying that only a fraction of the energy stored can be retrieved, increases cost of storage per unit of retrievable energy.

Storage capacity and *rated power*, determined by the energy and power densities of the storage devices. Together, these two properties determine the field of application of the energy storage technology. Storage capacity is the maximum amount of energy that a storage device can hold, and rated power determines at what rate the stored energy could be recovered. For energy storage at utility-scale, especially when storing off-peak excess power for later use, it is desirable for the energy storage unit to store several thousand MWh of energy, and release at rated power above several hundreds of MW [18].

Storage timescale, representing the time period for which energy can be stored using the technology, taking into account phenomena such as self-discharging. Since load placed on the power grid varies by time of day and by season, it is desirable for the chosen technology to be able to store energy for several hours, even up to months, without degradation.

Durability of equipment is represented by the number of charge-discharge cycles that the system can undergo without refurbishment or replacement. A short lifespan is undesirable, because it increases the costs of storage in the long term by multiplying the costs of replacement.

Cost of storage is a parameter that measures the economic competitiveness of the technology. It varies depending on the stage of development and the nature of a given technology. The values presented in this section are costs for the total energy storage system per unit of energy stored, whenever available. Since this is an exploratory project that simulates a future scenario, the cost is only given as indicators, not as a criterion. This ensures that options are not discarded purely by costs, for development following the current research will be able to affect future economics.

Other characteristics of a technology, such as *geographic requirement* or *auxiliary equipment requirement* are noted whenever applicable. They will be used to further refine the choice of a large-scale energy storage technology.

2.1.4.1 Battery Systems

All battery systems convert electrical energy to chemical energy for storage. When charging, an electrical potential is applied and the batteries undergo an internal chemical reaction. The discharge of stored energy occurs when the chemical reaction is reversed. The types of batteries listed below mainly differ by the material used for the electrodes and the electrolyte, since different chemical reactions are involved. Note that, since the electrodes in these batteries participate in the chemical reaction and store the products via solid state reactions, the energy and power densities of the battery are dependent on the size and geometry of the electrodes [6]. Also, most of them have lifetimes which are affected by operating conditions such as depth of discharge, operating temperature and fast charge/discharge cycling ([1]. Since batteries are direct current (DC) systems, a power conversion unit is required for them to interface with the grid, where energy is generated and transmitted as alternating current (AC).

2.1.4.1.1 Lead-Acid Batteries

The lead-acid battery is a very mature and established technology. It uses elemental lead as anode and lead dioxide as cathode; the electrodes are immersed in a dilute sulfuric acid. The round trip efficiency of a lead-acid system ranges from 70% to 80% [11]. Typical energy density values are about 30 Wh/kg, and the total stored energy can be discharged in tens of minutes to an hour [8], so

the power density is estimated to be around 150 W/kg. Because there is very little self-discharge (2% of rated capacity per month), lead-acid batteries are appropriate for long term storage. Currently, such systems are expected to last from 1000 to 2000 charge/discharge cycles at 70 % depth of discharge [9, 19]. Storage cost per installed storage capacity is $425-475/kWh, and relatively little maintenance is needed [10]. But, because of the maturity of the technology, no significant breakthrough is expected with respect to system lifetime and costs[9]. Lead-acid batteries are commonly used when low energy density is acceptable and high abuse tolerance is required, in applications such as automotive starting, lighting and ignition, and battery-powered uninterruptible power supply. The disposal of a large-scale lead-acid system causes environmental concern, for it contains a toxic heavy metal.

2.1.4.1.2 Nickel-Cadmium Batteries

A nickel-cadmium battery (Ni-Cd) consists of a cathode made of nickel hydroxide, anode made from metallic cadmium, with an aqueous potassium hydroxide solution as electrolyte [11]. Energy and power density ratings for this type of battery are 40-60 Wh/kg and 140-180 W/kg, with a round-trip efficiency of 60-90%. At 10% of rated capacity per month, the self –discharge rate is higher than that of lead-acid batteries, but still acceptable for hour-long storage purposes[8]. A Ni-Cd system has durability estimates of 1000-2500 charge/discharge cycles and 10-20 years, and is more durable than lead-acid batteries at higher operation temperatures [1, 9], The storage cost per installed capacity is $1000-2000/kWh, more expensive than that of lead-acid systems. One important disadvantage of the Ni-Cd battery is the toxicity of cadmium, which will require a complex recycling procedure if deployed, to minimize negative environmental impacts.

2.1.4.1.3 Sodium Sulfur Batteries

Sodium sulfur batteries (Na-S) has molten sulfur at the cathode and molten sodium at the anode; the two electrodes are separated by a solid beta alumina ceramic electrolyte, which only allow positive sodium ion to pass through [7]. The literature reports round-trip efficiency of around 75% [10]. Na-S batteries have energy density of 120 Wh/kg, and power density of 120 W/kg [11], Since there’s no noticeable degradation of stored energy through self-discharge, long-term storage using Na-S batteries is very favourable [19]. At 100% discharge, a Na-S battery can last up to 2500 cycles; its lifetime is further extended at shallow depth of discharge (40,000 cycles at 20% depth of

discharge)[1]. Cost-wise, most recent values for large-scale applications are $520-550/kWh [10]. Both sodium and sulfur are abundant low-cost material, making the battery suitable for mass production. The battery operates with molten compounds; therefore, the operating temperature, about 300 °C is much higher than the ambient temperature and requires heating in stand-by mode [19]. The auxiliary heating requirement places a parasitic load on the overall system and reduces its efficiency [7]. They have been used for load leveling, emergency power supply or UPS.

2.1.4.1.4 Lithium-Ion Batteries

Lithium ion batteries (Li-Ion), known to the public through their wide use to power portable equipment, laptops, cameras, cell phones and portable tools, are made up of lithiated metal oxide cathodes and graphitic carbon anodes with layer structure. Lithium salts dissolved in organic carbonates act as the electrolyte [7]. Very high round-trip efficiency has been reported for Li-Ion batteries: 87-92% [10]; energy and power densities are 100-200 Wh/kg and 360 W/kg, respectively [11]. Self-discharge occurs at the rate of 5% of rated power per month [8]. In its lifetime, the Li-Ion battery is able to complete more than 1500 charge/discharge cycles, 3000 cycles at 80% DOD [19]. The main obstacle to large-scale applications of Li-Ion batteries is its higher cost: $1500-3500/kWh [9]. Because of its high energy density, Li-Ion batteries are studied for use in plug-in hybrid and electrical vehicles.

2.1.4.1.5 Flow Batteries

As aforementioned, the electrodes of most batteries participate in storage, tying the energy and power densities of a system to the electrodes' size and shape. One exception exists: flow batteries. Flow batteries consist of two liquid electrolytes in an electrochemical cell with two compartments, physically separated by an ion-exchange membrane which only selected ions can pass through. In this case, the system is easily scalable, since the storage capacity is set by the electrolyte tank capacity, and the rated power, by the electrolyte flow rate and the area of the membrane [11].

There are three types of flow batteries: vanadium redox (VRB), polysulfide bromide (PSB) and zinc bromide (ZnBR). Of the three, VRB uses compounds of vanadium in both electrolyte tanks,

eliminating cross contamination of electrolytes, allowing for easy recycling [7]. It has also shown a longer lifetime and is more developed than the other two types of flow batteries. Therefore, VRB is used to represent flow batteries in general in this review of technologies.

Round-trip efficiency of VRB, also called AC to AC efficiency, is about 75% [9]. Energy density per mass of electrolyte is 25 Wh/kg and power density is 80-150 W/kg [11]. The battery can be fully discharged without adverse effects, and self-charge is negligible since little electrolyte is lost over time, encouraging its use for long term storage applications [7]. Lifetime is estimated to be 1000-2500 charge/discharge cycles, or 10 years [9]. Finally, by economy of scale, the storage cost per installed capacity decreases as the system size increases, $620-740$/kWh are the most recent values derived from calculations for a 250 MWh demo facility [10].

2.1.4.2 Flywheels

Flywheels convert electrical energy to kinetic energy for storage, in the form of a mass rotating about an axis. To charge the flywheel, a motor is used to accelerate the flywheel; for retrieval, the flywheel is slowed down via a decelerating torque to the motor, now reversely used as a generator [8]. The energy stored is a function of the moment of inertia of the rotor, and the square of its rotational velocity. Low speed flywheels are typically made of steel and high speed flywheels (>50,000 RPM) are made from composite materials. Containment vessels are required to deal with potential rotor failures. Magnetic bearings and vacuum chambers are sometimes used to reduce losses from friction [6].

The roundtrip efficiency of such systems is high for short periods of storage: 90% [9]. However, flywheels have very high standing losses. After five hours of storage, the overall efficiency is reduced to 78%, and 45% after one day [18]. In some instances, up to 20% of stored capacity could be lost per hour for non-continuous cycling [8]. Therefore, long term storage is not foreseeable with this technology. As for storage capacity, low speed flywheels have energy density between 5-30 Wh/kg, while high speed flywheels have ratings higher than 50 Wh/kg [11]. Flywheels have extremely high power density: 1000 W/kg for low speed flywheels and 5000 W/kg for high speed ones, although the peak power rating does depend on the power ratings of the power converter and the motor/generator.

Within the lifetime of one flywheel, it can support more than 100,000 complete charge/discharge cycles, operating for 10 years and longer [9].

Costs for flywheel storage are more reasonable when compared to other technologies on a storage cost per installed power capacity ($/kW) basis, not as cost per installed energy capacity ($/kWh). The per power value, ~$2000/kW compares well to other storage options, which mostly have values that range from $1000/kW to $5000/kW. But, the per energy value, $7800-$8800/kWh, is the highest among all existing options [10]. In other words, flywheels are not strong candidates for bulk energy storage, but are more suitable for power quality control applications which require high power delivery over short period of time.

2.1.4.3 Advanced Capacitors

Three types of advanced exist: electrochemical double layer supercapacitors (ECDL), pseudocapacitors, and hybrid capacitors. Out of the three, ECDL is the most fully developed and will be the focus of this review. Capacitors store energy by physically separating positive and negative charges with an insulating dielectric. In supercapacitors, the insulating material is replaced by an ionic electrolyte, in which conducting electrodes are submerged. When charging, the voltage applied creates an electric field that enables the ions in electrolyte to migrate towards electrodes of opposite polarity, forming an electrostatic electrical equilibrium at the surface of electrodes. The capacitance of supercapacitors is much larger than regular capacitors, because the separation of charge occurs at much smaller distances, and because electrodes are made of porous carbon with very large surface area [8].

Since the separation of charge is physical rather than chemical, the effect is easily reversible, leading to high efficiency such as 95% [11]. For the same reason, the rate of charge and discharge is faster than that of batteries, operating based on chemical reactions. ECDLs are capable of delivering 4000 W/kg, potentially 100,000 W/kg if electrodes are made of carbon nanotubes. Energy density is close to 5 Wh/kg, with hope of attaining 69 Wh/kg when carbon nanotube electrodes are used [8]. Supercapacitors have high self-discharge rate: about 14% of nominal energy is lost per month. The nature of energy storage in supercapacitors implies that degradation is minimal for deep discharge and over charge. A lifetime of 400,000 cycles at 100% depth of discharge is expected. Because of

their low energy density, investments per installed capacity for ECDLs are very high, around $20,000/kWh [8]. Overall, supercapacitors are more suitable for high peak-power, low-energy situations.

2.1.4.4 Superconducting Magnetic Energy Storage (SMES)

SMES stores energy in the magnetic field generated by DC current flowing through a superconducting coil. The operation mode of the superconducting coil is controlled by altering the voltage across the coil. Positive voltage charges the coil and negative voltage leads to discharge. In standby mode, there's no voltage difference across the coil. Because the superconductor needs to be maintained below its superconducting critical temperature, the SMES system needs a cryogenic cooling system, in addition to the power conversion/conditioning system and the coil [6].

The charge-discharge cycle of SMES systems can reach instantaneous efficiency of more than 95% [18]. The storage capacity of a superconducting coil is dependent on its size and temperature, among other properties. These units can respond to change of mode within a few milliseconds, then provide very high power output, but only for a very short while [1]. They are able to complete a great number of charge-discharge cycles at 100% DOD. In between charging and discharging, SMES systems have a small power loss in the non-superconducting part of the circuit, so a small trickle charge is necessary to replace the lost power. This is comparable to self-discharge in battery systems.

Large SMES projects might need to be contained underground in order to shield the effect of the enormous electromagnetic forces that are generated [18]. As with supercapacitors, SMES systems have competitive storage costs per installed power, but much higher storage costs per installed energy storage capacity. For example, for a hypothetical 100 MW, 500 kWh SMES project, the costs are $1970/kW and $394,000/kWh [20].

2.1.4.5 Compressed Air Energy Storage (CAES)

Conventional gas turbines consume up to two-thirds of the fuel used to compress air, before directing it to the combustor for combustion with fuel [6]. To compress the air needed by gas turbines, CAES systems use compressors powered by off-peak electricity instead more expensive natural gas. Compressed air can be stored in vessels, but the pressure that tanks can withstand limits the storage

capacity of this technology. Therefore, in for large-scale applications that absorb grid excess power, the compressed air is stored in underground mines, caverns or aquifers. A complete CAES system comprises of motors/generators, compressors, expansion turbines, an underground formation for storage and auxiliary equipment. Before being injected underground, air is cooled and pressurized. When it is extracted from storage, it must first be preheated in a recuperator before being mixed with gas to be combusted and expanded in the turbines [8]. There are three types of CAES technologies based on how heat exchange is managed for compression: isothermally, adiabatically or diabatically [11]. Isothermal systems allow the temperature to equalize with the surroundings by slow compression, thus limiting power delivery rate, is more suitable for small-scale projects. Adiabatic systems store heat released during compression for later use in the recuperator, requiring a heat-storing device. Diabatic systems use external energy to heat or cool air throughout the process and are most common.

The round trip efficiency of existing diabatic systems in operation is about 50%, lower than that of proposed adiabatic systems, 75% [9, 21]. CAES technology is typically used for very large-scale storage projects, having rather low energy density of between 10-30 Wh/kg [11]. The rate at which power can be delivered using CAES technology is dependent on the output specifications of the combustion turbines into which the compressed gas is fed. To recover energy stored, a combustion turbine power plant fitted with CAES is able to start-up rapidly in 9 to 12 minutes, compared to the required 20-30 minutes of conventional combustion turbine peaking plants [8]. The energy can be stored for more than a year, since losses are very small. A CAES project can have lifetime of more than 20 years, or more than 5000 cycles [9, 11], and the most recent storage costs per installed capacity is $60-120/kWh [10]. The obvious limitations of CAES technology are the requirement of an adequate underground storage facility and its dependence on an on-site combustion turbine power plant for energy recovery.

2.1.4.6 Pumped Hydro

Pumped hydro stores energy by circulating water between two reservoirs with a height difference. To charge the system, water is pumped from the lower reservoir to the upper reservoir, consuming power; to discharge, water stored by the upper reservoir is released and flow into the lower one through a turbine, generating power. The typical components of such a system are: reservoirs with

appreciable hydraulic head, connected through a set of reversible pumps/turbines [8]. Both freshwater and seawater systems exist, with the open sea being the lower reservoir. Sometimes, well-located abandoned mines can also act as the lower reservoir.

The overall efficiency of pumped hydro operations were 60% in their beginnings in the 1960s, currently, more recent values of about 80% are reported [7, 9, 11]. The losses mainly come from evaporation at exposed water surface and from energy conversion at pumps and turbines. The energy density for pumped water storage is very low (0.3 Wh/kg). Therefore, small-sized projects are rarely economical. The storage capacity of the technology is dependent on the body of water available and on the variation in height between the two reservoirs. The response time of a pumped hydro plant is on the order of seconds, like other conventional hydroelectric plants. Only 10 to 30 seconds is required for the plant to ramp up to full power from standby mode, and 10 minutes are needed to switch from complete shutdown to full power mode [1]. The self-discharge of this technology is negligible, and its lifetime, measured in decades, is from 20 to 50 years [9]. System development costs for pumped hydro projects are notably high, in the range of $420-430 for 280 to 530 MW facilities, and $250-270 for 90 to 1400 MW facilities [10].

Pumped hydro is the oldest and largest of all commercially available energy storage technologies. In 2010, more than 99% of the world’s installed energy storage capacity (127,841 MW) consists of pumped hydro energy storage. However, most of the easily exploitable operating sites have already been taken. The interest in pumped hydro waned after the 1980s, because of high capital costs and the difficulty in locating new operating sites [1]. Efforts in this field are now directed toward upgrading existing projects rather than launching new ones.

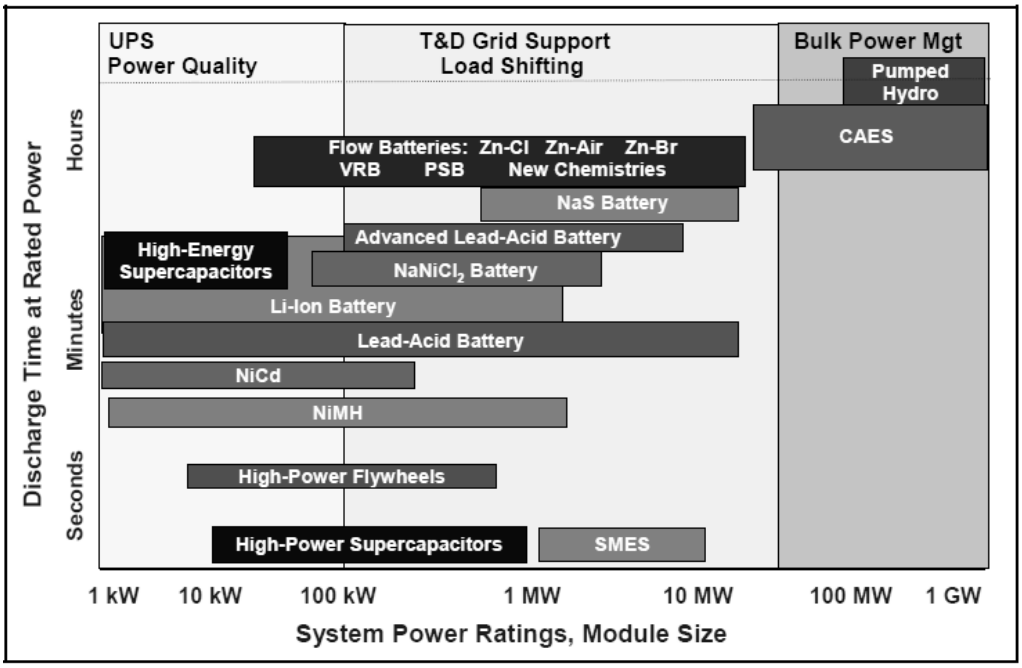

Figure 2.10 Energy storage technologies by power ratings and discharge time [10]

Table 2.2 Summary of existing energy storage technology benchmark parameters [6]-[20].

Technology Option	Efficiency AC-to-AC	Energy Density Wh/kg	Power Density W/kg	Self-Discharge Rate capacity per day	Durability cycles	Cost of Storage $/kWh installed	Geologic Requirement
Pb-Acid Battery	70-80%	30	150	0.1%	1000-2000	425-475	No
Ni-Cd Battery	60-90%	40-60	140-180	0.3%	1000-2500	1000-2000	No
Na-S Battery	75%	120	120	0.0%	2500	520-550	No
Li-Ion Battery	87-92%	100-200	360	0.2%	1500-3000	1500-3500	No
VRB	75%	25	80-150	0.0%	1000-2500	620-740	No
Flywheels	90%	5-30 OR 50[1]	1000 OR 5000[1]	45.0%	100,000	7800-8800	No
ECDL Capacitors	95%	5	4000	0.5%	400,000	20,000	No
SMES	95%	low to moderate	very high	very low	--	394,000	Sometimes
CAES	50%	10-30	N/A	N/A	>5000	60-120	Yes
Pumped Hydro	80%	0.3	N/A	N/A	>10,000	420-430 OR 250-270[2]	Yes
[1] The lower energy/power density values are for low-speed steel flywheels, and the other one, high-speed composite flywheels							
[2] The lower cost values are for pumped hydro projects with rated power > 900 MW							

2.2 The Case for Ontario

As of 2012, Ontario has over 34,000 MW of installed generation capacity. The breakdown of Ontario's generating capacity is shown by Figure 2.12.

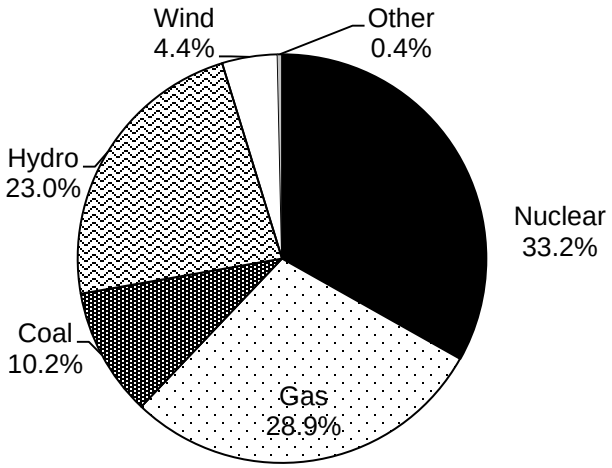

Figure 2.11 Ontario's installed generation capacity by type [22]

The real percentage of demand met by each type of energy supply differs from their percentage in the installed generation capacity. Because, the actual amount of generation actually available at any given time is dependent on outages and the capacity factor of each forms of supply. Power could also be imported from neighbouring jurisdictions. The actual use of energy by type of supply for the past few years are shown by Figure 2.13. We observe nuclear power to be the most important source of power supply at 55%. Some other trends could also be summarized from this figure: coal's share is decreasing, gradually replaced by natural gas; also growing is the power generation by wind, albeit a very small percentage of the total power output.

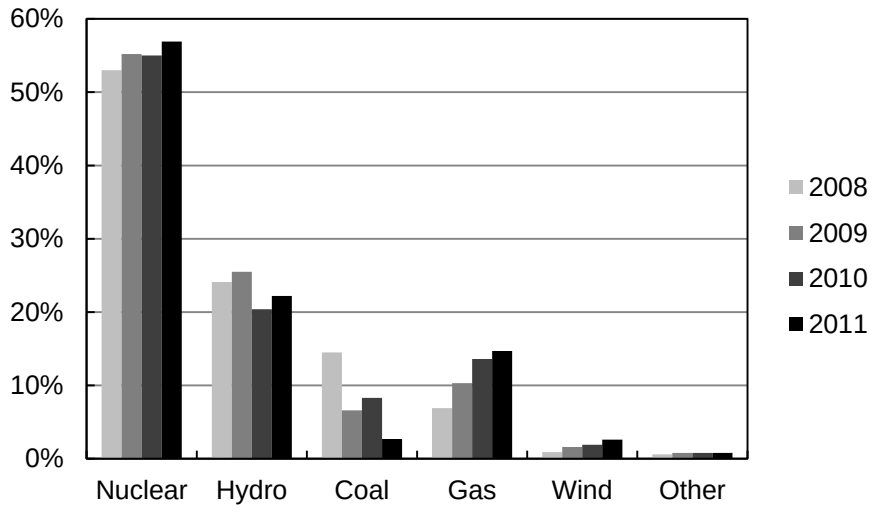

Figure 2.12 Total electricity output by fuel type [2]

In October 2012, two units at the Bruce Nuclear Facility with a combined capacity of 1500 MW have been restarted, achieving commercial operation after being shut down for 17 years. This further increases the installed capacity of nuclear power, which is conducive to surplus baseload generation conditions, until the refurbishment of the Darlington units (3800 MW) between 2016 to 2024 and the retirement of the Pickering nuclear units occur in 2020 ([23]). Meanwhile, aligned with the Supply Mix Directive issued by the Ministry of Energy of Ontario in February of 2011, non-hydro renewable power generators (wind, solar and bio-energy) are expected to increase their installed capacity to 10,700 MW in 2018, representing 10-15 % of total Ontario electricity generation [15].

The combined effect of increasing RE generators (mostly wind turbines) and plentiful baseload power supplied by nuclear power plants has already influenced Ontario's wholesale electricity market. Today, the wholesale electricity market is the mechanism through which electricity supply and demand in the province is balanced in real-time. In addition to the system and market operator (the IESO in Ontario), market participants come from all stages of the electricity life cycle: generators, distributors, electricity retailers, etc. Mandated to oversee Ontario's wholesale electricity market, the IESO administers a set of rules that govern the transactions of all the market participants, by authorizing market participants, publishing load forecasts and market information, producing statements and invoices, and performing financial settlement transactions.

One of its most important duties is to set the commodity price for electricity based on market conditions. Every five minutes, the IESO calculates the market clearing price, taking into consideration information submitted by all market participants: generation schedules, bids and offers to generate or purchase energy at different price points. Every hour, the Hourly Ontario Energy Price (HOEP) is determined by the average of the five-minute prices; it is the price applied to the non-dispatchable generators and loads; whereas dispatchable generators and loads make transactions at the five-minute real-time price.

Since 2007, the HOEP have dipped into the negative for increasing number of hours (Figure 2.14), for during those hours, the supply of electricity generated by the non-dispatchable generators has surpassed the provincial demand for electricity. Such a market signal has initiated a conversation about the implementation of energy storage technology in the province.

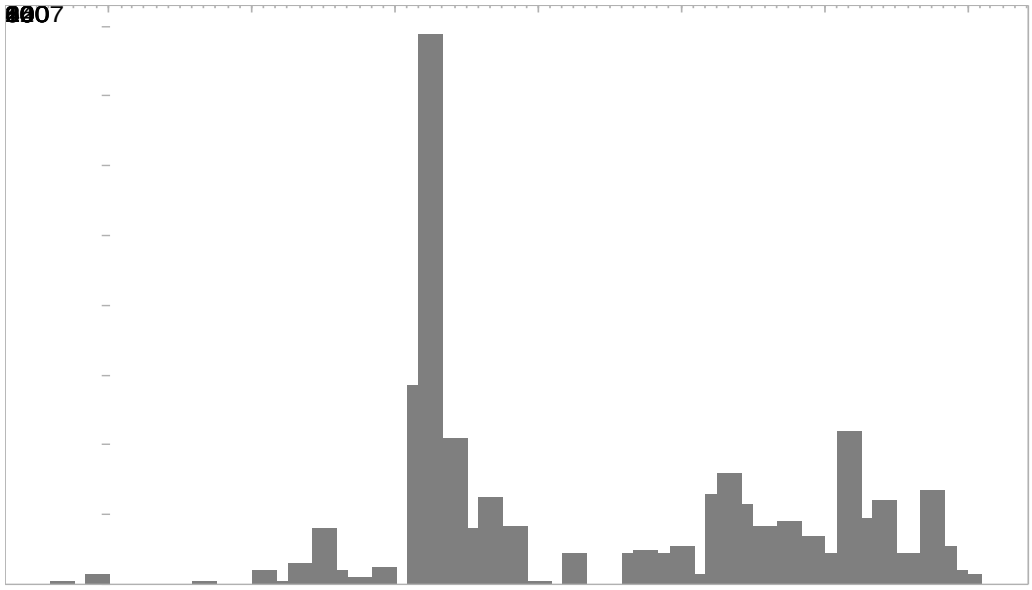

Figure 2.13 Number of hour per month with negative HOEP [14]

2.3 Energy Hub Framework

Since 2002, the project "Vision of Future Energy Networks", undertaken by researchers at the Swiss Federal Institute of Technology (ETH) Zurich, has produced a series of publications that focus on general system modeling framework for future energy networks. The development of such modeling frameworks are motivated by the challenges that the electric power infrastructure faces: aging assets approaching the end of their lifetime, requiring replacement; growing use of natural gas to supply combined-cycle turbines for power generation, increasing the coupling between the power and gas networks, while the supply of fossil fuels remains finite and uncertain; and the integration of small and distributed energy sources, sometimes involving several energy carriers. It is hoped that, using the modeling frameworks developed, the optimal system structure and operation strategies for future energy networks can be determined. The transition paths that bridge today's system with the future optimum can then be identified.

Three key concepts have emerged from their work: energy hubs is a modeling frameworks that can be extended or customized for modeling, analysis and planning of energy system scenarios.

2.3.1 Definition

An **energy hub** is an integrated system of units which is able to condition, convert and store multiple energy carriers. As illustrated by Figure 2.15, within an energy hub, there are several units that can convert or condition incoming energy carriers, so that the local load can be met. In other words, energy hubs can be viewed as interfaces between energy consumers, energy producers and the transmission infrastructure; equipped to store or convert in between energy carriers if necessary. Energy hubs allow connected consumers to access energy in the form that they desire, at the time that they desire, which may be different from the form or time in which energy supply is delivered to the hubs.

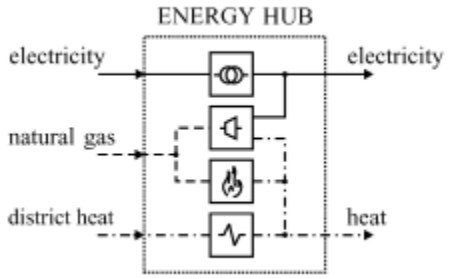

Figure 2.14 Generic schematic of an energy hub [24]

2.3.2 Methodology

There are three types of elements within an energy hub: converting units, conditioning units and storage units, and they are represented differently mathematically. The section above briefly outlines the "energy hub" approach developed by the research group at ETH.

The converters and conditioning units in the energy hub are abstracted and simplified to a level appropriate for analysis. So, it is assumed that they can be characterized by their efficiencies. In the case of multiple inputs and multiple outputs, the relationship between conversion/conditioning efficiency, energy input, energy output and different forms of energy carriers is represented by the coupling matrix **C**, which balances the input and output power flows [25]:

$$\underbrace{\begin{pmatrix} L_\alpha \\ L_\beta \\ \vdots \\ L_\omega \end{pmatrix}}_{\mathbf{L}} = \underbrace{\begin{pmatrix} c_{\alpha\alpha} & c_{\beta\alpha} & \cdots & c_{\omega\alpha} \\ c_{\alpha\beta} & c_{\beta\beta} & \cdots & c_{\omega\beta} \\ \vdots & \vdots & \ddots & \vdots \\ c_{\alpha\omega} & c_{\beta\omega} & \cdots & c_{\omega\omega} \end{pmatrix}}_{\mathbf{C}} \underbrace{\begin{pmatrix} P_\alpha \\ P_\beta \\ \vdots \\ P_\omega \end{pmatrix}}_{\mathbf{P}} \tag{2.1}$$

The vector **P** contains all values of energy inputs to the converters/conditioning units, and the vector **P**, all values of load placed on them; the set of energy carriers are denoted by small Greek letters α to ω. When the two subscript letters differ, the energy transaction taking place is a conversion process; when they are identical, the energy transaction taking place is a conditioning process, i.e. no change in energy carrier has occurred.

To account for the splitting of input among several type of converters (e.g. not all of Pα is transmitted/converted through one type of conversion units; instead, it is distributed to feed different

converters that transform energy vector α to several energy vectors), dispatch factors *v* are introduced to specify the input flow associated with a particular conversion. For converter κ, for example:

$$P_{\alpha\kappa} = v_{\alpha\kappa} P_{\alpha} \tag{2.2}$$

The entries of the coupling matrix represent the efficiencies of particular conversion; they can be constants or functions of the power flow through the unit, with values ranging between 0 to 100%.

Storage devices in energy hubs are conceptualized as an ideal storage equipped with an interface for energy exchange. Therefore, in addition to being characterized by conversion efficiency, as a converter, a storage device is also characterized by its energy content: the amount of energy that is in storage. At the interface, the storage device is modeled as follows:

$$\tilde{Q}_{\alpha} = e_{\alpha} Q_{\alpha} \tag{2.3}$$

Where: Q_{α} is the power flow to the storage device, $\tilde{Q}_{\alpha}$ is the power flow that has been converted into the form of the storage medium, also known as the internal power flow, and e_{α} is the charging/discharging efficiency, depending on the direction of power flow. Similar to conversion efficiency, charging and discharging efficiency values can be constants, or function of another variable.

$$e_{\alpha} = \begin{cases} e_{\alpha}^{+} \text{ if } Q_{\alpha} \geq 0 \text{ (charging/standby)} \\ 1/e_{\alpha}^{-} \text{ else} \qquad \text{(discharging)} \end{cases} \tag{2.4}$$

The energy that is in storage is the integral of the power flow over time, with a given initial value. Or, in other terms, the internal power flow is the time derivative of the stored energy. In this framework, it is assumed that the flow of power $\tilde{Q}_{\alpha}$ can be approximated to be constant during the time step Δt

$$E_{\alpha}(T) = E_{\alpha}(0) + \int_{0}^{T} \tilde{Q}_{\alpha}(t) dt \tag{2.5}$$

$$\tilde{Q}_{\alpha} = \frac{dE_{\alpha}}{dt} \approx \frac{\Delta E_{\alpha}}{\Delta t} \triangleq \dot{E}_{\alpha} \tag{2.6}$$

The subsequent combination of storage devices with converter elements is dependent on the location of storage within the energy hub: connected to the input energy carriers, the output energy carriers, or between the two sets of energy carriers.

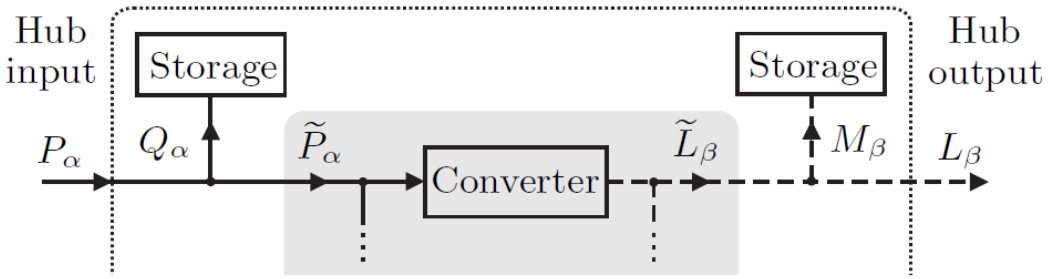

Figure 2.15 Storage elements in energy hubs [25]

Storage elements connected to the input energy carriers divert power from the input P_α, while storage elements connected to the output energy carriers divert from converted power $\tilde{L}_\beta$

$$\tilde{P}_\alpha = P_\alpha - Q_\alpha \tag{2.7}$$

$$\tilde{L}_\beta = L_\beta + M_\beta \tag{2.8}$$

In the shaded area in Figure 2.16 Storage elements in energy hubs [25], there are no storage element connections. Thus, the energy hub elements within can be described using the converter-only model in equation(2.1). The effect of storage flows can be added to this original equation through the following manipulation:

$$\mathbf{L + M = C(P \quad -Q)} \tag{2.9}$$

$$\mathbf{L = C(P \quad -Q) - M} \tag{2.10}$$

$$\mathbf{L = CP - CQ - M = CP - M^{eq}} \tag{2.11}$$

The equivalent storage flow vector $\mathbf{M^{eq}}$ is related to the approximated internal power flow $\dot{\mathbf{E}}$ through the storage coupling matrix.

$$M_\beta^{eq} = c_{\alpha\beta} Q_\alpha + M_\beta = \frac{c_{\alpha\beta}}{e_\alpha} \dot{E}_\alpha + \frac{1}{e_\beta} \dot{E}_\beta \tag{2.12}$$

Re-writing $\mathbf{M^{eq}}$ as a function of $\dot{\mathbf{E}}$ requires the use of $\mathbf{S}$, the storage coupling matrix, whose entry is derived individually according to equation(2.12):

$$\underbrace{\begin{pmatrix} M_{\alpha}^{eq} \\ M_{\beta}^{eq} \\ \vdots \\ M_{\omega}^{eq} \end{pmatrix}}_{\mathbf{M^{eq}}} = \underbrace{\begin{pmatrix} s_{\alpha\alpha} & s_{\beta\alpha} & \cdots & s_{\omega\alpha} \\ s_{\alpha\beta} & s_{\beta\beta} & \cdots & s_{\omega\beta} \\ \vdots & \vdots & \ddots & \vdots \\ s_{\alpha\omega} & s_{\beta\omega} & \cdots & s_{\omega\omega} \end{pmatrix}}_{\mathbf{S}} \underbrace{\begin{pmatrix} \dot{E}_{\alpha} \\ \dot{E}_{\beta} \\ \vdots \\ \dot{E}_{\omega} \end{pmatrix}}_{\dot{\mathbf{E}}} \tag{2.13}$$

After some matrix manipulation steps, the combined converter and storage energy hub energy balance equation can be written as:

$$\mathbf{L = CP - S\dot{E}} = \begin{pmatrix} \mathbf{C} & \mathbf{-S} \end{pmatrix} \begin{pmatrix} \mathbf{P} \\ \dot{\mathbf{E}} \end{pmatrix} \tag{2.14}$$

Other than the three types of hub elements described above, there are transmission networks that connect units within a hub and connect multiple hubs in the overall network. Several level of abstraction is possible [25]. In order of increasing accuracy and complexity, they are:

1. Neglecting physical losses, describing the networks using conservation laws only;
2. Approximate physical losses by expressing them as functions of the corresponding flow;
3. Calculate physical losses on constitutional laws, connecting current to electric voltage, and mass flow to hydraulic pressure, etc.

For the UHNG simulation project, only one energy hub is considered (i.e. there are no connections between multiple energy hubs), and the project is scoped to be a general investigation of system behaviour that focuses on dynamics between the conversion, conditioning and storage elements. Therefore the level 1 approximation is assumed to be adequate for such purpose.

2.3.3 Applications

The framework above has been used to derive several sub-models for different applications:

1. Optimal dispatch: optimizing the performance of a given energy hub in terms of cost, losses, or emissions, using the type of energy carriers used in conversions, their dispatch factors, and/or energy to storage as decision variables [25-27];

2. Optimal power flow: optimizing the performance of a system of interconnected energy hubs, using the type of energy carriers used in conversions and the dispatch of power among/within hubs as decision variables [25, 27, 28];
3. Reliability assessment: using failure rate and repair rate matrices that are analogous to the coupling matrix, the expected reliability of supply and the expected energy not supplied are derived for a given energy hub [29-31];
4. Distributed control: the optimization problem in "optimal power flow" is decomposed into several sub-problems, each representing an energy hub, and optimized as separate entities that exchange information in parallel or sequentially [32, 33];
5. Real options valuation: the Monte Carlo simulation method is used to evaluate the economic value of an energy hub, through real option analysis. The prices of different input energy carriers are modeled as distributions, and conversion/storage decisions are modeled as real options, not obligations [34-36];
6. Long-term portfolio planning: The optimal future generation portfolio is found through the use of a mean-variance portfolio model. The risks and returns associated with different shares of generation technology are computed, for a range of scenarios that contain different risk and cost drivers [37-39].

2.4 Key Technologies

Hydrogen, a storable fluid with very higher energy density (33,000 Wh/kg, based on lower heating value of hydrogen [40]), is attractive as a novel medium for utility-scale energy storage operations. As the section on conventional energy storage technologies indicate, among existing technologies, pumped hydro, CAES and NaS batteries the only cost-effective candidates for energy storage at very large scale (>>10 MW). These options either involve the physical storage and transport of fluids (water or air) in special formations, or storage via chemical energy in battery cells. Energy storage through hydrogen shares some similarities with each of them, but is entirely different when examined thoroughly (Table 2.3).

Table 2.3 Summary of utility-scale energy storage technologies

Technology	From electrical energy to…	Storage	From storable form to…
PHES	Potential energy in height difference	Maintaining height difference using special formation	Electrical energy through shaft work powering turbo generators
CAES	Pressure differential of gas with respect to atmospheric pressure	Maintaining pressure difference using special formation	Electrical energy through shaft work powering turbo generators
Battery	Internal energy in chemical compounds	Storing compound	Electrical energy through electrochemical reactions
UHNG*	Internal energy in hydrogen	Storing hydrogen with natural gas in special formation	Hydrogen-natural gas mixture: • Electrical energy through combustion as fuel for gas turbines • Thermal energy through combustion in boilers Pure hydrogen: • Electrical energy through fuel cell • Used as-is, without further conversion, as feedstock for chemical processes

Compared to the conventional technologies, energy storage via hydrogen offers some important advantages. The energy that can be stored per unit of common fluids (10-30Wh/kg compressed air, 0.3Wh/kg pumped water) is significantly less than the energy that can be stored in the form of hydrogen (lower heating value: 33,300 Wh/kg). This large difference is rooted in the differences of energy storage mechanism: electrical energy is converted to gravitational potential energy or energy associated with the pressure differential between the system and the atmosphere for pumped hydro and CAES, respectively; but, it is converted to internal energy when hydrogen is used as a storage medium. In addition, unlike pumped hydro, CAES and battery storage, the recovery of energy stored

does not need to take place at the energy storage facility. In addition to on-site energy recovery via fuel cells or combustion in gas turbines, hydrogen is in itself a valued industrial feedstock and transportation fuel, which has off-site applications. And, when stored together with natural gas, as proposed in this project, the downstream distribution of energy embodied in hydrogen can benefit from the vast distribution infrastructure already in place.

Energy storage through underground storage of hydrogen with natural gas requires a series of steps: electrolysis, underground gas storage, energy recovery through combined cycle gas turbines, and delivery of pure hydrogen or distribution of hydrogen-enriched natural gas. The individual technologies are outlined below and discussed with regard to the role that they play in the overall technology.

2.4.1 Electrolysis

Because the nature of this project is to tackle the problem of electrical energy storage, only production methods that produces hydrogen using electrical energy is of interest to this study. There are three technologies under electrolysis: alkaline electrolyzers, proton exchange membrane (PEM) electrolyzers and solid oxide electrolysis cells (SOEC) [41]. All three methods are briefly discussed.

2.4.1.1 Alkaline Electrolyzers

Alkaline electrolyzers are named after their use of an aqueous alkaline electrolyte, containing about 30 wt% KOH or NaOH. Electrodes, most commonly a platinum cathode paired with a nickel or copper anode coated by metal oxides, and a microporous separator complete the picture. At the cathode, water is decomposed into hydrogen and hydroxide. The hydroxide ion then reaches the anode, traveling though the electrolyte, and forms oxygen. As shown in Figure 2.17, oxygen and hydrogen thus produced need to be separated from the electrolyte, then purified and dried, depending on the purity requirement. Although the liquid electrolyte is not consumed during this process, it needs to be replenished periodically, because some losses occur during the gas-liquid separation. Alkaline electrolysis is a mature technology and available at operating pressures up to 25 bar. In commercial units, a number of electrolytic cells are arranged in a stack. The stack efficiency for units available on the market from Canadian manufacturer Hydrogenics is about 68% (4.44 kWh per Nm^3

of hydrogen, based on the LHV), with a lifetime of 60,000 hours [42] . The energy requirement of the stacks is assumed to represent 90% of the overall energy requirement, based on figures provided by Ivy [43], the rest being energy consumption of units supporting electrolysis occurring at the stack.

Electrolyte: $$4H_2O \rightarrow 4H^+ + 4OH^-$$

Anode: $$4OH^- \rightarrow O_2 + 2H_2O + 4e^-$$

Cathode: $$4H^+ + 4e^- \rightarrow 2H_2$$

Overall: $$2H_2O \rightarrow 2H_2 + O_2$$

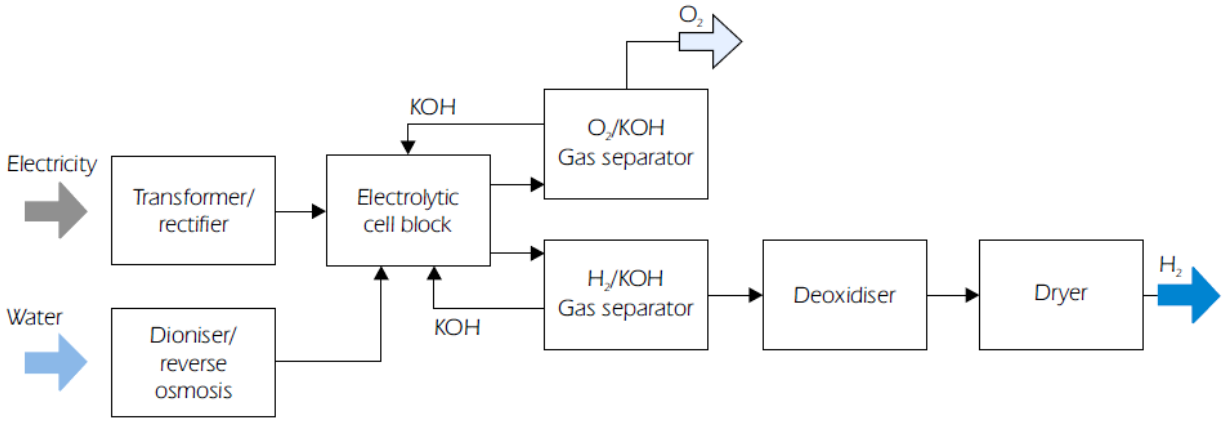

Figure 2.16 Process diagram of alkaline electrolysis [44]

2.4.1.2 Proton Exchange Membrane Electrolyzers

Building on the advances in PEM fuel cell technology, PEM electrolyzers use noble-metal catalysts, typically platinum, and an acidic polymer membrane which not only separates the electrodes, but also separates hydrogen from oxygen: the protons are able to travel across the membrane to form hydrogen at the cathode, while oxygen remains at the anode.

Anode: $$H_2O \rightarrow {}^{1}/_{2}\, O_2 + 2H^+ + 2e^-$$

Cathode: $$2H^+ + 2e^- \rightarrow H_2$$

Therefore, no gas separation unit is required, but the humid hydrogen might need drying, depending on application. Since no liquid electrolyte is present, the design of the PEM electrolyzers is much simpler and more compact when compared to alkaline electrolyzers, but it is less mature. Higher operating pressures are possible, potentially up to several hundred bar, and experimental units have shown stack efficiency of 73% [45].

2.4.1.3 Solid Oxide Electrolysis Cells

SOEC are solid oxide fuel cells run in reverse and require high operating temperature (700 to 1000 °C), it is one of the technologies that fall under the banner of high-temperature electrolysis [44]. Part of the electrical energy required to split water is replaced by thermal energy: when water is converted to hydrogen and oxygen, some energy is required to convert the liquid to a gas and to break the chemical bonds; at higher temperatures, some of that energy is supplied by heat. However, as shown in Figure 2.18, although increasing the temperature of electrolysis can lower the electrical energy demand, but the total energy demand, which is the sum of thermal and electrical energy required to split water, remains constant and can even increase slightly.

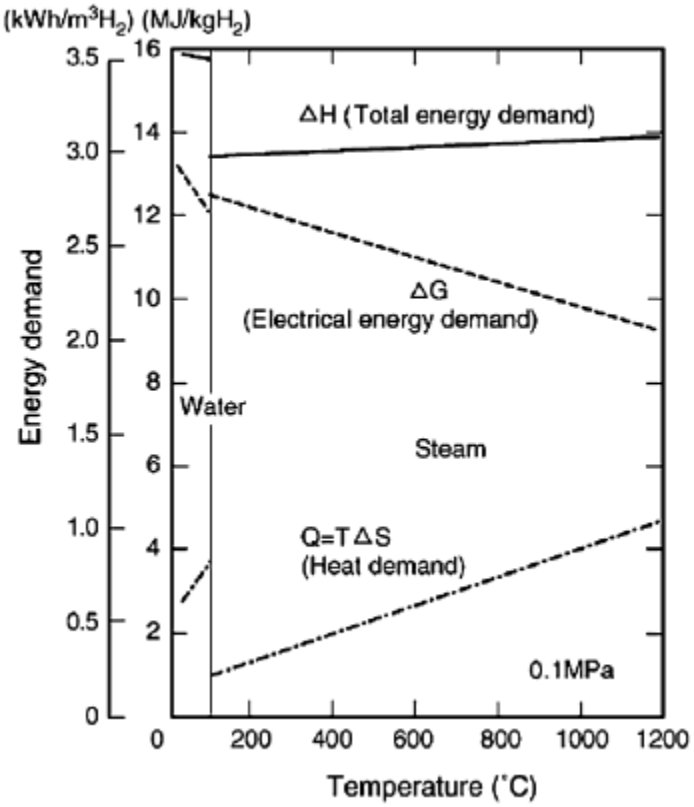

Figure 2.17 Energy demand for water and steam electrolysis [41]

Therefore, high-temperature electrolysis is only more efficient in a context where the thermal energy is available for free and readily accessible, in nuclear, geothermal or solar thermal based scenarios [46]. Efficiency of up to 60% has been achieved by SOEC operating from advanced high temperature nuclear reactors. At 85-90%, the efficiency based on electrical input alone is much higher [41].

2.4.1.4 Comparison

Currently, within the field of electrolysis, in between alkaline electrolyzers, PEM electrolyzers and SOEC, alkaline electrolyzers represent the most mature technology. Therefore, alkaline electrolyzers are chosen as the technology to be modeled for this simulation study. However, PEM electrolyzers could become a more suitable candidate technology in the mid-to-long-term, because its superior energy efficiency and compactness make it ideal for large-scale applications. SOEC would only be

considered if the electrolyzers are located next to large sources of waste heat or untapped geothermal/solar heat.

2.4.2 Underground Gas Storage

Once hydrogen is produced from water via electrolysis, the compound needs to be stored for later retrieval. Before that, the hydrogen produced needs to be compressed to storage pressure. For this step, reciprocating compressors are chosen, because the low molar weight of hydrogen requires the use of a volumetric compressor instead of a centrifugal compressor [47].

Current hydrogen storage methods can be categorized base on the phase in which hydrogen is stored. The first type of storage stores hydrogen as a compressed gas, either above ground or underground; the second type stores hydrogen as a cryogenic liquid; and the third type, as a solid hydride. The most appropriate type of storage on the final use of the hydrogen stored: high energy density and compactness are important for mobile applications, whereas stationary applications value lower storage costs and storage capacity. For all storage options, safety under normal use and acceptable risk under extreme conditions are essential for the well-being of communities and workers in proximity of storage locations. Energy storage at utility scale is a stationary application driven by scale, and the hydrogen stored will be mostly used in its gaseous form during energy recovery. Therefore, very large scale underground geologic storage of hydrogen gas is preferred to cryogenic hydrogen storage and hydride storage.

The successful storage of natural gas underground worldwide is seen as a precedent for the storage of hydrogen in underground geological formation. The existing storage infrastructure for natural gas could be leveraged by the co-storage of hydrogen with natural gas, in the form of a mixture. This will decrease the capital investment required for the development of underground storage facilities. In the future, if the need for hydrogen strengths, pure hydrogen storage reservoirs could become feasible as an operation independent of natural gas storage.

Natural gas is stored mainly to manage varying loads and uncertainties in supplies. Unlike the present power grid, in which flexible generation units, brought online or shut down, are used to deal with variations in load, the producers of natural gas have difficulty in scheduling production based on

demand: there is a very long response time to adjust production, so those adjustments would be costly and much delayed. Also, the physical storage of natural gas is quite straightforward and does not require conversion. Thus, large scale natural gas storage facilities became prevalent much earlier than their equivalents in electricity storage.

The practice of large-scale storage of natural gas is of primordial interest to large-scale storage of electricity. On one hand, the physical operation of UGS facilities contain insights on best practices that should be consulted by the future electrical energy storage sector; on the other hand, the financial transactions based on UGS facilities, providing contracted storage services under provincial regulations, are important precedents for the financial operations involving energy storage facilities.

According to a survey completed by the International Gas Union, there are more than 600 underground storage facilities operating worldwide[48]. In Canada there are 52 facilities; most of them are located in Alberta, Ontario and Saskatchewan. The types of underground reservoirs that have been used are presented in Figure 2.19.

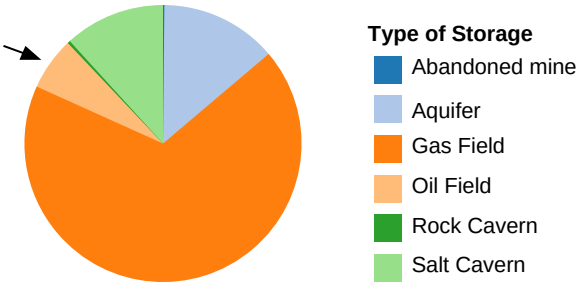

Figure 2.18 Type of reservoirs for worldwide UGS [48]

All types of underground storage reservoirs mentioned above fall into two categories: porous media storage, including aquifers and depleted gas or oil fields, and cavern storage, including solution-mined or excavated cavities. For porous media storage, the gas is contained in many naturally occurring small pores between mineral grains or crystals in sandstones or porous carbonates; for cavern storage, the gas is contained in a single large cavern located in salt beds or dense rock [49]. Regardless of types, sufficient capacity and containment are basic requirements that need to be met for all types of underground gas storage reservoirs. In porous media storage, the porous reservoir rock

provides the storage capacity, while an overlying confining enclosure, known as the cap rock, provides containment. In the case of cavern storage, the volume of the chamber is the storage capacity of the reservoir, and the surrounding impermeable host rocks are the containment agent.

Pressure is another important factor which influences the magnitude of storage and containment. Most rocks are not absolutely permeable; there exists a threshold pressure beyond which the rock's sealing effect will be compromised [49]. Thus, UGS facilities have maximum operating pressures that need to be respected. Within the operating range, increase in pressure decreases the volume required to store a given quantity of gas.

2.4.2.1 Porous Media Storage

Depleted gas fields constitute the bulk of UGS facilities, because they have been proved to be able to contain natural gas over prolonged period of time and a certain amount of cushion gas is already in place. Also, because of existing production history, the local geology is well-known and there are often many production/injection wells in place already. To convert a depleted gas field for storage, the old wells are inspected and upgraded, plugged wells are investigated, and new wells are drilled if necessary [50]. A gathering/injection pipeline system should also be installed. To increase pipeline gas pressure to field pressure, a compression station is set up. Compression is sometimes also required to deliver gas at pipeline pressure after withdrawal.

The original objective of injecting gas into *depleted oil fields* has been to enhance oil recovery. *C*ompared to the gas fields, they have similar behaviour, only with additional complexity because of presence of liquids in the wellbore, possible enrichment of the gas, and condensate formation inside pipelines. The gas sometimes went into solution in crude oil, complicating the assessment of stored volume. Depleted oil fields are less preferable if there is no gas present, because the injection of cushion gas to displace oil, preparing the reservoir will take many years [51]. In addition, the absence of gas cap might indicate that the cap rock is permeable to gas, since the proven ability to contain oil is not equivalent to the ability to contain gas.

Aquifers used for storage are water-filled porous sedimentary formations bound above and below by impermeable layers. They are different from depleted gas fields in that they have not previously

contained natural gas, so containment ability and other reservoir characteristics needs to be established. It is necessary to differentiate near-surface aquifers that provide drinking water from confined aquifers used for storage (Figure 2.20). In order to access confined aquifers, drilling through the phreatic aquifer is needed. Therefore, well casings are very important for preventing leakage of gas into the phreatic aquifer which could contaminate near-surface water.

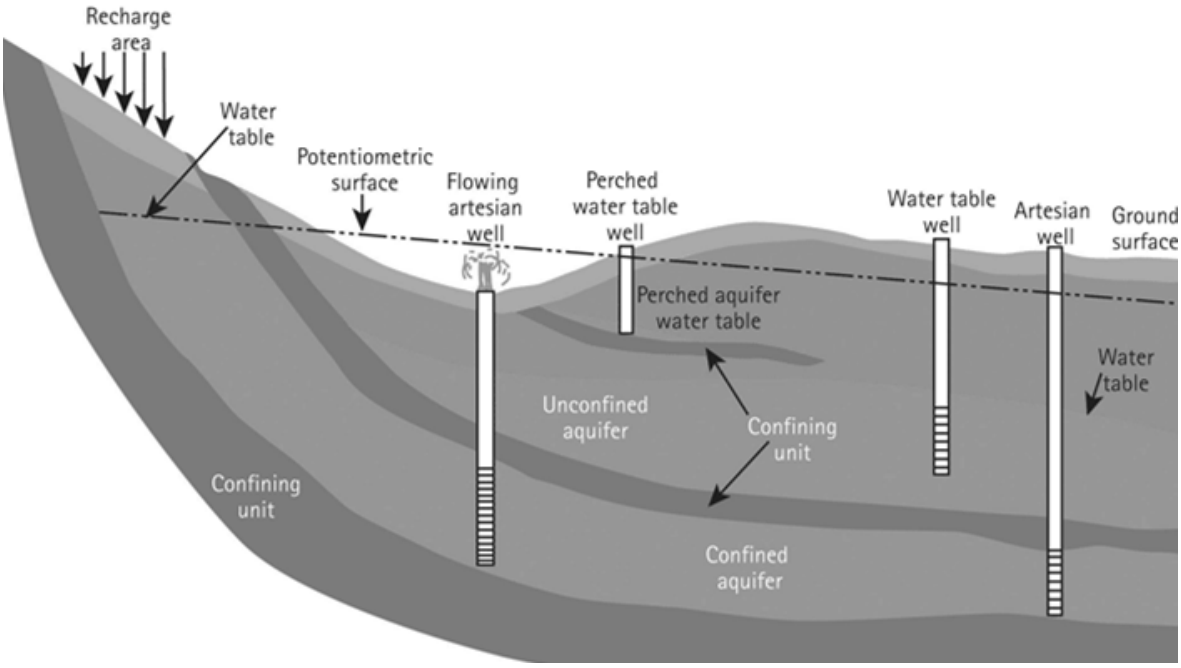

Figure 2.19 Confined and unconfined aquifers (National Ground Water Association, 2007)

2.4.2.2 Cavern Storage

Using solution mining techniques, s*alt caverns* can be formed by dissolving the rock salt present in the subsurface. It is a time consuming process that might take from many months to several years. The porosity and permeability of salt to liquid and gaseous hydrocarbons are near zero, so containment for those species can be established. Compared to porous media storage, salt cavern storage has high deliverability, since gas withdrawn does not experience the pressure loss from flow through pores. Similarly, because the same quantity of gas is stored in one large void space instead of many microscopic ones, the total volume of the reservoir is smaller. The ease to cycle – switch from injection to production – and the large working gas/cushion gas ratio makes salt caverns desirable for

applications that require frequent cycling and high deliverability/injectability [52]. Although salt have moderately high tensile strength, and its ability to flow plastically enables the closing of fracture that could otherwise develop into leaks, the same plasticity causes salt creep: salt moving slowly under large pressure differences, being squeezed by the surrounding toward the centre of the cavern, reducing volume [51].

The remaining types of reservoirs, *abandoned mines and man-mined rock caverns,* are in the extreme minority. In the past, mines of limestone, salt, and coal have been converted for storage. Failure to ensure air tightness has led all three storage facilities to be abandoned following gas leakage to the surface. The only operating UGS facilities of these types are Haje (granite tunnel) in Czech Republic, Skallen (lined rock cavern) in Sweden and Burggraf-Bernsdorf (abandoned salt mine) in Germany [48].

2.4.2.3 Safety Hazards of UGS

Existing experience in the operation of UGS facilities is crucial to the underground storage of hydrogen proposed by this project. By examining the history of accidents and incidents in the storage of natural gas, possible safety hazards associated with the underground storage of hydrogen can be identified and controlled through preventive measures.

Different technical and geological parameters determine the suitability of a give UGS facility and its potential safety hazards. Inaccurate technical evaluations of those parameters could result in subsequent lateral and vertical gas migration from a UGS facility: the gas released could escape from the inadequate reservoir confinement – compromised cap rock, faults or leaking wells –and migrate to the surface or into shallow ground water. The escape of gas has economic, environmental and safety implications and must be avoided at all costs.

Porous media storage and cavern storage facilities, because of their different storage mechanism, cannot be directly compared in terms of their safety hazards [53]. The flow of gas out of porous media is constrained by the permeability of the rock and the pressure gradient driving it. Consequently, leaks or releases from this type of facilities are typically small volumes at low rates. Comparatively, the flow of gas out of cavern-type large cavities, deemed more dangerous, is

essentially uncontrolled, limited only by the well capacity. Once ignited, the uncontrolled release could cause dramatic explosions. It should be noted that leak from porous-media-type storage reservoirs could also lead to explosions, if the escaped gas is undetected and left to accumulate inside ground-level structures.

In order to detect any unwanted gas leakage, UGS facility operators regularly conduct monitoring tests. For example, the Stenlille porous-media-type facility located in Denmark, operating since 1989, monitor reservoir pressure through a series of specifically designed wells to detect major losses of gas. Minor leaks which could develop over time, possibly undetected by pressure monitoring, require the regular analysis of subsurface fluids. If abnormal concentration of natural gas is measured in shallow ground water, isotope analysis and radiocarbon dating could be performed on the fluids to deduce the origin of the gas [54].

In areas with significant oil and gas exploration history, such as Southwestern Ontario, the integrity of sealing in abandoned well is a major safety concern. Wells originally drilled in the earlier half of the 20th century might not have been completed according to modern design and construction practices, increasing their potential for leaking. In the Los Angeles Basin area, where many abandoned wells exist, the Division of Oil Gas and Geothermal Resources of the California State Government found that many wells abandoned to the current standards were leaking upon testing [53].This calls for careful evaluation of all abandoned wells connected to the confined reservoir, prior to and during UGS operations.

Other than reservoir selection, physical property determination, and safety hazards monitoring, the design of the storage facility, based on knowledge of the local transmission facilities, various gas supplies and customer loads, is equally important to the success of the UGS project. Undertaken by pipeline engineers and planners, the design of a specific storage facility also has to comply with the economic and operating philosophies of the particular company in question.

2.4.2.4 Comparison

In a 2009 survey completed by International Gas Union, the total working volume of storage facilities in Ontario is given as 244 Bcf, divided between 27 depleted gas field type storage reservoirs and 5 depleted oil type storage reservoirs [48]. All but one of the 32 UGS facilities store gas in the Guelph

formation, inside carbonate and dolomite type reservoirs. The 32 storage facilities have highly varied working volumes which range from 290 to 26424 MMcf. The distribution of working volume for Ontario UGS facilities is illustrated by Figure 2.21, and the average working volume for each type is shown in Table 2.4. Most of the depleted gas field reservoirs fall within the 3000-6000 MMcf range, a size slightly under the average volume of 7155 MMcf.

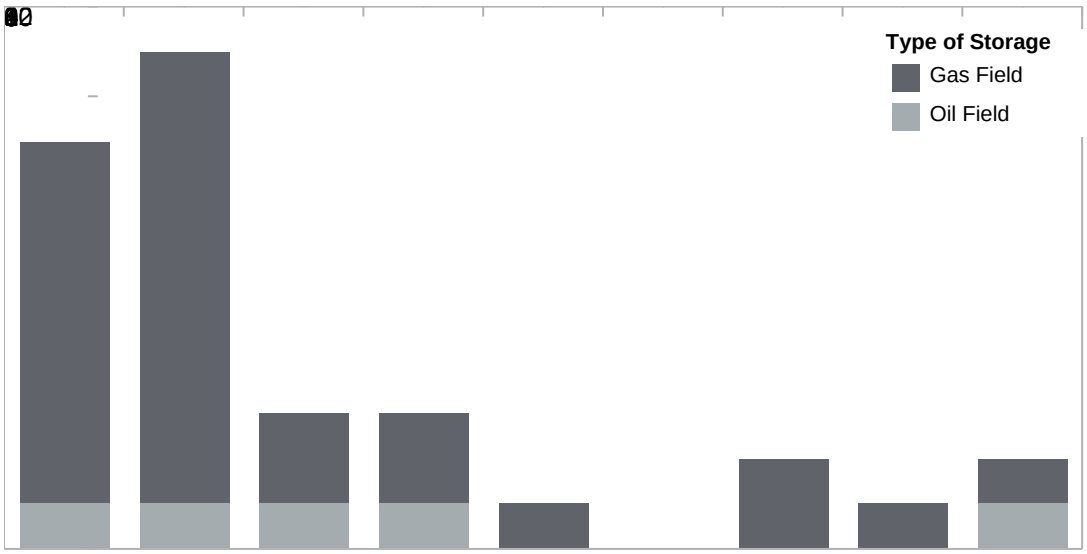

Figure 2.20 Installed maximum working volumes of Ontario UGS facilities

Table 2.4 Total and Average working volume of Ontario UGS facilities by type

	Facilities	**Working Volume (MMcf)**	
	Count	Sum	Average
Gas Field	27	193190	7155
Oil Field	5	50947	10189
Total	32	244137	7629

By comparison, in 2003, 73 solution-mined salt caverns located in the Sarnia and Windsor areas were in operation for liquefied petroleum product storage [55]. The total storage capacity reached 3.5 million m^3 (123.6 MMcf), which is almost 2000 times smaller than the total storage capacity of depleted hydrocarbon reservoirs (244 Bcf).

Since this project focuses on the use of existing natural gas distribution and storage infrastructure for the storage of electrolytic hydrogen, porous media storage reservoirs, the types currently used in Ontario to store natural gas, will be studied in detail and modeled. The use of solution-mined salt caverns of much smaller scales, common in Western Canada for underground gas storage and in Ontario for liquid petroleum product storage, are beyond the scope of this project.

2.4.3 Gas Turbines

A gas turbine harnesses the energy contained within a fluid, be it kinetic energy or potential energy in pressurized air, to generate rotary motion. Windmill is the earliest device of this type. Thus, the modern version of windmills, the wind turbine, is related to gas turbines through their fundamental principle. The first direct ancestor to the modern turbine made the use of an axial compressor, mounted on the same shaft as the turbine, which harvests the energy in the compressed air, after it has been mixed with fuel and ignited in the intermediate combustor (Figure 2.22). Prior to that, the compressor operated separately from the turbine.

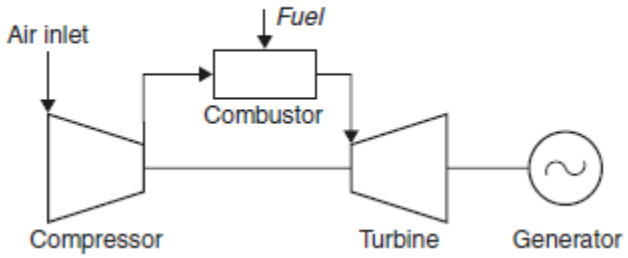

Figure 2.21 Block diagram of a gas turbine for power generation [56]

Modern gas turbines for power generation use multi-stage axial compressors to compress atmospheric air to 15-19 times of its original pressure. The compressors have efficiencies of about 87%.

Pressurized air is then routed into a combustion chamber, mixed with fuel and ignited. Combustion chambers can be designed to be separate from the turbine body, or positioned between the compressor and the turbine. The turbine component of a gas turbine system operates with an efficiency of about 90%. Because the energy to operate the compressor is provided by the turbine itself, the energy output of the turbine must be greater than the energy consumption of the compressor, for the system to function. The additional energy is provided by the combustion of fuel which heats the gas flow entering the turbine. Therefore, the turbine must be capable of operating at very high temperatures. The improvement in turbine material made the increase in inlet gas temperature possible, from 900 °C in the 1960's to 1425 °C by 2000, thereby increasing the maximum efficiency of gas turbines [56]. The overall efficiency of small gas turbines (35-45 MW) is about 38%. Larger turbines (>100MW) have usually shown slightly lower efficiencies.

2.4.3.1 Combined Cycle Gas Turbines

As the exhaust leaves the gas turbine, it is still extremely hot and contains a very important amount of thermal energy. This is energy from fuel combustion which has not been converted into electricity. Strategies that capture the heat in gas turbine exhaust gas, otherwise wasted, can offer significant efficiency improvement to the overall system. Two examples are cogeneration (also known as Combined Heat and Power), the generation of hot water or steam as forms of heat for industrial processes or residential use, and combined cycle operations, recovering heat through the installation of steam boilers and a subsequent steam turbine, generating additional electricity (Figure 2.23).

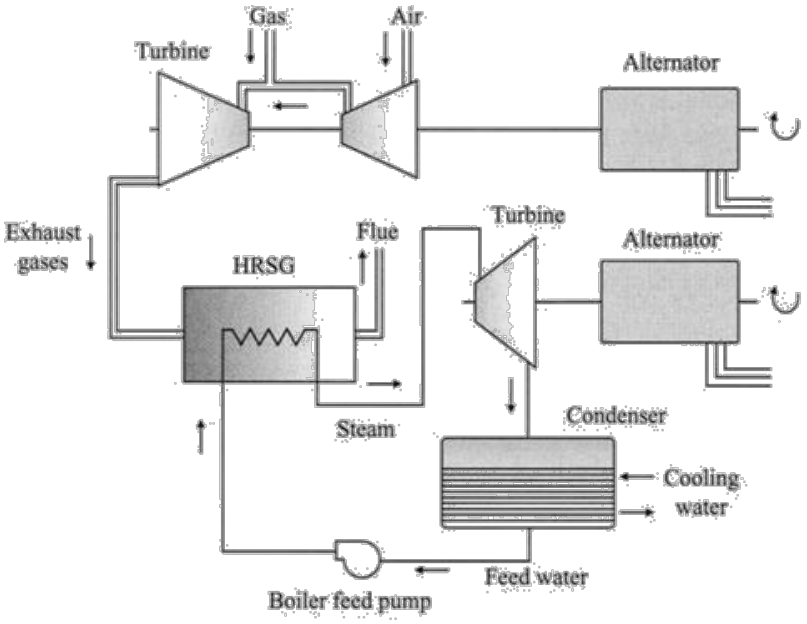

Figure 2.22 Block diagram for combined cycle gas turbine

As any typical steam power plant, the steam cycle of a combined cycle power plant requires other pieces of equipment: steam turbine condenser and boiler feed pump, most notably, to form a closed steam loop. The steam boiler which uses gas turbine exhaust gas as the heat source is called a Heat Recover Steam Generator (HRSG). In some combined-cycle installations, power output of the facility is further increased through supplementary firing in the HRSG. The current generation of combined cycle power plants, such as the H-System from GE Power Systems, boasts efficiency of up to 60% [56]. In those high-performing units, the gas and steam turbines are closely coupled to optimize performance.

2.4.3.2 Fuel Flexibility

To recover energy that is stored in hydrogen via the UHNG technology, one of the pathways proposed is to produce electricity from hydrogen, closing the energy storage cycle (Power to Power). Fuel cells and the use of hydrogen-oxygen semi-closed cycle are seen as future options for converting hydrogen to electricity, but for the moment, combined cycle power plants are considered to be the short to mid-term solution for energy recovery due to its maturity and availability.

The typical standard fuel for gas turbine fuel supply systems and combustors is natural gas from pipelines, whose main component is methane. Compared to methane, hydrogen has a higher burning

velocity, a wider flammability range, higher heating value per unit weight but lower per unit volume (Table 2.5).

Table 2.5 Combustion characteristics for hydrogen and methane

	Flammability Limits (in air), T=20°C		Laminar Flame Speed	Heating Value	
	Lower (vol %)	Upper (vol %)	(cm/s)	(MJ/kg)	(MJ/Nm^3)
Hydrogen	4.1	74	306	120	10.8
Methane	5.3	13.9	33.8	50	36

Robust designs and less specialized combustion systems allow stationary gas turbines to handle a wide range of commercial and process by-product fuels: natural gas, petroleum distillates, gasified coal or biomass, gas condensates, alcohols, and ash-forming fuels [57]. Among gaseous fuels, the heating value of the fuel is not the only criterion for comparison. The Wobbe index is used by the gas supply and transport utilities to indicate the interchangeability of gaseous fuels. It is a measure of volumetric energy of fuel, being defined as:

$$Wi = \frac{Q}{\sqrt{\rho/\rho_D}}$$

Where Wi is the Wobbe index, Q is the heat input based on LHV, ρ and ρ_D are the density of fuel gas and the density of air, respectively, both at standard conditions. Gases with the same Wobbe index can be used in the same combustor, because they produce identical heat load at the same combustion pressure. For premix combustors, the range of interchangeability is ± 5% [58]. The effect of hydrogen addition on the Wobbe index of the mixture is shown in Figure 2.24. For the natural gas used in Ontario, the Wobbe index without hydrogen addition is 47. Therefore, the admissible range of hydrogen concentration is 0-20% for it has Wobbe index above 44.5, within 95% of the original index.

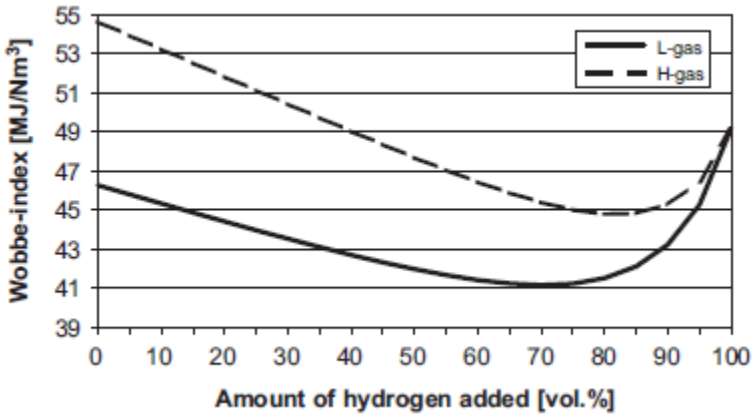

Figure 2.23 Effect of hydrogen-natural gas mixtures on the Wobbe Index [59]

2.4.3.3 Emissions

The main pollutants present in combustion exhaust are carbon oxides, unburned hydrocarbons and nitrogen oxides. Carbon dioxide is the product of complete hydrocarbon combustion. In the case that there is not enough oxygen present during combustion (fuel-rich), carbon monoxide can also be formed. Unburned hydrocarbons occur in cases of incomplete combustion, in regions of the combustor where the flame is quenched, for instance. As for NO_x, there are three formation mechanisms, broadly labeled as thermally-generated, flame-generated or fuel-bound. Thermal NO_x is formed by oxidation of nitrogen in air; it is aided by high temperature and long combustion time. Flame-generated NO_x, or the prompt NO_x mechanism, is associated with the primary combustion reactions. It is connected to the intermediate combustion species that take place in the reaction of the flame. It is less temperature dependent and much faster than the thermal NO_x mechanism. For the fuel-bound case, fuel nitrogen, in the form of NH_3 or HCN, most commonly, is converted to NO_x through a series of elementary reaction steps.

The combustion of hydrogen enriched natural gas produce less carbon dioxide than that of pure natural gas, by virtue of its chemical composition: the combustion product of hydrogen is water, since it does contain any carbon. Therefore, reduction of CO_2 emissions is a direct function of H2 content in the blend, assuming the same combustion efficiency (Figure 2.25).

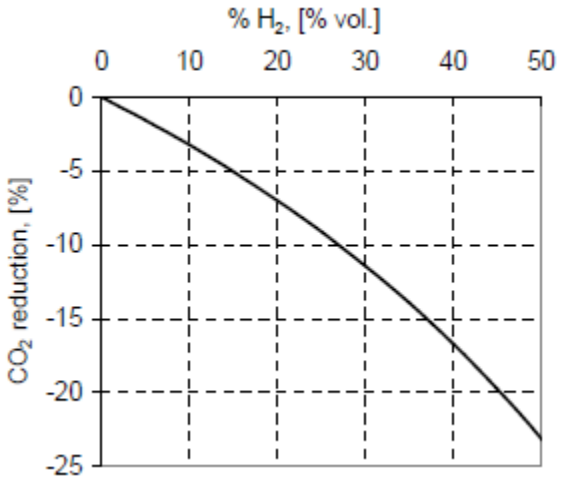

Figure 2.24 Effect of hydrogen concentration in a CH4-H2 mixture on carbon emissions, relative to pure CH4 [60]

The stoichiometric air/fuel mass ratio required for the complete combustion of hydrogen in air is about 34:1, much higher than that of natural gas (17.2:1). This means that an air/fuel mass ratio that is rich to hydrogen combustion is lean for natural gas combustion. Therefore, lean mixtures are possible when burning hydrogen blended with natural gas, encouraging complete combustion. The high flame velocity and the small quenching distance of hydrogen – the hydrogen flame is quenched closer to the combustor than other fuels, increasing the reach of the flame – also encourage complete combustion. Consequently, the carbon monoxide and unburned hydrocarbon emissions are reduced.

Dry low-emission premix combustors are proposed by manufacturers for natural gas applications. They can reduce NO_x emissions from gas turbines by mixing air to fuel before the combustion, so that the air-fuel ratio in the primary zone of the turbine is higher than the stoichiometric ratio. For natural gas with lower heating values -- hydrogen-enriched natural gas or coal syngas used in IGCC plants, for example -- premixing becomes a questionable practice, because, hydrogen can react when mixed to air at typical gas turbine conditions (wider flammability limits). Therefore, for fuels with hydrogen content larger than 10%, premixing is excluded due to the potential of flashback [61]. In addition to the risk of flashbacks, when ***pure*** hydrogen is fired, the higher flame temperature produces more thermal NO_x than the combustion of natural gas, if left untreated.

In these cases, fuel dilution by steam or nitrogen is required to bring emission levels within power industry standards (22-45 ppmvd) by reducing flame temperature. In the case that a combined cycle is present, steam is chosen as the diluent and extracted from the steam turbine. The combustion of pure hydrogen, combined with the addition of diluent can impact the operation of a gas turbine in three ways: the enthalpy drop during turbine expansion will vary, the flow rate of gas at the turbine inlet will be different, and the heat-transfer coefficient, affecting the cooling of the turbine blades, will differ.

2.4.4 Hydrogen Recovery and Use

The second of three pathways proposed for energy recovery is to use hydrogen by itself (Power to Hydrogen), in specific downstream applications such as powering fuel cell vehicles, forklifts and other vehicle prototypes, supplying needs of the manufacturing, food industries, and meeting industrial and academic research uses. According to the Commodity Specification for Hydrogen issued by the Compressed Gas Association, hydrogen used for general industrial applications (Grade B) need to meet 99.95% overall hydrogen purity, and hydrogen for fuel, hydrogenation and water chemistry applications (Grade D), 99.99%.

In the case that hydrogen is not produced "just-in-time", at the moment of its delivery, gas separation technologies are required to produce hydrogen that meets end-user specifications, from the hydrogen-natural gas mixture stored underground. Due to constraints in other energy recovery pathways (material compatibility and fuel flexibility), the concentration of hydrogen in the mixture stream is expected to be controlled to remain under 10%.

The driving force for all gas separation methods is the difference between one or more physical/chemical properties of the components in a mixture. The properties behind the operating principle of the most common gas separation technologies have been listed in Table 2.6. A given method can only succeed, achieving the degree of separation wanted, if the components to be separated differ in properties significantly.

Table 2.6 Separation methods and their corresponding properties [62]

Separation Method	Properties
Cryogenic distillation	Relative volatility
Physical absorption	Chemical family
Chemical absorption	Chemical family
Catalytic conversion	Chemical family
Membrane permeation	Critical temperature, van der Waals volume
Molecular sieve adsorption	Kinetic diameter
Equilibrium-limited adsorption	Equilibrium loading
Condensation	Relative volatility

There are three categories of gas-phase separations based on the purity, recovery and magnitude of the separation: enrichment separation, sharp separation and purification separation. The separation for hydrogen and natural gas, in this project, can be described as a sharp separation, for two high-purity high-recovery product streams are desired. The technologies that are suitable for a sharp separation in a single step are: cryogenic distillation, physical absorption, molecular sieve adsorption, and equilibrium adsorption. Separation by membrane permeation is not selected, because the typical selectivity of that process is inadequate for the purity required in a sharp separation. On the other hand, it may be appropriate as the first unit operation for a multiple-step separation process, in which the feed stream is first enriched, and then further separated.

2.4.4.1 Cryogenic Distillation

Cryogenic distillation is very similar to high-temperature distillation, in which relativity volatility of the key components are used to separate the mixture into different fractions. Because of the larger range of boiling point for gases, the relative volatilities of condensed gaseous systems tend to be larger than those of the liquid systems. Generally, industrial applications are considered feasible, when the relative volatility is larger than 2. The volatility of hydrogen is higher relative to that of methane and other components present in natural gas, as suggested by the ranking of their boing point (Table 2.7). However, not all processes with large relative volatility automatically favor cryogenic distillation. The economics of this separation method are rarely cost-efficient for scales smaller than 10-20 tons per day of product gas.

Table 2.7 Boiling points of gas mixture components

Compound	K
Butane	272
Propane	231
Carbon Dioxide	216
Ethane	184
Methane	109
Nitrogen	77.2
Hydrogen	20.1

In this approach, the components with higher condensation temperature (same as boiling temperature) are condensed by Joule-Thompson refrigeration, derived from throttling the condensed liquid hydrocarbons. Cryogenic distillation works best when the feed pressure is low, hydrogen concentration in the feed is lower than 40%, and the heavier hydrocarbons are present in higher concentrations and easily condensed. Hydrogen purity, recovery and pressure of the natural gas stream are correlated, so not all of them can be optimized at the same time. If the natural gas stream, produced after separation of hydrogen, has low pressure (0.7 bar), purities achievable is moderate (90-95%) and the recovery of hydrogen is relatively high (90-95%) [63].

2.4.4.2 Physical Absorption

In absorption processes, the solute molecules are assimilated into a solid or liquid substance. Physical and chemical absorption differ in the nature of the interaction between the absorbent material and the solute molecules. The driving force in selective physical absorption is the difference in solubility. Different gaseous solutes experience solubility in the absorptive liquid, due to different intermolecular forces at play. Because of the use of a liquid absorbent, the physical absorption process is sometimes called gas-liquid contacting.

The gas-liquid contacting process can be set up with a mixer and a separator unit. In this process, a high pressure hydrogen-natural-gas stream is contacted with a liquid in a high pressure mixer unit, in which the components of natural gas are selectively absorbed in the liquid. Solvents proposed for the

absorption of light hydrocarbons include iso-octane, n-octane, 1-octane or methyl cyclohexane. Then, the gas and liquid phases are separated in a high pressure separator to obtain purified hydrogen (Hydrogen has remained in the gas phase). The liquid containing dissolved natural gas is flashed at a low pressure for regeneration, then returned to the mixer. The desorbed gas will still contain some hydrogen, albeit at a lower concentration. Countercurrent version of this process has been proposed to provide higher purity (85-95%) and recovery (85-95%) [63].

2.4.4.3 Adsorption

A molecular sieve is a material with holes small and precise enough to block large molecules, allowing smaller molecules to pass. They select for adsorbent based on its molecular structure and size. On the other hand, in equilibrium-limited adsorption, the extent of adsorption is determined by the equilibrium loading of the adsorbent, typically expressed as isotherms. The most prevalent adsorption process to separate hydrogen from other gases is the Pressure Swing Adsorption (PSA) technology. In PSA, both driving forces for molecular adsorption and equilibrium-limited adsorption may be in place, since molecular sieve is often used as adsorbent, and the force of adsorption is dependent on the equilibrium loading of the adsorbent.

In this technology, the adsorbent attract other gases more strongly than it does hydrogen. So that hydrogen is left free, while the rest is adsorbed. The adsorption takes place at a high pressure (10-40 bar) until the equilibrium loading is reached. At that point, no more adsorption capacity is available. Once hydrogen has been removed from the chamber, partial pressure is lowered and the non-hydrogen gases are desorbed, and the adsorbent, regenerated. After that, pressure is increased back to adsorption level and the process resumes.

Separation through PSA is completed in batches, cyclically. Therefore, there is usually more than one adsorption bed, so the overall process can be operated continuously: one unit desorbs while the other begins absorption. Up to 12 units can be operated in concert. Hydrogen can be recovered at almost the same pressure as feed pressure, since there is little pressure drop through the unit. Hydrogen purity achievable is very high (99.99%), and moderate hydrogen recovery is possible (65-90%), depending on the final pressure of the natural gas stream [63]. PSA systems are insensitive to changing feed composition and provide constant product purity and recovery, once the exit gas stream pressure is

set. As the only separation technology that is able to meet the high purity requirement for fuel-grade hydrogen, PSA is selected and modeled in this simulation study.

Different compounds have different potential for physical adsorption, conditional to operating pressure, temperature and the component concentration inside the mixture. For PSA processes, inside adsorption beds, the total system pressure is varied to control the adsorption equilibrium between the adsorbed molecules and the adsorbent. Using a cycle of carefully designed operational steps that take adsorbent regeneration into account, it is possible to use a batch of adsorbent to repeatedly separate a continuously-fed stream of mixture.

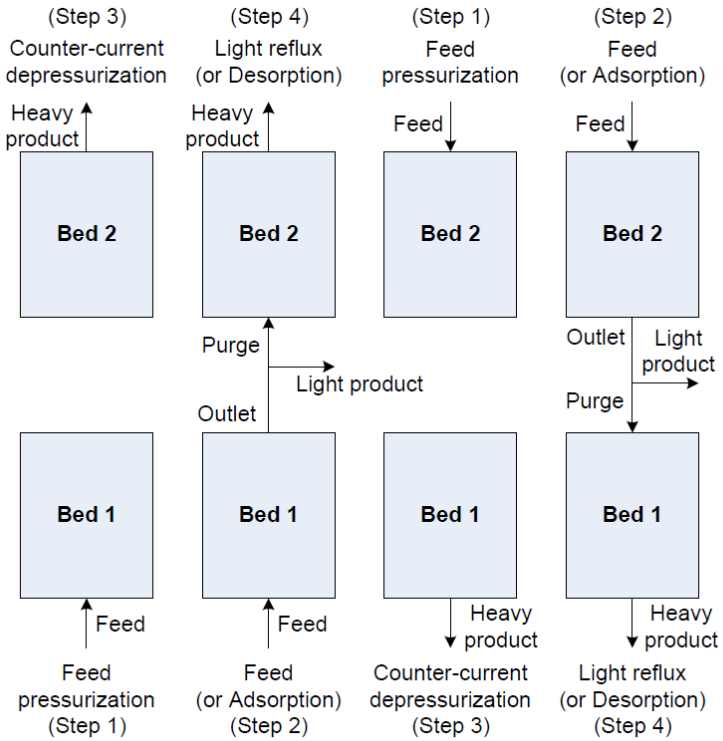

Figure 2.25 Two-column four-step Skarstorm cycle [64]

2.4.5 Distribution of Hydrogen Enriched Natural Gas

The last energy recovery pathway considered for this project is the direct delivery of stored mixture, a blend of hydrogen with natural gas, to gas end-users, through the existing local distribution pipelines (Power to Gas). Hydrogen enriched natural gas (HENG) is not entirely new; prior to wide adoption of

natural gas as the key gaseous fuel, numerous countries used manufactured gas (or town gas), consisting of 10 to 50% hydrogen, for lighting, heating and cooking through most of the 19th century and the first half of 20th century. The distribution of HENG using existing natural gas infrastructure is suggested by several authors, as an interim measure prior to large-scale pipeline delivery of pure hydrogen or an opportunity to reduce the carbon emissions associated with natural gas use [59, 65, 66]. A project of special relevance is NaturalHy, a research project funded by the European Commission's Sixth Framework Programme, reuniting 39 partners to investigate the impact that the additional to natural gas may have on the existing system.

Pipelines, compression stations and pressure-reduction stations form the existing natural gas transportation infrastructure. The pressure drop in the pipeline between different compression stations drives the flow of natural gas. The relationship between pipeline flow rate and the pressure drop is:

$$Q = CD^{2.5}e\sqrt{\frac{p_1^2 - p_2^2}{dZTLf}}$$

Where Q is the normal flow rate, Nm^3/h; C is a dimensionless proportionality constant = 0.000129; D is the pipeline inner diameter, mm; e the dimensionless pipeline efficiency, p_1 and p_2 are inlet and outlet pressures, kPa; d the relative density compared to air; Z the compressibility factor; T the gas temperature, K; L the pipeline length, K; f the dimensionless friction factor.

Because hydrogen has lower volumetric heating value compared to natural gas (Table 2.5), if pure hydrogen is transported in the pipelines instead of natural gas, in order to maintain the same energy flow, the volumetric flow of hydrogen Q needs to be three times that of natural gas. This increase in Q is balanced by the decrease in density: hydrogen is approximately 9 times lighter than natural gas (specific gravity of H_2: 0.0696, specific gravity of natural gas: 0.6-0.7), so that the pressure drop across the same section of pipeline can be maintained constant, despite of the change in gas transported. Factoring changes in compressibility factor and friction factor, for the same pipeline and pressure difference, pure hydrogen can transport 98% of the energy carried by lean natural gas under the same conditions, and 80% of the energy carried by rich natural gas. For mixture of hydrogen with natural gas at different concentration, the relative energy content is shown in Figure 2.27. It can be observed that, for hydrogen concentration smaller than 20%, the energy flow carried by the mixture is within 5% of that of pure natural gas.

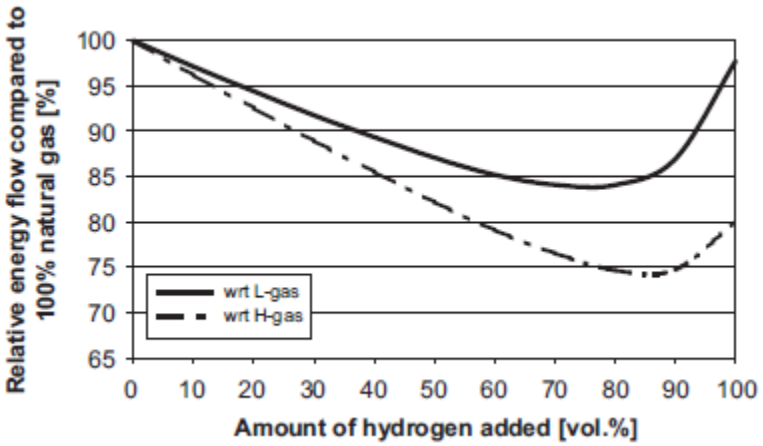

Figure 2.26 Energy-transport losses for hydrogen and hydrogen-natural gas mixtures, assuming an unchanged pressure drop [59]

In principle, the addition of hydrogen into the existing natural gas network can occur at the high pressure grid level, the medium pressure grid level, or the low pressure distribution level. But, for practical considerations, the first trials should take place at the medium or low-pressure levels, after the pressure-reduction stations. The advantages are: backflow from lower pressure network to the high pressure level is impossible, reducing unwanted mixing prior to full conversion; and, compressors are unnecessary at the medium or low pressure distribution grid, reducing possible complications.

Other than considerations for the energy content, the material compatibility of hydrogen with existing equipment also requires investigation: the suitability of existing compression and pressure-reduction stations, the possibility of hydrogen embrittlement and leaks, among others.

There are two common types of compressors for industrial use: reciprocating and centrifugal. Although reciprocating compressors are insensitive to nature of the working gas, the design and operations of centrifugal compressors are tied to the molecular weight of the working gas. To carry the same amount of energy, the volume flow rate of pure hydrogen needs to be three times that of natural gas. Given this new feed rate, assuming the same feed condition and compression ratio as for natural gas, the rotational velocity of the centrifugal compressors needs to be increased. The maximum rotational velocity of a given compressor is limited by the strength of its material;

therefore, the compression of pure hydrogen may be unsuitable with centrifugal compressors currently in use.

Hydrogen embrittlement is the diffusion of hydrogen atoms through various metals (especially steel), creating pressures within the metal that reduces their ductility and tensile strength, leading up to hydrogen induced cracking. The risk of damage to pipelines is dependent on its material of construction and its history: larger fluctuations experienced by the pipeline increase the risk of hydrogen embrittlement and material fatigue. Results from fracture toughness tests and fatigue tests performed in the NaturalHy project suggest that up to 50% hydrogen can be accommodated in pipelines, without significant effect on embrittlement for the pipeline material tested. Other studies have provided more conservative values, showing that up to 17 % of hydrogen can be accommodated.

Diffusion losses of gas occur through seals, gaskets, valves and fittings. The diffusion loss of hydrogen will be larger than natural gas, for the same equipment designed to contain natural gas. The hydrogen molecule has a smaller size and lower viscosity. Since the 1980’s, polyethylene pipelines have been used by many gas distributors at the low pressure distribution network level. Diffusion of hydrogen loss through such pipelines is five times more important than that of natural gas. Overall, the diffusion losses are considered negligible, at approximately 0.0005-0.001% of the totally transported volume [59].

Chapter 3
Model Overview

Prior to the formal development of the physical and the performance models, as indicated by the research objectives, the key decision variables, equivalent to user-manipulated inputs, and the performance indicators, equivalent to model outputs from simulation, need to be outlined. The inputs and outputs are of key interest, since they determine the level of detail of model development. In this chapter, after a detailed view of the energy hub, the key decision variable and performance indicators identified are described.

3.1 Energy Hub Overview

The energy hub, first sketched in Figure 1.4, can be further broken down to show its internal components and interconnections in Figure 3.1. Within the confine of the dashed line, which represents the physical boundary of the energy hub, the main technological components are labelled: the wind turbines, the electrolyzers, the storage reservoir, the CCGT plant and the PSA separator. The compressor units needed are numbered from C1 to C4; they are identical blocks, only the feeds are at different conditions. Additionally, because this modeling study is not intended for optimization, additional specifications that define the relationship between two or more variables are required, so that the model can become fully specified. The colored diamonds (D1 through D6) represent such decision points.

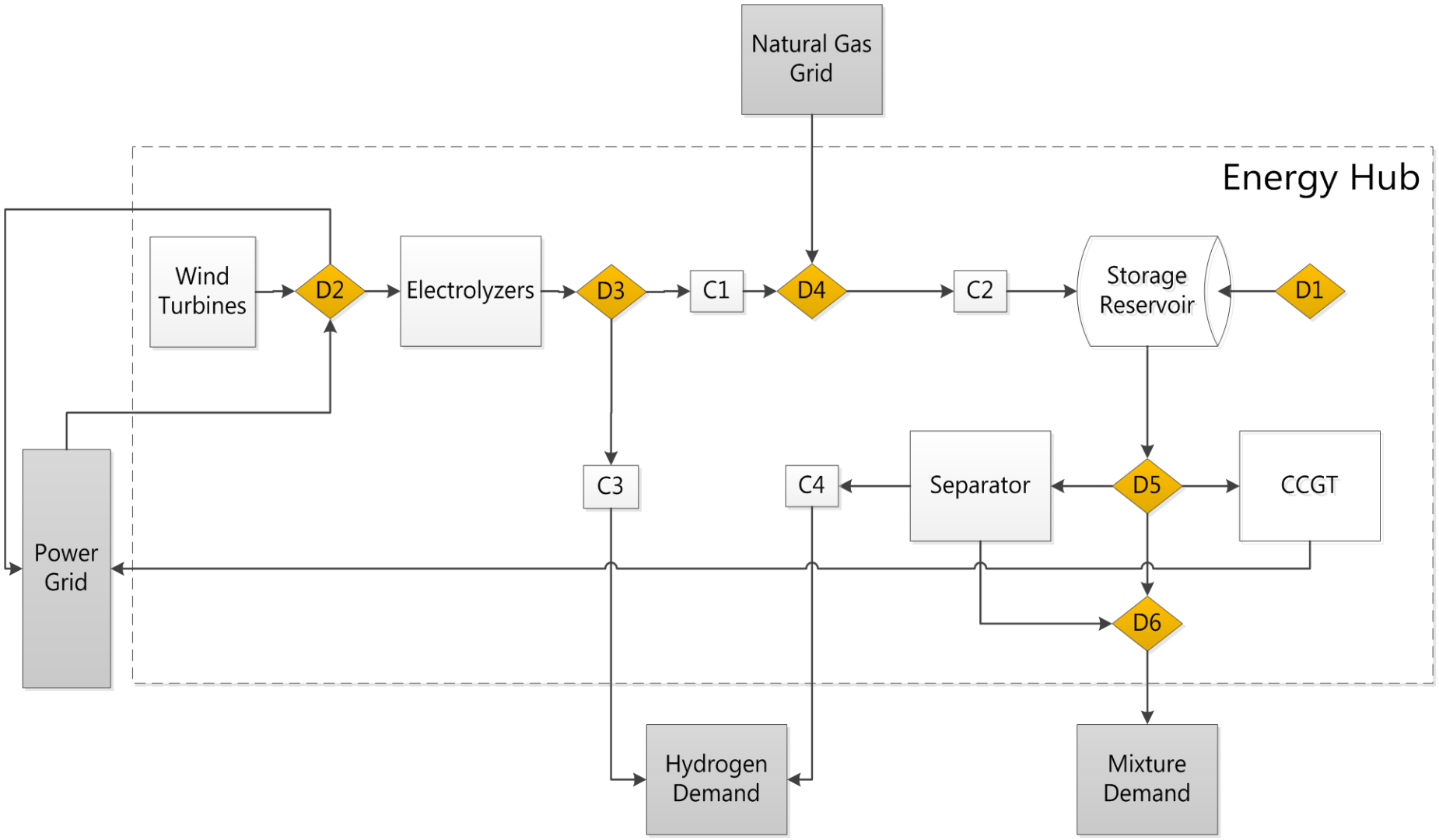

Figure 3.1 Detailed view of the energy hub

3.2 Decision Variables

The decision variables are also known as experimental factors or model inputs; they are elements of the model which can be altered to effect better understanding of the real world system. They are also known as experimental factors. Three types of decision variables have been identified for the simulation of the energy hub:

1. Variables that describe the configuration of energy hub components (Ex: with or without separator, with or without CCGT);
2. Variables that describe the rated capacity of energy hub components (Ex.: the rated input/output of the electrolyzer, the rated input/output of the separator);
3. Relationships that can determine the value of unspecified variables based on specified ones.

Type 1 and 2 variables have been identified and listed in Table 3.1. Note that the storage reservoir is always set to be available; otherwise, the energy hub project wouldn't be physically meaningful. Also, its storage capacity and rated input/output (known as injectability/deliverability for reservoirs) are taken to be fixed, for they cannot be freely adjusted as for individual man-made parts.

Table 3.1 List of system configuration and capacity variables

Component	Variable	Symbol	Value	Unit	Reference
Reservoir (ON)	Rated capacity	$V_{\max,s}$	7.6	Bcf	[67]
Electrolyzers (ON/OFF)	Rated capacity per unit	$P_{E,rated,i}$	0.29	MW	[68]
	Number of units	N_E	integer ≥ 0		
Wind turbines (ON/OFF)	Rated capacity per unit	$P_{W,rated,i}$	2	MW	[69]
	Number of units	N_T	integer ≥ 0		
CCGT (ON/OFF)	Rated capacity	$\dot{W}_{CC,rated}$	40-800	MW	[58]
Separator (ON/OFF)	Rated capacity	$\dot{V}_{feed,rated}$	300-400,000	Nm^3/h	[70]

The last type of decision variables/relationships is necessary because this modeling project is not based on optimization, which can be set up to determine the optimal values of unspecified variables automatically. For the model simulation to arrive at results, the system of equations that is the model needs to be completely specified.

Each of the six decision points, shown in Figure 3.1, represents the logic for one or more of the relationships required. The pairs of variables that they connect are shown in Table 3.2.

1. At decision points 1, it is necessary to determine whether to inject into the reservoir, produce from the reservoir, or shut-in the reservoir based on exogenous power and gas market conditions. The reservoir model then translates the "mode", also referred to as the reservoir dispatch order, into injectability or deliverability terms;
2. At decision point 2, it is necessary to determine the utilization level of the electrolyzer and the mix of power supply used;
3. At decision point 3, it is necessary to determine whether the electrolytic hydrogen produced is sent to storage, or directly delivered to meet local demand for hydrogen;
4. At decision point 4, it is necessary to determine how much natural gas to blend with the hydrogen produced;
5. At decision point 5, it is necessary to determine the amount of mixture is withdrawn from storage, and the amount dispatched to different energy recovery pathways;
6. Finally, at decision point 6, the destination of the natural gas-rich stream from the separator needs to be decided. For simplicity, it is assumed that it is merged with the mixture dispatched to the gas distribution network.

Compared to the first two types of decision variables, for which binary values (ON/OFF) or a simple number suffice, the decision points require inputs which are more complex. In Chapter 7, when describing inputs for different scenarios, the decision points are illustrated by logic flow diagrams.

Table 3.2 List of decision point inputs and outputs

	Description	Inputs	Symbol	Unit	Outputs	Symbol	Unit
D1	Reservoir operation regime	Sets of exogenous environmental variables and their derivatives			Reservoir mode	Mode	N/A
		H_2 produced	$\dot{n}_{H_2,E}$	kmol/h			
D2	Electrolyzer power supply	Sets of exogenous environmental variables and their derivatives			Wind power stored	P_{Wts}	MW
		Wind power available	P_W	MW	Wind power sold to grid	P_{WtG}	MW
		Rated power of electrolyzers	$P_{E,rated}$	MW	Grid power stored	P_{Gts}	MW
					Electrolyzers supply	P_E	MW
D3	Hydrogen bypass	H_2 produced	$\dot{n}_{H_2,E}$	kmol/h	H_2 stored	$\dot{n}_{H_2,s}$	kmol/h
		Injectability/deliverability	$\dot{n}_s$	kmol/h	H_2 bypassed	$\dot{n}_{H_2,b}$	kmol/h
		H_2 demand schedule	$\dot{n}_{H_2,load}$	kmol/h	H_2 curtailed	$\dot{n}_{H_2,c}$	kmol/h
D4	NG/H_2 blending	H_2 stored	$\dot{n}_{H_2,s}$	kmol/h	NG stored	$\dot{n}_{NG,in}$	kmol/h
		Injectability/deliverability	$\dot{n}_s$	kmol/h	Mixture stored	$\dot{n}_{mix,in}$	kmol/h
					H_2 conc.	$c_{H_2,in}$	mol %
D5	Mixture dispatch	Injectability or deliverability	$\dot{n}_s$	kmol/h	Fuel to CCGT	$\dot{n}_{fuel}$	kmol/h
		Rated fuel capacity of CCGT	$\dot{n}_{fuel,rated}$	kmol/h	Feed to separator	$\dot{n}_{feed}$	kmol/h
		Rated feed capacity of separator	$\dot{n}_{feed,rated}$	kmol/h	Mixture delivered	$\dot{n}_{mix}$	kmol/h
					Mixture withdrawn	$\dot{n}_{mix,out}$	kmol/h
D6	Separator recycle	Waste stream from separator	$\dot{n}_{sep,mix}$	kmol/h	Mixture delivered	$\dot{n}_{mix,tot}$	kmol/h
		Curtailed separator feed	$\dot{n}_{feed,c}$	kmol/h	H_2 conc. in mixture delivered	$c_{H_2,mix,tc}$	mol %
		Mixture delivered	$\dot{n}_{mix}$	kmol/h			
		H_2 concentration in waste	$c_{H_2,sep,mix}$	mol %			
		Reservoir H_2 conc.	$c_{H_2,res}$	mol %			

3.3 Exogenous Variables

The exogenous variables are variables describing elements which are outside of the scope of this modeling study. They are presented here, because they are the basis of many operational decisions at decision points. In the following sections, each of the external components that interact with the energy hub is discussed in terms of the direction for material flow, the realistic scale of supply and/or demand, and the information available to energy hub operators for decision making.

The exogenous environmental variables are dependent on the geographic location and the temporal coverage of the energy hub project. For this simulation study, they are taken to be constants, but they can be updated with different values to assess the same energy hub project planned for other locations and/or time periods.

In this study, it is assumed that they interact with the energy hub but are not changed by outputs from the energy hub. For example, it is assumed that the market price of electricity is not influenced by the electricity consumed or supplied by the energy hub. Such assumptions may be valid for energy hubs with relatively limited inputs and outputs; once their scale and number multiply, it will be necessary to re-evaluate such assumptions.

Also, in this modeling project, external components are usually represented by their aggregated behaviour – for example: the overall Ontario demand for electricity –, but, in reality, each of them is made up of many smaller constituents, for example: the power grid is made up of many other power suppliers and loads. If the previous assumption is found to be invalid, then such aggregated representation of the external components will need to be revised; the inner details of the power grid and the natural gas grid will need to be modeled, thus transforming them from exogenous variables endogenous variables of the modeling efforts.

Table 3.3 List of exogenous environmental variables

Component	Variable	Symbol	Value	Unit	Reference
Power grid	Market price of electricity	$HOEP$	Figure 3.4 Historic HOEP from 2010-2012	$/MWh	[14]
	Ontario demand	P_{load}	Figure 3.5 Historic Ontario electricity demand for 2010-2012	MW	[14]
	FIT price schedule	FIT	Weekdays 11am-6pm: 135% of 115 Rest of the week: 90% of 115	$/MWh	[71]
	Emission factor of power from grid	EF_G	Figure 3.8 Hourly emission factor for power generation in Ontario for 2010-2012	kg CO_2 /MWh	[106]
Natural gas grid	Market price of natural gas	C_{NG}	Figure 3.11 Historic natural gas spot price at Henry Hub for 2010-2012	$/MMBtu	[72]
Mixture demand	Price of mixture	C_{mix}	Identical to natural gas market prices	$/MMBtu	Estimated in section 3.3.3
Hydrogen demand	Price of hydrogen	C_{H_2}	5	$/kg	Estimated section 3.3.4
	Hydrogen pick-up schedule	$\dot{n}_{H_2,load}$	Weekdays 10am – 5pm: >0 Rest of the week: 0	kmol/h	Assumed

3.3.1 Power Grid

The power grid is both a source and a sink for electricity. The energy hub, since it has the capability to generate and consume electricity, has a bidirectional relationship with the power grid (Figure 3.2). But, for any given hours, it is assumed that the energy is either producing or consuming electricity, not both simultaneously.

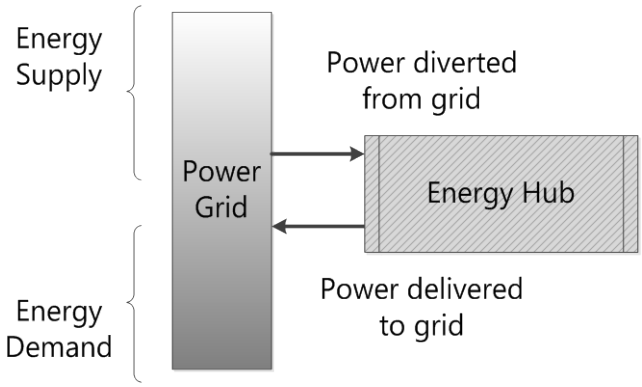

Figure 3.2 Interaction between the power grid and energy hub

In reality, the Ontario power grid is an extended network made up of 30,000 km of high-voltage transmission lines, spanning all regions of Ontario, connecting power generators with loads. It would be necessary to capture the geographic disaggregated nature of the power grid, if it were modeled as an endogenous component of the project, including the location of different generators and loads, the status of connections between them (congested or not), and the status of generators and loads (Figure 3.3). However, given that the power grid is considered to be exogenous to the scope of the current project, it is modeled as a single connection to the energy hub, through which electricity can be procured and delivered.

The power grid interacting with the energy hub can be viewed as a provincial system. For the volumes of imports and exports are small compared to the overall volumes of intra-province production and consumption. For the year of 2011, imported electricity fulfilled 3% of the total Ontario demand, whereas 9% of electricity produced in Ontario was exported (calculated from IESO market data). Given the scale of the Ontario power grid (34,000 MW installed by end of 2011 and 150.4 TWh generated for the year of 2011), it is assumed that the planned energy hub (1 to 50 MW in scale) will not have significant influence over the grid-wide power supply and demand.

Figure 3.3 Ontario's power grid and its transmission zones [73]

The wholesale market price of electricity (HOEP) is the main tool through which the operations of many different electricity market participants are coordinated. The historic HOEP for 2010 through 2012 is published as part of the market data archive by the IESO (Figure 3.4).

Other than the market price, the IESO also publishes the actual level of demand in Ontario at an hourly resolution (Figure 3.5). Upon inspection, it is found that the market price shows some correlation with the power demand (correlation coefficient r = 0.44, suggesting modest correlation). Also, comparing the two measures by plotting the relative change with respect to the previous value in the time series, it is observed that the market price for electricity is much more volatile than the demand for electricity (Figure 3.7). Therefore, in some scenarios, the HOEP is interpreted as an indicator of the level of demand and supply within the electricity market, guiding the operations of the energy hub as it is the only information realistically available in real-time. But, in some other scenarios which have particular focus on better serving the electricity demand in Ontario, the actual

market demand data is used as the indicator, for it is a more accurate measure for hourly demand in Ontario.

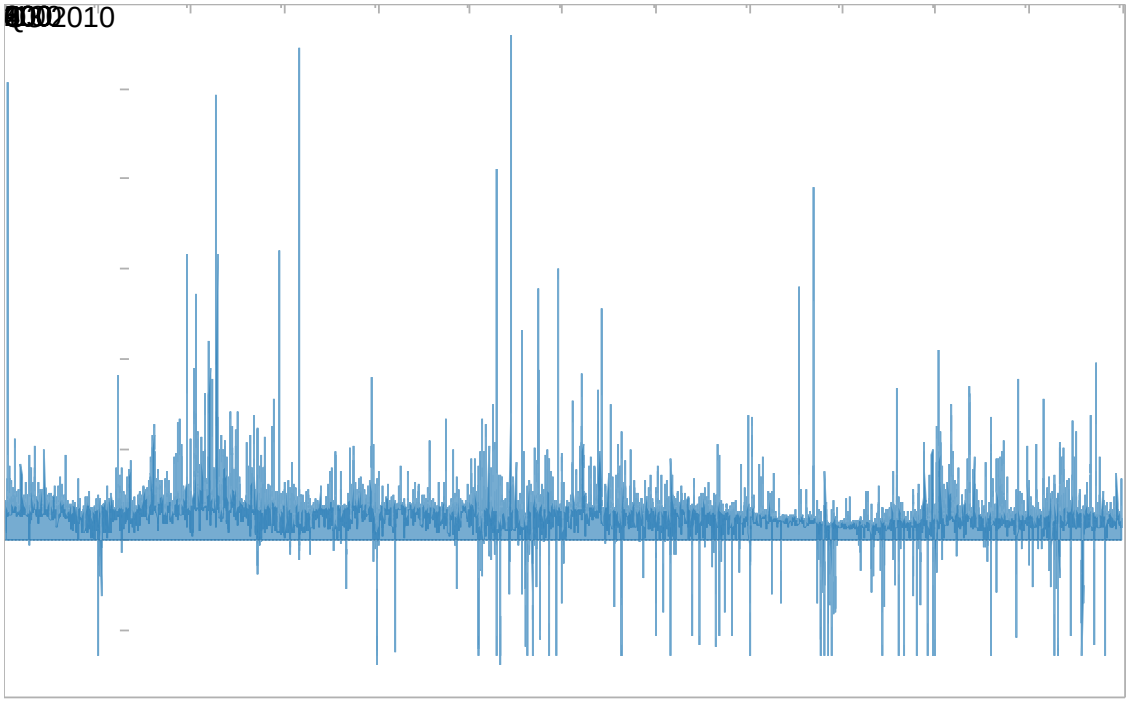

Figure 3.4 Historic HOEP from 2010-2012

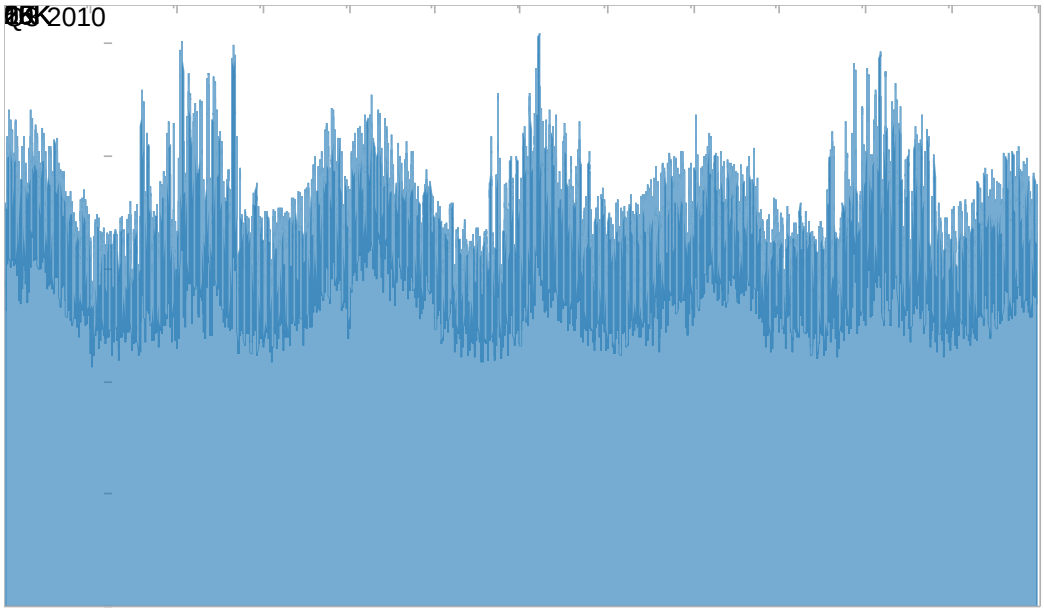

Figure 3.5 Historic Ontario electricity demand for 2010-2012

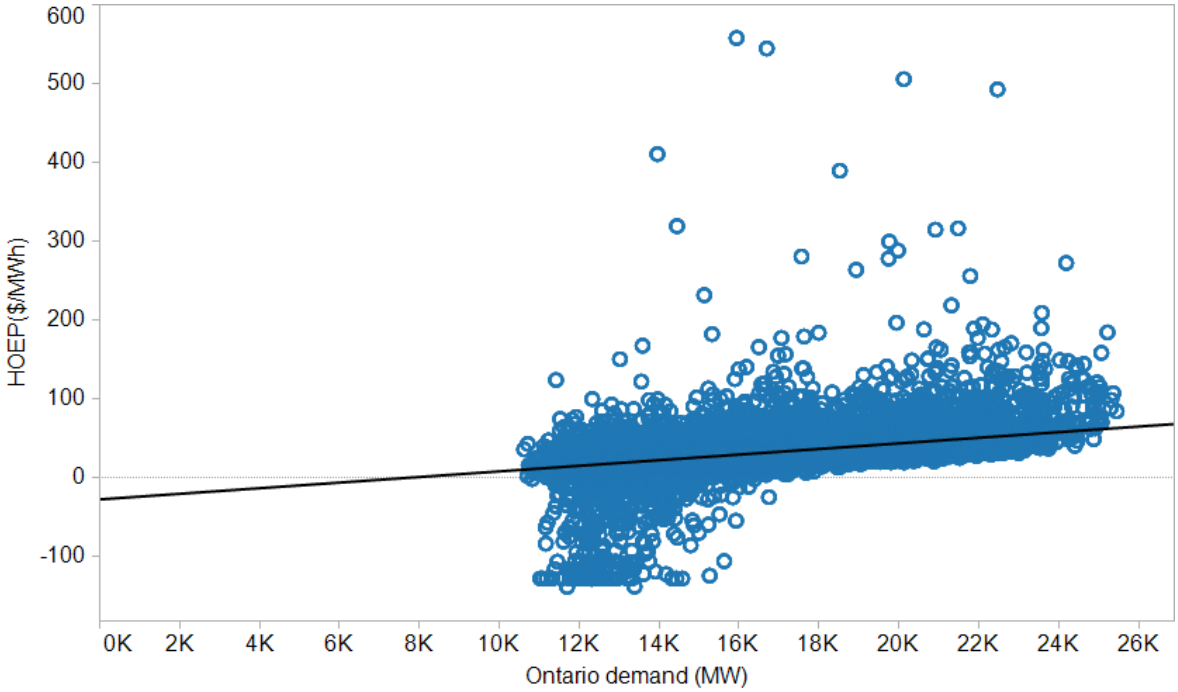

Figure 3.6 Correlation between 2010-2012 electricity demand and HOEP for Ontario

Because of the existence of the Feed-In Tariff (FIT) program in Ontario, a participating renewable energy generator is paid a price different than the HOEP. The FIT price is fixed and reviewed annually; for current wind projects, it is $115/MWh [71]. For technologies which are dispatchable, the FIT schedule is multiplied to a factor to incentivise production during peak periods. The rate paid during peak periods (weekdays from 11am to 6pm, inclusively) is 135% of the fixed FIT price, and the rate paid ruing off-peak periods (rest of the time, including weekends) is 90% of the fixed FIT price. In this project, it is assumed that wind power generated on-site, given that it can be directed to storage, is considered to be dispatchable, being paid the time-differentiating FIT schedule instead of the fixed price.

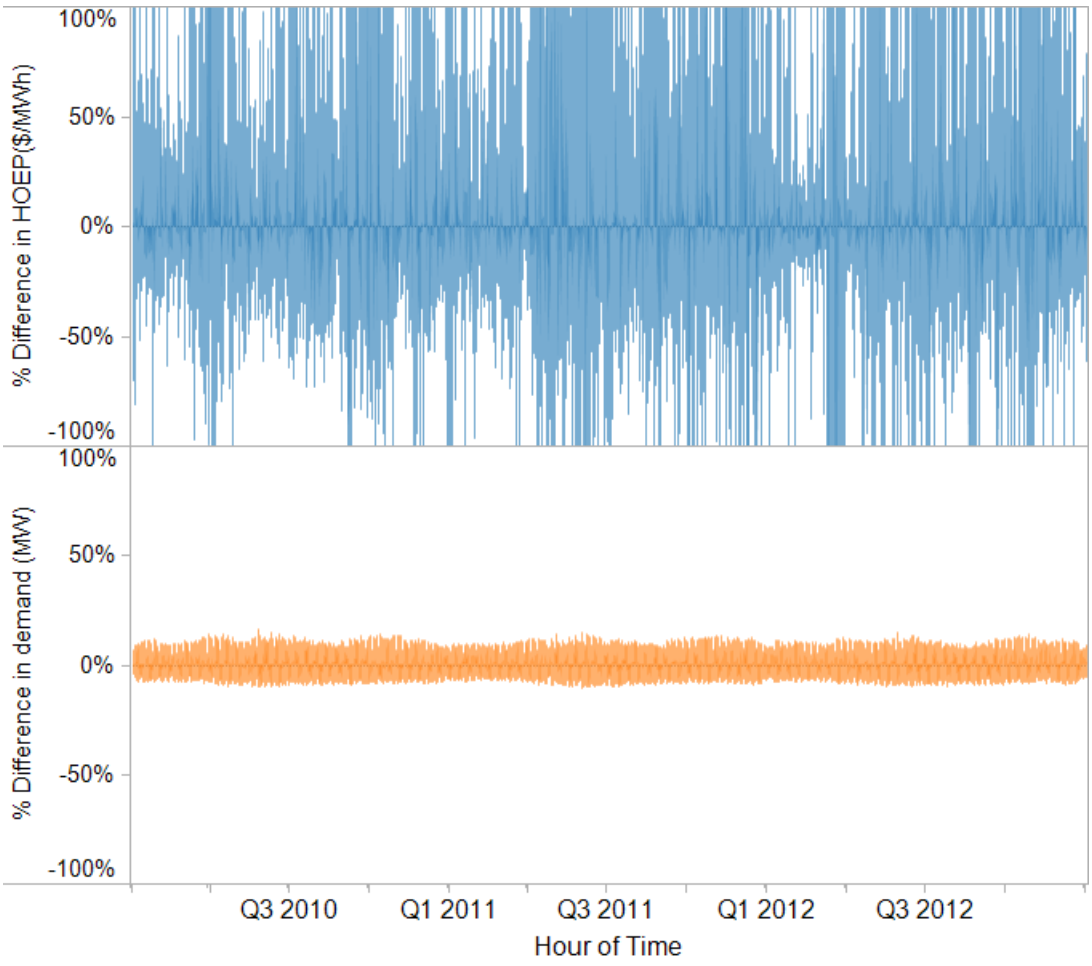

Figure 3.7 Relative hourly changes in HOEP and Ontario demand

Finally, in order to assess the carbon dioxide emissions incurred when the energy hub consumes electricity purchased from the grid, it is necessary to have access to the emission factor of grid power in Ontario. Currently, an annual greenhouse gas intensity factor is available for Ontario's electricity system in general, but it does not reflect the hourly variation in emission caused by the different types of generators engaged. For this project, the hourly emission factor for electricity generation in Ontario is estimated from the hourly total generation, the hourly wind power generated, percentage of energy by fuel type (annual values), and an approximate merit order (Figure 3.8).

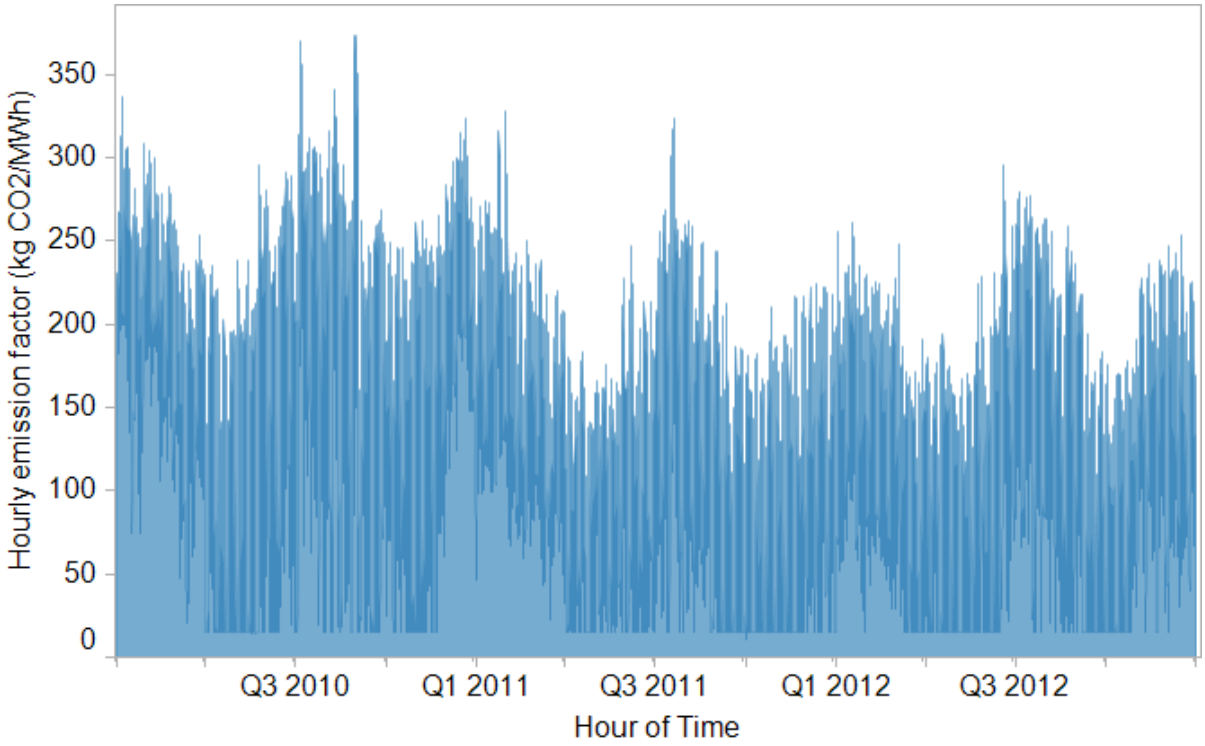

Figure 3.8 Hourly emission factors for power generation in Ontario for 2010-2012

3.3.2 Natural Gas Grid

The natural gas that is stored in the underground reservoir, along with hydrogen, is supplied by the high pressure transmission pipelines of the natural gas grid (Figure 3.9). The mixture withdrawn from storage is not sent back to the original natural gas grid: it is assumed that the gas exiting the energy hub, in the form of a natural gas/hydrogen mixture, is distributed directly to local consumers via a series of dedicated mid-to-low pressure distribution pipelines. These dedicated pipelines might be assets formerly belonging to the natural gas grid, but they are differentiated from the natural gas grid in general because of their dedicated content (discussed in Section 3.3.3).

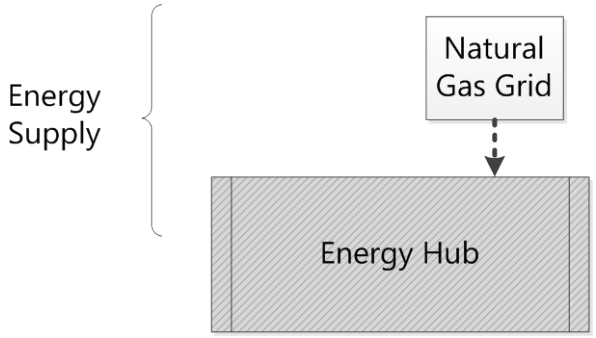

Figure 3.9 Interaction of the natural gas grid with the energy hub

Ontario is the largest market for natural gas in Canada, with a peak demand of 3 Bcf per day. Compared to the total annual consumption of 756.5 Bcf, the annual marketed production in Ontario is only 8.32 Bcf [74]. Therefore, Ontario is largely dependent on external producers, mostly form the Western Canada Sedimentary Basin, for its own natural gas needs. The province receives natural gas from producers in western Canada through the northern mainline TransCanada Pipeline (TCPL, 4.1 Bcf per day), and through Dawn Hub in southwestern Ontario (3.9 Bcf per day) [75]. The major natural gas pipelines entering and leaving Ontario are shown in Figure 3.10. Pipeline capacity in excess of Ontario's needs, approximately 60 percent of the gas entering Ontario, is used to supply Eastern Canada and the North Eastern US markets. Compared to the Ontario power market, which is essentially provincial, the natural gas market of Ontario is tightly coupled to the supply and demand in other jurisdictions.

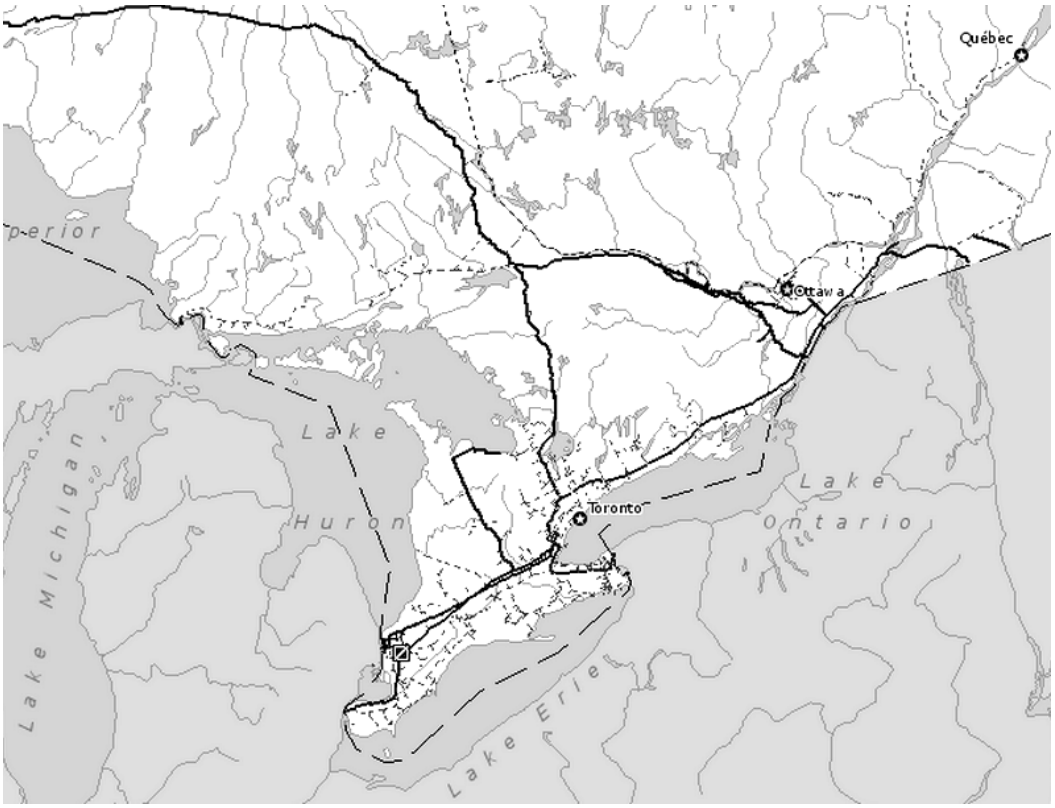

Figure 3.10 Pipeline Infrastructure in Ontario [76]

The natural gas grid is modeled as a single point of connection that supplies natural gas to the energy hub. It is assumed that the geographically disaggregated details of the natural gas grid can be simplified. Also, it is assumed that the energy hub, modeled on a gas storage facility with maximum throughput of 0.3 Bcf per day at absolute open flow conditions, less than 10% of the daily intake of Dawn Hub, is a price-taker. For all hours, it is assumed that the natural gas grid has enough capacity to supply the energy hub at its maximum intake capacity.

The market price of natural gas is the key indicator available to participants in the natural gas market to gauge the level of supply and demand within the whole sector. The Ontario market price for natural gas is mainly set at the Dawn Hub, where several pipelines intersect, but its historic values are not readily available to the public. In its absence, the historical spot price at the Henry Hub, a major price-setting point and natural gas distribution hub in the United States, is used as a substitute. Some discrepancy between the Henry Hub price and the Ontario wholesale price is expected, but it is

assumed to be negligible; the natural gas price in Canada is linked to the American natural gas market, for natural gas is imported and exported extensively across international borders and the prices are competitively set.

Unlike electricity, whose market price is set every hour (or at even shorter intervals), the historic price of natural gas is only available at a daily resolution (weekdays only, excluding week days and holidays, [72]). Consequently, in order to generate an hourly time series for the simulation, weekly averages of the Henry Spot price are computed and expanded to hourly resolution (i.e. all hours in the same week has the same natural gas price).

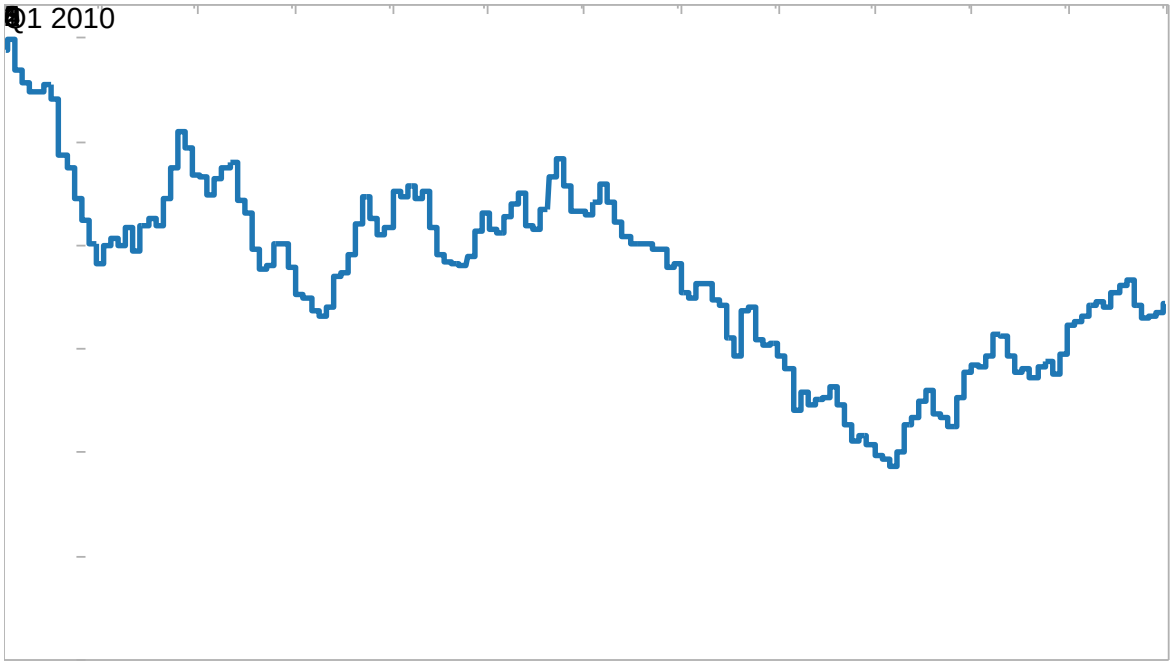

Figure 3.11 Historic natural gas spot price at Henry Hub for 2010-2012

3.3.3 Mixture Demand

The mixture demand is the sink for which all mixture produced from the energy hub for off-site use. In this project, it is assumed that the demand for hydrogen-enriched natural gas is fulfilled via the use of existing natural gas distribution network, but, in order to assess the scale of demand, it is treated separately from the natural gas demand in general.

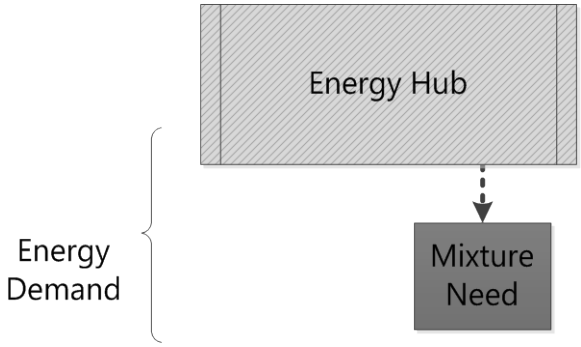

Figure 3.12 Interaction of the mixture need with energy hub

In the near future, hydrogen enriched natural gas is expected to be used as an alternative to conventional natural gas; therefore, the projection of demand for such mixture is based on the current demand for natural gas in Southwestern Ontario, the region in which the energy hub is to be located. The Ontario total natural gas consumption for year 2010-2012 is shown in Figure 3.13. Assuming natural gas use is proportional to population, then the annual natural gas consumption of Southwestern Ontario is estimated to be 27% of the total Ontario demand. Then, it is assumed that 10% of the Southwestern Ontario demand can be converted to use hydrogen-enriched natural gas as a substitute. The resulting estimate for mixture demand for the period of interest is shown by the line in the same figure.

Since the hydrogen/natural gas mixture a new product without an established market price, a selling price needs to be established, considering the possible end-users and competitors. The price that newly converted industrial customers are willing to pay is likely to be the price that they are currently paying for natural gas. Therefore, the selling price of the mixture is set to be identical to the price of natural gas; note that the price is expressed in terms of energy content, not mass or volume.

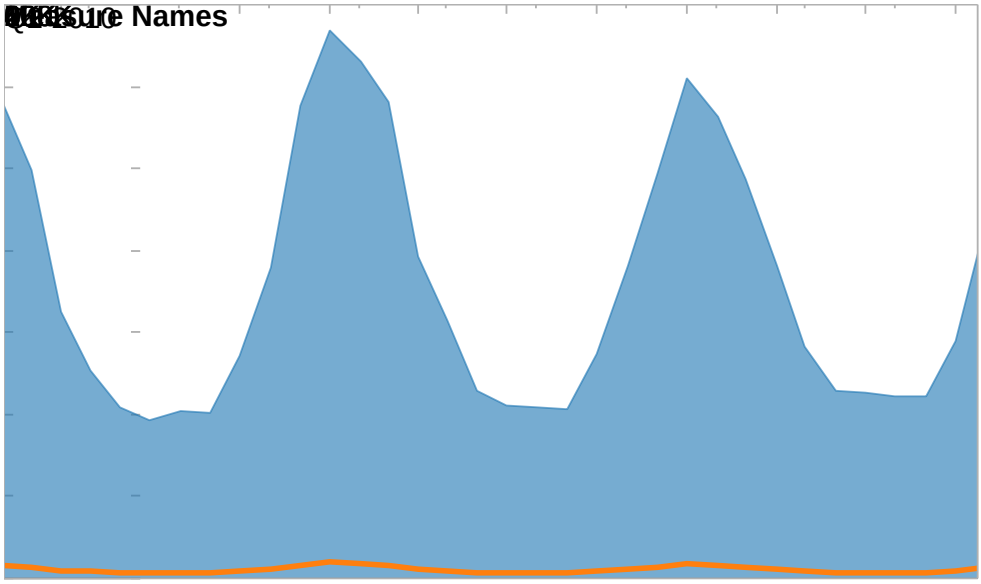

Figure 3.13 Ontario monthly natural gas demand for 2010 – 2012 [77]

3.3.4 Hydrogen Demand

The hydrogen demand is the sink for all pure hydrogen delivered from the energy hub (Figure 3.14). Compared to other sinks (the power grid and the demand for mixture), the demand for hydrogen is different in that is does not yet have dedicated transport infrastructure, such as power lines or gas distribution pipelines, so that the demand is not always present: hydrogen demand is present only when there is a scheduled delivery to be made. Therefore, during simulation, the effect of constrained delivery needs to be investigated.

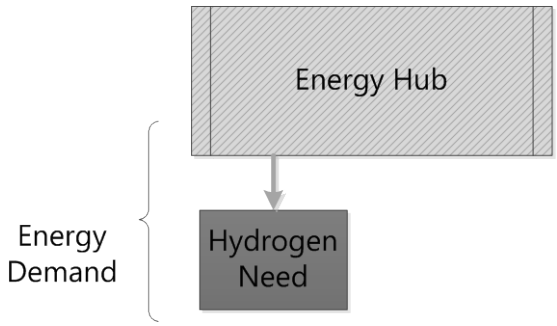

Figure 3.14 Interaction of Hydrogen Need with Energy Hub

Proponents of the hydrogen economy propose that, as part of the efforts to decarbonize modern society's energy use, hydrogen can be and should be used as an energy vector. But, at the present stage, hydrogen is still mainly used as an industrial commodity, a feedstock to be used in other industrial processes. The main industrial usages of hydrogen include heavy oil upgrading, oil refining, ammonia and methanol production. These constitute 85% of hydrogen consumption in Canada. The other 15% of consumption, outside of process need, include the heat treatment of metals, glass making, microelectronics fabrication, power generator cooling, hydrogenation of food oils, as well as the nascent fuel cell applications [78].

In 2008, 3 megatonnes of hydrogen was produced in Canada, of which 70% was produced from natural gas, via steam methane reforming [79]. Using the information above, it is calculated that the per capita hydrogen consumption in Canada is about 87 kg per year. The region of interest to this simulation project, Southwestern Ontario, centered on the city of London, containing Lambton County, in which the storage reservoir is to be located, has a population of 3,443,484 in 2006. Therefore, a first estimate for the regional consumption of hydrogen would be about 300,000 tonnes

annually. For the scale of electrolyzer operations envisaged (1MW to 20 MW), supposing 100% utilization and 70% efficiency converting power to hydrogen, a maximum annual production in the order of 3000 tonnes is possible, or 1% of the projected regional demand. Therefore, it seems reasonable to assume that the existing demand for hydrogen can absorb the hydrogen produced at the energy hub.

Unlike for natural gas and electricity, there is no publicly disclosed market price for hydrogen. Therefore, the price at which hydrogen is delivered to consumers is estimated according to the following guidelines:

In accounting, two long-run pricing approaches are common: the market-based approach and the cost-based approach [80]. Because hydrogen is a commodity product, as opposed to differentiated products such as cameras and cars, the market-based approach is recommended, for competition between producers is an important market force in this case. The market-based pricing approach requires knowledge of the price that potential customers are willing to pay. This price can be estimated based on the understanding of the value that customers perceive in the product, and on the knowledge of the price of competing products.

Of all the applications for electrolytic hydrogen, using it as an alternative fuel to replace gasoline or using it in conventional industrial and research applications to replace hydrogen produced via SMR are perceived as the most important.

Assuming that the main value that the customers perceive in the energy-hub produced hydrogen is its value as an alternative fuel, the price that the customers are willing to pay for hydrogen will be the expected price of retail gasoline, perhaps at a premium, given that hydrogen is a cleaner-burning fuel. The historic retail price of gasoline is, obtained from the Energy Information Administration, shown in Figure 3.15 suggests that for the future five years, the per-gallon price of gasoline will vary in between $2 and $4. Given that 0.997 kg of hydrogen constitutes 1 gasoline gallon equivalent, the price that the customers are willing to pay should also vary from $2 to $4.

Assuming that the main value that the customers perceive in the energy-hub produced hydrogen is its ability to replace hydrogen produced from natural gas, then the cost of such fossil-fuel based hydrogen needs to be examined. As shown by Figure 3.11, natural gas prices in recent years vary between $2/MMBtu to $5/MMBtu (~ $2 to $5/GJ). Thus, using the correlation given by Figure 3.16,

the cost of hydrogen should range from $10 to $25/GJ ($1.2 to $3/kg hydrogen), for centralized SMR and distributed SMR respectively.

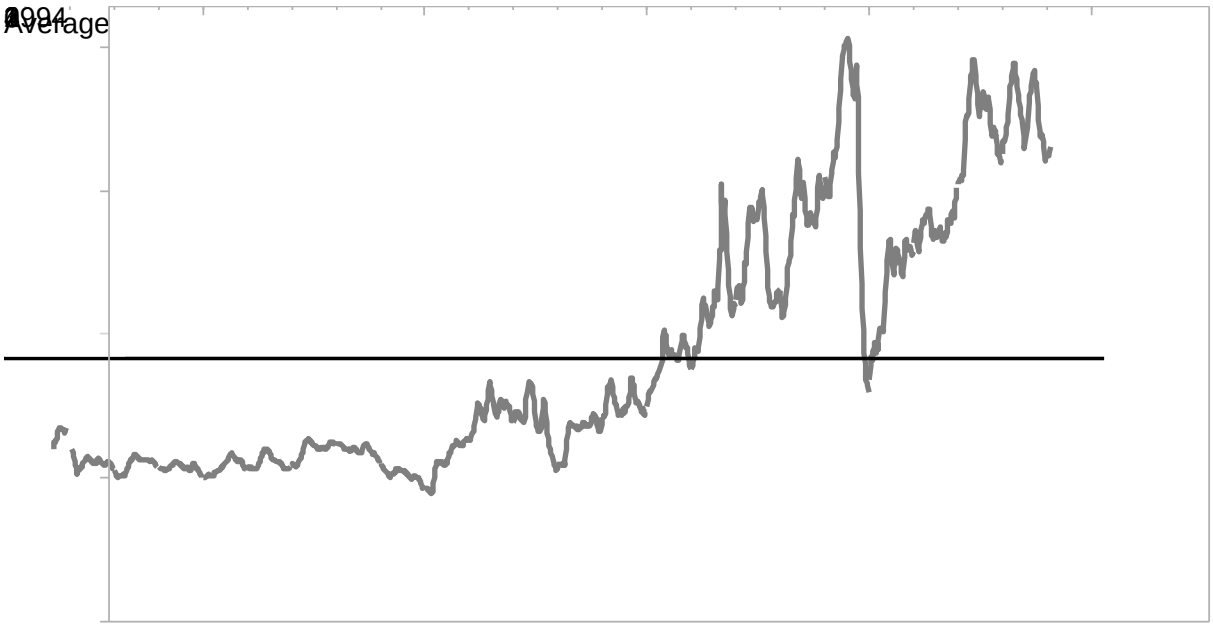

Figure 3.15 Historic retail price of regular gasoline from 1991 to 2012

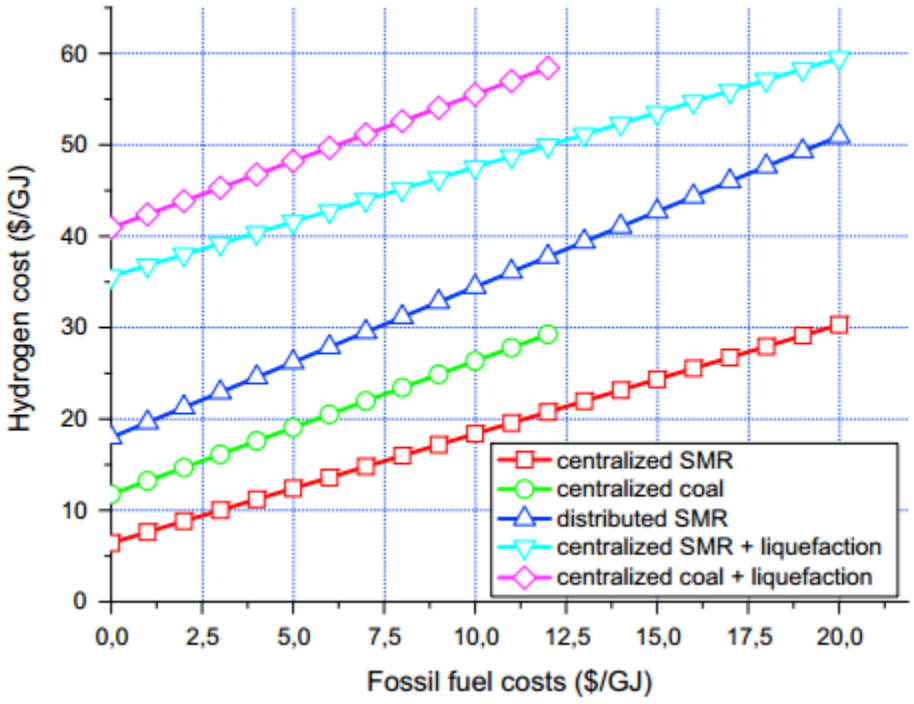

Figure 3.16 Linear dependences of natural gas and coal prices to centralized and distributed SMR and coal based hydrogen costs [81]

After deliberation, the long-term price of hydrogen delivery by the energy hub is set to be $5/kg, with the knowledge that, in the future, for hydrogen to become a widely used fuel, the price of per gasoline gallon equivalent needs to be decreased to $2-3/gge (untaxed), according to the US Department of Energy's Hydrogen Program [82] .

Finally, in the context of energy hub operations, in the absence of dedicated pipelines, hydrogen is picked up at scheduled times. Consequently, pure hydrogen cannot be produced at points other than those pick-up points. It is assumed that hydrogen is collected and delivered to end-users in tube trailers at 180 bar, each capable of transporting 340 kg hydrogen. The frequency of pick-up points and the number of tube trailer available at each pick-up are independent variables that are varied in different scenarios. The cost of pure hydrogen delivery is excluded from this study.

3.4 Performance indicators

Performance indicators are the results generated by the model based on the inputs provided. The interpretation of those indicators is the source of much insights gained from a modeling and simulation study. As discussed previously, there are three types of performance indicators: physical, financial and environmental. The financial and environmental performance indicators are evaluated using the physical indicators. The physical model outputs of interest are summarized by the Table 3.4.

All of the physical performance indicators are available as hourly time series for the time period simulated. They can also be compared in their aggregate form. The outputs are separated into two types: stock variables, for which the annual average of the time series is more meaningful, and flow variables, for which the annual sum of the time series is more meaningful.

Table 3.4 List of physical performance indicators

Component	Variable	Symbol	Description	Type	Unit
D1	Dispatch order to the reservoir	$Mode$	The dispatch order indicates the decision of the operators to inject/withdraw gas from the reservoir	Stock	N/A
Storage reservoir	Inventory	n_{total}	The total amount of gas in storage	Stock	kmol
	H_2 conc.	$c_{H_2,res}$	Hydrogen concentration of the gas mixture in storage	Stock	mol %
	Reservoir pressure	p_{res}	Pressure that the gas in storage exerts on the reservoir, assumed to be uniform throughout	Stock	bar
	Wellhead pressure	p_{wh}	The pressure at the wellhead, which is controlled by the operators of the energy hub	Stock	bar
	Injectability/deliverability	$\dot{n}_s$	The physical limits to flow rates in/out of the reservoir, given the conditions of the reservoir	Flow	kmol/h
	Actual flow rate	$\dot{n}_{s,act}$	The actual flow rate of gas injected or withdrawn, maybe lower than or equal to the injectability / deliverability	Flow	kmol/h
Wind turbines	Wind power produced	P_W	Wind power generated by the on-site wind turbine	Flow	MW
	Utilization factor	U_W	The capacity utilization factor for the individual component	Stock	
D2	Wind power stored	P_{Wts}	The amount of wind power produced that is supplied to the electrolyzers	Flow	MW
	Wind power sold to grid	P_{WtG}	The amount of wind power produced that is supplied to the power grid	Flow	MW
	Grid power stored	P_{Gts}	The amount of grid power that is supplied to the electrolyzers	Flow	MW
Electrolyzers	H_2 produced	$\dot{n}_{H_2,E}$	Amount of hydrogen produced by the electrolyzers	Flow	kmol/h
	Utilization factor	U_E	The capacity utilization factor for the individual component	Stock	
D3	H_2 stored	$\dot{n}_{H_2,s}$	The amount of hydrogen produced by the electrolyzers that is injected into the reservoir	Flow	kmol/h
	H_2 bypassed	$\dot{n}_{H_2,b}$	The amount of hydrogen that is delivered to meet demand upon production from the	Flow	kmol/h

			electrolyzers		
	H_2 curtailed	$\dot{n}_{H_2,c}$	The amount of hydrogen produced that cannot be stored or delivered to meet demand	Flow	kmol/h
D4	NG stored	$\dot{n}_{NG,in}$	The amount of natural gas that is injected into the reservoir	Flow	kmol/h
	H_2 conc. of mixture injected	$c_{H_2,in}$	Hydrogen concentration at the blending point prior to injection into the reservoir	Stock	mol %
D5	Fuel to CCGT	$\dot{n}_{fuel}$	The amount of mixture that is dispatched to the CCGT as fuel	Flow	kmol/h
	Feed to separator	$\dot{n}_{feed}$	The amount of mixture that is dispatched to the separator as feed	Flow	kmol/h
	Mixture delivered	$\dot{n}_{mix}$	The amount of mixture that is dispatched for distribution to off-site end-users via gas pipelines	Flow	kmol/h
CCGT	Power delivered to grid	$\dot{W}_{CC}$	The amount of power that is generated by the CCGT plant	Flow	MW
	Utilization factor	U_{CCGT}	The capacity utilization factor for the individual component	Stock	
Separator	H2 delivered	$\dot{n}_{H_2,sep}$	The amount of hydrogen that is produced via the separator	Flow	kmol/h
	Utilization factor	U_{sep}	The capacity utilization factor for the individual component	Stock	
D6	Revised mixture delivery	$\dot{n}_{mix,tot}$	Mixture delivered, after the merging of original stream with the natural gas-rich by-product stream from the separator	Flow	kmol/h
	H_2 conc. of mixture delivered	$c_{H_2,mix,tot}$	Final concentration of hydrogen in the mixture delivered to off-site end-users	Stock	mol %
Compressors	Compressor work required	$P_{comp,tot}$	Energy consumed by compressors to inject gas	Flow	kWh

As outlined in the conceptual model, the financial is one of the evaluative models that assess the performance of the energy hub project. The key indicators developed and used is the: net present value of project which captures the main economic benefits directly associated with the operations of the energy hub. The constituents required for the calculation of the net present value are many. Each of the shadowed boxes in Figure 3.17 can be further divided into its constituents; they are described in Chapter 5. The default project life time used is 20 years; and the discount rate is 8% for final reporting.

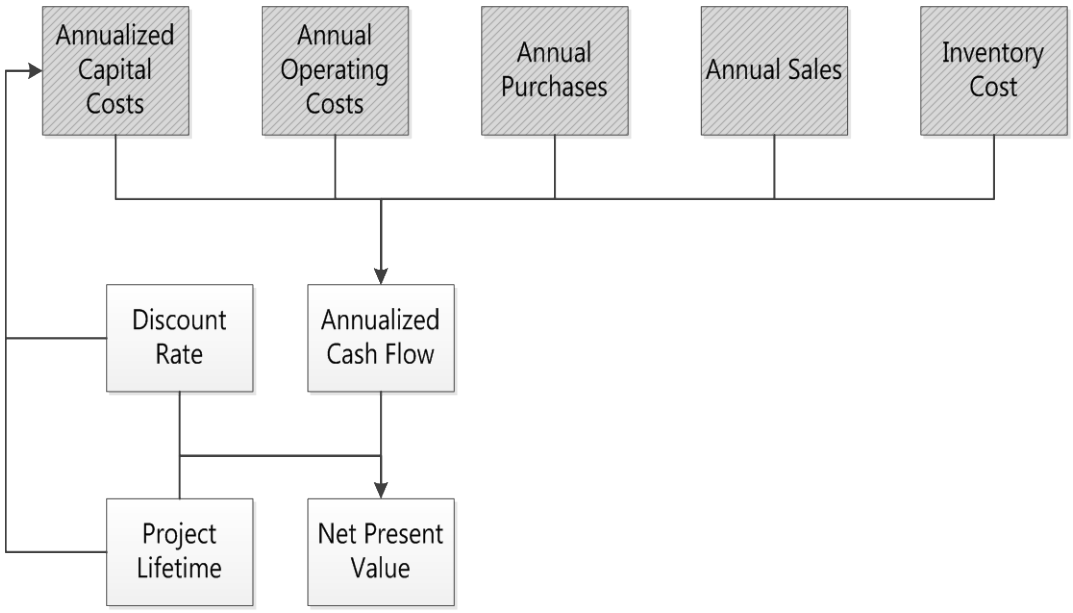

Figure 3.17 Scope for financial model

For this study, only carbon dioxide emissions are included as part of the emission model to facilitate model development. The scope of emission model is drawn to include emissions incurred while operating the energy hub and emissions that are displaced by the operations of the energy hub, so that the net emissions associated with the energy hub can be assessed (Figure 3.18).

The sources of emissions associated with the energy hub are: emissions from power generators which produce the electricity for hydrogen production, including both the grid-connected generators and the on-site wind turbines; emissions from on-site use of hydrogen-enriched natural gas at the CCGT; emissions from the off-site use of the hydrogen/natural gas mixture by the end-users reached by the distribution pipeline, and emissions from the natural gas-driven compressors that enable gas injection.

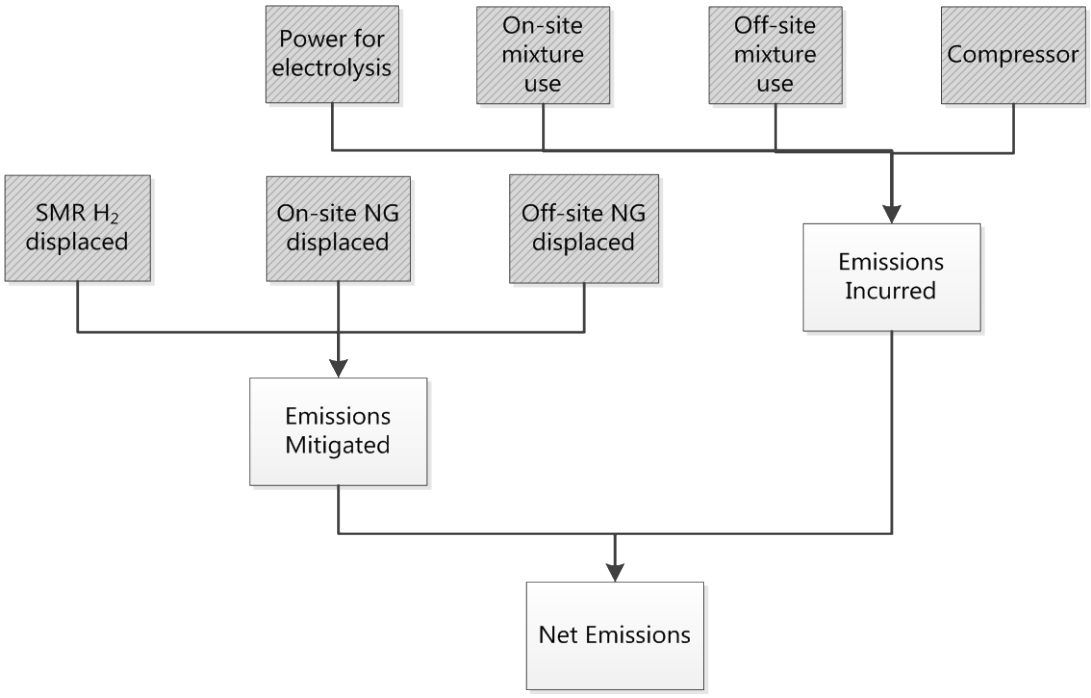

Figure 3.18 Scope for emission model

Also associated with the energy hub are carbon dioxide emissions which have been mitigated: by producing electrolytic hydrogen, the use of hydrogen produced from fossil fuel (SMR process) is displaced; by using hydrogen-enriched natural gas in the on-site CCGT, the use of natural gas in the gas turbine is displaced; and by distributing hydrogen-enriched natural gas to end-users, their use of conventional natural gas is also displaced.

Finally, as indicated by the research objectives, in order to be able to compare the UHNG technology with other energy storage alternatives, it is necessary to evaluate its performance in terms of a few benchmark parameters, commonly used for the assessment of storage options. Rated capacity and rated power are preferred over energy density and power capacity, since it is unrealistic and impractical to evaluate the “weight” of an underground storage reservoir, for it is not a device with finite dimensions and weight.

Table 3.5 List of energy storage benchmark parameters

Parameter	Description	Unit
Round trip efficiency	Defined as the AC to AC efficiency, involving all conversion steps in between	
Rated capacity	The maximum amount of electrical energy that can be stored (usually in the form of another vector)	MWh
Rated power	The maximum rate at which electricity can be stored or discharged	MW
Self-discharge rate	The rate at which stored energy is lost from storage	
Durability	The physical life time of the project	years
Cost of storage	The capital cost required to setup storage facility, expressed both in terms storage capacity ($/MWh) and rated power ($/MW)	$/MWh $/MW

Chapter 4
Physical Model Development

The physical model is made up by smaller models, each representing a component of the energy hub: the storage reservoir, wind turbines, electrolyzers, the gas turbine, the separator, and compressors. The decision points connect individual component models and allow for interaction with the exogenous environmental variables.

The architecture of the overall physical model is illustrated by Figure 4.2: Information flow from the top to the bottom. Decision points are shown as diamonds and the component technologies sub-models, are shown as double-sided boxes. Once simulation is initiated, information about the decision variables: configuration of energy hub, ratings of components, and the model logic of all decision points are loaded into the model. After initialization, the model logic at D1 and D2 drives the key activities at the storage reservoir: dictating the operations occurring at the storage reservoir and the electrolyzer, respectively. Their outputs are in turn routed toward D3, D4, D5, D6 and other sub-models, which determines the value of all other relevant physical variables based on prescribed decision point logic and physical constraints.

The decision point logic used for each scenario is described in Chapter 7. In this chapter, the physical constraints contained by each physical sub-model are described. The most important constraints are the constraint connecting physical input to output, the constraint on maximum or minimum output from a component, and the constraint connecting consecutive physical output in time. Depending on the type of component, the nature of the above-mentioned constraints differs (Table 4.1).

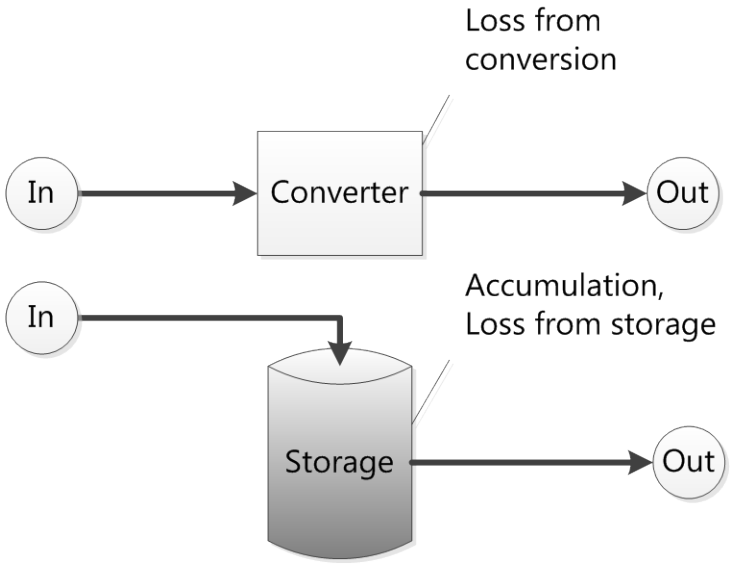

Figure 4.1 Mass balance difference between converters and storage devices

Table 4.1 Differences in constraints for converters and storage devices

	Converter	Storage reservoir
Relationship between input and output for a given period	Coupled, usually through efficiency	Decoupled because of the presence of inventory, which is limited by the storage capacity
Maximum input/output	Limited by rated power/feed	Limited by injectability/deliverability, which is dependent on surface and reservoir conditions
Maximum difference allowed between consecutive outputs in time	Limited by ramp rate	Limited by rate of change of injectability/deliverability, which is dependent on rate of change of surface and reservoir conditions

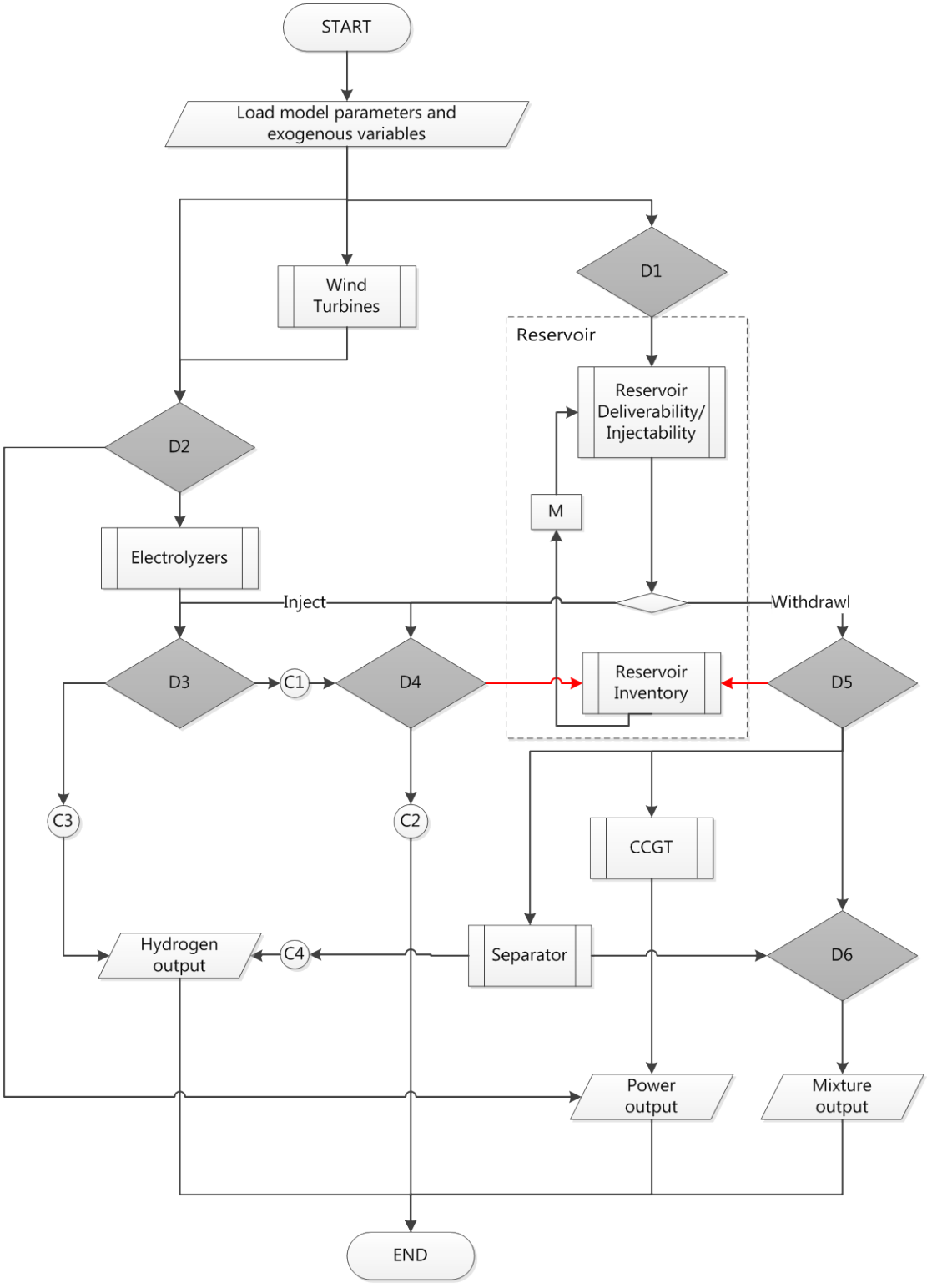

Figure 4.2 Architecture of the energy hub physical model

4.1 Storage Reservoir

The storage reservoir is at the center of the concept of UHNG and the most important component of the energy hub. It is the only component in which accumulation can occur, which influences the possible flow rates to/from it. The input that this sub-model is expected to accept is the reservoir dispatch order, the flow rate of injected gas or withdrawn gas, the quantity of hydrogen injected (if applicable), and the initial reservoir conditions; the outputs that are expected are the reservoir inventory, the reservoir pressure, the wellhead pressure, the concentration of hydrogen of the stored gas, and the injectability/deliverability allowed by the most recent reservoir conditions. For this study, the physical storage capacity and well injectability/deliverability of the geological reservoir is not altered at will as a decision variable. The information on storage capacity is obtained for a specific reservoir in Southwestern Ontario. If the model is to be adapted for any other reservoir, those parameters in the original model also need to be adapted.

4.1.1 Storage Capacity and Inventory

The reservoir modeled is a depleted gas reservoir in Ontario, chosen for its representativeness of reservoir available in the region.

4.1.1.1 Determination of Reservoir Capacity

If the capacity of a gas reservoir is not already known, it can be estimated by calculating its pore space volume available for gas storage, using values measured by geological surveys. But, this scenario is highly unlikely, because reservoirs which are candidates for gas storage are depleted ones with well-known configurations and a long production history.

$$V_{\max} = Ah\varphi(1 - S_{wi}) \tag{4.1}$$

V_{max}: Maximum reservoir pore volume, m^3

A: Original productive area of reservoir, m^2

For cylindrical reservoirs, $A = \pi r^2$,where r is the radius of the reservoir

h: Net effective formation thickness, m

φ: Porosity

S_{wi}: Interstitial water saturation

For this model, it is assumed that the reservoir may be treated as a constant-volume tank whose volume does not change with reservoir pressure, because the change in porosity with pressure is negligible; and the change in interstitial water volume and the evolution of gas dissolved in the water are also negligible. Therefore, V_{max} is treated as a constant.

For a reservoir with known capacity, the value reported $V_{max,s}$ is typically expressed in terms of standard volume of natural gas that can be stored at maximum reservoir pressure. The standard volume is the space that the maximum amount of storable gas occupies under standard conditions. The two values are related through the use of gas formation volume factor B_g.

$$V_{max} = B_g V_{max,s} \tag{4.2}$$

$$B_g = \frac{p_s T_{res} z_{res}}{p_{res} T_s z_s} \tag{4.3}$$

V_{max}: Maximum reservoir pore volume, m^3

$V_{max,s}$: Maximum reservoir capacity for natural gas, sm^3

B_g: Gas formation volume factor for maximum reservoir pressure, m^3sm^{-3}

p_s: Standard pressure, 14.7 psi = 1.01 bar

$p_{res,max}$: Maximum reservoir pressure, bar

T_s: Standard temperature, 520 °R = 288 K

T_{res}: Reservoir temperature, K

z_s: Compressibility factor under standard conditions = 1

$z_{res,max}$: Compressibility factor at maximum reservoir pressure

Once $V_{max,s}$ is known, it is possible to determine the actual reservoir pore volume V_{max} for subsequent inventory calculations. The standard conditions used in Equation (4.3) are the base conditions recognized in North America for large-volume fuel gas measurements [83]. For the determination of reservoir capacity in standard volume units, the average reservoir pressure is equivalent to the maximum allowable reservoir pressure.

The compressibility of a gas is a function of its pressure, temperature and composition. Since the reservoir conditions are constantly changing pressure and composition-wise, it is necessary to

establish the values of the compressibility factor for the range of reservoir conditions expected. In this project, the bulk of the gas stored in the reservoir is natural gas blended with some hydrogen. The range of pressure expected for this model is between 1 bar to 111 bar, the reservoir temperature is assumed to be constant at 298 K. The compressibility factor for the mixture is estimated for the full range of hydrogen concentration (mole %) possible, from 0 to 100%, while natural gas that makes up the rest of the mixture has composition as shown in Table 4.2. The compressibility factor for mixtures of different pressure and composition at four temperatures between 273 to 323K is determined using the physical property methods included within Aspen Plus, using the SRK equation of state. Then, the data obtained is used for subsequent interpolation, through the interface of a three dimensional lookup table in Simulink. Viscosity values for the same pressure range and concentration range are also computed similarly. The outputs of Aspen Plus are tabulated and shown in Table 4.3and Table 4.4.

Table 4.2 Molar Composition of Natural Gas [84]

Compound	mole %
Methane	95.0%
Ethane	2.5%
Propane	0.2%
Butane	0.1%
Pentane + heavier	0.0%
Nitrogen	1.6%
Carbon Dioxide	0.7%
Hydrogen Sulphide	0.0%
Water	0.0%

Table 4.3 Compressibility factor of hydrogen/natural gas mixture as a function of pressure, composition and temperature

Pressure (bar)	1	11	21	31	41	51	61	71	81	91	101	111
0% H_2												
273 K	1.00	0.97	0.95	0.92	0.90	0.88	0.86	0.84	0.82	0.80	0.79	0.78
323 K	1.00	0.99	0.97	0.96	0.95	0.94	0.93	0.92	0.92	0.91	0.90	0.90
373 K	1.00	0.99	0.99	0.98	0.98	0.97	0.97	0.97	0.96	0.96	0.96	0.96
423 K	1.00	1.00	1.00	0.99	0.99	0.99	0.99	0.99	0.99	0.99	0.99	0.99
20% H_2												
273 K	1.00	0.98	0.97	0.96	0.95	0.93	0.92	0.91	0.91	0.90	0.89	0.89
323 K	1.00	0.99	0.99	0.98	0.98	0.97	0.97	0.97	0.96	0.96	0.96	0.96
373 K	1.00	1.00	1.00	0.99	0.99	0.99	0.99	0.99	0.99	0.99	1.00	1.00
423 K	1.00	1.00	1.00	1.00	1.00	1.00	1.01	1.01	1.01	1.01	1.01	1.02
40% H_2												
273 K	1.00	0.99	0.99	0.98	0.98	0.98	0.97	0.97	0.97	0.97	0.97	0.97
323 K	1.00	1.00	1.00	1.00	1.00	1.00	1.00	1.00	1.00	1.00	1.00	1.01
373 K	1.00	1.00	1.00	1.00	1.01	1.01	1.01	1.01	1.01	1.02	1.02	1.02
423 K	1.00	1.00	1.00	1.01	1.01	1.01	1.02	1.02	1.02	1.03	1.03	1.03
60% H_2												
273 K	1.00	1.00	1.00	1.00	1.00	1.00	1.01	1.01	1.01	1.01	1.02	1.02
323 K	1.00	1.00	1.00	1.01	1.01	1.01	1.02	1.02	1.02	1.03	1.03	1.03
373 K	1.00	1.00	1.01	1.01	1.01	1.02	1.02	1.02	1.03	1.03	1.04	1.04
423 K	1.00	1.00	1.01	1.01	1.01	1.02	1.02	1.03	1.03	1.03	1.04	1.04
80% H_2												
273 K	1.00	1.00	1.01	1.01	1.02	1.02	1.03	1.03	1.04	1.04	1.05	1.05
323 K	1.00	1.00	1.01	1.01	1.02	1.02	1.03	1.03	1.04	1.04	1.05	1.05
373 K	1.00	1.00	1.01	1.01	1.02	1.02	1.03	1.03	1.04	1.04	1.05	1.05
423 K	1.00	1.00	1.01	1.01	1.02	1.02	1.03	1.03	1.03	1.04	1.04	1.05
100% H_2												
273 K	1.00	1.01	1.01	1.02	1.02	1.03	1.03	1.04	1.05	1.05	1.06	1.06
323 K	1.00	1.01	1.01	1.02	1.02	1.03	1.03	1.04	1.04	1.05	1.05	1.06
373 K	1.00	1.00	1.01	1.01	1.02	1.02	1.03	1.03	1.04	1.04	1.04	1.05
423 K	1.00	1.00	1.01	1.01	1.02	1.02	1.02	1.03	1.03	1.04	1.04	1.04

Table 4.4 Viscosity of hydrogen/natural gas mixture as a function of pressure, composition and temperature

Visc.(μPa·s)	1	11	21	31	41	51	61	71	81	91	101	111
0% H_2												
273 K	10.3	10.5	10.7	10.9	11.2	11.6	12.0	12.5	13.0	13.5	14.2	14.8
323 K	11.9	12.0	12.2	12.4	12.6	12.9	13.1	13.4	13.8	14.1	14.5	14.9
373 K	13.4	13.5	13.7	13.8	14.0	14.2	14.4	14.6	14.8	15.1	15.4	15.6
423 K	14.9	14.9	15.0	15.2	15.3	15.5	15.6	15.8	16.0	16.2	16.4	16.6
20% H_2												
273 K	10.9	11.0	11.2	11.4	11.6	11.8	12.1	12.4	12.7	13.1	13.4	13.8
323 K	12.6	12.7	12.8	12.9	13.1	13.3	13.5	13.7	13.9	14.1	14.4	14.6
373 K	14.1	14.2	14.3	14.4	14.5	14.6	14.8	15.0	15.1	15.3	15.5	15.7
423 K	15.6	15.6	15.7	15.8	15.9	16.0	16.1	16.2	16.4	16.5	16.7	16.8
40% H_2												
273 K	11.4	11.5	11.6	11.7	11.9	12.0	12.2	12.4	12.6	12.8	13.0	13.3
323 K	13.0	13.1	13.2	13.3	13.4	13.5	13.6	13.8	13.9	14.1	14.2	14.4
373 K	14.5	14.6	14.7	14.7	14.8	14.9	15.0	15.1	15.3	15.4	15.5	15.6
423 K	16.0	16.0	16.1	16.1	16.2	16.3	16.4	16.5	16.6	16.7	16.8	16.9
60% H_2												
273 K	11.6	11.6	11.7	11.8	11.9	12.0	12.1	12.2	12.3	12.4	12.6	12.7
323 K	13.1	13.2	13.2	13.3	13.3	13.4	13.5	13.6	13.7	13.8	13.9	14.0
373 K	14.6	14.6	14.6	14.7	14.8	14.8	14.9	15.0	15.0	15.1	15.2	15.3
423 K	15.9	16.0	16.0	16.0	16.1	16.1	16.2	16.3	16.3	16.4	16.4	16.5
80% H_2												
273 K	11.0	11.0	11.1	11.1	11.2	11.2	11.3	11.3	11.4	11.5	11.5	11.6
323 K	12.4	12.4	12.4	12.5	12.5	12.6	12.6	12.6	12.7	12.7	12.8	12.9
373 K	13.7	13.7	13.7	13.7	13.8	13.8	13.8	13.9	13.9	14.0	14.0	14.1
423 K	14.9	14.9	14.9	15.0	15.0	15.0	15.0	15.1	15.1	15.1	15.2	15.2
100% H_2												
273 K	8.6	8.6	8.6	8.7	8.7	8.7	8.7	8.7	8.8	8.8	8.8	8.9
323 K	9.6	9.6	9.6	9.7	9.7	9.7	9.7	9.7	9.7	9.8	9.8	9.8
373 K	10.6	10.6	10.6	10.6	10.6	10.6	10.6	10.7	10.7	10.7	10.7	10.7
423 K	11.5	11.5	11.5	11.5	11.5	11.5	11.6	11.6	11.6	11.6	11.6	11.6

4.1.1.2 Reservoir Inventory

The reservoir inventory is the amount of gas that has accumulated within the storage reservoir; it changes with the flow rate of gas coming in and out of the reservoir. Assuming no water influx into the reservoir, and negligible loss from the reservoir during storage, the simplest material balance can be applied (time is treated as discrete steps).

$$n_{tot} = n_{tot,0} + \left(\dot{n}_{in} - \dot{n}_{out}\right)\Delta t \tag{4.4}$$

n_{tot}: Total amount of gas in-place at end of time step, kmol

$n_{tot,0}$: Initial amount of gas in-place, kmol

$\dot{n}_{s,in}$: Injection rate during time step, kmol/h

$\dot{n}_{s,out}$: Production rate during time step, kmol/h

Δt: Time step = 1 h

In this model, it is assumed that injection and withdrawal cannot take place at this same time (i.e. $\dot{n}_{s,in}$ and $\dot{n}_{s,out}$ cannot be both non-zero during the same time step. Therefore, Equation (4.4) is simplified to the following:

$$n_{tot} = n_{tot,0} + \left(\dot{n}_{s,act}\right)\Delta t \tag{4.5}$$

Here, $\dot{n}_{s,act}$ is a value which can take on both positive and negative values: it is positive when injection takes place; it is negative when gas is withdrawn from the reservoir.

As the value of reservoir inventory is update at every time step, the concentration of hydrogen in the stored gas is also updated:

$$c_{H_2,res} = \frac{n_{H_2,tot}}{n_{tot}} \tag{4.6}$$

$$c_{H_2,res,0} = \frac{n_{H_2,tot,0}}{n_{tot,0}} \tag{4.7}$$

$$n_{H_2,tot} = \begin{cases} n_{H_2,tot,0} + \dot{n}_{H_2,in}\Delta t, \text{ if } \dot{n}_{s,act} \geq 0 \\ n_{H_2,tot,0} + \left(\dot{n}_{s,act} c_{H_2,res,0}\right)\Delta t, \text{ if } \dot{n}_{s,act} < 0 \end{cases} \tag{4.8}$$

$c_{H_2,res}$: Concentration of hydrogen in stored gas, mol %

$n_{H_2,tot}$: Amount of hydrogen in storage, kmol

n_{tot}: Total amount of gas in storage, kmol

$\dot{n}_{H_2,in}$: Injection rate of hydrogen, kmol/h

$\dot{n}_{s,act}$: Injection/withdrawal rate, kmol/h

Δt: Time step = 1 h

Since the reservoir can be perceived as a constant volume vessel, as the amount of gas in place fluctuates, the pressure inside the reservoir also changes. For this model, instead of defining pressure as a function of the radial distance from the production/injection well, the average reservoir pressure is used. Once the amount of gas in-place is known, the pressure of gas in storage can be related through the real gas law.

$$\overline{p}_{res} = \frac{n_{tot} z_{res} R T_{res}}{V_{\max}} \tag{4.9}$$

$\overline{p}_{res}$: Average reservoir pressure, bar

V_{max}: Maximum reservoir pore volume, m^3

z_{res}: Gas compressibility factor at reservoir conditions

R: Gas constant, $8.314 \times 10^{-2}\, m^3 bar \left(K \times kmol\right)^{-1}$

T_{res}: Reservoir temperature = 298 K

However, because compressibility factor z is a function of reservoir pressure and gas composition, only $\overline{p}_{res}/z$ can be calculated from the amount of gas in-place. In this model, a three dimensional lookup table is generated to interpolate pressured based on the temperature, composition and $\overline{p}_{res}/z$ values associated with the pressure.

While injecting or producing from the reservoir, the average reservoir pressure – and the gas inventory by extension – is subjected to two constraints:

1. The average reservoir pressure cannot exceed the maximum allowable reservoir pressure:

$$\overline{p}_{res} \leq p_{res,\max} \tag{4.10}$$

The maximum allowable reservoir pressure, also known as the maximum design pressure, is the operating pressure beyond which the structural integrity of the cap rock might be compromised. The recommended range of P_{max} is 0.65 to 0.70 psi/ft of depth (0.15 to 0.16 bar/m of depth) [83]. This value is typically provided by the operator of the UGS facility in question. In order to maintain reservoir pressure below the maximum allowable value at all times, once reservoir pressure has surpassed a certain threshold value, no more injection into the reservoir will be able to take place unless reservoir pressure is lowered below threshold from gas production.

Since reservoir pressure is dependent on the gas in inventory, this upper-bound on reservoir pressure also limits how much gas can be stored safely inside the reservoir. As shown in the equation below, the maximum gas inventory differs for different mixture composition, because the term $z_{res,\max}$ is a function of composition.

$$n_{tot,\max} = \frac{V_{\max} p_{res,\max}}{RT_{res}} \left(\frac{1}{z_{res,\max}} \right) \tag{4.11}$$

As the concentration of hydrogen in the mixture increases, the compressibility factor of the mixture also increases, leading to a reduced amount of gas in inventory, for the same maximum reservoir pressure (Figure 4.3). At 0% H_2, the maximum amount of inventory allowed by the reservoir is 7641 MMscf; at 100% H_2, this number is lowered to 6163 MMscf.

Physically, this means that the reservoir's storage capacity is reduced when natural gas enriched hydrogen is stored, when compared to its original storage capacity that is rated for pure natural gas. For, if the inventory is not reduced, the gas in storage will be at a pressure which is superior to the upper threshold that can be supported by the reservoir rock.

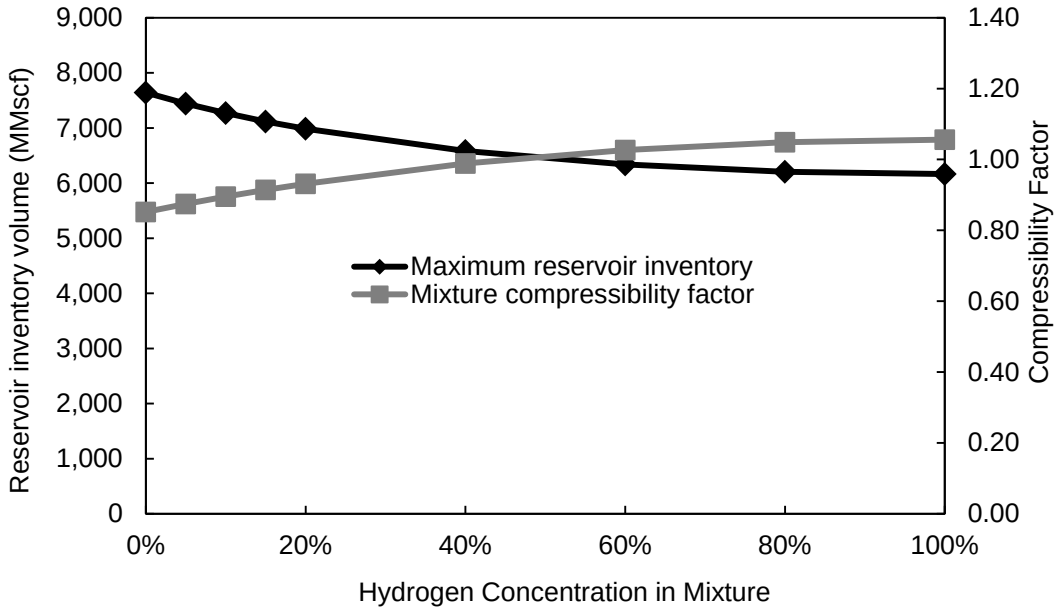

Figure 4.3 Reservoir maximum inventory and mixture compressibility factor for stored gas mixture of different hydrogen concentrations

2. The average reservoir pressure cannot fall below the minimum allowable reservoir pressure:

$$\overline{p}_{res} \geq p_{res,\min} \tag{4.12}$$

Below the minimum reservoir pressure, gas production from the reservoir becomes economically unattractive. Since gas is produced from the reservoir using reservoir pressure as the main driving force, the wellhead (surface) pressure is limited by the reservoir pressure. Once the wellhead pressure falls below the minimum operating pressure of the distribution network, additional energy is required to compress gas, adding to the cost of storage.

Oftentimes, the minimum reservoir pressure is not provided directly. Instead, the cushion gas volume in standard units is given, cushion gas being the minimum amount of gas that must remain within the reservoir while it is in operation. In order to maintain reservoir pressure above the minimum allowable value at all times, once reservoir pressure has dropped below a threshold value, no more gas production is allowed from the reservoir, unless reservoir pressure is increased from gas injection. The cushion gas volume is related to the minimum reservoir pressure as follows:

$$n_{tot,\min} = \frac{p_{res,\min} V_{\max}}{z_{res,\min} R T_{res}} = \frac{p_s V_{cushion,s}}{R T_s} \tag{4.13}$$

$$\frac{p_{res,\min}}{z_{res,\min}} = \frac{p_s V_{cushion,s} T_{res}}{T_s V_{\max}} \tag{4.14}$$

$n_{tot,min}$: Minimum gas inventory level in reservoir (cushion gas), mol

p_{min}: Minimum reservoir pressure, bar

$V_{cushion,s}$: Amount of cushion gas required, sm^3

Analogous to the change in maximum reservoir inventory, the minimum inventory, or the amount of cushion gas needed, is also affected by the composition of the mixture in storage; the volume of gas needed to maintain the minimum reservoir pressure is reduced (Table 4.7). At 0% H_2, the cushion gas requirement of the reservoir is 1246 MMscf; at 100% H_2, this number is lowered to 1190 MMscf.

The difference between the maximum inventory and the cushion gas required is the maximum working gas volume. In Figure 4.5, the maximum working gas volume is shown as a function of hydrogen concentration. It can be seen that the maximum working gas volume available decreases as the mixture becomes richer in hydrogen. At 0% H_2, the cushion gas requirement of the reservoir is 6395 MMscf; at 100% H_2, this number is 4974 MMscf, or 78% of the original value.

An important simplifying assumption has been made when applying the two constraints: there is no variation in pressure inside the reservoir, the pressure is distributed uniform throughout the structure; its value is represented by the average reservoir pressure. As reservoir pressure increases or decreases, it does so by the same extent at every point within the reservoir.

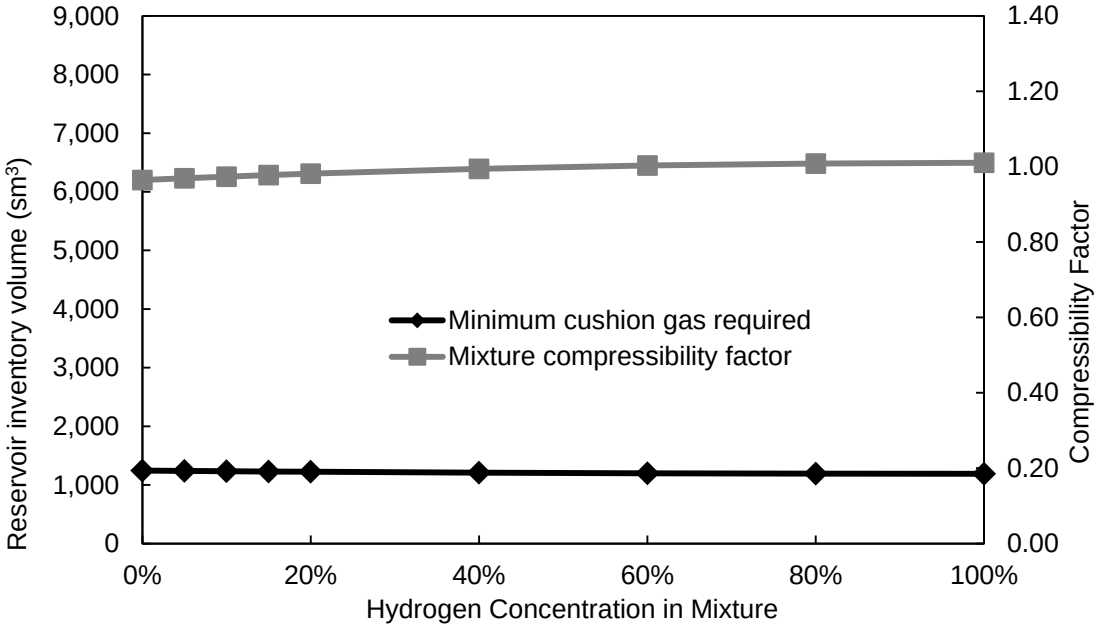

Figure 4.4 Reservoir cushion gas requirement and mixture compressibility factor for stored gas mixture of different hydrogen concentrations

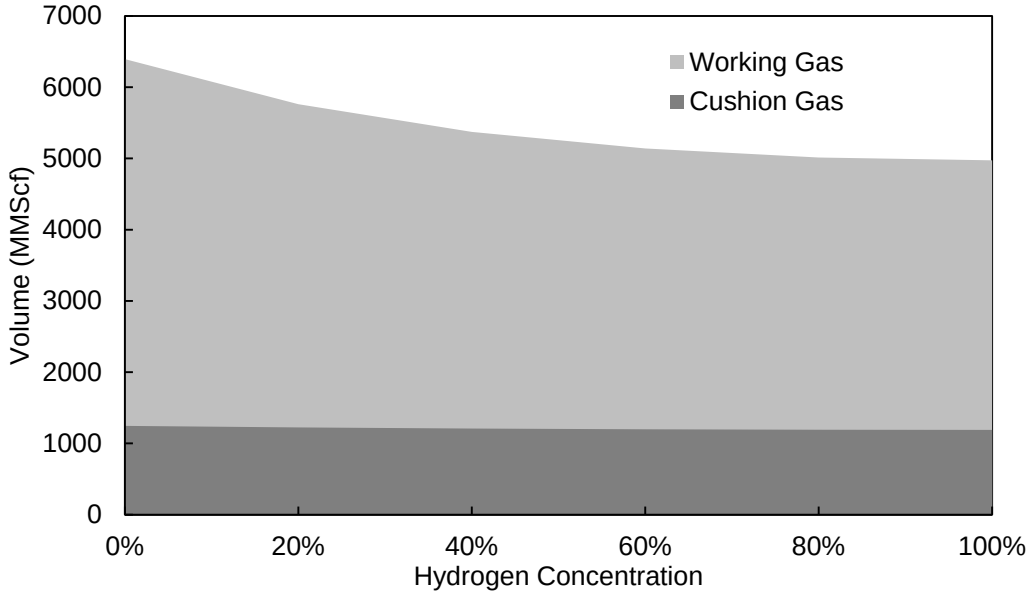

Figure 4.5 Maximum working gas volume available and cushion gas requirement for different hydrogen concentration in stored mixture

4.1.2 Injectability and Deliverability

For the reservoir modeled, assumed to be without an active water drive, the driving force for gas injection and production is the pressure difference between the reservoir and the surface [67]. Therefore, the flow of gas that can be injected or delivered is mainly dependent on reservoir and wellhead pressures. The possible values of average reservoir pressure are delimited by the constraints outlined in the previous section. As for the wellhead pressure: during injection, it is limited by maximum allowable pressure; during production, it is limited by the minimum operating pressure of the distribution network.

At all times, operating regime of the storage reservoir is controlled by changing the wellhead pressure. The wellhead pressure is changed as a function of the dispatch order to the reservoir. Three types of dispatch order are expected:

1. The well is shut-in and there is no flow in or out of reservoir;
2. The well produces gas from reservoir;
3. The well injects gas into reservoir;

These three types of situation can all be related to the pressure at different points of the reservoir-well system:

$$\underbrace{p_{wh} - \overline{p}_{res}}_{\text{1. overall } \Delta p} = \underbrace{(p_{wh} - p_{bh})}_{\substack{\text{2. } \Delta p \text{ from tubing-flow} \\ \text{(height diff. and friction)}}} + \underbrace{(p_{bh} - \overline{p}_{res})}_{\text{3. } \Delta p \text{ driving reservoir flow}} \tag{4.15}$$

p_{wh}: Wellhead pressure, bar
$\overline{p}_{res}$: Average reservoir pressure , bar
p_{bh}: Bottom-hole pressure, bar

4.1.2.1 Shut-in Well

For the first case, there is no flow from the reservoir, so $p_{bh} = \overline{p}_{res}$, therefore the only difference between the wellhead pressure and the reservoir pressure is the hydrostatic pressure caused by the height difference. The following equation between the two can be derived from extended the Bernoulli equation:

$$p_{wh,shut-in} = \frac{p_{bh}}{\exp\left(N_{gp}\right)} = \frac{\overline{p}_{res}}{\exp\left(N_{gp}\right)} \tag{4.16}$$

$$N_{gp} = \frac{M_{mix} g L \cos\alpha}{\overline{z} R \overline{T}} \tag{4.17}$$

N_{gp} is a dimensionless number characterizing the ratio of gravitational forces to pressure forces

M_{mix}: Molecular weight of gas mixture, kg/kmol

g: Acceleration of gravity = 9.8N/kg

L: Length of borehole, m

α: Angle of tubing with vertical = 0°

$\overline{z}$: Average compressibility factor

R: Gas constant

$\overline{T}$: Average temperature, K

For the pressure range of interest (p_{res} from 20 to 110 bar), the wellhead pressure required to maintain shut-in conditions is shown in Figure 4.6.

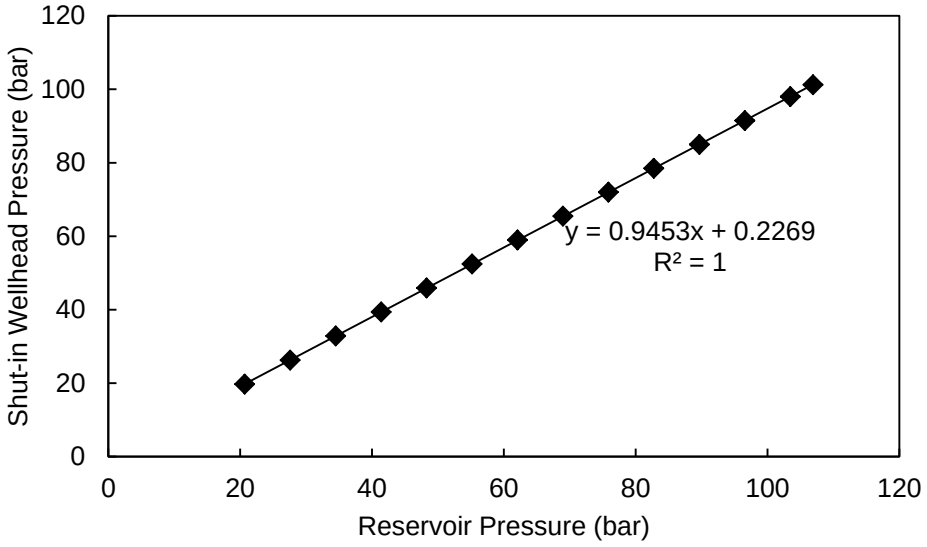

Figure 4.6 Shut-in wellhead pressure as a function of reservoir pressure

For this project, the values of injectability and deliverability are pre-established outside of the physical model using physical correlations. During modeling and simulation, the pre-established values are used as a two-dimensional look-up table to facilitate computation. The pressure range for

which injectability and deliverability needs to be established is as follows: p_{wh} ranging from 300 to 1400 psi (20.4 to 95.2 bar) and $\overline{p}_{res}$ ranging from 400 to 1550 psi (27.2 bar to 105.4 bar).Whenever the wellhead pressure exceeds the shut-in pressure corresponding to a given reservoir pressure, injection occurs, and production occurs when the well-head pressure is lower than the shut-in pressure.

4.1.2.2 Producing Well Deliverability

For the second case, in which gas is produced from the reservoir, the bottom-hole pressure is different from the average reservoir pressure, because this pressure difference must exist so that the reservoir gas can be driven through the porous rock of the reservoir from the outer region to reach the bottom-hole. The pressure difference between the bottom-hole pressure and the reservoir pressure is no longer static; it is now also a function of the frictional losses that occur as gas from the reservoir travels through the wellbore toward the surface.

The flow of gas through the porous rock, also called well-inflow performance, can be described by the Schelhard backpressure equation. The backpressure equation, an empirical exponential equation, is used to express the relationship between flow rate, reservoir pressure and the bottom-hole pressure for a well flowing at stable conditions or semi-steady-state conditions. The value of the empirical parameters C and n are determined from well test data provided by the UGS facility operator [67]. There are six injection/withdrawal wells at the storage site. But, to simplify the solution, only the well with the largest deliverability is considered.

$$Q_{s,out} = C\left(\overline{p}_{res}^{2} - p_{bh}^{2}\right)^{n} \tag{4.18}$$

$Q_{s,out}$:Gas production flow rate in standard volume per unit time, MMscf/day
C: Empirical coefficient for backpressure equation
n: Empirical exponent for backpressure equation

In order to fully describe the path of produced gas, it is still necessary to quantify the relationship between the bottom-hole pressure and the wellhead pressure. To do so, it is necessary to understand the vertical flow in the wellbore, also known as tubing-flow performance which causes the pressure difference. The pressure difference is determined by the combined effects of gravity, wall friction and kinetic energy. Friction and kinetic energy are both dependent on the flow rate in the wellbore. The

bottom-hole pressure for a given wellhead pressure can be calculated through the following relationships, derived from the extended Bernoulli equation [85] :

$$p_{bh} = p_{wh}\left\{\exp\left(2N_{gp}\right) - \frac{N^*_{fp}}{2N_{gp}}\left[1-\exp\left(2N_{gp}\right)\right]\right\}^{1/2} \tag{4.19}$$

$$N^*_{fp} = \frac{4\bar{z}\bar{f}w^2_{mix}2\bar{T}L}{p^2_{wh}A^2 d_i M_{mix}} \tag{4.20}$$

N_{gp} is defined as in the case above; N^*_{fp} is a dimensionless number characterizing the ratio of friction forces to pressure forces.

$\bar{f}$: Average fanning friction factor

w_{mix}: Mass flow rate of gas mixture, kg/s

A: Cross-sectional area of tubing, m^2

d_i: Internal tubing diameter, m

The friction factor can be estimated using an empirical correlation which closely approximates the Colebrook equation [85]:

$$f = a + b\,\mathrm{Re}^{-c} \tag{4.21}$$

$$a = 0.026\left(\delta/d_i\right)^{0.225} + 0.133\left(\delta/d_i\right)$$

$$b = 22\left(\delta/d_i\right)^{0.44}$$

$$c = 1.62\left(\delta/d_i\right)^{0.134}$$

δ: Absolute wall roughness, m

Re: Reynolds number $= \dfrac{\rho v d_i}{\mu}$

ρ: Density of fluid, kg/m^3

ν: Mean velocity of fluid, m/s

μ: Dynamic viscosity of the fluid, $\mathrm{Pa}\cdot\mathrm{s}$

Note that, because of the effect of frictional losses within the wellbore, the bottom-well pressure is also a function of gas flow rate via w_{mix} ; therefore, Equations (4.18) and (4.19) need to be solved simultaneously. The backpressure equation is rewritten to express bottom-hole pressure as a function of the well flow rate and the average reservoir pressure.

$$p_{bh} = \sqrt{\overline{p}_{res}^2 - \left(\frac{Q_{s,out}}{C}\right)^{\frac{1}{n}}} \tag{4.22}$$

For each pair of well-head pressure and reservoir pressure, the Excel solver is used to find the value of $Q_{s,out}$ $Q_{s,out}$ which satisfies both Equation (4.19) and Equation (4.22), i.e. p_{bh} p_{bh} calculated through both methods are equal within a small margin. The flow rate thus determined is known as the deliverability of the well: it is the maximum amount of gas that can be produced from the reservoir given the reservoir and surface conditions. $Q_{s,out}$ $Q_{s,out}$ (MMscf/day) can be converted to $\dot{n}_s$ $\dot{n}_s$ $\dot{n}_s$ (kmol/h) through the use of conversion factors. Note that, because it is the withdrawing flow rate, which decreases the reservoir inventory, the corresponding $\dot{n}_s$ $\dot{n}_s$ values are negative.

4.1.2.3 Injecting Well Injectability

Injection of gas into the reservoir is the mirror image of the production process, and the same method described in the section above is used to determine the allowable injection flow rate, or injectability, for given pairs of reservoir and surface pressure.

During gas production, the gas from the reservoir needs to counter the effect of gravitational forces, whereas during gas injection, the injection is facilitated by the hydrostatic pressure from the gas column. The revised version of Equation(4.19), which contains a reversed sign in the term between braces to indicate the change in flow direction, is shown below:

$$p_{bh} = p_{wh}\left\{\exp\left(2N_{gp}\right) + \frac{N_{fp}^*}{2N_{gp}}\left[1 - \exp\left(2N_{gp}\right)\right]\right\}^{1/2} \tag{4.23}$$

N_{gp} and N_{fp}^* are defined as in the case above.

As for the case of the producing well, solving for the bottom-well pressure requires the knowledge of the gas injection rate. Therefore, the solution of the reservoir inflow performance equation is also required. Reservoir inflow performance is the relationship between the average reservoir pressure and the bottom-hole pressure during injection under semi-steady-state conditions, Equation (4.18)

also need to be modified to account for the reversed direction of gas flow [86], and the resulting expression of p_{bh} is updated.

$$Q_{s,in} = C\left(p_{bh}^2 - \overline{p}_{res}^2\right)^n \tag{4.24}$$

$$p_{bh} = \sqrt{\left(\frac{Q_{s,in}}{C}\right)^{\frac{1}{n}} + \overline{p}_{res}^2} \tag{4.25}$$

The pre-generated injectability and deliverability for all possible reservoir and wellhead pressure pairs are illustrated in Figure 4.7. In this figure, negative gas flow rates indicate that it is a withdrawal, whereas positive gas flow rates indicate that it is a case of injection. At low reservoir pressure, high injection rates are observed, and at high reservoir pressure, high withdrawal rates are observed. For the same reservoir pressure, if the wellhead pressure increases, then injection rate increases, while withdrawal rate decreases.

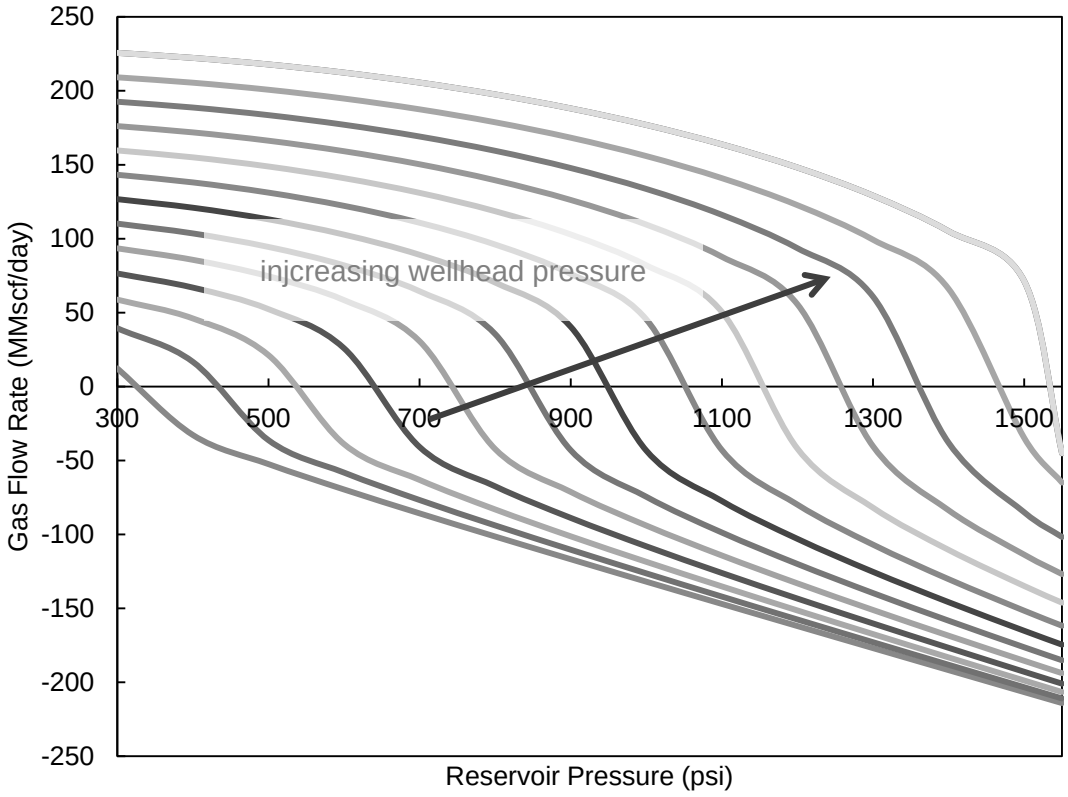

Figure 4.7 Reservoir flow rate as function of reservoir and wellhead pressure

It is assumed that the deliverability and injectability of the reservoir-well system is independent of hydrogen concentration. The values presented above are used in injectability/deliverability look-up regardless of hydrogen concentration.

Often, the gathering system at the reservoir is not sized to handle the flow rate corresponding to maximum deliverability, so that the deliverability that can be achieved is capped by the capacity of the gathering pipelines. In this model, such a limiting value is used on both injectability and deliverability:

$$\dot{n}_s = \begin{cases} \dot{n}_s, \text{ if } \left|\dot{n}_s\right| \le \dot{n}_{cap} \\ -\dot{n}_{cap}, \text{ if } \dot{n}_s < \dot{n}_{cap} \\ \dot{n}_{cap}, \text{ if } \dot{n}_s > \dot{n}_{cap} \end{cases} \tag{4.26}$$

4.1.3 Rate of Change for Injectability and Deliverability

It has been established that the deliverability and injectability of the reservoir well are functions of reservoir pressure and wellhead pressure, and that the reservoir pressure is a function of the inventory of the gas in storage. Thus, for a given reservoir state, the deliverability or injectability is adjusted by changing the wellhead pressure. The rate at which the wellhead pressure can be altered limits the rate at which deliverability and injectability can be ramped up or down. It is assumed that, for the reservoir modeled, the ramp rate of wellhead pressure is limited to 1 bar per hour. The possible values of wellhead pressure ranges from 20 bar to 110 bar. Thus, under the current assumption of ramp rate of 1 bar per hour, it will require about 90 hours to increase wellhead pressure from its minimum to the maximum value, in other words, slightly less than four days. The relationship between wellhead pressure and the dispatch order to the reservoir model is presented in Figure 4.8.

As Figure 4.2 shows, the reservoir model is broken down into two main blocks, one block is responsible for the computation of reservoir inventory and H_2 concentration at all times, the other one is responsible for determining the injectability/deliverability of the reservoir based on surface and reservoir conditions. In this case, reservoir conditions are communicated to the injectability deliverability block through the use of a memory block, which retains the value of inventory and hydrogen in storage from the previous time step; surface conditions, the wellhead pressure, is determined by the block based on the reservoir dispatch order and the value of wellhead pressure from the previous time step.

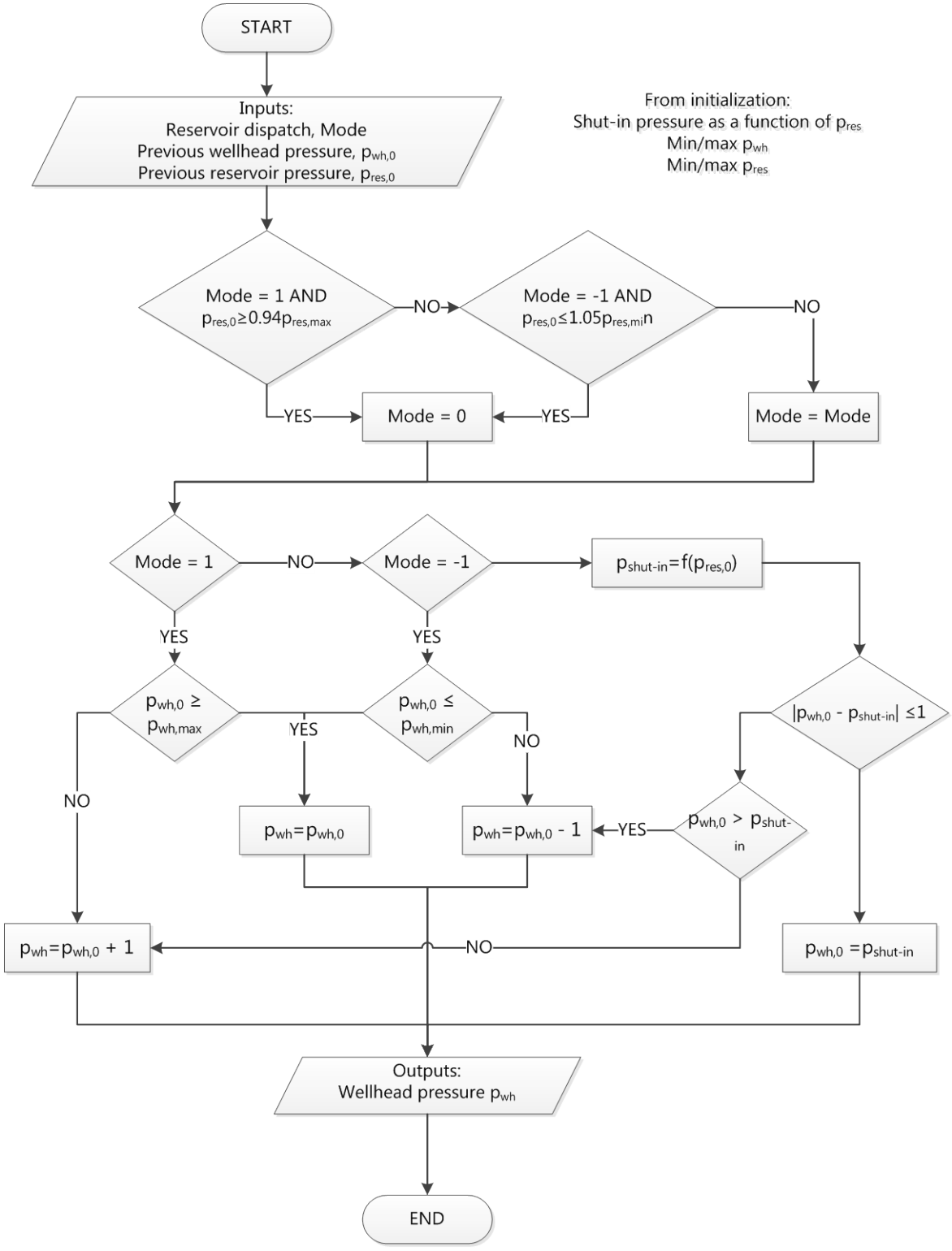

Figure 4.8 Wellhead pressure as a function of reservoir dispatch order

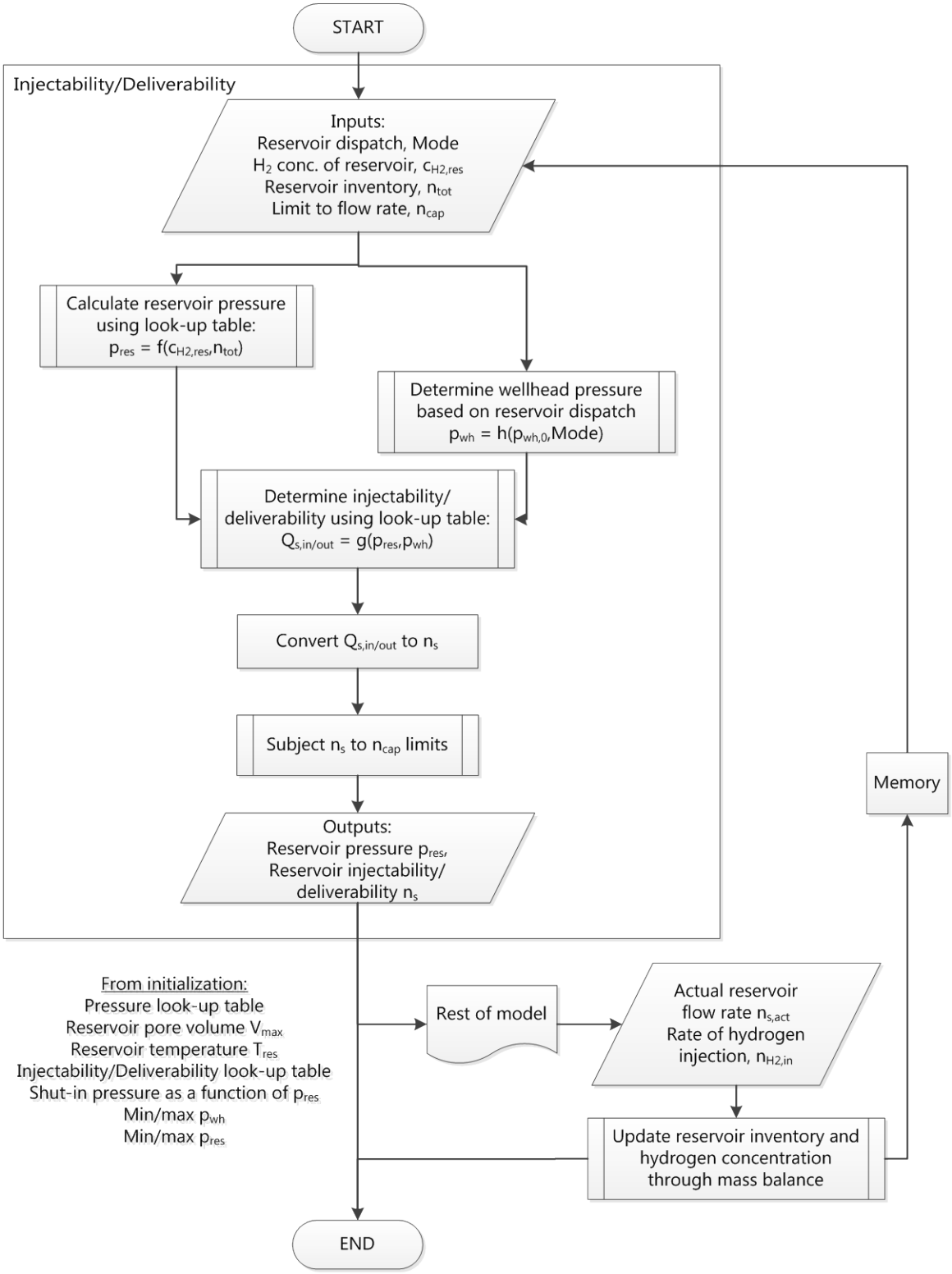

Figure 4.9 Model flow diagram for electrolyzers

Table 4.5 List of key variables and parameters for the reservoir model

Type	Description	Symbol	Value	Unit	Ref.
Input	Reservoir dispatch	$Mode$			
Output	Reservoir injectability/deliverability	$\dot{n}_s$		kmol/h	
	Reservoir inventory	n_{tot}		kmol	
	Reservoir H_2 conc.	$c_{H_2,res}$		mol. %	
Parameters	Maximum reservoir pore volume	$V_{\max}$	1.83E+06	m^3	Based on [67]
	Maximum reservoir capacity for natural gas	$V_{\max,s}$	7639	MMscf	[67]
	Standard pressure	p_s	1.01	bar	[83]
	Maximum reservoir pressure	$p_{res,\max}$	105.5	bar	[67]
	Standard temperature	T_s	288	K	[83]
	Reservoir temperature	T_{res}	298	K	Assumed
	Amount of cushion gas required	$V_{cushion,s}$	1271	MMscf	[67]
	Minimum reservoir pressure	$p_{res,\min}$	19.5	bar	Based on [67]
	Compressibility factor	z_{res}	Table 4.3		Aspen Plus
	Initial amount of gas in place	$n_{tot,0}$	2.40E+06	kmol	Assumed
	Initial amount of H_2 in place	$n_{H_2,tot,0}$	0	kmol	Assumed
	Initial wellhead pressure	$p_{wh,0}$	20.7	bar	Assumed
	Maximum wellhead pressure	$p_{wh,\max}$	103.4	bar	Estimated from $p_{res,\max}$
	Minimum wellhead pressure	$p_{wh,\min}$	20.7	bar	Assumed
	Limits to injectability and deliverability	$\dot{n}_{cap}$	5000	kmol/h	Estimated from range of $\dot{n}_s$
	Length of borehole	L	687.6	m	[67]
	Angle of tubing with vertical	α	0	degree	Assumed
	Empirical coefficient for backpressure equation	C	0.14		Based on [67]
	Empirical exponent for backpressure equation	n	0.53		Based on [67]
	Cross-sectional area of tubing	A	0.020		Based on [67]
	Internal tubing diameter	d_i	0.16	m	[67]
	Absolute wall roughness	δ	0.0015	mm	Estimated
	Dynamic viscosity of the fluid	μ	Table 4.4	Pa•s	Aspen Plus

4.2 Wind Turbines

The inputs that the wind turbine sub-model accepts are rated capacity, and local wind speed; the outputs expected from the wind turbines model are the quantity of wind power generation achievable given the local weather conditions.

4.2.1 Efficiency

Modern wind turbines are horizontal-axis type designs that harvest the kinetic energy present in wind. The power curve, the empirical relationship between the power output of an individual turbine and different wind speeds, such as the one shown below, is often available from wind turbine manufacturers.

$$P_{W,i} = f\left(u_{80}\right) \tag{4.27}$$

u_{80}:Wind speed at 80m above ground

$P_{W,i}$: Rated capacity of individual wind turbine

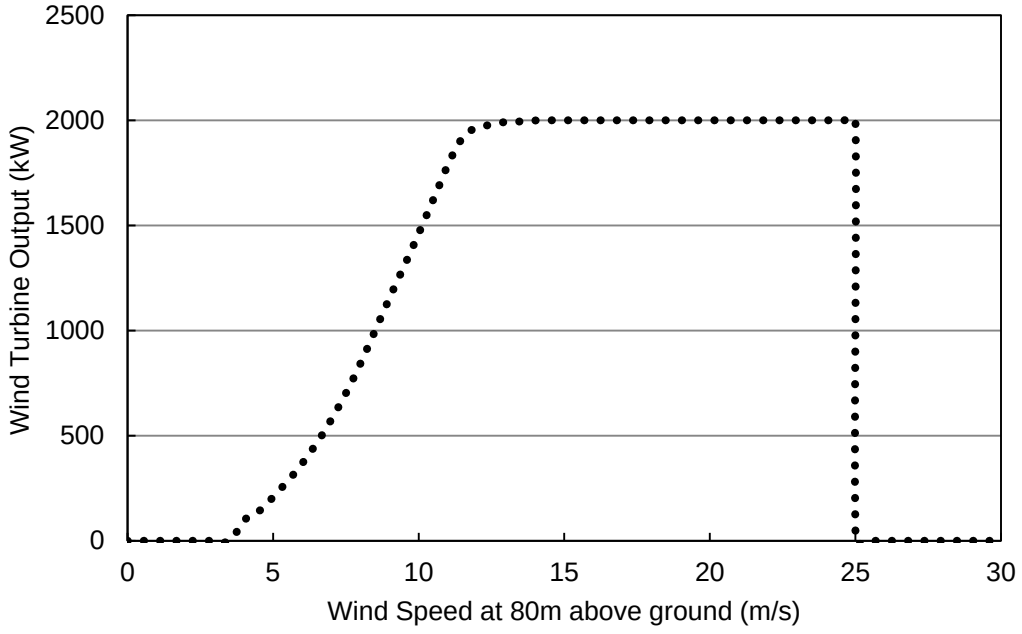

Figure 4.10 Power curve for V90 2.0MW wind turbine [69]

V90 2.0MW is a pitch regulated wind turbine with variable speed that is suitable for sites with medium to low wind speeds. For wind speed lower than 14m/s, the power curve is a function of wind speed. For wind speed ranging between 14 and 25m/s, the V90 wind turbine generates power at its rated capacity, 2.0MW. At wind speed lower than 4m/s (cut-in speed) or higher than 25m/s (cut-out speed), the wind turbine is not operated and the power output is zero.

The hourly wind speed for the region of Sarnia, where the reservoir is located, is known for the period simulated (2010-2012). The original measurements were conducted at 10m above ground level; the measured values are adjusted to match the height of the nacelle, at 80m above ground level.

$$u_{80} = u_{10}\left(\frac{80m}{10m}\right)^{\alpha} \tag{4.28}$$

u_{80}: Wind speed at 80m above ground
u_{10}: Wind speed at 10m above ground
α: Hellman exponent

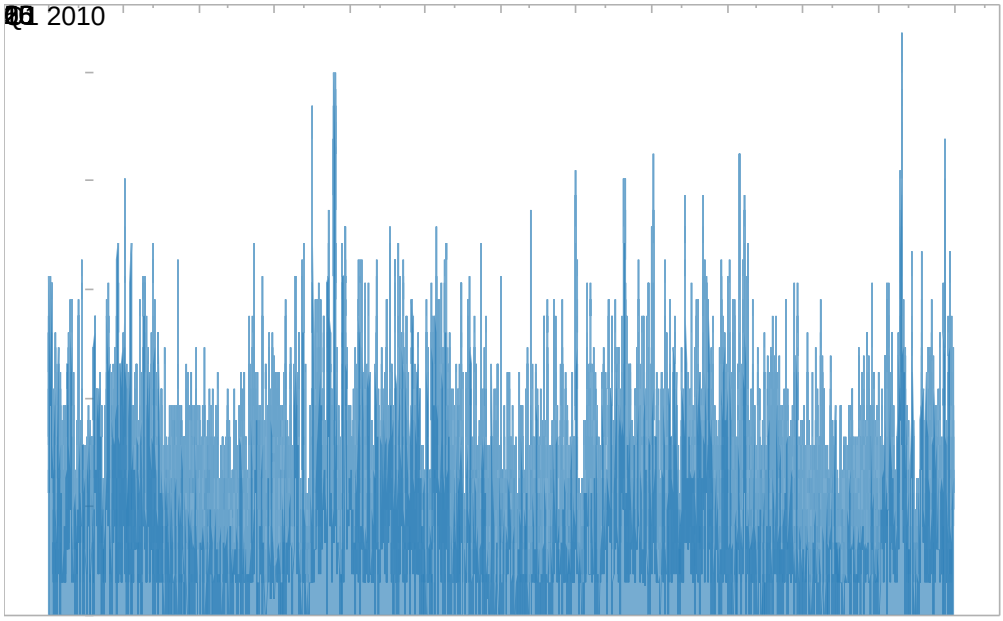

Figure 4.11 Hourly wind speed at Sarnia for 2010-2012 [87]

4.2.2 Rated power

The rated power output of the wind turbines is the total of rated power for individual units. For identical units:

$$P_{W,rated} = N_T P_{W,i,rated} \tag{4.29}$$

Since the rated power of individual unit is fixed, in order to change the rated capacity of the wind turbines overall, it is necessary to change the number of turbines in place n_T n_T n_T .Assuming that the individual wind turbines do not interfere with each other; the power generated on a wind farm is the sum of generation from individual turbines.

$$P_W = N_T P_{W,i} \tag{4.30}$$

The utilization factor of wind turbines can be calculated using the actual hourly power output and the rated power:

$$U_W(t) = \frac{P_W(t)}{P_{W,rated}} \tag{4.31}$$

4.2.3 Ramp rate

It is assumed that the wind turbines are able to ramp up and ramp down completely within one hour. In other words, the output of individual wind turbines can change from non-producing (0 MW) to maximum capacity (2 MW) within an hour.

Table 4.6 List of key variables and parameters for wind turbines model

Type	Description	Symbol	Value	Unit	Ref.
Input	Local wind speed at 80m of height	u_{80}	Time series for Sarnia from 2010-2012	m/s	[87]
Output	Wind power	P_W		MW	
	Utilization factor	U_W			
Parameters	Power curve for Vestas V90		See Figure 4.10		[69]
	Rated power of individual turbine	$P_{W,i,rated}$	2	MW	[69]
	Hellman constant	α	0.14		Estimated
	Number of wind turbines	N_T	From initialization		

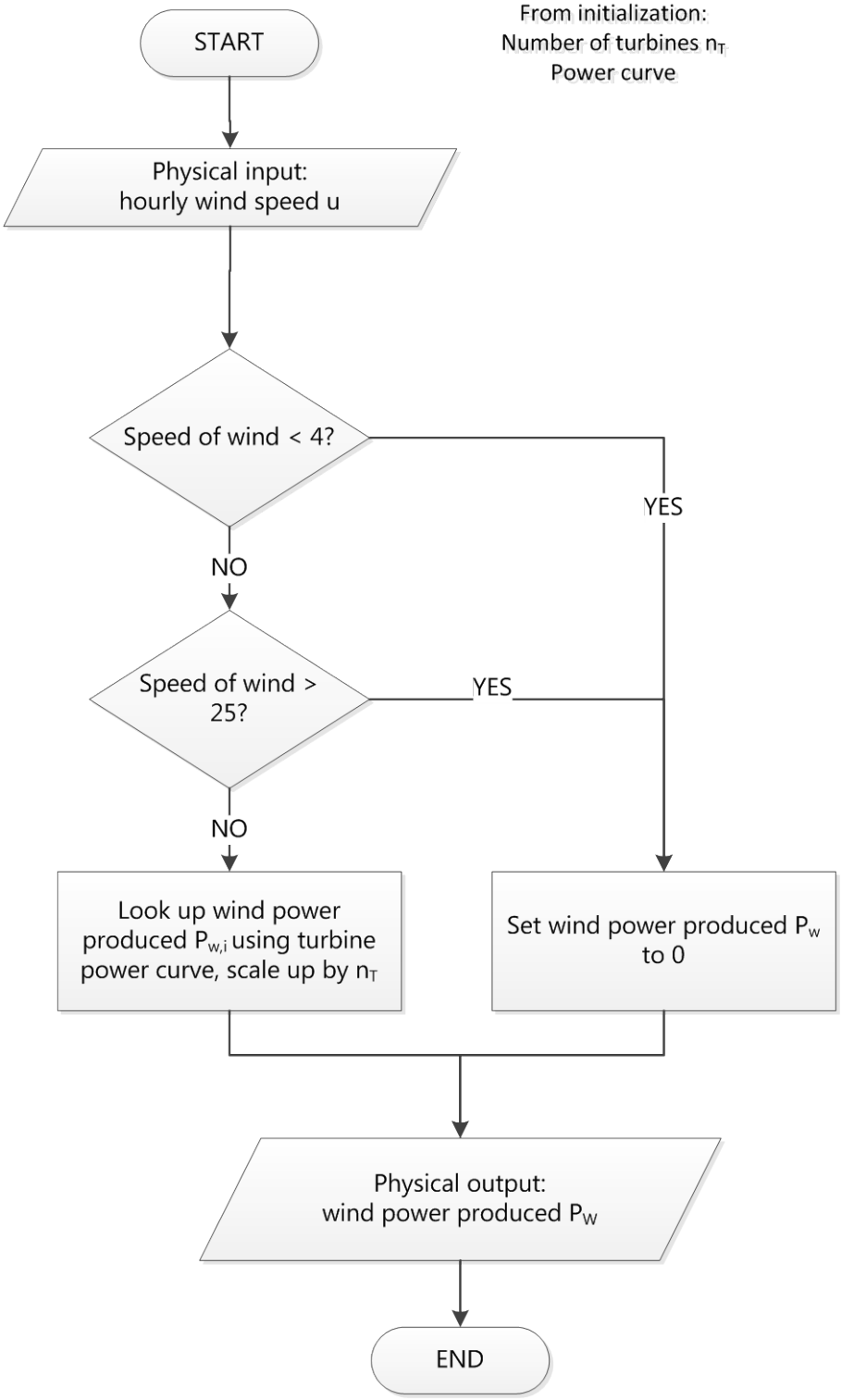

Figure 4.12 Model flow diagram for wind turbines

4.3 Electrolyzer

The input accepted by the electrolyzer sub-model is the actual power supplied. The output expected from this sub-model is the quantity of hydrogen produced from power available.

4.3.1 Efficiency

The energy requirement of an electrolyzer varies with its hydrogen production and the energy required per unit of hydrogen production. The energy required for production consists of two parts: the energy required by the electrolyzer itself (stacks) and the energy required by the auxiliary equipment such as water pumps. The energy requirement of the stacks is assumed to represent 90% of the overall energy requirement, based on figures provided by Ivy [43]. The energy requirement of the stacks changes with the stack efficiency; at 100% stack efficiency, the theoretical work required to produce hydrogen via electrolysis is equivalent to the higher heating value (HHV) of hydrogen.

$$P_{E,i} = \dot{n}_{E,H_2,i} E_E \tag{4.32}$$

$$E_E = E_{E,s} + E_{E,a} = E_{E,s} / 0.90 \tag{4.33}$$

$$E_{E,s} = \frac{E_{HHV}}{\eta_{E,s}} \tag{4.34}$$

$$\dot{n}_{E,H_2,i} = \frac{0.90 \eta_{E,s}}{E_{HHV}} P_{E,i} \tag{4.35}$$

The efficiency of the electrolyzer stacks is a dynamic parameter that is the function of cell operating voltage, which is then a function of current density. As the cell operating voltage decreases and approaches the thermoneutral voltage, the electrolyzer stacks efficiency approaches 100%. For low-temperature electrolysis, the thermoneutral voltage can be assumed to be constant.

$$\eta_{E,s} = \frac{V_{TN}}{V_E} \tag{4.36}$$

The following empirical function between efficiency and current density of commercial electrolyzers is used for interpolation [88]. More advanced electrolyzers will have lower cell voltage (higher efficiency) for the same current density values; also, they will be able to operate at higher ratings of current density. The correlation between cell voltage and current density is also a function of

temperature, but it is assumed that the temperature is maintained constant for any stage, thus the only variable is current density.

$$\eta_{E,s} = f\left(j\right) \tag{4.37}$$

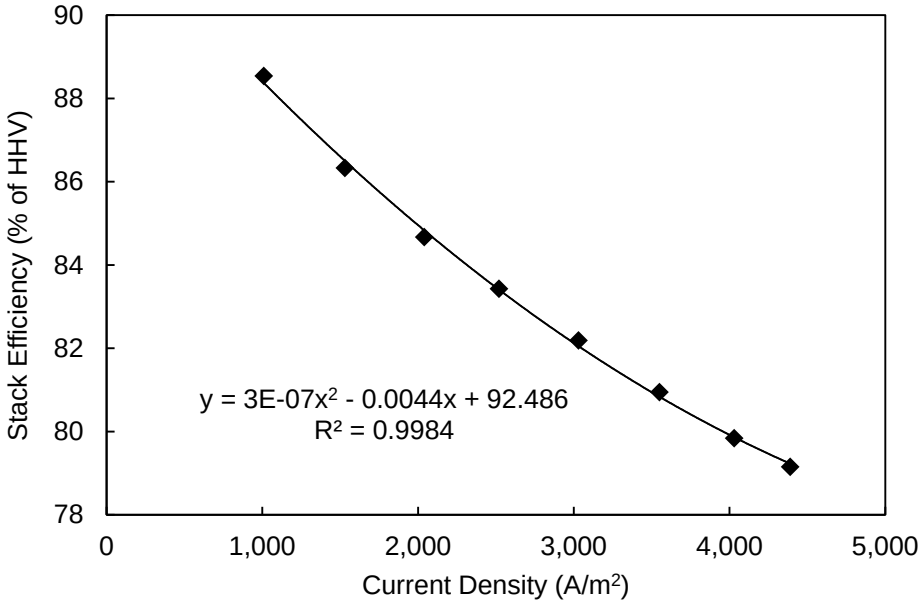

Figure 4.13 Electrolyzer stack efficiency as a function of current density

The current density is a variable that directly controls the actual amount of hydrogen produced, for a given electrolyzer configuration, i.e. constant separator area; it is only limited by the electrolyzer technology available on the market. For electrolyzers with the same performance curve (Figure 4.13), the total separator area of the electrolyzer unit is different, depending on the desired rated capacity of the unit. For the electrolyzers modeled, it is assumed that the current density value has upper and lower caps, at 400 mA/cm^2 and 100 mA/cm^2, respectively, for the electrolyzer to operate normally.

$$\frac{j_{\min}}{j_{rated}} = 0.25 \tag{4.38}$$

Assuming that pressure is constant and that current efficiency is 100%, for a single electrolyzer unit, the rated hydrogen production capacity is related to current density through the following equation.

$$\dot{n}_{E,H_2,i} = \frac{A_E}{nF} j \tag{4.39}$$

For part-load operation of the electrolyzer, the amount of hydrogen produced is lowered by decreasing the current density. From the equations above, it is obvious that current density is linearly related to the hourly production of hydrogen per unit of electrolyzer, since A_E, n, F are all constants.

To recapitulate, the production of hydrogen is not only limited by the power supply available, but it is also controlled by the current density, which determines the efficiency at which the power supplied to electrolyzers is used.

$$\dot{n}_{E,H_2,i} = \frac{P_{E,i}}{E_E(j)} = j\frac{A_E}{nF} \tag{4.40}$$

4.3.2 Rated Power

The rated capacity of the electrolyzer unit can be expressed in terms of rated power or hydrogen output. Here, it is expressed in terms of the rated electrolyzer hydrogen production. Given that the rated output of a single electrolyzer unit is fixed by manufacturer design (fixed A_E, j_{rated}, n and F are physical constants), changing the total rated output of all electrolyzer involve altering the number of units in place N_E. Because the current density has a lower limit, thus a minimum load requirement per unit and, by extension, an overall minimum load requirement, also exist.

$$\dot{n}_{E,H_2,rated} = N_E\left(\dot{n}_{E,H_2,rated,i}\right) = N_E\left(\frac{A_E}{nF} j_{rated}\right) \tag{4.41}$$

$$\dot{n}_{E,H_2,\min} = N_E\left(\dot{n}_{E,H_2,\min,i}\right) = N_E\left(\frac{A_E}{nF} j_{\min}\right) \tag{4.42}$$

To convert rated capacity expressed in terms of hydrogen production to units of power consumption, the following relationship can be used, where $E_{E,rated}$ is the energy consumption per unit of hydrogen production at rated conditions.

$$P_{E,rated} = \dot{n}_{E,H_2,rated} E_{E,rated} \tag{4.43}$$

$$P_{E,\min} = \dot{n}_{E,H_2,\min} E_{E,\min} \tag{4.44}$$

The utilization factor of the electrolyzer unit can also be expressed differently, depending on the basis of calculation. The hydrogen production-based utilization factor also describes the relationships between actual and rated current density:

$$U_E = \frac{\dot{n}_{H_2}}{\dot{n}_{H_2,rated}} = \frac{N_E \frac{A_E}{nF} j}{N_E \frac{A_E}{nF} j_{rated}} = \frac{j}{j_{rated}} \tag{4.45}$$

$$U_{E,\min} = \frac{\dot{n}_{H_2,\min}}{\dot{n}_{H_2,rated}} = \frac{j_{\min}}{j_{rated}} = 0.25 \tag{4.46}$$

This factor is different from the utilization factor based on power consumption, but the two are related through the following relationship, valid with the condition that all electrolyzer units operate at the same level, all the time (i.e. $E_E = N_E E_{E,i}$):

$$\frac{P_E}{P_{rated}} = \frac{\dot{n}_{E,H_2}}{\dot{n}_{E,H_2,rated}} \frac{E_E}{E_{E,rated}} \tag{4.47}$$

$$U_P = U_E \frac{E_E}{E_{E,rated}} \; U_P = U_E \frac{E_E}{E_{E,rated}} \tag{4.48}$$

$$U_E = U_P \frac{E_{E,rated}}{E_E} \tag{4.49}$$

For U_E ranging from 0.25 to 1 (thus j ranging from 100 to 400 mA/cm^2, the value of E_E / E_{rated} has been determined, so that U_E can be easily converted to U_P. The relationship between the two is plotted and the regression equation found is shown in Figure 4.14.

$$\frac{E_E}{E_{E,rated}} = \frac{E_{HHV}}{0.90 \eta_{E,s} E_{E,rated}} \tag{4.50}$$

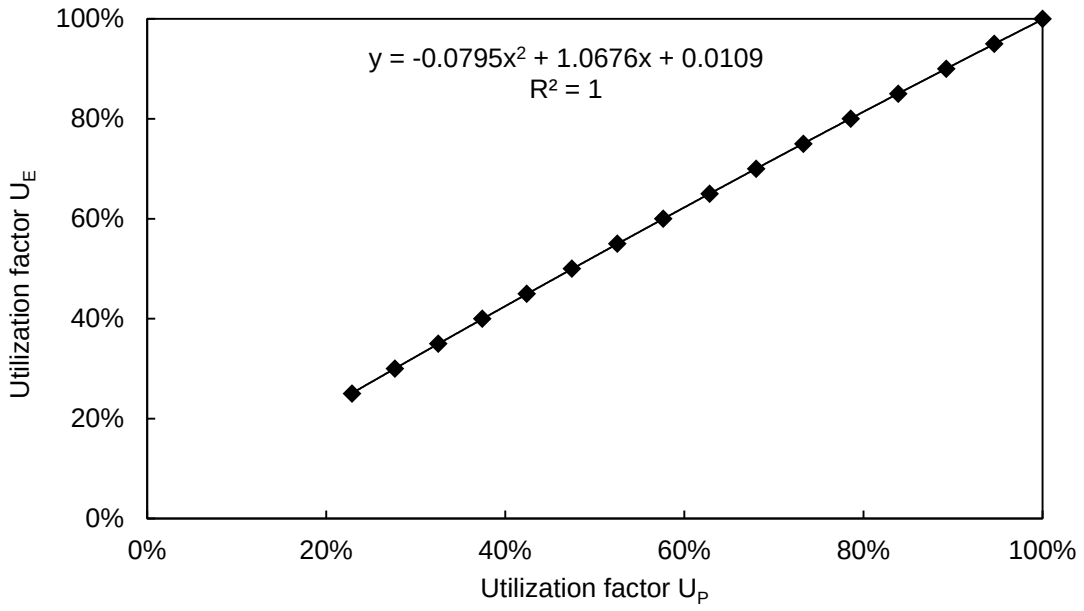

Figure 4.14 Correlation between the hydrogen output based utilization factor and the power consumption based utilization factor for the electrolyzer

This relationship is also used to simplify the solving of input-output relationship for all electrolyzer units:

$$\dot{n}_{E,H_2} = \frac{P_E}{E_E} \tag{4.51}$$

$$\dot{n}_{E,H_2} = U_E \dot{n}_{E,H_2,rated} = f\left(U_P\right)\dot{n}_{E,H_2,rated} \tag{4.52}$$

$$\dot{n}_{E,H_2} = f\left(\frac{P_E}{P_{E,rated}}\right)\dot{n}_{E,H_2,rated} \tag{4.53}$$

In the equation above, because $P_{E,rated}, \dot{n}_{E,H_2,rated}$ are constants and the relationship between U_E, U_P is known, once P_E is provided, the corresponding hydrogen production can be determined.

4.3.3 Ramp Rate

Studies have found that the proposed electrolyzer unit has dynamic performance that is suitable for rapid ramping (i.e. operating with intermittent power supply that emulates wind power profile): the

electrolyzer efficiency was only little affected by the transient regime of operation [89]. Therefore, it can be safely assumed that from one hour to the next, it is possible for the electrolyzers to ramp up and down at the rate that the power supply is changing.

Table 4.7 List of key variables and parameters for the electrolyzer model

Type	Description	Symbol	Value	Unit	Ref.
Input	Power supply available to electrolyzers	P_E	MW		
Output	Hydrogen produced	$\dot{n}_{H_2,E}$		kmol/h	
	Utilization factor	U_P	(based on rated power)		
Parameters	Number of electrolyzer units	N_E	From initialization		
	Rated power of a single unit	$P_{E,rated,i}$	0.29	MW	[68]
	Rated hydrogen production of a single unit	$\dot{n}_{H_2,E,rated,i}$	2.7	kmol/h	[68]
	Correlation between stack efficiency and current density		See Figure 4.13		[88]
	Rated current density	j_{rated}	400	mA/cm^2	[88]
	Minimum current density	$j_{\min}$	100	mA/cm^2	[88]

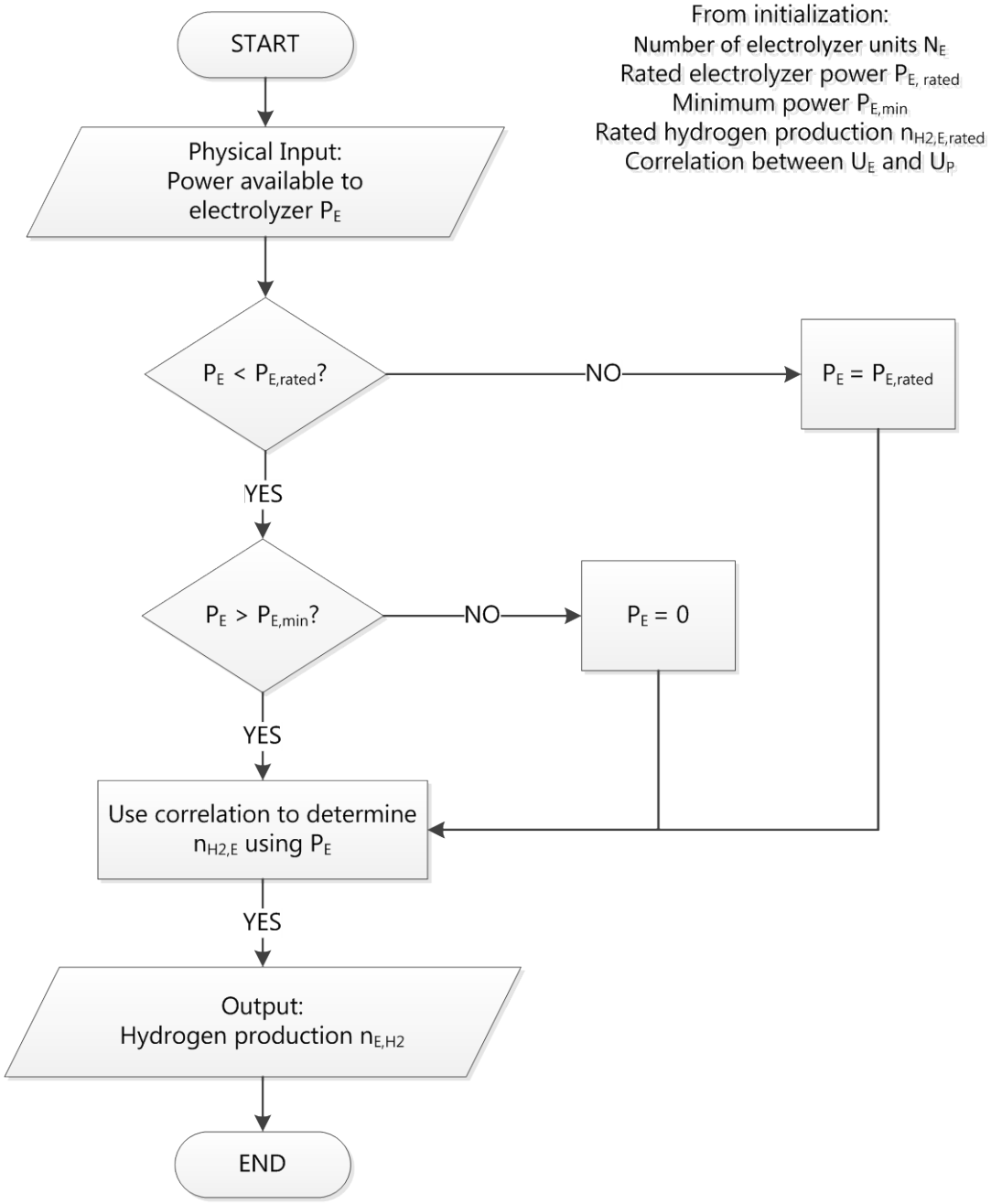

Figure 4.15 Model flow diagram for electrolyzers

4.4 Gas Turbine

The inputs accepted by the gas turbine are the amount of fuel dispatched to the CCGT plant and the hydrogen concentration in the fuel; the outputs expected from the gas turbine model are the power generated by the unit, given the fuel input.

4.4.1 Efficiency

Figure 4.16 shows the simple process flow diagram proposed for the combined cycle plant operating at energy hub. The flows are numbered and used in the development of the model.

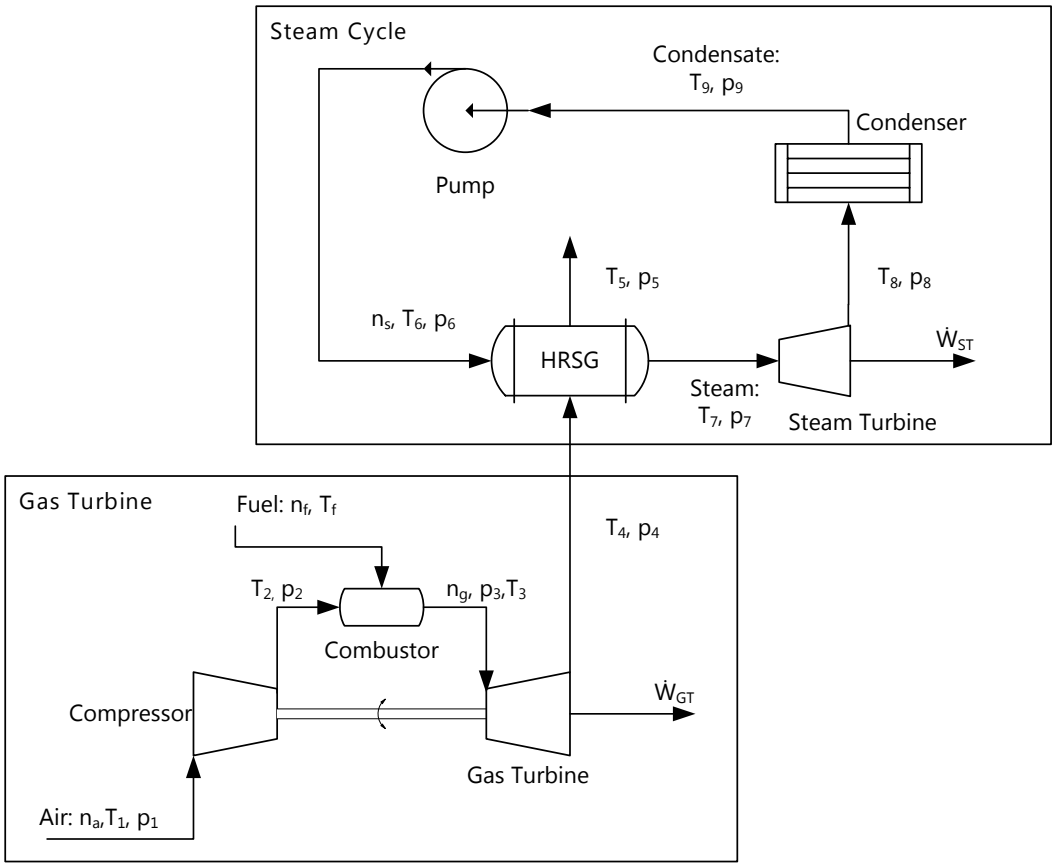

Figure 4.16 Process flow diagram for the combined-cycle plant

The overall efficiency of the CCGT is dependent on the gas turbine efficiency and the steam turbine efficiency. The two thermal cycles are connected through the HRSG, in which the exhaust gas from

the gas turbine exchanges heat with the condensate of the steam cycle, to form steam again. It can be defined as a function of the steam turbine and gas turbine power outputs.

$$\eta_{CC} = \frac{\dot{W}_{GT} + \dot{W}_{ST}}{\dot{H}_{GT} + \dot{H}_{SF}} \tag{4.54}$$

Since it is assumed that no supplemental firing (the addition of fuel to the exhaust of the gas turbine, to increase the inlet temperature of the HSGT) occurs, the supplementary firing fuel consumption $\dot{H}_{SF}$ $\dot{H}_{SF}$ is 0. By applying the definition of gas turbine and steam turbine efficiencies, the previous equation can be rewritten, showing that the combined efficiency is higher than that of the gas turbine or the steam turbine.

$$\eta_{GT} = \frac{\dot{W}_{GT}}{\dot{H}_{GT}} \tag{4.55}$$

$$\eta_{ST} = \frac{\dot{W}_{ST}}{\dot{H}_{GT,Exh}} \cong \frac{\dot{W}_{ST}}{\dot{H}_{GT}\left(1-\eta_{GT}\right)} \tag{4.56}$$

$$\eta_{CC} = \eta_{GT} + \eta_{ST}(1-\eta_{GT}) \tag{4.57}$$

4.4.1.1 Gas Turbine Efficiency

The gas turbine in a CCGT operates as an open Brayton cycle. In an ideal Brayton cycle, the incoming air first undergoes isentropic compression, followed by heat addition at constant pressure in the combustor, isentropic expansion in the turbine. Finally, in the HRSG, the exhaust gas rejects heat at constant pressure.

The theoretical efficiency of an ideal Brayton cycle – using the assumptions of a cold air-standard analysis: air behaves as an ideal gas, the working fluid is air and does not change composition, the working fluid has constant heat capacity – is calculated as follows:

$$\eta_{GT,th} = 1 - \frac{T_1}{T_{2,s}} = 1 - \frac{1}{r_p^{\frac{k-1}{k}}} \tag{4.58}$$

r_p: Compressor pressure ratio = p_2 / p_1

k: Air heat capacity ratio

r_p: Compressor pressure ratio = p_2 / p_1

k: Air heat capacity ratio

For isentropic compression and expansion, the outlet temperature of the compressor and the turbine can be calculated. Since heat rejection and heat addition is assumed to be done at constant pressure conditions, $p_2 = p_3$ and $p_4 = p_1$.

$$T_{2,s} = T_1 \left(\frac{p_2}{p_1} \right)^{k-1/k} \tag{4.59}$$

$$T_{4,s} = T_3 \left(\frac{p_4}{p_3} \right)^{k-1/k} = T_3 \left(\frac{p_1}{p_2} \right)^{k-1/k} \tag{4.60}$$

The actual gas turbine cycle efficiency deviates from the ideal efficiency because the compressor and the turbine are not ideal isentropic machines. The actual work done/required by the turbine and the compressor can be calculated if the isentropic efficiencies are known. Note that a negative sign is present in the work equation for the turbine to reverse the sign of the calculated value, for all work terms are considered as positive values in the following calculations.

$$W_{GTc,act} = \frac{W_{GTc,th}}{\eta_{GTc}} = \frac{RT_1 \frac{k}{k-1} \left[\left(\frac{p_2}{p_1} \right)^{k-1/k} - 1 \right]}{\eta_{GTc}} \tag{4.61}$$

$$W_{GTt,act} = \eta_{GTt} W_{GTt,th} = \eta_{GTt} RT_3 \frac{-k}{k-1} \left[\left(\frac{p_1}{p_2} \right)^{k-1/k} - 1 \right] \tag{4.62}$$

η_{GTc}: Gas turbine cycle compressor efficiency

η_{GTt}: Gas turbine cycle turbine efficiency

At the combustor, the combustion reaction provides the heat that increases the temperature of the reactant gas, which then expands in the turbine. Ignoring the components other than methane and hydrogen in the fuel mixture, the following combustion reaction equation can be found:

$$2O_2 + CH_4 \rightarrow CO_2 + 2H_2O \tag{4.63}$$

$$\frac{1}{2}O_2 + H_2 \rightarrow H_2O \tag{4.64}$$

Since the fuel will be containing both methane and hydrogen, the two combustion reactions above are combined to form the combustion reaction of the pseudo-compound that is the fuel mixture, for 1 unit of fuel, where x represents the concentration of hydrogen per mole of fuel:

$$(1-x/2)O_2 + \underbrace{\left[xH_2 + (1-x)CH_4\right]}_{\text{fuel}} \rightarrow xH_2O + (1-x)CO_2 \tag{4.65}$$

If 100% combustion efficiency is assumed, then the number of moles of carbon dioxide emitted is the same as the number of moles of methane present in the fuel mixture.

$$\dot{n}_{CO_2} = \left(1-c_{H_2}\right)\dot{n}_f \tag{4.66}$$

Assuming the combustor to be adiabatic and the combustion gas has constant heat capacity for the range of interest, the temperature of the working gas at the exit of the combustor is:

$$T_3 = T_2 + \frac{-\left(\Delta H_{R,f}\right)}{\sum \Theta_i c_{p_i}} \; T_3 = T_2 + \frac{-\left(\Delta H_{R,f}\right)}{\sum \Theta_i c_{p_i}} \tag{4.67}$$

Where $\Delta H_{R,f}$ $\Delta H_{R,f}$ is the heat of reaction (kJ/ kmol of fuel reacted) for the reaction represented in Equation(4.65). It is assumed that the heat or reaction is constant regardless of combustion temperature.

$$\Delta H_{R,f} = \Delta H_{R,H_2} c_{H_2} + \Delta H_{R,NG}\left(1-c_{H_2}\right) \tag{4.68}$$

$\Theta_f = 1$

$$\left.\begin{aligned}\Theta_{O_2} &= 0.21\dot{n}_a/\dot{n}_f \\ \Theta_{N_2} &= 0.79\,\dot{n}_a/\dot{n}_f\end{aligned}\right\}\Theta_{air} = \dot{n}_a/\dot{n}_f$$

$\Theta_{H_2O} = 0$

$\Theta_{CO_2} = 0$

The fuel and air heat capacities are assumed to be constants. The combustion heat from the fuel is also the main source of energy for the combined-cycle.

$$\dot{H}_{GT} = \dot{n}_f\left(-\Delta H_{R,f}\right) \tag{4.69}$$

The actual temperatures at the exit of the compressor and the turbine, T_2 and T_4, need to be determined for use in the combustor calculations and the HRSG calculations, respectively. Assuming that the working gas has properties compare to that of pure air even after combustion, we can determine the temperature of the working gas based on the stream enthalpies and the ideal gas properties table for air. Similarly, if the temperature of an air stream is known, its enthalpy can be looked up from the ideal gas properties table.

$$T_2 = f\left(h_2\right) \qquad h_2 = h_1 + W_{GTc,act} \tag{4.70}$$

$$T_4 = f\left(h_4\right) \qquad h_4 = h_3 - W_{GTt,act} \tag{4.71}$$

$$h_1 = f\left(T_1\right) \tag{4.72}$$

$$h_3 = f\left(T_3\right) \tag{4.73}$$

To calculate the actual gas turbine cycle efficiency, the following equation is used:

$$\eta_{GT} = \Theta_a \left(\frac{W_{GTt,act} - W_{GTc,act}}{-\Delta H_{R,f}} \right) \tag{4.74}$$

It is assumed that the number of moles of working gas is constant.

$$\dot{n}_{GT} \approx \dot{n}_a + \dot{n}_f \approx \dot{n}_g = \dot{n}_a \tag{4.75}$$

The net power output from the gas turbine cycle is:

$$\dot{W}_{GT} = \dot{n}_a \left(W_{GTt,act} - W_{GTc,act} \right) = \Theta_a \dot{n}_f \left(W_{GTt,act} - W_{GTc,act} \right) \tag{4.76}$$

4.4.1.2 Exhaust Heat Recovery Efficiency

The design and operation of a HRSG is limited by the quality of the gas turbine exhaust gas available. Compared to the boiler used for conventional steam generation, the temperature of the heating medium is much lower, in the order of 750-800K instead of 1400K. Thus, a rather large gas/steam ratio is required to produce steam that is adequate for power generation in a turbine.

Typically, a HRSG is a large heat exchanger consists of three parts: the superheater, the evaporator and the economizer. The exhaust gas from the gas turbine travels from the superheater to the economizer, while water and the resulting steam travels from the economizer to the superheater. For

this model, it is assumed that there is no pressure drop within the HRSG and all parts are operating at pressure. p_7 . The temperature at which water is evaporated is the corresponding saturation temperature. $T_{7,sat}$.

Water is first pre-heated to a temperature slightly below the saturation temperature in the economizer. Then, in the evaporator, water is heated to the saturation temperature and completely boiled, to exist as a saturated vapor of the same temperature. Finally, water is heated to a temperature above the saturation temperature, resulting in superheated steam (Figure 4.17).

The temperature difference between the saturation temperature and that of the exiting exhaust gas is known as the pinch temperature; it is an important design parameter. Another parameter is the temperature difference between the saturation temperature and that of the entering water, known as the approach temperature. It is important to specify those temperatures, so that at no point during the heat transfer, the temperature of the exhaust gas crosses the temperature of the heated steam. Once the pinch and approach temperatures have been set, the ratio between the steam and exhaust gas flows inside the HRSG can be determined as below (molar enthalpies are written as function of temperature):

$$T_{pinch} = T_4^{"} - T_{7,sat} \tag{4.77}$$

$$T_{approach} = T_{7,sat} - T_6^{'} \tag{4.78}$$

$$SGR = \frac{\dot{n}_s}{\dot{n}_a} = \frac{h_g\left(T_4\right) - h_g\left(T_4{"}\right)}{h_v\left(T_7\right) - h_w\left(T_6{'}\right)} \tag{4.79}$$

T_4: Gas turbine exhaust temperature, K

$T_4^{"}$: Temperature of gas leaving evaporator, K

T_7: Steam turbine inlet temperature, K

$T_6^{'}$: Temperature of water entering evaporator, K

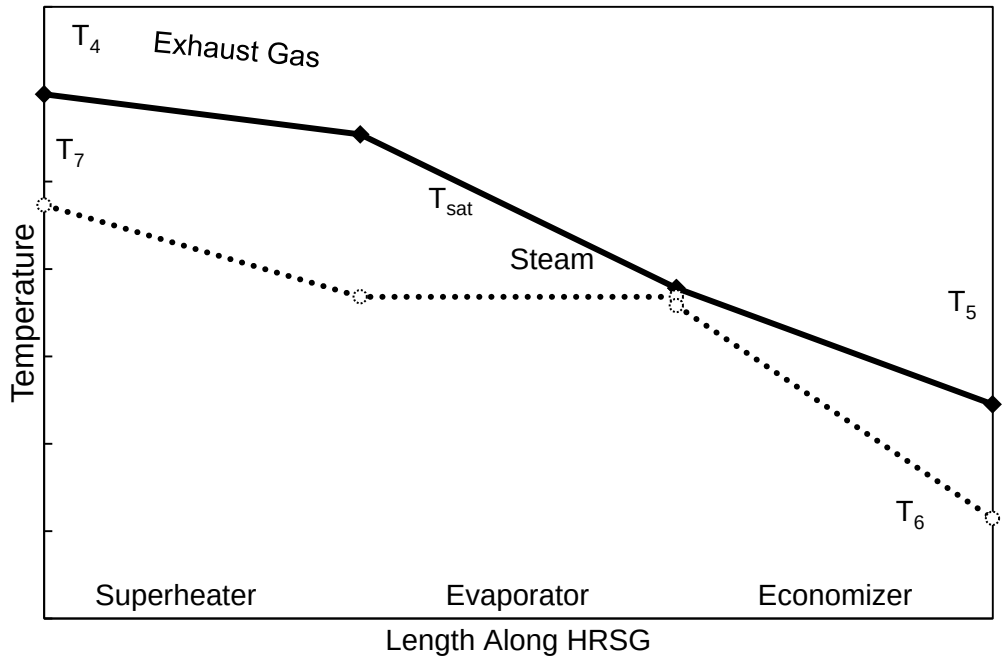

Figure 4.17 Temperature profile along the HRSG

The HRSG heat exchanger is designed for the design value of gas turbine exhaust temperature (T_4), during part-load operations ($c_{H_2} > 0,\ \dot{n}_f < \dot{n}_{f,rated}$), it is possible that exhaust temperature drops below the rated value. Decreased exhaust temperature then leads to decreased steam turbine efficiency, for the steam temperature in the Rankine cycle is reduced.

4.4.1.3 Steam Turbine Efficiency

The steam turbine in a CCGT operates as a closed Rankine cycle. In an ideal Rankine cycle, the working fluid, water, first undergoes isentropic compression through a pump, then heat addition at constant pressure occurs in a heat exchanger, followed by isentropic expansion in the turbine. Finally, the used steam is condensed to water and resumes the cycle. Given that this is a closed cycle, the flow rate of working fluid $\dot{n}_s$ is the same throughout. The maximum theoretical efficiency of an ideal Brayton cycle is the Carnot efficiency:

$$\eta_{ST,th} = 1 - \frac{T_{9,sat}}{T_{7,sat}} \tag{4.80}$$

However, because of practical concerns, the Rankine cycle is different from the Carnot cycle in that the hot stream used for heat exchange with steam is cooled more extensively, and the used steam is condensed fully into a liquid prior to pumping. Assuming a turbine and pump efficiency of 90%, the actual efficiency of the Rankine cycle plant can be determined as follows:

$$\eta_{ST,act} = \frac{\dot{W}_{STt,act} - \dot{W}_{STp,act}}{\dot{H}_{ST}} \tag{4.81}$$

$$W_{STt,act} = \eta_{STt}\left(h_7 - h_{8,s}\right) \tag{4.82}$$

$$W_{STp,act} = \frac{v_9\left(p_6 - p_9\right)}{\eta_{STp}} \tag{4.83}$$

$$\dot{H}_{ST} = \dot{n}_s\left(h_7 - h_6\right) \tag{4.84}$$

At the exit of the condenser (state 9), the working fluid is assumed to be in the state of saturated liquid, so that its enthalpy can be located using the specified pressure of the stream.

$$h_9 = f\left(p_9, T_{9,sat}\right) \tag{4.85}$$

At the exit of the pump (state 6), the temperature of the working fluid remains the same as before, only the pressure has changed because of the work done by the pump.

$$h_6 = f\left(p_6, T_6\right) \qquad T_6 = T_{9,sat} \tag{4.86}$$

At the exit of the turbine (state 8), the working fluid is a saturated mixture containing both vapor and liquid. The steam quality can also be determined from the saturation pressure of the turbine inlet stream, assuming isentropic expansion:

$$h_{8,s} = f_1\left(s_8\right) = f_2\left(s_7\right) = f_3\left(p_7, T_7\right) \tag{4.87}$$

It is assumed that, since constant heat addition and rejection is taking place, $p_6 = p_7$ and. $p_8 = p_9$. Liquid water is assumed to be incompressible, so v_9 v_9 is considered a constant. The enthalpy of the heat exchanger outlet (state 6) is coupled to the enthalpy in the gas turbine exhaust stream through the use of the heat recovery steam generator.

The net power output from the gas turbine cycle is:

$$\dot{W}_{ST} = \dot{n}_s \left(W_{STt,act} - W_{STp,act} \right) \tag{4.88}$$

$$\dot{W}_{CC} = \dot{W}_{GT} + \dot{W}_{ST} \tag{4.89}$$

For the design case (100% load and natural gas fuel), the ratio of air to fuel flow rate is a fixed number. But, for off-design operating conditions (part-load or use of hydrogen-enriched fuel); where the heat of reaction is lower than the design value, it is necessary to vary the ratio of air to fuel Θ_{air} in order to maintain the temperature of the combustion gas T_3. Because, as demonstrated in the section above, the temperature of working gas from the gas turbine directly impacts the efficiency of the steam turbine cycle. But, the ratio needs to follow certain constraints: it is known that gas turbines can operate with reduced air flow, as long as the air flow maintained above 85% of the design value. Once that value has been reached, it is no longer possible to further reduce air flow; in consequence, the combustion temperature starts to decline [58].

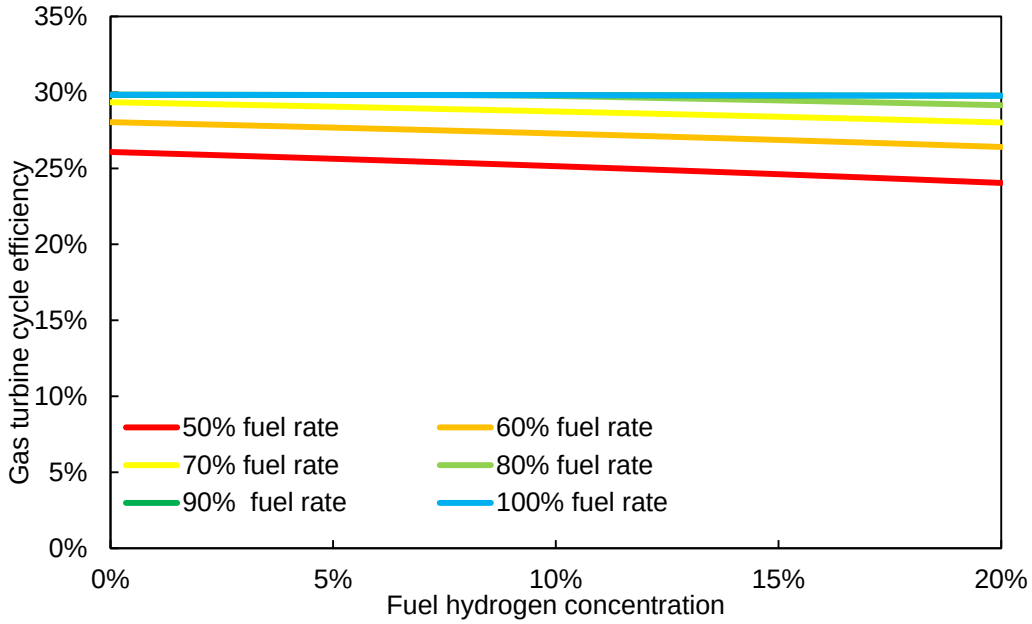

Figure 4.18 Gas turbine cycle efficiency as a function of fuel hydrogen concentration and relative fuel rate

For this model, the efficiency of the gas turbine cycle is pre-determined using the relationships outlined in 4.4.1.1; the range of input variables used is: fuel hydrogen concentration from 0% to 20% and relative fuel flow rate from 50% to 100% (Figure 4.18). The relative fuel flow rate is defined as the actual amount of fuel available (kmol/h) divided by the rated amount of fuel that can be used.

Once the part-load gas turbine cycle efficiency is known, it is used to find the part-load combined cycle efficiency. The efficiency of the gas turbine cycle is dependent on the heat rate (work load) of the gas turbine, which then influences the efficiency of the overall combined cycle with its own change and its effect on the steam turbine cycle efficiency. The efficiency of the gas turbine cycle at partial load (40% to 100%) and the corresponding combined cycle efficiency are presented in Figure 4.19. The logarithmic functions fitted have R^2 of 0.9971 and 0.9944; they are used to calculate fixed pairs of combined cycle and gas turbine efficiency at given load levels, which are then correlated in Figure 4.20 is derived from the empirical relationship in Figure 4.19.

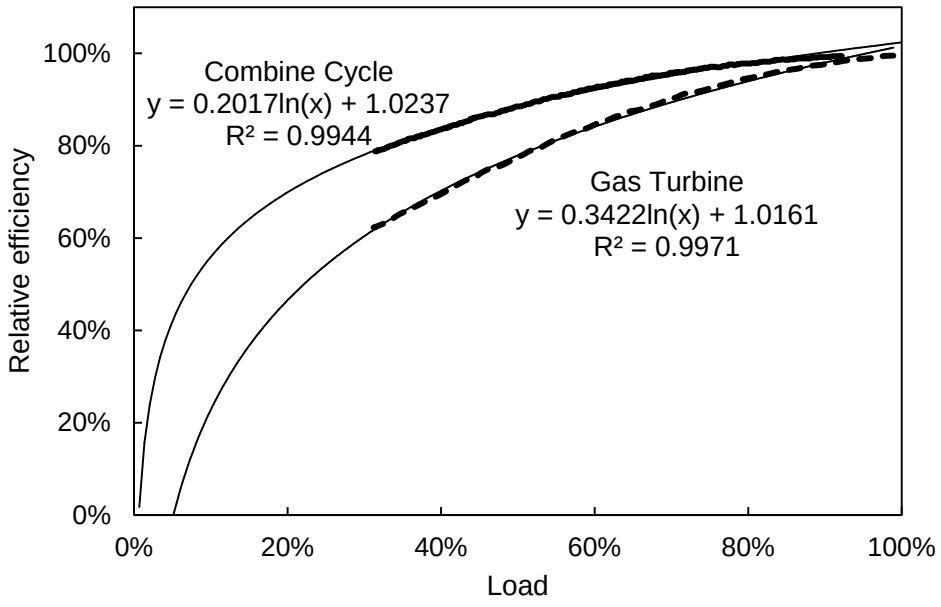

Figure 4.19 Relative efficiencies of the gas turbine cycle and of the combine cycle at part-load conditions [58]

The correlation between the gas turbine cycle efficiency and the relative combined cycle efficiency is used as a simple look-up function. For a R^2 of 0.9912 and 27 pairs of data, the correlation is significant for p-value <0.0005.

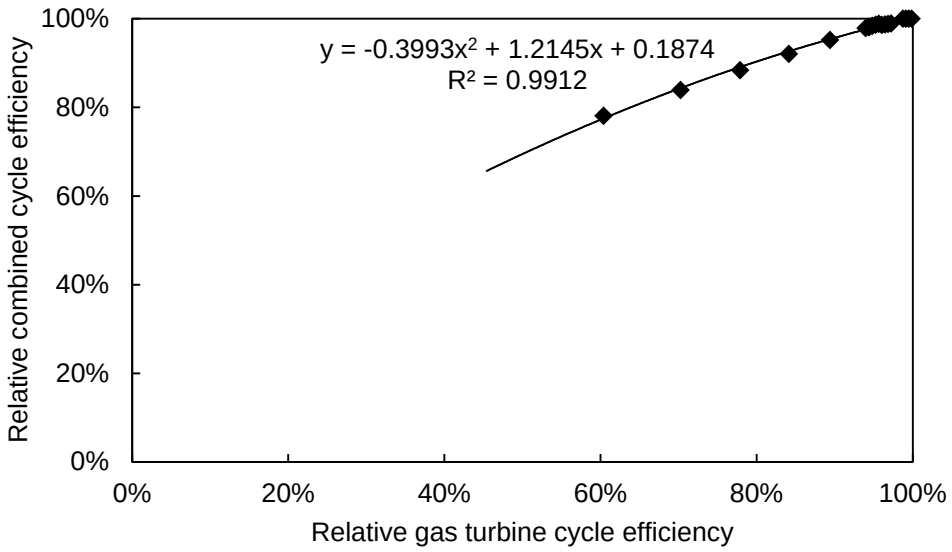

Figure 4.20 Relative combined cycle efficiency as a function of relative gas turbine cycle efficiency

4.4.2 Rated power

Individual gas turbines are available a wide range of sizes, from 500 kW to 300 MW in terms of power output. The size of the overall unit is dependent on the maximum flow rate of working fluid that the gas turbine cycle and the steam turbine cycle are expected to process at design conditions (100% load, natural gas as fuel). The relationship between the rated power in terms of MW is related to the rated power expressed in terms of fuel intake rate is the following:

$$\dot{W}_{CC,rated} = \eta_{CC,rated}\dot{n}_{f,rated}\left(-\Delta H_{R,NG}\right) \tag{4.90}$$

$$U_{CCGT}\left(t\right) = \frac{\dot{W}_{CC}\left(t\right)}{\dot{W}_{CC,rated}} \tag{4.91}$$

4.4.3 Ramp rate

Combined cycle power plants are known to have short start-up time. The following start times are expected for different standstill periods:

- After 8 hours of standstill: 40 – 60 minutes, simplified to be 1 hour;
- After 48 hours of standstill: 80- 120 minutes, simplified to be 2 hours;
- After 120 hours of standstill: 120-170 minutes, simplified to be 3 hours.

Furthermore, combine cycle units have quick load change capability, especially the gas turbine section. It is reported that, while operating, a CCGT plant can ramp its generation by 5-10% of its rated output per minute [90]. In 10 to 20 minutes, it is possible for the CCGT unit to ramp up or down completely, provided that it has not been in standstill. To simplify the overall model, the start time of the CCGT, in the order of a few hours, is assumed to be negligible. In other words, even 100% start-up from a standstill state is assumed to be completed within an hour.

Table 4.8 List of key variables and parameters for the CCGT model

Type	Description	Symbol	Value	Unit	Ref.
Input	Fuel dispatched to CCGT unit	$\dot{n}_{fuel}$		kmol/h	
	H_2 conc. in fuel	$c_{H_2,fuel}$		mol. %	
Output	Power generated by CCGT unit	$\dot{W}_{CC}$		MW	
	Utilization factor	U_{CCGT}			
Parameters	Inlet air temperature	T_1	288	K	Assumed
	Inlet air pressure	p_1	1.01	bar	Assumed
	GT compressor outlet pressure	p_2	15	bar	Example from [91]
	Air heat capacity ratio	k	1.4		Estimated
	GT compressor efficiency	η_{GTc}	84%		Example from [91]
	GT turbine efficiency	η_{GTt}	88%		Example from [91]
	Heat of reaction of natural gas	$\Delta H_{R,NG}$	8.04E+05	kJ/kmol	Calculate from composition
	Heat of reaction of hydrogen (LHV)	$\Delta H_{R,H_2}$	2.44E+05	kJ/kmol	

	Heat capacity of air	$c_{p,a}$	29.0	kJ/kmol·K	Estimated
	Heat capacity of natural gas	$c_{p,NG}$	68.8	kJ/kmol·K	Estimated
	Heat capacity of H_2	c_{p,H_2}	30.0	kJ/kmol·K	Estimated
	Evaporator pressure/Steam turbine inlet pressure	p_7	80	bar	Example from [91]
	Evaporator saturation temperature	$T_{7,sat}$	568.1	K	Steam table
	Pinch temperature	T_{pinch}	10	K	Assumed
	Approach temperature	$T_{approach}$	10	K	Assumed
	ST turbine efficiency	η_{STt}	90%		Example from [91]
	Molar volume of water	v_9	0.01802	m^3/kmol	Steam table
	Pump outlet liquid pressure	p_6	80	bar	Example from [91]
	Condenser outlet saturated liquid pressure	p_9	0.08	bar	Example from [91]
	ST pump efficiency	η_{STp}	80%		Example from [91]
	Rated CCGT efficiency	$\eta_{CC,rated}$	52.8%		Calculated
	Rated GT cycle efficiency	$\eta_{GT,rated}$	29.8%		Calculated
	Rated ST cycle efficiency	$\eta_{ST,rated}$	32.7%		Calculated
	Correlation between GT efficiency and CCGT efficiency		Figure 4.20		Adapted from [58]
	Rated power of CCGT	$\dot{W}_{CC,rated}$	From initialization	MW	

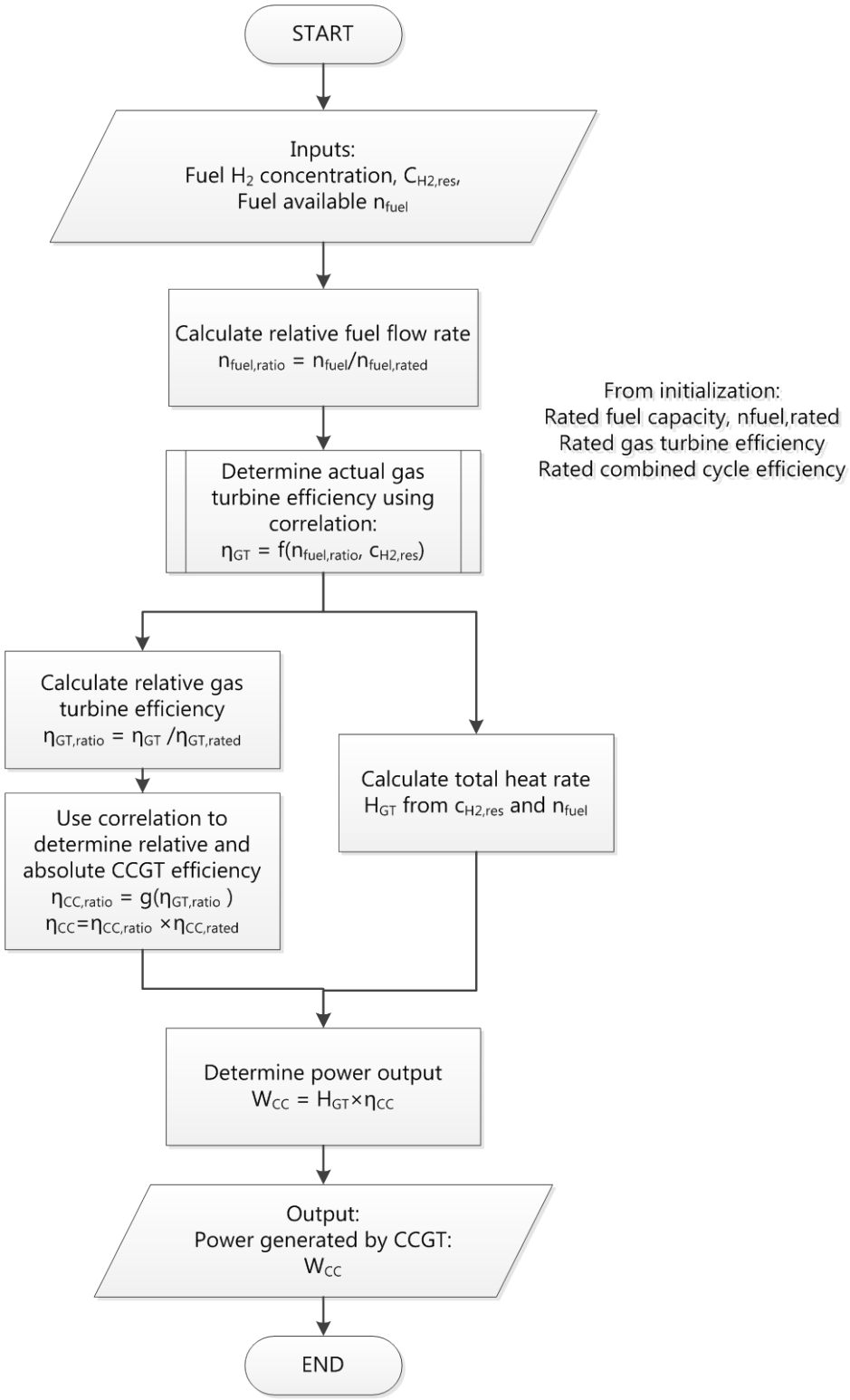

Figure 4.21 Model flow diagram for CCGT

4.5 Separator

The inputs that the separator model accepts is the feed dispatched toward it and the concentration of hydrogen in the feed; the outputs expected from this model are the amount of hydrogen recovered, the quantity of natural-gas rich adsorbate released, and the concentration of hydrogen in the adsorbate.

4.5.1 Efficiency

The efficiency of the PSA process is characterized by its recovery: the percentage of desired product present in the mixture that is recovered after separation. For this energy hub, the recovery of hydrogen is calculated as follows:

$$\eta_{sep} = \frac{\dot{n}_{H_2}}{\dot{n}_{H_2,\,feed}} = \frac{c_{H_2,\,product}\dot{n}_{product}}{\dot{n}_{feed}c_{H_2,\,feed}} \tag{4.92}$$

$$\dot{n}_{H_2,sep} = \eta_{sep}\dot{n}_{Feed}c_{H_2,Feed} \tag{4.93}$$

$c_{H_2,\,product} = 0.999 \simeq 1$

$\dot{n}_{H_2,sep} \simeq \dot{n}_{product}$

The adsorbate, which consists of natural gas and the hydrogen that cannot be recovered:

$$\dot{n}_{sep,mix} = \dot{n}_{feed} - \dot{n}_{H_2} \tag{4.94}$$

$$c_{H_2,sep,mix} = \frac{\left(1-\eta_{sep}\right)\dot{n}_{H_2,\,feed}}{\dot{n}_{sep,mix}} = \frac{\dot{n}_{H_2,\,feed} - \dot{n}_{H_2}}{\dot{n}_{sep,mix}} \tag{4.95}$$

The actual hydrogen recovery of any PSA process is dependent on the multicomponent adsorption equilibrium over the temperature, pressure and concentration range of interest, the physical properties of the gases and the adsorbent, the fluid dynamics and heat transfer inside the adsorption beds, the feed gas conditions, and the sequence of PSA cycle steps and their duration.

The hydrogen-containing gas mixture fed to PSA processes typically contains from 60-90 mol% hydrogen. The two most common sources of mixture are the steam-methane reformer off-gas, after treatment in a water-gas shift reactor, and the refinery off-gas, available at 8-28 bar and at 21-38°C. The composition of the first mixture is 70-80% H_2, 15-25% CO_2, 3-6% CH_4, 1-3% CO, and traces of

N_2. The second mixture contains 65-90% H_2, 3-2-% CH_4, 4-6% C_2H_6, 1-3% C_3H_8, and less than 0.5% C_4+ hydrocarbons. For such feed conditions, the PSA units can produce a product stream containing 98-99.999 mol% H2 at the feed gas pressure, with a hydrogen recovery of 70-90%, if state-of-the-art commercial units are used [92]. The waste stream which contains unrecovered hydrogen and what remains from the feed gas is released at a pressure between 1 to 2 bar. One example of such PSA process is the 11 step cycle Polybed process.

Table 4.9 Summary of hydrogen purification PSA processes [92]

Cases	Polybed	Lofin	Gemini
Feed H_2 Conc.	77.1%	78.8%	75.4% with co-production of high purity CO_2
Feed Pressure	20.7 atm	28 atm	18 atm
Feed Temp.	294 K	288 K	288 K
Gas Type	SMROG	ROG	SMROG
Adsorbent Type	Activated carbon and 5A zeolite	Silica gel and activated carbon	N/A
No. of Columns	10	4 + tank	6 + 3
No. of Cycle Steps	11	9	6 or 7
Cycle Time	13.33 min	30.0 min	N/A
Hydrogen Purity	99.999%	99.96%	99.999%
Hydrogen Recovery	86.0%	86.3%	87.1%
Adsorbent Productivity	34.9 ft^3 feed/ft^3 adsorbent/cycle	153.0 ft^3 feed /ft^3 adsorbent/cycle	N/A

In the literature, for hydrogen/methane mixtures with lower than typical hydrogen concentration, the following values have been reported.

Table 4.10 PSA Process parameters for various feed concentration [93, 94]

Cases	Yang & Doong	Waldron & Sircar
Feed H_2 Conc.	50%	60 to 90%
Feed Pressure	34 atm	14.61 atm
Feed Temp.	298 K	303 K
Adsorbent Type	Activated carbon	Activated carbon
No. of Columns	1	4
No. of Cycle Steps	5	7
Cycle Time	7 min	16 min
Hydrogen Purity	93-98%	99.999%
Hydrogen Recovery	80-95%	82.5 to 85.51%
Adsorbent Productivity	36 to 66 ft^3 feed /ft^3 adsorbent/cycle	12.8 to 32.1 ft^3 feed /ft^3 adsorbent/cycle

There is evidence that the hydrogen recovery is relatively insensitive to feed composition: for hydrogen concentration ranging from 50 to 90%, the value of hydrogen recovery has always remained above 80%. Therefore, the hydrogen recovery of the PSA process at the energy hub used is estimated to be 80%, regardless of feed hydrogen concentration.

4.5.2 Rated power

PSA systems can be procured from small scale plants of a few hundred Nm^3/h to large scale plants with capacity over 400,000 Nm^3/h in terms of feed gas flow [70]. The output of hydrogen that is realizable from the PSA unit with a given capacity is a function of hydrogen concentration in the feed stream. Because the concentration of hydrogen varies in between of simulation time steps, the rated output of hydrogen from PSA also varies.

$$\frac{p_s}{RT_s}\dot{V}_{feed,rated} = \dot{n}_{feed,rated} \tag{4.96}$$

$$\dot{n}_{feed,rated} c_{H_2,feed} \eta_{sep} = \dot{n}_{H_2,rated} \tag{4.97}$$

Given different combination of feed concentration with process scale, the possible rated hydrogen outputs are listed:

Table 4.11 Range of rated hydrogen output for PSA unit

		Hydrogen Concentration in Feed	
		2%	**20%**
Rated Feed	**300 Nm^3/h**	0.20 kmol/h	2.0 kmol/h
Flow rate	**40,000 Nm^3/h**	27.08 kmol/h	270.8 kmol/h

The utilization factor of the separator can be calculated as follows:

$$U_{sep}(t) = \frac{\dot{n}_{sep,feed}(t)}{\dot{n}_{feed,rated}} \tag{4.98}$$

4.5.3 Ramp rate

At this stage, to simplify the model, it is assumed that the PSA unit operates with a constant cycle time of 30 minutes, independent of hydrogen concentration in feed and of actual PSA throughput. It is also assumed that the PSA unit can be started completely within a single simulation time step.

Table 4.12 List of key variables and parameters for the separator model

Type	Description	Symbol	Value	Unit	Ref.
Input	Feed to separator	$\dot{n}_{feed}$		kmol/h	
	H_2 conc. in feed	$c_{H_2,feed}$		mol. %	
Output	Amount of hydrogen recovered	$\dot{n}_{H_2,sep}$		kmol/h	
	Amount of NG-rich adsorbate produced	$\dot{n}_{sep,mix}$		kmol/h	
	H_2 conc. in adsorbate	$c_{H_2,sep,mix}$		mol. %	
	Utilization factor	U_{Sep}			
Parameters	Separator hydrogen recovery	η_{sep}	90%		Estimated
	Concentration of hydrogen in separated stream	$c_{H_2,product}$	$0.999 \simeq 1$	mol. %	Estimated
	Rated input capacity	$\dot{n}_{feed,rated}$	from initialization	kmol/h	

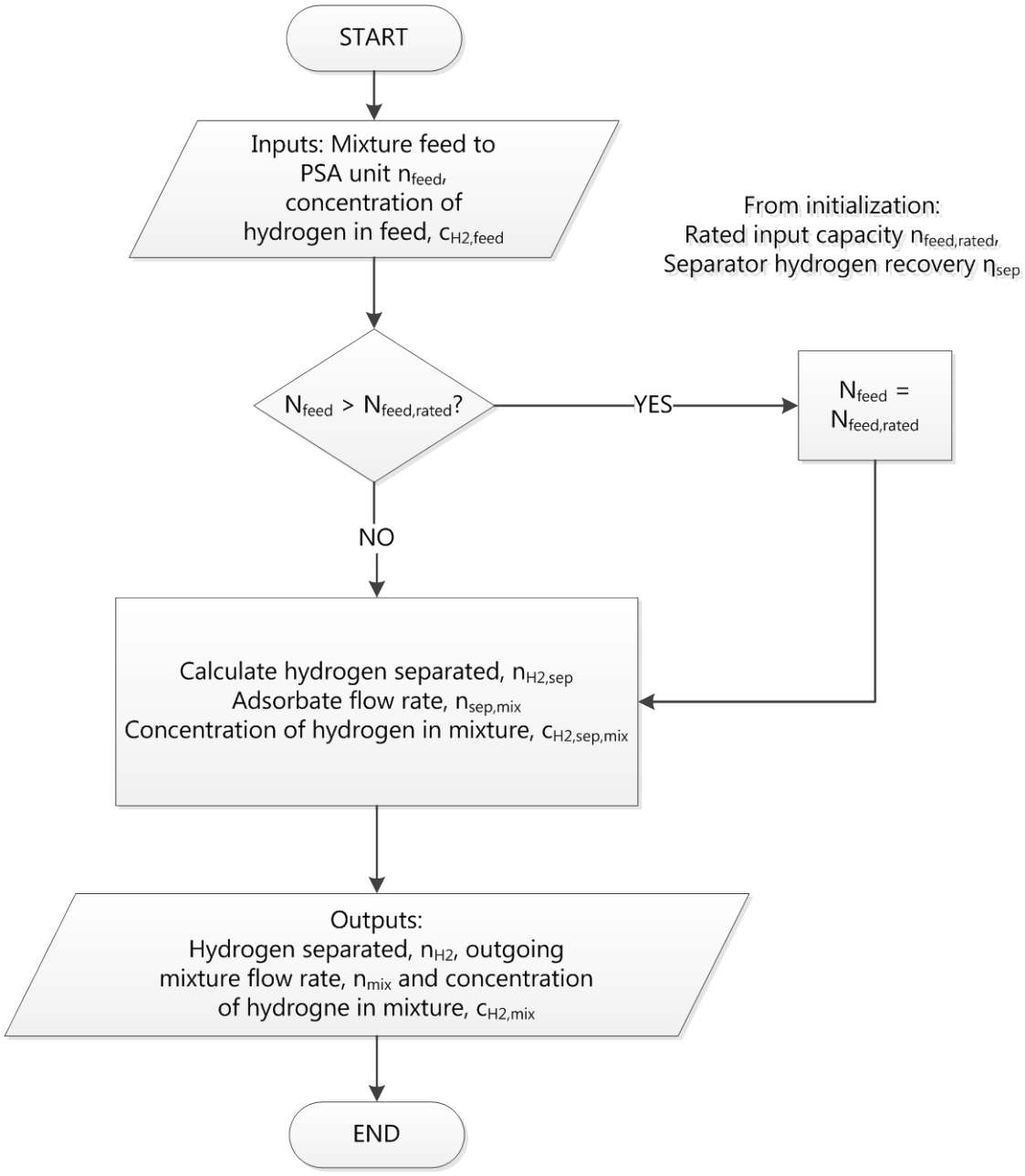

Figure 4.22 Model flow diagram for the separator

4.6 Compressor

At various point in the energy hub, stand-alone compressors are used to pressurize natural gas, hydrogen, or their mixture. In Figure 4.2, four compressors can be identified: C1, located at the electrolyzer outlet, to compress hydrogen to the pipeline pressure of incoming natural gas; C2, located before the injection well, to compress hydrogen enriched natural gas to wellhead pressure; C3, located at the electrolyzer outlet, to compress hydrogen to the pressure needed for gas delivery (if bypass of storage is an available option); C4, located at the separator outlet, to compress hydrogen to the pressure needed for gas delivery.

The inputs accepted by a compressor sub-model are compressor inlet and outlet pressure, inlet temperature, quantity and the hydrogen concentration of the gas to be compressed; the output expected from the compressor model is the work that is required for the compression described. All compressor units have identical code, only the inputs have been changed.

4.6.1 Compression Efficiency

The power required by the compressor at any given time is a function of gas flow rate and inlet/outlet conditions. Typically, the work requirement and the effluent conditions are estimated based on inlet conditions and the discharge pressure, assuming isothermal, adiabatic (isentropic) or polytropic process conditions. The isothermal compression calculations represent the minimum amount of power required, supposing that there exist an infinite number of intercoolers between stages of compression, so that the temperature of gas is kept constant during the compression [95]. The isentropic process assumes that no heat is added or removed from the gas during compression, and that friction is absent, so that the entropy of the gas is kept constant during the compression. As for the polytropic compression, it is assumed that infinite isentropic steps are conducted in series, each separated by isobaric heat transfer, yielding the discharge temperature for the actual process. For this particular model, isentropic conditions are assumed.

Because the compression pressure is expected to range from atmospheric pressure to hundreds of bar, when calculating the theoretical compressor work, the deviation from the ideal gas behaviour needs to be accounted for through the use of the compressibility factor, z, which is a function of temperature, pressure and composition. The values of compressibility factor for the full range of temperature,

pressure and composition expected have already been compiled for reservoir inventory calculations. The same values are used to populate the look-up table in the compressor model (Table 4.3)

$$P_{comp} = \dot{n}_{comp} \frac{W_{comp,th}}{\eta_{comp}} \tag{4.99}$$

$$W_{comp,th} = \overline{z}RT_{in} \frac{k_{mix}}{k_{mix} - 1} \left[\left(\frac{p_{out}}{p_{in}} \right)^{k_{mix}-1/k_{mix}} - 1 \right] \tag{4.100}$$

$W_{comp,th}$: Isentropic work done by compressor, kJ/kmol

P_{comp}: Actual power required by compressor, kJ/h

$\dot{n}_{comp}$: Compression gas flow rate, kmol/h

η_{comp}: Compressor isentropic efficiency

k_{mix}: Heat capacity ratio of compression gas

The isentropic efficiency of typical reciprocating compressors at different pressure ratio can be looked up from [96]. In this model, the average of the range provided is chosen as the basis of calculations. Since the compression is simplified to be a one-stage process, scenarios with compression ratio larger than 4 are deemed to be acceptable, with an isentropic efficiency of 87.5%.

Table 4.13 Isentropic efficiencies of reciprocating compressors

Compression Ratio	Efficiencies (Engine-driven)
1.1	50-60
1.2	60-70
1.3	65-80
1.5	70-85
2.0	75-88
2.5	80-89
3.0	82-90
4.0	85-90

The heat capacity ratio, another important parameter in the determination of isentropic work needed for compression, is also a function of mixture composition.

$$k_{mix} = \frac{c_{p,mix}}{c_{v,mix}} = \frac{\sum y_i c_{p,i}}{\sum y_i c_{v,i}} \tag{4.101}$$

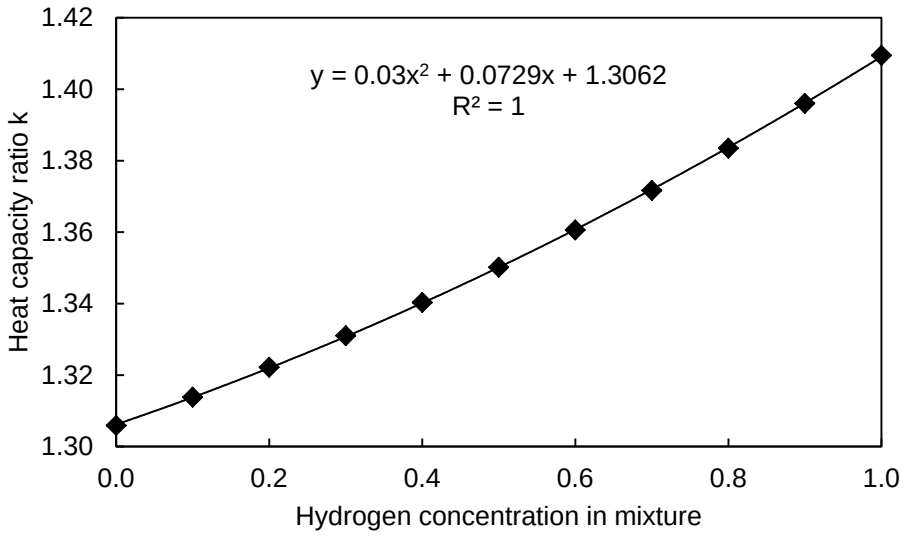

Figure 4.23 Heat capacity ratio as a function of hydrogen concentration in compression mixture

4.6.2 Rated Power

In this model, the compressor is not provided a fixed size at the start of the simulation. Instead, the compressor unit is sized to accommodate the maximum compressor head that it will need to provide. The rated compressor power is obtained by querying the maximum from the hourly indexed values of actual compressor power required and applying a safety factor to allow for operation above design load:

$$P_{comp,rated}\,0.95 = P_{comp,\max} \tag{4.102}$$

4.6.3 Ramp Rate

It is assumed that compressors, as a gas conditioning unit, do not pose constraints in terms of ramp rate. In other words, from one simulation time step to the next, it is assumed that the compressors can be started-up and shut-down completely.

Table 4.14 List of key variables and parameters for the compressor model

Type	Description	Symbol	Value	Unit	Ref.
Input	Gas to be compressed	$\dot{n}_{comp}$		kmol/h	
	H_2 conc. of gas	$c_{H_2,comp}$		mol. %	
Output	Compression work requirement	P_{comp}		kWh/h	
Parameters	Compressor isentropic efficiency	η_{comp}	Table 4.13		[96]
	Compressor gas heat capacity ratio	k_{mix}	Figure 4.23		Estimated
	Compressibility factor correlations		Table 4.3		Aspen Plus
C1	Inlet pressure	$p_{in,1}$	16	bar	[68]
	Outlet pressure	$p_{out,1}$	60	bar	Estimated
	Inlet temperature	$T_{in,1}$	288	K	Assumed
	H_2 conc. of gas	$c_{H_2,comp,1}$	100%		
C2	Inlet pressure	$p_{in,2}$	$P_{out,1}$	bar	
	Outlet pressure	$p_{out,2}$	p_{wh}	bar	
	Inlet temperature	$T_{in,2}$	288	K	Assumed
C3	Inlet pressure	$p_{in,3}$	16	bar	[68]
	Outlet pressure	$p_{out,3}$	180	bar	[97]
	Inlet temperature	$T_{in,3}$	288	K	Assumed
	H_2 conc. of gas	$c_{H_2,comp,3}$	100%		
C4	Inlet pressure	$p_{in,4}$	20	bar	Assumed
	Outlet pressure	$p_{out,4}$	180	bar	[97]
	Inlet temperature	$T_{in,4}$	288	K	Assumed

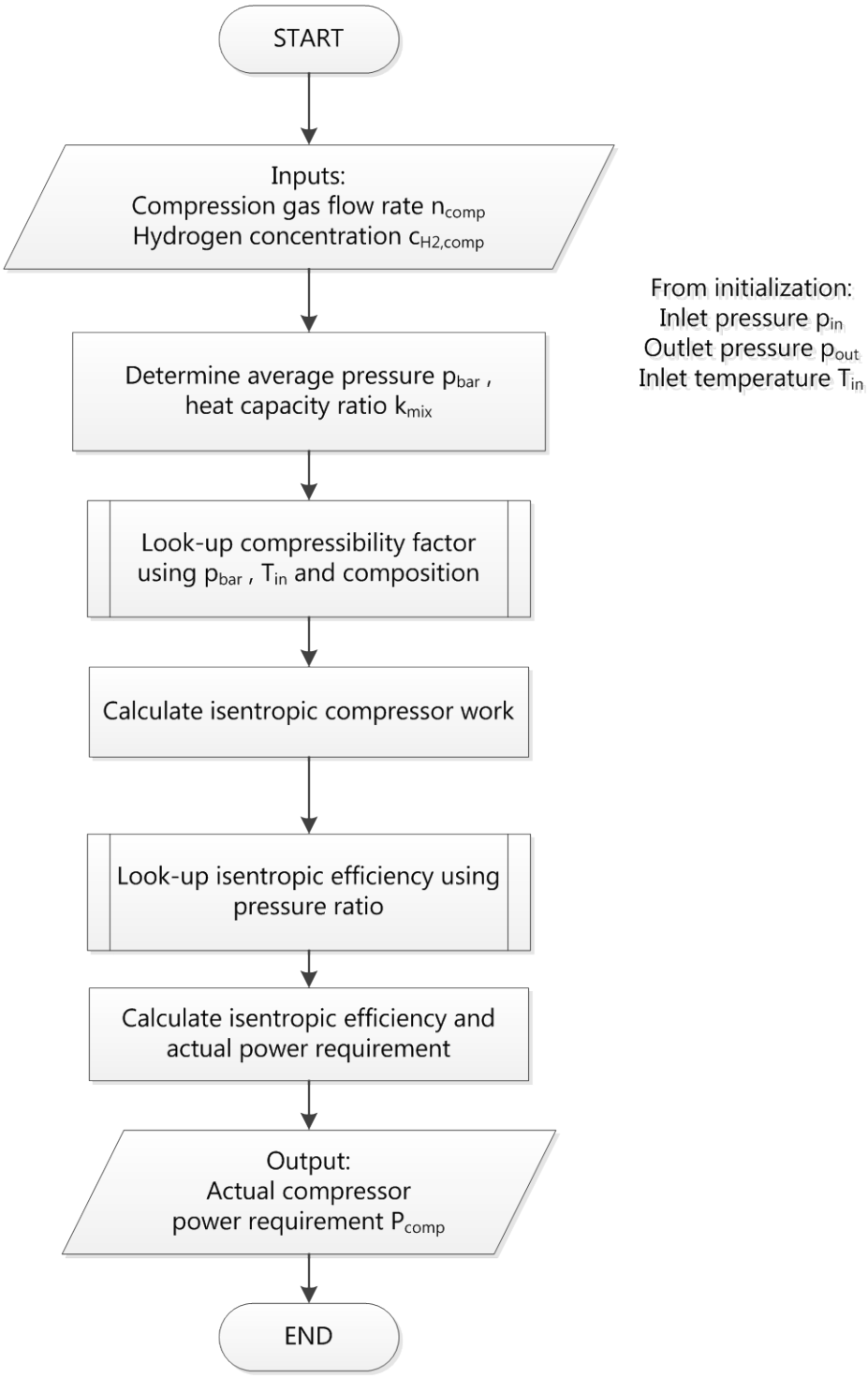

Figure 4.24 Model flow diagram for the compressor

Chapter 5
Financial Model Development

The most important financial indicator used in this project is the net present value (NPV). NPV is calculated by discounting the expected annual cash flow of the project into its present value. Because the project is not simulated for the entirety of its economic lifetime, a typical annual cash flow is estimated and projected over the lifetime of the project. The following equation is used to discount the uniform future cash flow to its present value:

$$NPV = \frac{CF_{annual}}{i}\left[1 - \frac{1}{(1+i)^n}\right] \tag{5.1}$$

CF_{annual}: Average annual net cash flow, $/year
i: Discount rate
n: Project lifetime expected, years

The estimated annual cash flow is made up of the following components: revenues from sales of energy products (power, hydrogen, and hydrogen-enriched natural gas), expense from purchases of energy products (natural gas, power), the inventoriable cost of purchase, the amortized capital cost for all equipment, as well as the annual operating and maintenance costs.

$$CF_{annual} = S_{annual} - (C_{annual} - I) - C_{inv,annual} - C_{OM,annual} \tag{5.2}$$

S_{annual}: Annual sales of energy products, $/year
C_{annual}: Annual purchases of energy inputs, $/year
I : Inventoriable cost of purchase, $/year
$C_{inv,annual}$: Amortized capital cost, $/year
$C_{OM,annual}$: Annual O&M cost, $/year

5.1 Annual Sales of Energy Products

The energy hub components which produce energy products for sales are shaded in Figure 5.1: wind power from the wind turbines, bypassed hydrogen from compressor 3, and hydrogen from the separator via compressor 4, power delivered by the CCGT, and hydrogen-enriched natural gas from the reservoir and/or the natural gas rich adsorbate from the separator. The value of the sales

transactions is determined by multiplying the hourly flow rate of the material with the corresponding market price in place for the hour in question. The prices have been first presented in the section on exogenous environmental variables (section 3.3).

$$S_{wtG}(t) = P_{WtG}(t)\,FIT(t) \tag{5.3}$$

$$S_{H_2}(t) = \left[\dot{n}_{H_2,sep}(t) + \dot{n}_{H_2,b}(t)\right] MW_{H_2} C_{H_2} \tag{5.4}$$

$$S_{CCGTtG}(t) = \dot{W}_{CC}(t)\,HOEP(t) \tag{5.5}$$

$$S_{mix}(t) = \dot{n}_{mix,tot} E_{mix}(t) C_{mix}(t) \tag{5.6}$$

S_{WtG}: Sales of wind power to the grid, $/h

S_{H_2}: Sales of hydrogen to customers, $/h

S_{CCGTtG}: Sales of CCGT power to the grid, $/h

S_{mix}: Sales of mixture to customers, $/h

Since the flow rates are expressed in terms of kmol/h, whereas the market prices are often expressed in other basis (mass or energy units), sometimes conversion is necessary. Converting a molar flow rate to a mass flow rate is quite straightforward, but converting the molar flow rate of hydrogen enriched natural gas into energy flow rates require the knowledge of the hydrogen concentration of the mixture delivered:

$$E_{mix}(t) = c_{H_2,mix,tot}(t)\,E_{H_2} + \left[1 - c_{H_2,mix,tot}(t)\right] E_{NG} \tag{5.7}$$

E_{mix}:Energy content of mixture, MMBtu/kmol

E_{H_2}: Energy content of hydrogen, MMBtu/kmol

E_{NG}: Energy content of natural gas, MMBtu/kmol

$c_{H_2,mix,tot}$: Hydrogen concentration of mixture delivered

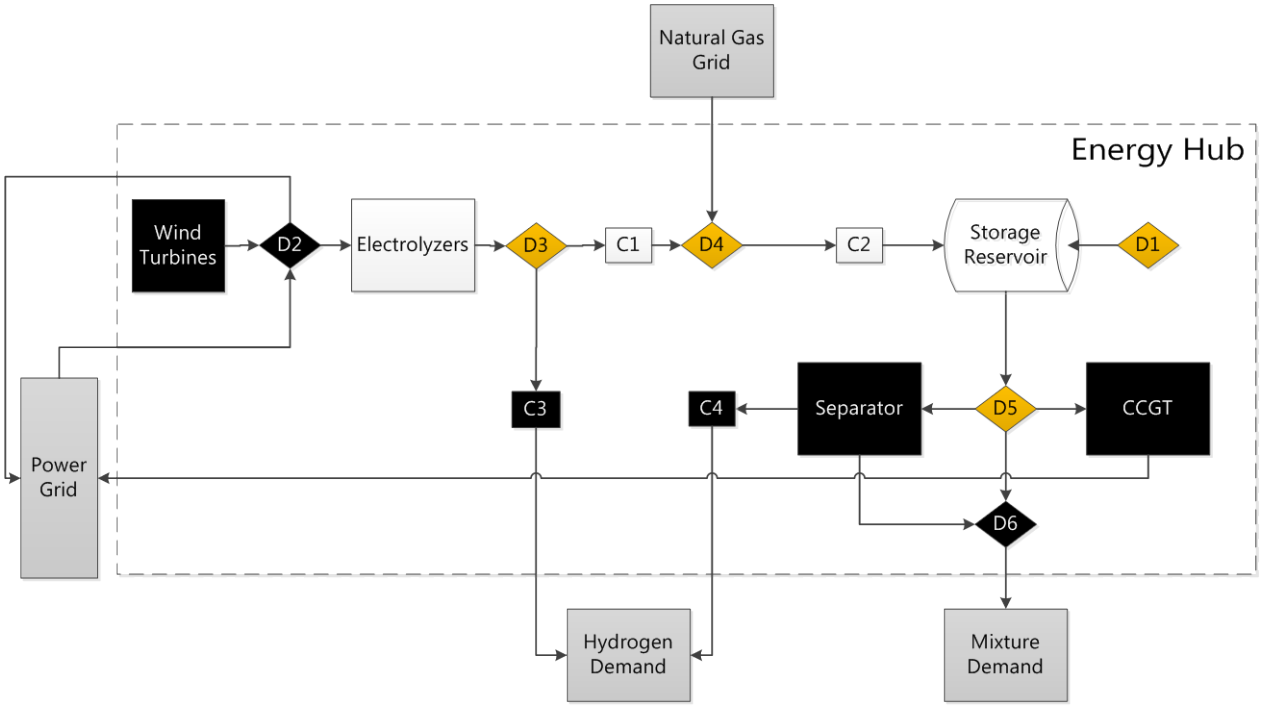

Figure 5.1 Points of sales of energy products from the energy hub

Once the revenues from all four types of sales have been calculated, the total sales are calculated by summing the hourly values over the period of interest (2010, 2011 and 2012, respectively). In this case, for year-based financial evaluation, the sales are summed over each of the three years simulated.

$$S_{annual} = \sum_{1}^{t}\left[S_{wtG}(t) + S_{H_2}(t) + S_{CCTGtG}(t) + S_{mix}(t)\right] \tag{5.8}$$

Table 5.1 List of key variables and parameters for the annual sales model

Type	Description	Symbol	Value	Unit	Ref.
Input	Wind power delivered to the grid	P_{WtG}		MW	
	Hydrogen delivered by separator	$\dot{n}_{H_2,sep}$		kmol/h	
	Hydrogen delivered from bypass	$\dot{n}_{H_2,b}$		kmol/h	
	Power delivered by CCGT to the grid	$\dot{W}_{CC}$		MW	
	Mixture delivered to customers	$\dot{n}_{mix,tot}$		kmol/h	
	Hydrogen concentration of mixture delivered	$c_{H_2,mix,tot}$		mol. %	
Output	Annual sales of energy products	S_{annual}		\$/year	
	Sales of wind power to the grid	S_{WtG}		\$/h	
	Sales of hydrogen to customers	S_{H_2}		\$/h	
	Sales of CCGT power to the grid	S_{CCGTtG}		\$/h	
	Sales of mixture to customers	S_{mix}		\$/h	
Parameters	FIT time differentiated schedule	FIT	Feed-in tariff prices for different hours of the week	\$/MWh	[71]
	Market price for H_2	C_{H_2}	5	\$/kg	Section 3.3.4
	Market price for electricity	$HOEP$	Hourly Ontario Energy Price for 2010 to 2012, time series	\$/MWh	[14]
	Energy content of hydrogen	E_{H_2}	0.2272	MMBtu/kmol	LHV of hydrogen
	Energy content of natural gas	E_{NG}	0.7618	MMBtu/kmol	Based on Table 4.2
	Market price of mixture	C_{mix}	Identical to natural gas market prices	\$/MMBtu	Estimated in section 3.3.3

5.2 Annual Purchases of Energy Inputs

The annual costs incurred by the purchases of energy products consist of two components, the purchase of natural gas from the gas grid and the purchase of electricity from the power grid. Similar to the calculation of sales, the costs of purchases is calculated by multiplying the flow rate of the material purchased with the corresponding market price.

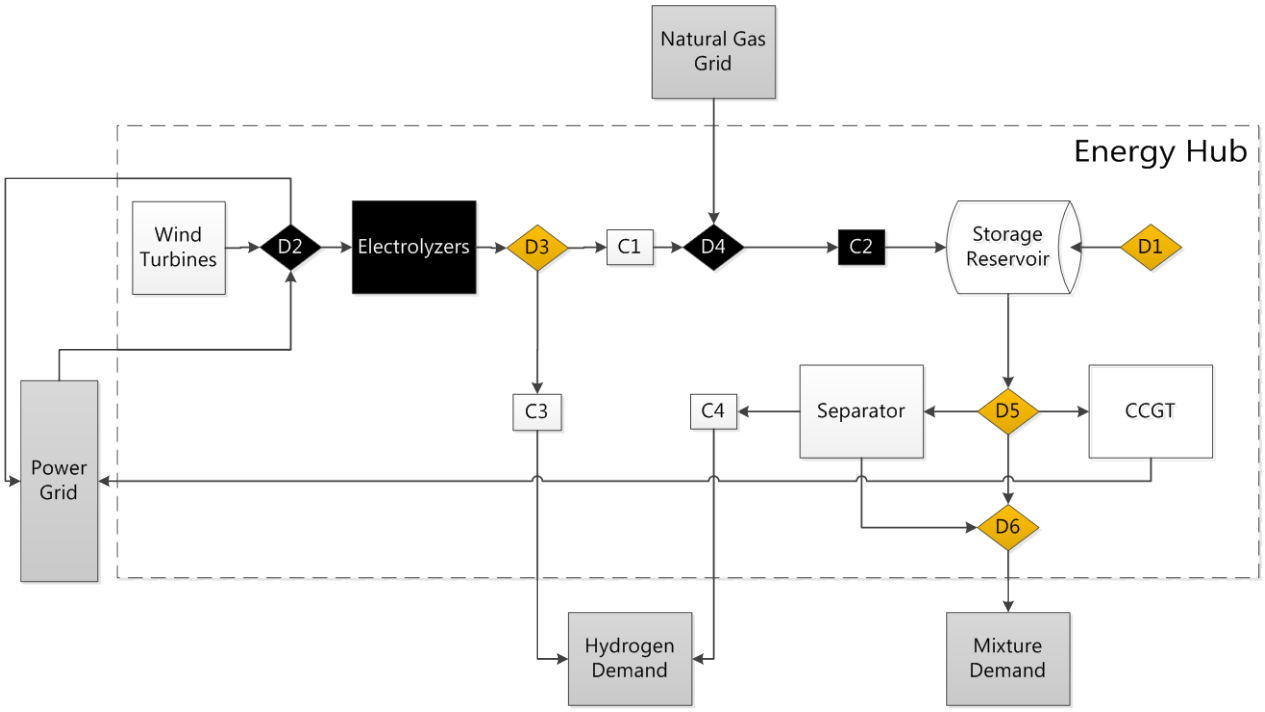

Figure 5.2 Points of purchases of energy products for the energy hub

$$C_{Gts}(t) = P_{Gts}(t)\,HOEP(t) \tag{5.9}$$

$$C_{NGts}(t) = \dot{n}_{NG,in}(t)\,E_{NG}\,C_{NG}(t) \tag{5.10}$$

C_{Gts}: Cost of power from the grid, \$/h

C_{NGts}: Cost of natural gas from pipelines, \$/h

Because wind turbines are considered to be an integral part of the energy hub, wind power supplied to the electrolyzer do not constitute a purchase, for money has not been transferred between two entities: the operators of the wind turbines are also the operators of the energy hub.

The total cost of all energy purchases over a period interest is summed as follows:

$$C_{annual} = \sum_{1}^{t} \left[C_{Gts}(t) + C_{NGts}(t) \right] \tag{5.11}$$

Table 5.2 List of key variables and parameters for the annual purchase model

Type	Description	Symbol	Value	Unit	Ref.
Input	Power stored from grid	P_{Gts}		MW	
	Natural gas injected for storage	$\dot{n}_{NG,in}$		kmol/h	
Output	Annual purchase of energy inputs	C_{annual}		$/year	
	Cost of power from the grid	C_{Gts}		$/h	
	Cost of natural gas from pipelines	C_{NGts}		$/h	
Parameters	Energy content of natural gas	E_{NG}	0.7618	MMBtu/kmol	Based on Table 4.2
	Market price of electricity	$HOEP$	Hourly Ontario Energy Price for 2010 to 2012, time series	$/MWh	[14]
	Market price of natural gas	C_{NG}	Weekly average of the Henry Hub spot price from 2010 to 2012, time series	$/MMBtu	[72]

5.3 Inventoriable Cost of Purchase

The total purchase cost for starting material, incurred at the time of purchase, can be separated into two components: the cost of material incurred, which represents the portion of annual purchase cost attributable to the sales made in that year, and the inventoried purchase cost, which represents the portion of annual purchase cost which is attributable to the inventory accrued over the year under consideration..

$$C_{annual} = I + C_{incurred} \tag{5.12}$$

$$C_{incurred} = C_{annual} - I \tag{5.13}$$

C_{annual}: Annual purchase of energy inputs, $/year
I: Inventoriable cost of purchase, $/year
$C_{incurred}$: Incurred cost of purchase, $/year

The inventoriable cost of purchase is equivalent to the change in inventory value over the course of a year. It is also the portion of the annual expenses that can be deducted from the annual income statement, for not all of the material purchased is processed and delivered to the customers within the same year. This value can be positive or negative. It is positive in the case that there is a net gain in the value of inventory compared to the beginning of the year. It is negative if there is a net loss in the value of inventory.

To determine the inventoriable cost of purchase, it is necessary to obtain the value of material in storage at the beginning and end of each year.

$$I_i = \frac{I_{i,f} - I_{i,0}}{\Delta t} \; I_i = \frac{I_{i,f} - I_{i,0}}{\Delta t} \tag{5.14}$$

$$I_{2010,0} = C_{res,tot}\left(t_0\right) \tag{5.15}$$

$$I_{2010,f} = I_{2011,0} = C_{res,tot}\left(t_1\right) \tag{5.16}$$

$$I_{2011,f} = I_{2012,0} = C_{res,tot}\left(t_2\right) \tag{5.17}$$

$$I_{2012,f} = C_{res,tot}\left(t_3\right) \tag{5.18}$$

I_i: Inventoriable cost of purchase of year i, $/year

$I_{i,f}$: Cost of inventory at end of year i, $

$I_{i,0}$: Cost of inventory at beginning of year i, $

Δt: Period of inventory accumulation/depletion = 1 year

$C_{res,tot}(t)$: Cost of gas in storage at time t, $

At the beginning of the simulation, the value of gas in storage is estimated using the initial physical inventory n_{total} n_{total} n_{total} and the estimated unit cost of the gas stored.

$$C_{res,tot}(t_0) = C_{mix,unit,0} n_{tot,0} \; C_{res,tot}(t_0) = C_{mix,unit,0} n_{tot,0} \; C_{res,tot}(t_0) = C_{mix,unit,0} n_{tot,0} \tag{5.19}$$

$C_{mix,unit,0}$: Initial unit cost of gas in storage, $/kmol

$n_{tot,0}$: Initial amount of gas in storage, kmol

Then, the value of inventory and the unit cost of store gas are updated hourly using the following logic:

$$C_{res,tot}(t) = \begin{cases} C_{res,tot}(t-1) + \dot{n}_{s,act}(t) n_{mix,unit}(t-1), \text{ if } \dot{n}_{s,act}(t) < 0 \\ C_{res,tot}(t-1) + C_{NGts}(t) + C_{Gts}(t) \dfrac{\dot{n}_{H_{2,S}}(t)}{\dot{n}_{H_2,E}(t)}, \text{ if } \dot{n}_{s,act}(t) \geq 0 \end{cases} \tag{5.20}$$

$$C_{mix,unit}(t) = \frac{C_{res,tot}(t)}{n_{tot}(t)} \tag{5.21}$$

$\dot{n}_{s,act}$: Actual flow rate into/out of the reservoir, kmol/h

$\dot{n}_{H_2,S}$: Amount of hydrogen stored, kmol/h

$\dot{n}_{H_2,E}$: Amount of electrolytic hydrogen produced, kmol/h

Only a portion of the cost of grid power is allocated to the gas in storage, because not all hydrogen produced using the electricity consumed is stored.

Table 5.3 List of key variables and parameters for the inventoriable purchase cost model

Type	Description	Symbol	Value	Unit	Ref.
Input	Annual purchase of energy inputs for year i	$C_{annual,i}$		$/year	
	Actual flow rate into/out of the reservoir	$\dot{n}_{s,act}$		kmol/h	
	Cost of power from the grid	C_{Gts}		$/h	
	Cost of natural gas from pipelines	C_{NGts}		$/h	
	Amount of hydrogen stored	$\dot{n}_{H_2,S}$		kmol/h	
	Amount of hydrogen bypassed	$\dot{n}_{H_2,b}$		kmol/h	
Output	Inventoriable cost of purchase for year i	I_i		$/year	
	Incurred cost of purchase for year i	$C_{incurred,i}$		$/year	
	Cost of gas in storage	$C_{res,tot}$		$	
Parameters	Initial unit cost of gas in storage	$C_{mix,unit,0}$	5.88	$/kmol	Estimated from C_{NG}
	Initial amount of gas in storage	$n_{tot,0}$	2.40E+06	kmol	Assumed

5.4 Capital Cost

The capital cost of the energy hub is determined based on the rated input or output capacity of its constituents. Wind turbines, electrolyzers, compressors, the separator unit and the combined-cycle gas turbine plant make up the bulk of the capital cost. For this model other components of the capital cost are assumed to be negligible. In the case that the configuration of energy hub excludes a given component, the component in question does not contribute to the total capital cost.

$$C_{inv,tot} = C_{W,inv} + C_{E,inv} + C_{sep,inv} + C_{CCGT,inv} + C_{comp,inv} \tag{5.22}$$

Once the total capital cost value is obtained, the capital recovery factor is used to transform the total capital investment, a one-time cash flow at the beginning of the project, into a series of constant annuities over the course of project life. By definition, it is calculated as follows:

$$CRF = \frac{i(1+i)^n}{(1+i)^n - 1} \tag{5.23}$$

$$C_{inv,annual} = C_{inv,tot} CRF \tag{5.24}$$

5.4.1 Wind Turbines

The capital cost of wind power projects in Canada is given as a function of project rated capacity [98]:

$$C_{W,inv} = \$2,000,000 \frac{CEPCI_{2008}}{CEPCI_{2006}} P_{W,rated} \tag{5.25}$$

$CEPCI_{2008}$: Chemical Engineering Plant Cost Index for 2008
$CEPCI_{2006}$: Chemical Engineering Plant Cost Index for 2006

A technical lifetime of 20 years is expected for wind turbines. As long as the economic lifetime of the project falls below 20 years, it is not necessary to incur replacement costs.

5.4.2 Electrolyzers

This section to determine the capital cost of electrolyzers is adapted from [99-101]. It is known that for hydrogen production scale ranging from 0.05kmol/h to 50kmol/h, only one unit of electrolyzer is needed, and economies of scale is possible.

$$C_{E,inv} = 224,490\left(2\dot{n}_{E,H_2,rated}\right)^{0.6156} \qquad 0.05 \le \dot{n}_{E,H_2,Rated} \le 50 \tag{5.26}$$

Modules of a given rating (2.7kmol/h, HySTAT-60 from Hydrogenics Corps.) have been chosen for this model. The capital cost required for an individual unit is thus:

$$C_{E,inv,i} = \$224,490\left(2\dot{n}_{E,H_2,rated,i}\right)^{0.6156} \tag{5.27}$$

The total capital cost for electrolyzers depend on the number of units procured:

$$C_{E,inv,0} = N_E C_{E,inv,i} \tag{5.28}$$

The typical lifetime of alkaline electrolyzers is estimated to be 10 years. Therefore, if the economic lifetime of the project is set to more than 10 years, replacement costs are incurred for electrolyzers in the 10th year of operation. Replacement costs are estimated to be 50% of the original capital cost at the time of replacement. It is discounted to its present value.

$$C_{E,inv,rep} = \frac{0.5C_{E,inv,0}}{(1+i)^{10}} \tag{5.29}$$

$$C_{E,inv} = C_{E,inv,0} + C_{E,inv,rep} \tag{5.30}$$

5.4.3 Separator

The main initial investment for a PSA system consists of the purchase of the adsorption beds (adsorbent and the vessel). Compressors are not required for feed pressurization, because reservoir gas is available at pressures higher than 20 bar, the stated operating pressure of the adsorption columns.

$$C_{sep,inv} = C_{sep,ads} + C_{sep,col} \tag{5.31}$$

$C_{sep,ads}$: Capital cost of adsorbent, $

$C_{sep,col}$: Capital cost of separation columns, $

The total adsorption volume required for the separation is calculated using the values of adsorbent productivity. The adsorbent productivity (MAR) for the operation conditions considered: 20 bar and 298 K, is approximated to be 30 volumetric units of feed per volume unit of active carbon per cycle, or 60 volumetric units of adsorbent for an hour (2 cycles occur per hour, 30 minutes per cycle).

$$MAR_h = MAR_{cycle} \frac{t_h}{t_{cycle}} \tag{5.32}$$

$$V_{ads} = \frac{\dot{V}_{feed,rated}}{MAR_h} \tag{5.33}$$

MAR_h: Adsorbent productivity, Nm^3/m^3h

MAR_{cycle}: Adsorbent productivity, Nm^3/m^3cycle

t_h: Time in an hour = 60 min

t_{cycle}: Duration of a cycle, min

V_{ads}: Volume of adsorbent required, m^3

$\dot{V}_{feed,rated}$: Rated input capacity of separator, Nm^3/h

Then, the cost of adsorbent used in the process can be calculated using its market price ($/weight)

$$C_{sep,ads} = V_{ads} \rho_{ads} C_{ads} \tag{5.34}$$

ρ_{ads}: Density of adsorbent (active carbon), kg/m^3

C_{ads}: Unit cost of adsorbent (active carbon), $/kg

The cost of the containing vessels is an important part of the overall unit cost. It is assumed that vessels 20 ft long, and 6 ft in diameter are used. Approximating the volume of vessels as cylinders, the number of vessels required to contain the adsorbent needed can be calculated. In order to ensure continuous process operation, the minimum number of adsorption beds is 2. The unit cost of vessels is computed using the Guthrie method, adjusted for its size, then updated from 1969 dollars to 2008 dollars using the Chemical Engineering Plant Cost Index (CEPCI) [102].

$$V_{col} = \pi \left(D_{col}/2 \right)^2 L_{col} \tag{5.35}$$

$$N_{col} = \begin{cases} 2, & \frac{V_{ads}}{V_{col}} < 2 \\ round\left(\frac{V_{ads}}{V_{col}} \right), & \frac{V_{ads}}{V_{col}} \geq 2 \end{cases} \tag{5.36}$$

$$C_{sep,col} = N_{col} C_{col} = N_{col} \left[\$690 \frac{CEPCI_{2008}}{CEPCI_{1969}} \left(\frac{L_{col}}{4\,ft} \right)^{0.78} \left(\frac{D_{col}}{3\,ft} \right)^{0.98} \left(3.18 + 1.05 - 1 \right) \right] \tag{5.37}$$

V_{col}: Volume of a column, m^3
D_{col}: Diameter of a column, m
L_{col}: Length of a column, m
N_{col}: Number of columns required
C_{col}: Unit cost of column, $/column

It is assumed that the technical lifetime of the vessels as well as the adsorbent is longer than the economic lifetime of the project; therefore, there are no replacement costs to be considered.

5.4.4 CCGT

For the range of capacity foreseen (< 200 MW), the investment cost of CCGT power plants is estimated to be $650/kW in 2006 dollars [58]. This figure is converted to 2008 dollars as in the rest of costing calculations:

$$C_{CCGT,inv} = \$650,000\left(\frac{CEPCI_{2008}}{CEPCI_{2006}}\right)\dot{W}_{CC,rated} \tag{5.38}$$

The technical lifetime of CCGT plants are in the order of 30 years, longer than the economic lifetime specified for this project, therefore there is no replacement cost for the turbines.

5.4.5 Compressors

The compressor cost model in this section is based on the work of [103] on the compression costs for carbon dioxide sequestration. The capital investment required by the compression unit is:

$$C_{comp,inv} = P_{comp,rated} C_{comp} \tag{5.39}$$

The cost factor for a range of rated capacity is shown in the figure below; as the rated capacity increases, the per unit cost decreases because of economies of scale. It is assumed that the service life of the compressors is longer than the life time of the project, and no replacement investment is required.

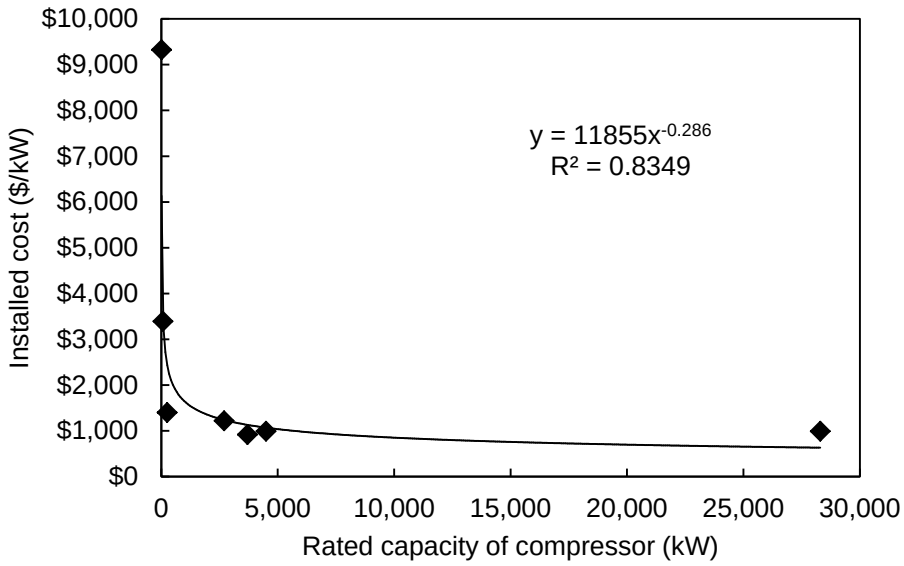

Figure 5.3 Capital cost factor of compressors for different installed capacity[104]

Note that there are four compression units of different rated capacities; the calculations above are completed for all four. The final capital cost reported includes for all units.

Table 5.4 List of key variables and parameters for the capital cost model

Type	Description	Symbol	Value	Unit	Ref.
Input	Rated capacity of wind turbines	$P_{W,rated}$		MW	
	Number of electrolyzer units	N_E			
	Rated input capacity of separator	$\dot{V}_{feed,rated}$		Nm3/h	
	Rated capacity of CCGT	$\dot{W}_{CC,rated}$		MW	
	Rated capacity of compressor	$P_{comp,rated}$		kW	
Output	Total capital cost required	$C_{inv,tot}$		$	
	Amortized capital cost	$C_{inv,annual}$		$/year	
	Capital cost of wind turbines	$C_{W,inv}$		$	
	Capital cost of electrolyzers	$C_{E,inv}$		$	
	Capital cost of the separator	$C_{sep,inv}$		$	
	Capital cost of the CCGT	$C_{CCGT,inv}$		$	
	Capital cost of compressors	$C_{comp,inv}$		$	
Parameters	Discount rate	i	8%		Assumed
	Expected project lifetime	n	20	years	Estimated
	CEPCI index for 2008	$CEPCI_{2008}$	575.4		
	CEPCI index for 2006	$CEPCI_{2006}$	499.6		
	CEPCI index for 1969	$CEPCI_{1969}$	119		
	Unit cost factor for wind turbines		2E+06	$/MW	[98]
	Rated capacity of electrolyzer unit	$\dot{n}_{E,H_2,rated,i}$	2.7	kmol/h	[68]
	Adsorbent productivity	MAR_{cycle}	30	$Nm^3/(m^3$-cycle)	Estimated
	Duration of a separation cycle	t_{cycle}	30	min	Estimated
	Density of adsorbent	ρ_{ads}	481	kg/m^3	[64]

	Unit cost of adsorbent	C_{ads}	1	$/kg	Estimated
	Diameter of a column	D_{col}	1.83	m	[94]
	Length of a column	L_{col}	6.1	m	[94]
	Correlation between column volume and column unit cost				[102]
	Unit cost factor for CCGT		6.5E+05	$/MW	[58]
	Unit cost factor for compressors		See Figure 5.3	$/kW	[104]

5.5 Operating and Maintenance Cost

Operating and maintenance cost for the energy hub is divided into two types: fixed and variable. Fixed maintenance cost is assumed to be a percentage of the annual capital cost:

$$C_{OM,\,fixed} = R_{OM} C_{inv,annual} \tag{5.40}$$

R_{OM}:Fixed operating cost ratio, % of $C_{inv,annual}$

The variable operating cost is mainly attributed to the consumption of energy by reciprocating compressors used on-site. Reciprocating compressor can have two types of driver: natural gas engines or electric motors. It is assumed that the compressors used at the energy hub are powered by natural gas engines. The energy consumption of the compressors is converted expressed in terms of natural gas consumption, through the use of conversion factors.

$$P_{comp,NG} = P_{comp} \frac{GPR}{E_{NG}} \tag{5.41}$$

$P_{comp,NG}$: Natural gas required by compressors, kmol/h

P_{comp}: Power requirement of compressors, kWh/h

GPR: Gas energy required per unit of electrical energy, MMBtu/kWh

E_{NG}: Energy content of natural gas, MMBtu/kmol

The cost of energy consumed by compressors is calculated as follows:

$$C_{comp,E}(t) = P_{comp,NG}(t) C_{NG}(t) \tag{5.42}$$

The annual operating and maintenance is the sum of the fixed cost and the annual variable cost:

$$C_{OM,annual} = C_{OM,\,fixed} + \sum_{1}^{t} C_{comp,E}(t) \tag{5.43}$$

Table 5.5 List of key variables and parameters for the O&M cost model

Type	Description	Symbol	Value	Unit	Ref.
Input	Amortized capital cost	$C_{inv,annual}$		\$/year	
	Power requirement of compressors	P_{comp}		kWh/h	
Output	Fixed annual O&M cost	$C_{OM,fixed}$		\$/year	
	Energy cost for compression	$C_{comp,E}$		\$/h	
	Annual O&M cost	$C_{OM,annual}$		\$/year	
Parameters	Fixed operating cost ratio	R_{OM}	4%	% of $C_{inv,annual}$	
	Gas energy required per unit of electrical energy	GPR	0.010	MMBtu/kWh	[96]
	Energy content of natural gas	E_{NG}	0.7618	MMBtu/kmol	Based on Table 4.2

Chapter 6
Emission Model Development

The emission model complements the financial model by assessing the environmental performance of the energy hub. The key indicator used is the net emissions (incurred or mitigated) due to the operation of the energy hub during the simulated year.

6.1 Net Emissions

The carbon dioxide emissions associated with the operation of the energy hub are divided into two types: the emissions which are incurred during the operation of the energy hub, and emissions which are mitigated by the operation of the energy hub. The net amount of emissions mitigated is given by the following difference:

$$m_{CO_2,\,net} = m_{CO_2,\,incurred} - m_{CO_2,\,mitigated} \tag{6.1}$$

$m_{CO_2,\,net}$: Net emissions, kg CO_2/year

$m_{CO_2,\,incurred}$: Emissions incurred, kg CO_2/year

$m_{CO_2,\,mitigated}$: Emissions mitigated, kg CO_2/year

A positive net emissions value means that more carbon dioxide have been emitted because of the operation of the energy hub; a; a negative value means that, overall, carbon emissions have been mitigated due to the operation of the energy hub.

6.2 Emissions Incurred

The carbon dioxide associated with the operation of the energy hub is attributed to five sources: on-site use of natural gas driven compressors for gas compression, consumption of grid-generated electricity, electricity generation from on-site wind turbines, on-site use of the CCGT for energy recovery, and the off-site use of hydrogen-enriched natural gas, once it reaches the end-users through the distribution pipelines.

$$m_{CO_2,incurred} = m_{CO_2,comp} + m_{CO_2,G} + m_{CO_2,W} + m_{CO_2,CCGT} + m_{CO_2,mix} \tag{6.2}$$

6.2.1 Gas Compression

The amount of compressor work required is known from the simulations. It is still necessary to calculate the emissions associated with this known compression duty. Assuming that all compressors present at the energy hub have natural gas-driven engines, the following conversion factors are used:

$$n_{CO_2,comp} = n_{NG,comp} = \sum \left[P_{comp}(t) \right] \frac{GPR}{E_{NG}} \tag{6.3}$$

$$m_{CO_2,comp} = n_{CO_2,comp} MW_{CO_2} \tag{6.4}$$

6.2.2 Electrolyzer Power Supply

The carbon dioxide emitted by grid-connected generators that supply the electrolyzer is a function of two variables. First of all, the emission factor of grid-supplied power, which is function of time and estimated as described in section 3.3.1. Secondly, the emissions of grid-connected generators that can be attributed to the operation of the energy hub are limited to the amount of grid power delivered to the electrolyzer. Obviously, the absolute value of carbon dioxide emitted from all grid-connected generators is a much higher value, but only the portion that is consumed by the energy hub is counted in these calculations.

$$m_{CO_{2,G}} = \sum \left[EF_G(t) P_{Gts}(t) \right] \tag{6.5}$$

The carbon dioxide emissions associated with wind power generation from existing life cycle analysis is low but non-negligible. Unlike the emission factor for the grid which is transient, the emission factor for wind turbines is assumed to be a number that is constant over the lifetime of the turbine. Note that the power generated by wind turbines is not only used to supply the electrolyzer (P_{wts} P_{wts} P_{wts}), but it may also be delivered to the grid directly P_{wtG} (P_{wtG} P_{wtG}) when market conditions are favourable.

$$m_{CO_{2,W}} = \sum \left[P_W(t) \right] EF_W \tag{6.6}$$

$$P_W(t) = P_{wts}(t) + P_{wtG}(t) \tag{6.7}$$

6.2.3 On-Site CCGT Generation

Assuming 100% combustion within the gas turbine, the number of moles of carbon dioxide produced by the combustion of fuel is the same as the number of moles of natural gas consumed. Upon combustion, hydrogen does not form carbon dioxide.

$$m_{CO_2,CCGT}(t) = \sum \left\{ \left[1 - c_{H_2,fuel}(t) \right] \dot{n}_{fuel}(t) \right\} MW_{CO_2} \tag{6.8}$$

6.2.4 HENG Mixture Consumption

Another important source of carbon emissions come from the use of hydrogen-enriched natural gas mixture once it has reached the end-users. Similarly to fuel combustion at the on-site CCGT, only the natural gas contained in the mixture contributes to carbon dioxide formation, whereas the hydrogen added produces mainly water vapour as a combustion product.

$$m_{CO_2,mix} = \sum \left\{ \left[1 - c_{H_2,mix(t)} \right] n_{mix,tot}(t) \right\} MW_{CO_2} \tag{6.9}$$

6.3 Emissions Mitigated

On the other hand, carbon dioxide emissions which are mitigated due to the operation of the energy hub can also be attributed to three sources. The delivery of electrolytic hydrogen displaces the need for hydrogen produced via steam methane reforming. The delivery power from the mixture-fired CCGT allows for the displacement of emissions from other gas turbines which run on pure natural gas. Finally, the gas end-users no longer consume pure natural gas, since they are now supplied with the hydrogen-enriched gas mixture.

$$m_{CO_2,mitigated} = m_{CO_2,SMR} + m_{CO_2,fuel} + m_{CO_2,NG} \tag{6.10}$$

6.3.1 Hydrogen from Steam Methane Reforming

The amount of electrolytic hydrogen delivered displaces the same amount of hydrogen produced via the traditional steam methane reforming process. The carbon dioxide emissions associated with unit production of hydrogen via SMR is documented in the literature [105].

$$m_{CO_2,SMR} = \sum \left[\dot{n}_{H_2,b}(t) + \dot{n}_{H_2,sep}(t) \right] MW_{H_2} EF_{SMR} \tag{6.11}$$

6.3.2 Gas-Fired CCGT Generation

It is assumed that, in the case that the energy hub did not operate, the power generated by the on-site CCGT plant would still be delivered to the grid, but by a competing CCGT operator that supplies the gas turbine with pure natural gas.

$$m_{CO_2,\,fuel} = \sum \left[\dot{n}_{fuel}\left(t\right) \right] MW_{CO_2} \tag{6.12}$$

6.3.3 Natural Gas Consumption

Analogous to the section above, it is assumed that, in the case that the energy hub did not operate, then the off-site customers would have used pure natural gas instead of hydrogen-enriched natural gas. The emissions that would have been produced from the combustion of natural gas are:

$$m_{CO_2,NG} = \sum \left[\dot{n}_{mix,tot}\left(t\right) \right] MW_{CO_2} \tag{6.13}$$

Table 6.1 List of key variables and parameters for the emission model

Type	Description	Symbol	Value	Unit	Ref.
Input	Power requirement of compressors	P_{comp}		kW	
	Power stored from grid	P_{Gts}		MW	
	Wind power generated	P_W		MW	
	Fuel dispatched to CCGT	$\dot{n}_{fuel}$		kmol/h	
	H2 concentration of fuel	$c_{H_2,\,fuel}$		mol. %	
	Mixture delivered to client	$\dot{n}_{mix,tot}$		kmol/h	
	H2 concentration of mixture delivered	$c_{H_2,mix,tot}$		mol. %	
	Hydrogen delivered by separator	$\dot{n}_{H_2,sep}$		kmol/h	
	Hydrogen delivered from bypass	$\dot{n}_{H_2,b}$		kmol/h	
Output	Net emissions	$m_{CO_2,\,net}$		kg CO_2/year	
	Emissions incurred	$m_{CO_2,\,incurred}$		kg CO_2/year	

	Emissions mitigated	$m_{CO_2,\,mitigated}$		kg CO_2/year	
	Emissions from gas compression	$m_{CO_2,comp}$		kg CO_2/year	
	Emissions from grid power generation	$m_{CO_2,G}$		kg CO_2/year	
	Emissions from wind power generation	$m_{CO_2,W}$		kg CO_2/year	
	Emissions from on-site CCGT power generation	$m_{CO_2,CCGT}$		kg CO_2/year	
	Emissions from off-site use of mixture	$m_{CO_2,mix}$		kg CO_2/year	
	Emissions displaced from SMR hydrogen	$m_{CO_2,SMR}$		kg CO_2/year	
	Emissions displaced from on-site CCGT fuel use	$m_{CO_2,\,fuel}$		kg CO_2/year	
	Emissions displaced from off-site NG use	$m_{CO_2,NG}$		kg CO_2/year	
Parameters	Gas energy required per unit of electrical energy	GPR	0.010	MMBtu/kWh	[96]
	Energy content of natural gas	E_{NG}	0.7618	MMBtu/kmol	Based on Table 4.2
	Emission factor of grid power in Ontario	EF_G	Figure 3.8	kg CO_2/MWh	Estimated from [106] and Ontario demand
	Emission factor of wind power	EF_W	19	kg CO_2/MWh	[106]
	Emission factor for hydrogen production via SMR	EF_{SMR}	10.6	kg CO_2/kg H_2	[105]
	Molar mass of H_2	MW_{H_2}	2	kg/kmol	
	Molar mass of CO_2	MW_{CO_2}	44	kg/kmol	

Chapter 7
Scenario Generation

In order to understand the impact of proposed underground storage of hydrogen, one base case scenario and four additional scenarios are generated, each focusing on one particular use of the hydrogen storage technology.

7.1 Base Case Scenario: Underground Gas Storage

The base case scenario describes the operation of an underground gas storage facility without the production and storage of hydrogen. Conventionally, natural gas is injected into UGS facilities from April through October and withdrawn from November through March, completing a gas storage cycle in a year. The underlying driving force is the typical natural gas profile: low prices during summer and higher prices during winter, the heating season. But, in recent years, the seasonal variation in natural gas prices is dwarfed by the year-to-year variation. In order to factor in the effect of year-to-year natural gas price fluctuation on UGS facilities, a three calendar year simulation time frame is chosen. The results obtained from the base case scenario allows one to differentiate between the variability inherent to UGS facilities and the effect of underground storage of hydrogen, which is performed in addition to regular UGS operations.

7.1.1 Summary

In this scenario, the energy hub is operated as a conventional natural gas storage facility, thus it is simplified to its core component: the storage reservoir (and compressor required for gas injection). The updated diagram illustrating the configuration of the base case scenario is shown below:

Table 7.1 Configuration and capacity of energy hub components for the base case scenario

Component	Status	Rated Capacity
Reservoir	*ON*	6.1-7.6 MMscf
Electrolyzers	*OFF*	N/A
Wind Turbines	*OFF*	N/A
CCGT	*OFF*	N/A
Separator	*OFF*	N/A

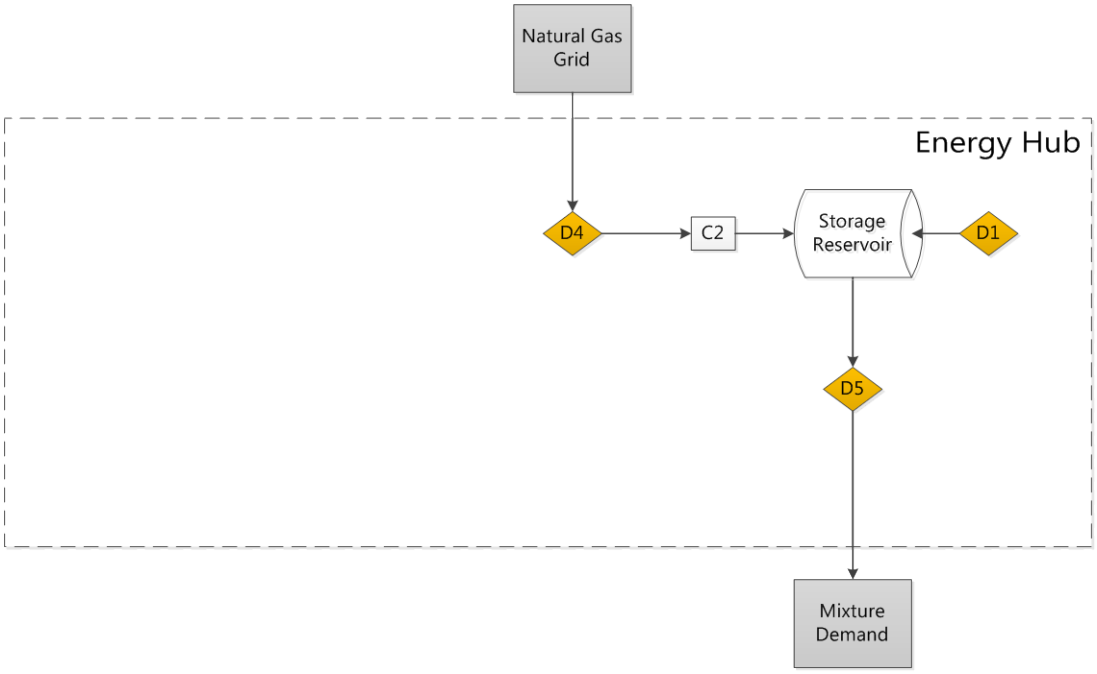

Figure 7.1 Model scope for the base case scenario

Table 7.2 Summary of decision point logic for the base case scenario

	Description	Action
D1	Reservoir operation regime	Inject when the NG market price is low; withdrawal when the NG market price is high
D2	Electrolyzer power supply	N/A
D3	Hydrogen bypass	N/A
D4	NG/H_2 blending	Set NG stored to injectability limit
D5	Mixture dispatch	Set NG produced to deliverability limit
D6	Separator recycle	N/A

7.1.2 Decision Point Model Logic

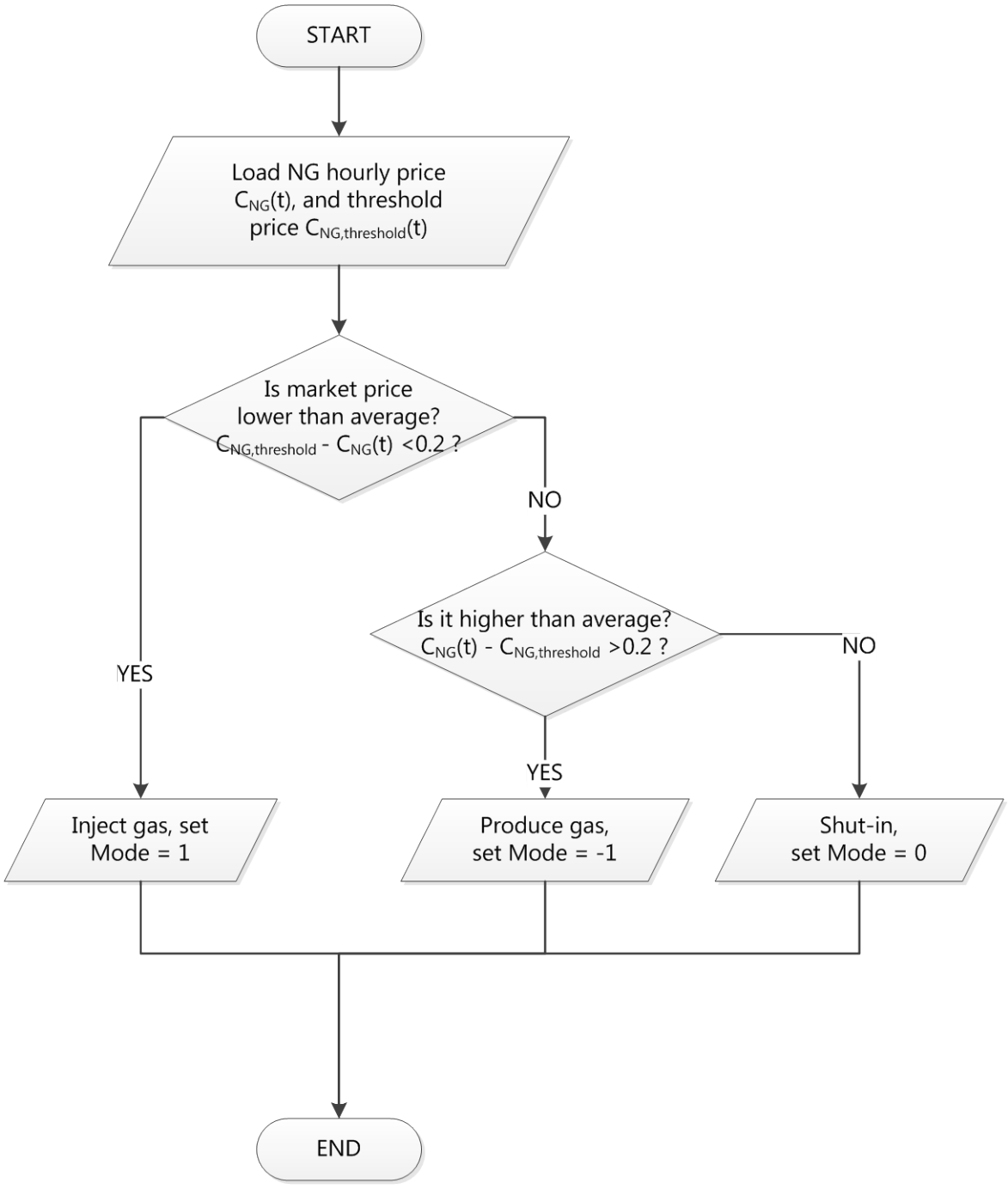

Figure 7.2 Reservoir operation decision point (D1) for the base case scenario

The key decision point present in this scenario is D1, depicted below: the reservoir enters injection mode whenever the market of natural gas is lower than the threshold value by $0.20. On the other

hand, whenever the market price of natural gas is $0.20 higher than the threshold value, the reservoir enters withdrawal mode. When the prices are equal, the reservoir remains in shut-in mode.
For this case, the threshold price used is the moving average of the Henry Hub spot price for a 26 weeks window. The moving average value is preferred over a static value, because, for the three years selected as basis years of simulation (2010-2012), the price of natural gas has changed significantly. Compared to its seasonal fluctuations; a static threshold value is incapable of reflecting this change in the market.

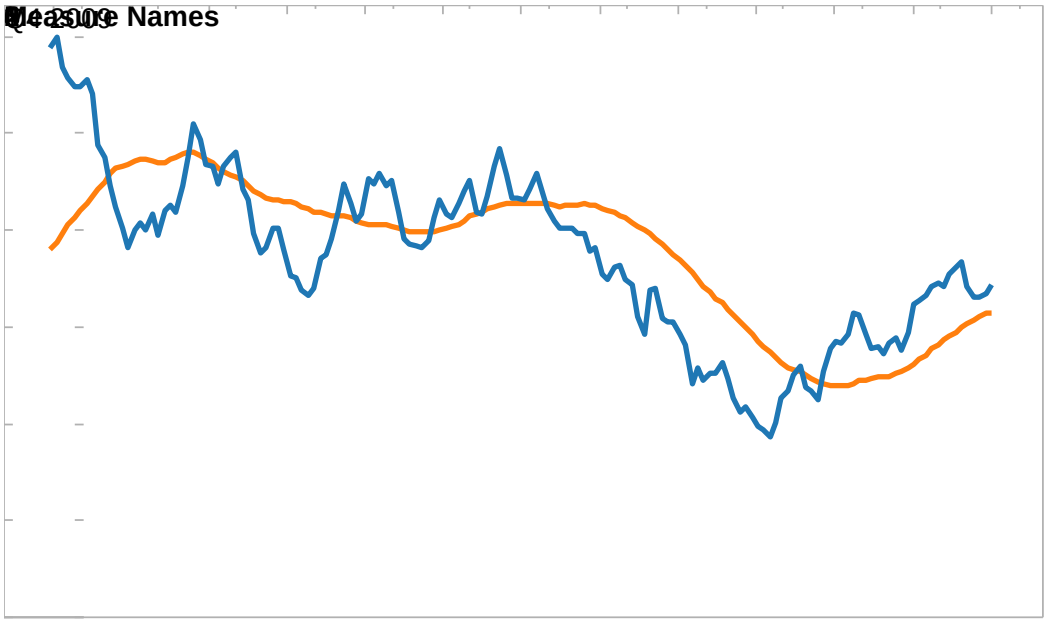

Figure 7.3 Natural gas market price and its 26 weeks moving average for years 2010-2012

The deliverability and injectability are outputs of the reservoir model, upon receiving and interpreting the dispatch order made by D1. Based on the inventory level and the limits placed on wellhead pressure, the wellhead pressure is adjusted, and the corresponding flow rate limit is determined. It is possible for the reservoir to remain in shut-in (deliverability/injectability~ 0) even when there is

dispatch order to inject or to withdrawal, if it violates a given physical constraint that is associated with the storage reservoir.

At D4, the amount of natural gas stored is set to be equal to the injectability of the reservoir at that given hour. Since no hydrogen is produced, the concentration of hydrogen in the injected stream is always zero.

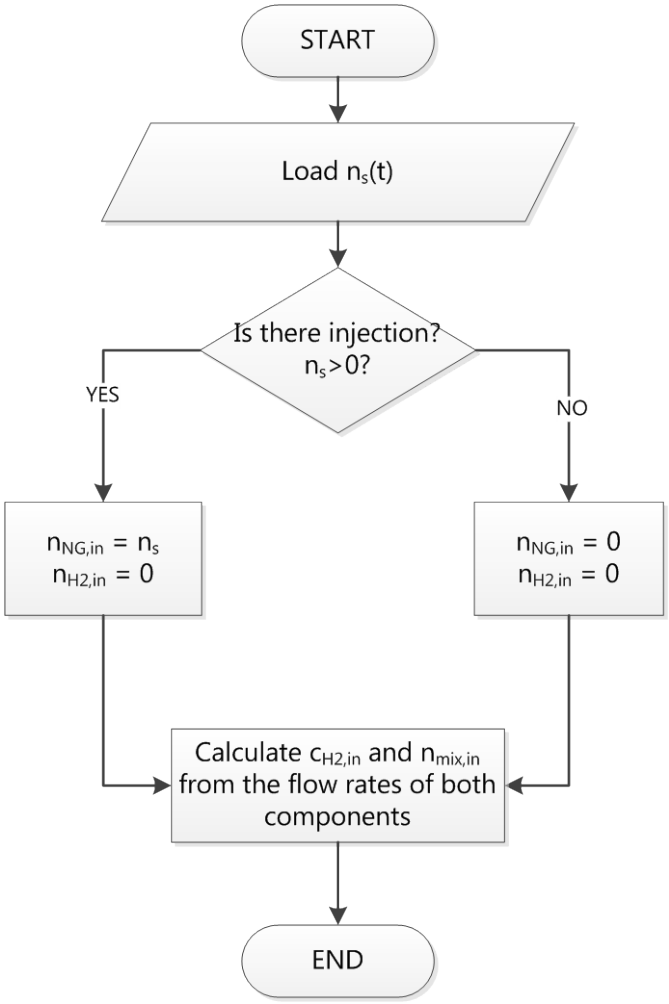

Figure 7.4 Gas blending decision point (D4) for base case scenario

For D5, the amount of natural gas delivered to the grid is set to be equal to the deliverability for the reservoir at that given hour.

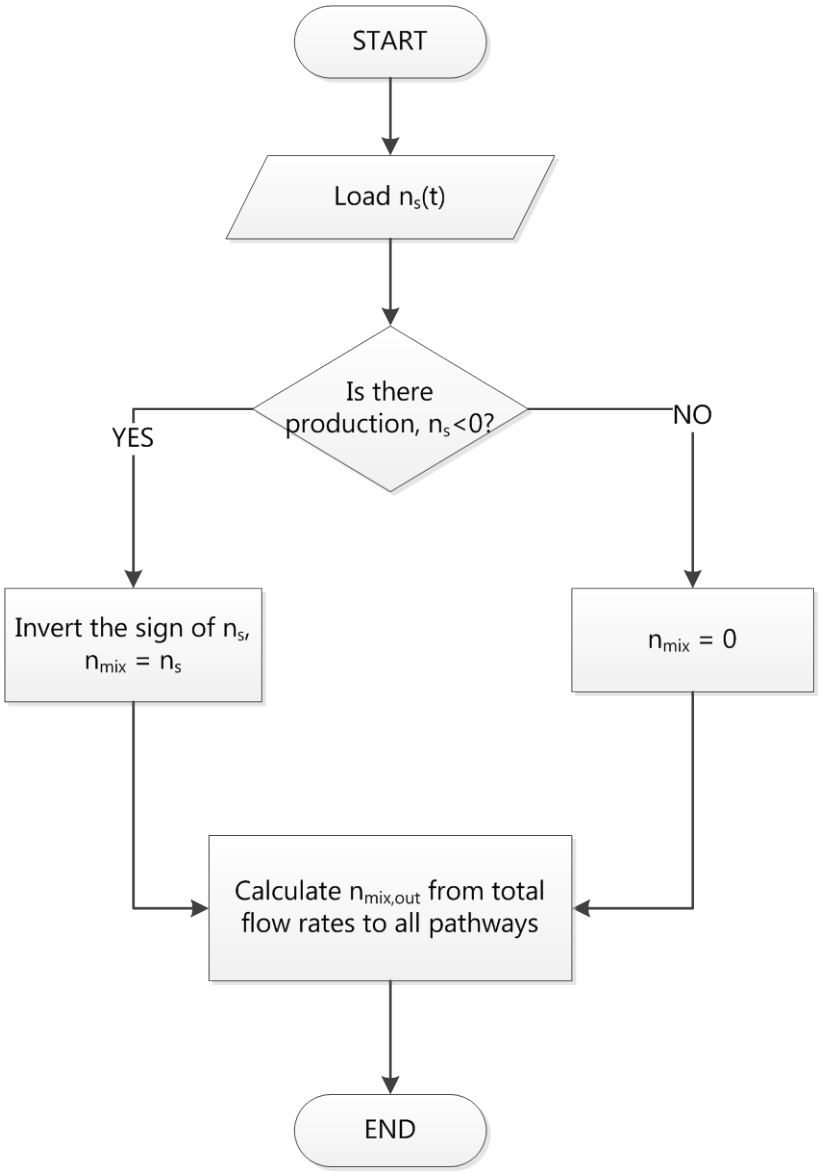

Figure 7.5 Mixture dispatch decision block (D5) for the base case scenario

7.2 Mid-Term Scenario: Hydrogen Injection

This second scenario is different from the other non-base case scenarios, for it simulates conditions which are likely to be in place a short time after the implementation of the underground storage of hydrogen: hydrogen is produced and injected into the natural gas storage system in relative small proportions (Figure 1.6). The hydrogen injection scenario is a mid-term scenario because, compared to the three later scenarios, it requires relatively little capital investment.

7.2.1 Summary

Compared to the previous scenario, electrolyzers are added as another key component of the energy hub, bring with it connectivity to the power grid and to demand for hydrogen (Table 1.3).

Table 7.3 Configuration and capacity of energy hub components for the hydrogen injection scenario

Component	Status	Rated Capacity
Reservoir	*ON*	6.1-7.6 MMscf
Electrolyzers	*ON*	8.7 MW or 30 units
Wind Turbines	*OFF*	N/A
CCGT	*OFF*	N/A
Separator	*OFF*	N/A

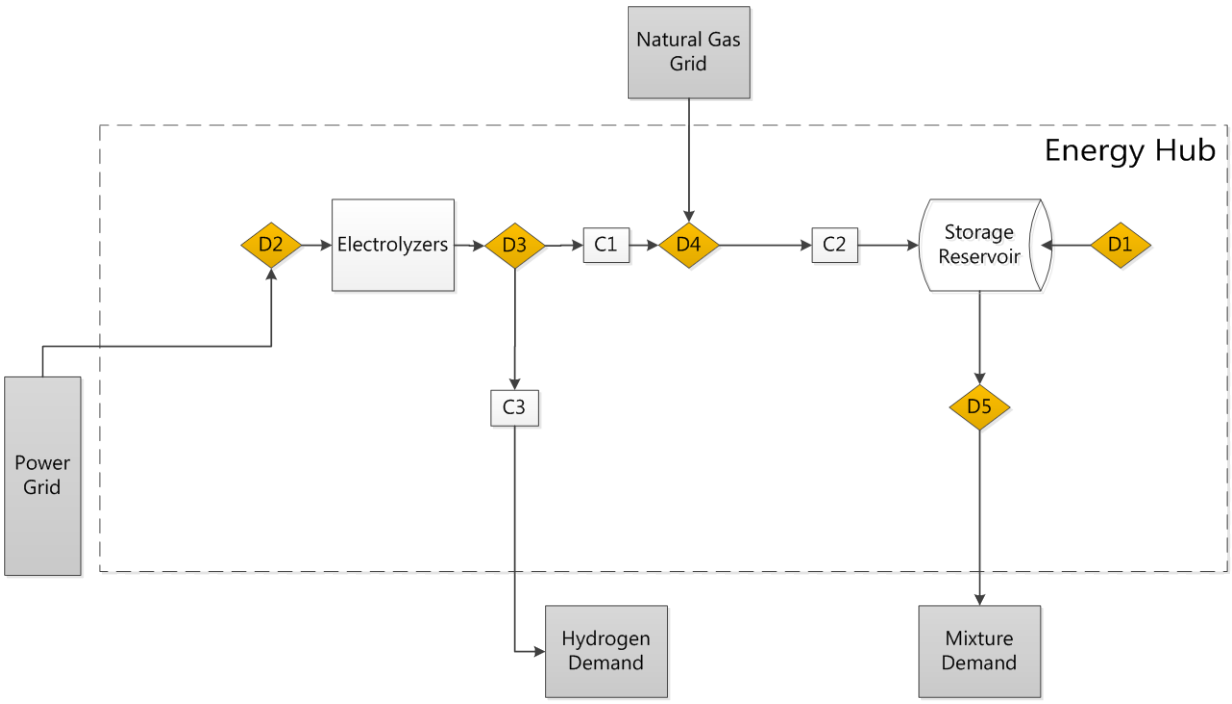

Figure 7.6 Model scope for hydrogen injection scenario

Table 7.4 Summary of decision point logic for the hydrogen injection scenario

	Description	Action
D1	Reservoir operation regime	Inject when the NG market price is low; withdrawal when the NG market price is high
D2	Electrolyzer power supply	Produce H_2 when the market price of electricity is low; stay in stand-by when the market price of electricity is high
D3	Hydrogen bypass	Bypass if the reservoir is withdrawing or H_2 produced exceeds the injectability limit
D4	NG/H_2 blending	Prioritize H_2 storage; complete with NG so that mixture storage meets injectability limit
D5	Mixture dispatch	Set mixture produced to the deliverability limit
D6	Separator recycle	N/A

7.2.2 Decision Point Modeling Logic

The decision point D2 determines whether the electrolyzer is operated to produce electricity, depending on the hourly price of grid power. The threshold value used in determination is the 24 hours moving average of the Hourly Ontario Energy Price (HOEP) from the IESO (Figure 1.8). It has

been found that the HOEP is a good indicator of the degree of demand for electricity in the Ontario market. In this scenario, it is estimated that, whenever the HOEP is lower than its daily moving average, the demand for electricity is lower than average. Thus it is preferable to use grid power to supply electrolytic hydrogen production, when surplus baseload generation is more plentiful. Vice versa, when HOEP is higher than its daily moving average, the electrolyzers are in stand-by as to not increase electricity demand during those hours. This practice ensures that the electrolyzer is operated daily during the off-peak hours.

This second scenario shares the same decision point logic with the base case scenario at D1 and D5: reservoir dispatch is based on natural gas prices, and once the reservoir has been dispatched to withdrawal, all the gases that can be produced is directed toward distribution via the natural gas distribution network. This scenario also contains two new decision points (D2 and D3) and an altered version of D4, for hydrogen is present (Figure 1.7, Figure 1.9 and Figure 1.10).

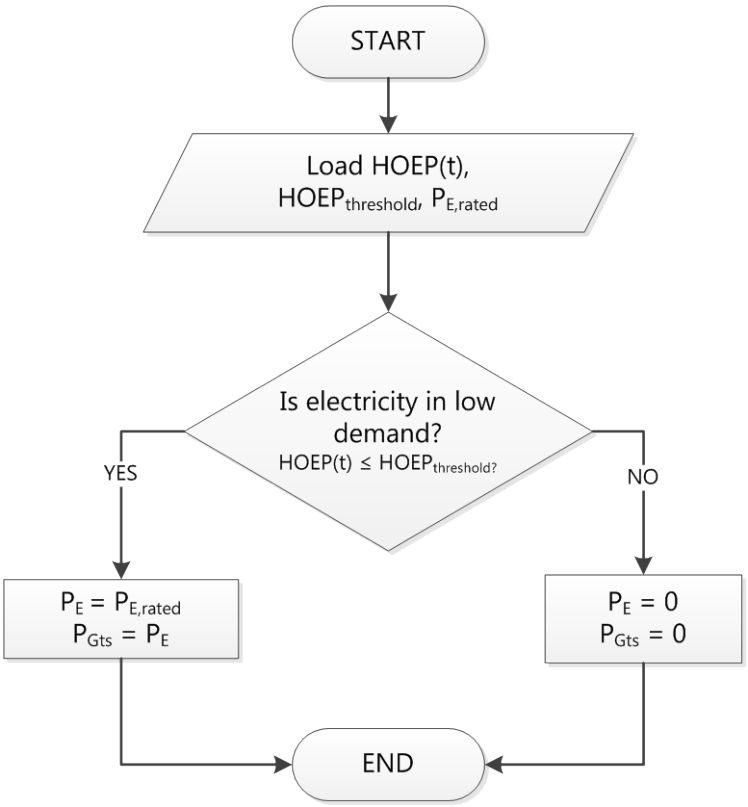

Figure 7.7 Electrolyzer power supply decision point (D2) for the hydrogen injection scenario

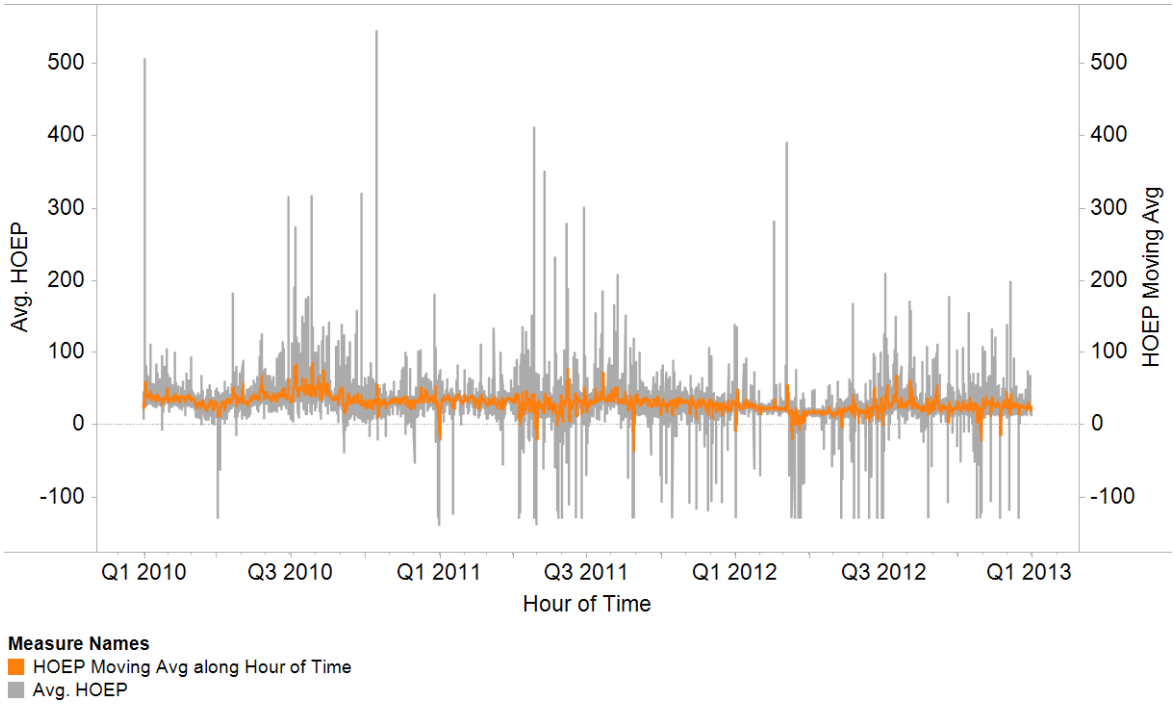

Figure 7.8 Ontario power price and its 24 hours moving average for years 2010-2012

The decision D3 determines whether the hydrogen produced by the electrolyzer is sent to storage. As input, it requires the knowledge of the reservoir injectability/deliverability and the flow rate of hydrogen produced. Hydrogen is sent for storage if it has been produced and if the reservoir is accepting injected gas. In the case that the hydrogen produced exceeds the injectability of the reservoir, or in the case that the reservoir is producing gas from storage, the portion of hydrogen that cannot be injected is assumed to be absorbed by local hydrogen demand, immediately. This assumption can be verified by examining the amount of hydrogen thus consumed from simulation results.

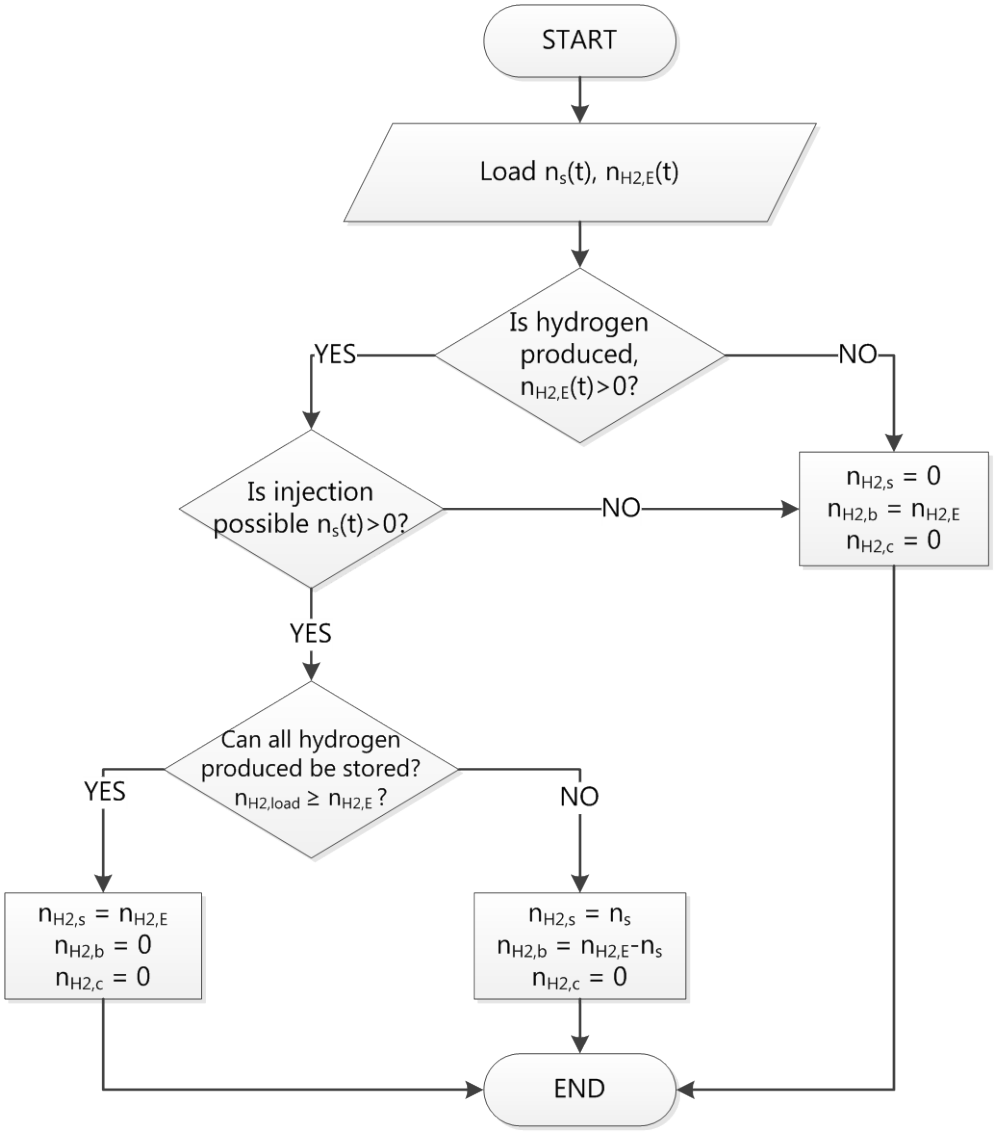

Figure 7.9 Hydrogen bypass decision point (D3) for the hydrogen injection scenario

The penultimate decision point, D4, determines how much natural gas is blended with the hydrogen that is to be injected. In this scenario, the amount of natural gas alongside hydrogen is calculated based on the injectability of the reservoir. It is set up so that the combined mixture fulfills the injectability limit exactly, so that the maximum amount of gas is injected into the reservoir during its operations. At decision point D5, as in the scenario before, the amount of mixture delivered $\dot{n}_{mix}$ remains matched to the deliverability limit $\dot{n}_s$ (Figure 1.5).

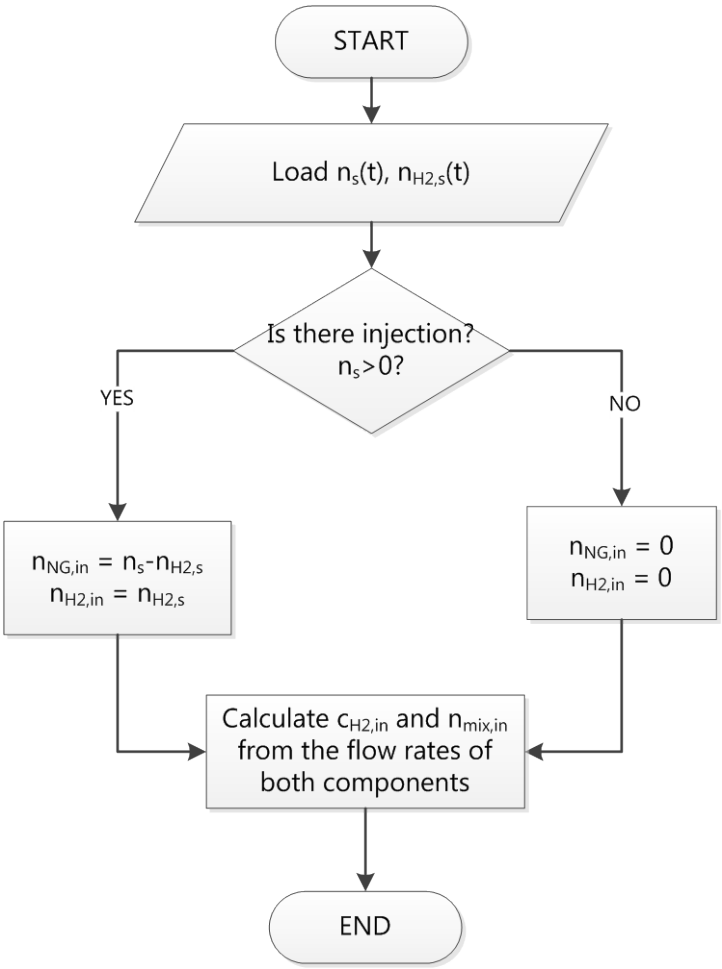

Figure 7.10 Gas blending decision point (D4) for hydrogen injection scenario

7.3 **Long-Term Scenario: Reduction of Surplus Baseload (SGB) Generation**

The surplus baseload generation reduction scenario is the first of three long-term scenarios. It differs from the hydrogen injection scenario in that an on-site combined cycle gas turbine plant is included in the energy hub, so that the stored energy can be recovered in the form of electric power at the energy hub (Figure 1.11 and Table 1.5). This configuration allows the energy hub operators to store electricity from the grid and to deliver electricity to the grid at the same physical location.

7.3.1 Summary

In order to be able to compare scenarios in a meaningful way, the rated capacity of the electrolyzer unit has been maintained to be the same as in the mid-term scenario at 8.7 MW. But, realistically, the full absorption of the surplus baseload generation in Ontario will require a much larger capacity. In that case, the number of energy hubs such as the one described within this scenario can be multiplied to scale up.

Table 7.5 Configuration and capacity of energy hub components for the SBG reduction scenario

Component	Status	Rated Capacity
Reservoir	*ON*	6.1-7.6 MMscf
Electrolyzers	*ON*	8.7 MW or 30 units
Wind Turbines	*OFF*	N/A
CCGT	*ON*	40 MW
Separator	*OFF*	N/A

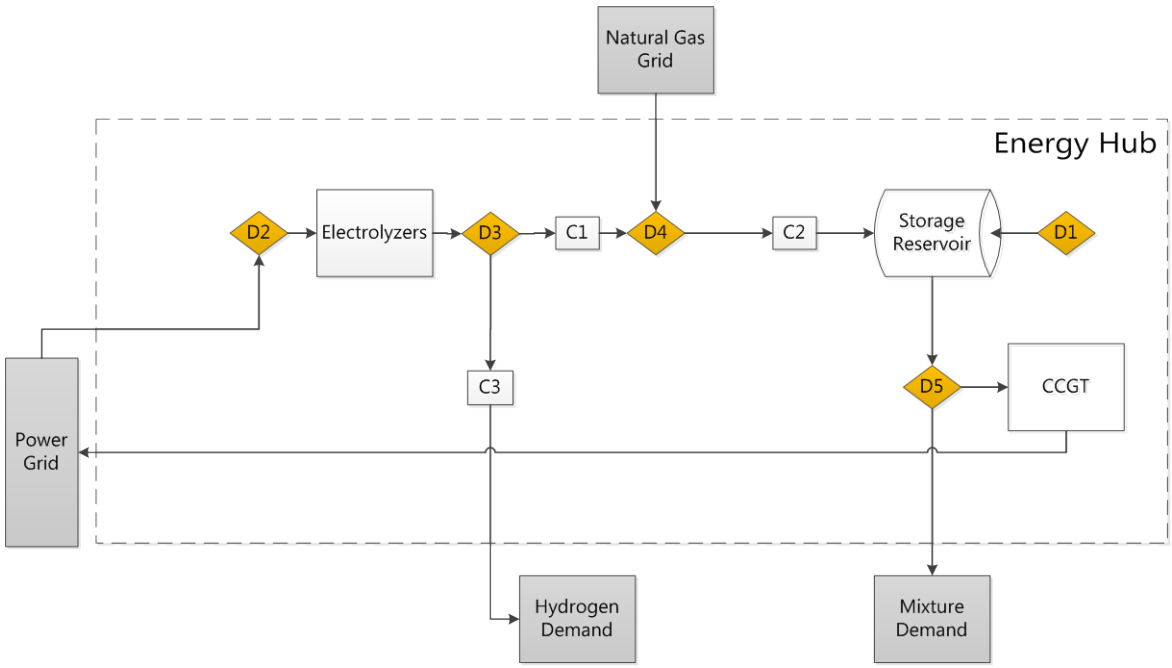

Figure 7.11 Model scope for the SBG reduction scenario

For long-term scenarios, the dispatch logic for the reservoir and for the energy hub as a whole is significantly different from the base case.

Table 7.6 Summary of decision point logic for the SBG reduction scenario

	Description	Action
D1	Reservoir operation regime	Inject when the demand for electricity is low; withdrawal when the demand for electricity is high
D2	Electrolyzer power supply	Produce H_2 when the demand for electricity is low; stay in stand-by when the demand for electricity is high
D3	Hydrogen bypass	Bypass if the reservoir is withdrawing or H_2 produced exceeds the injectability limit
D4	NG/H_2 blending	Prioritize H_2 storage; complete with NG so that mixture storage meets injectability limit
D5	Mixture dispatch	Set mixture produced to deliverability limit; prioritize supplying CCGT before sending the mixture to the NG distribution pipelines
D6	Separator recycle	N/A

7.3.2 Decision Point Modeling Logic

To begin, at decision point D1, when deciding whether to inject or withdrawal from the reservoir, the triggering signals are no longer the natural gas market price. Instead, the hourly demand for electricity in the province is compared to a threshold value, which triggers hydrogen production. This is followed by injection when electricity demand is low, mixture withdrawal when demand is high (Figure 1.12).

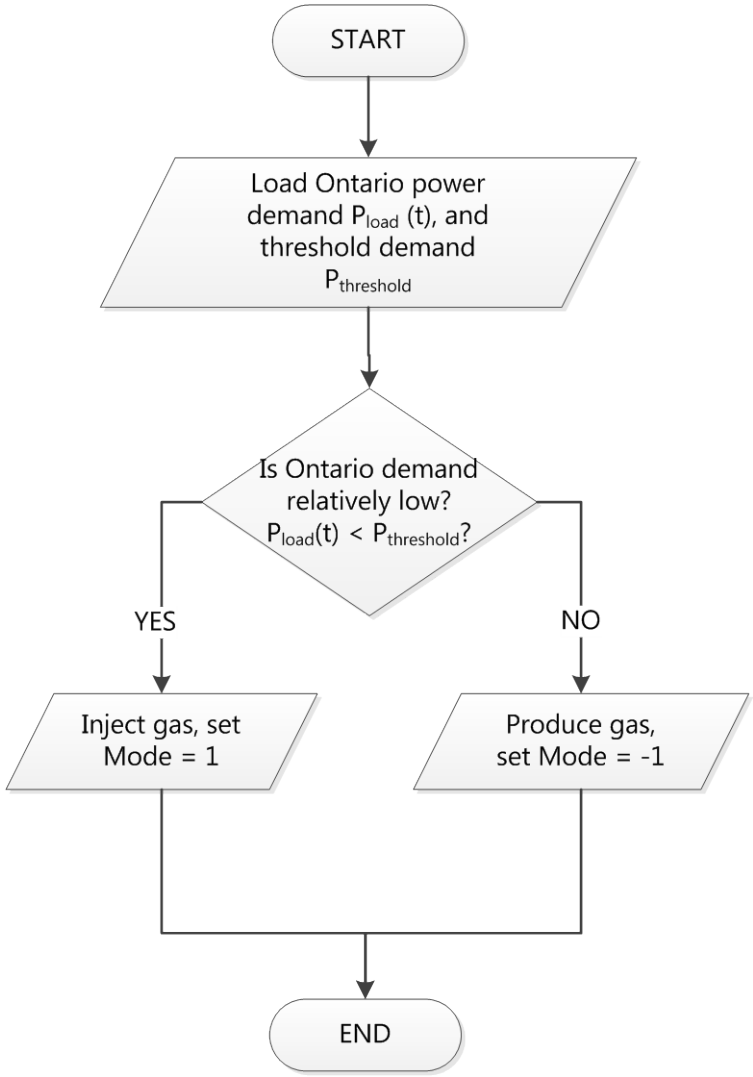

Figure 7.12 Reservoir operation decision point (D1) for the SBG reduction scenario

The threshold value used in this scenario is the one year moving average of Ontario-wide electricity demand (Figure 1.13).

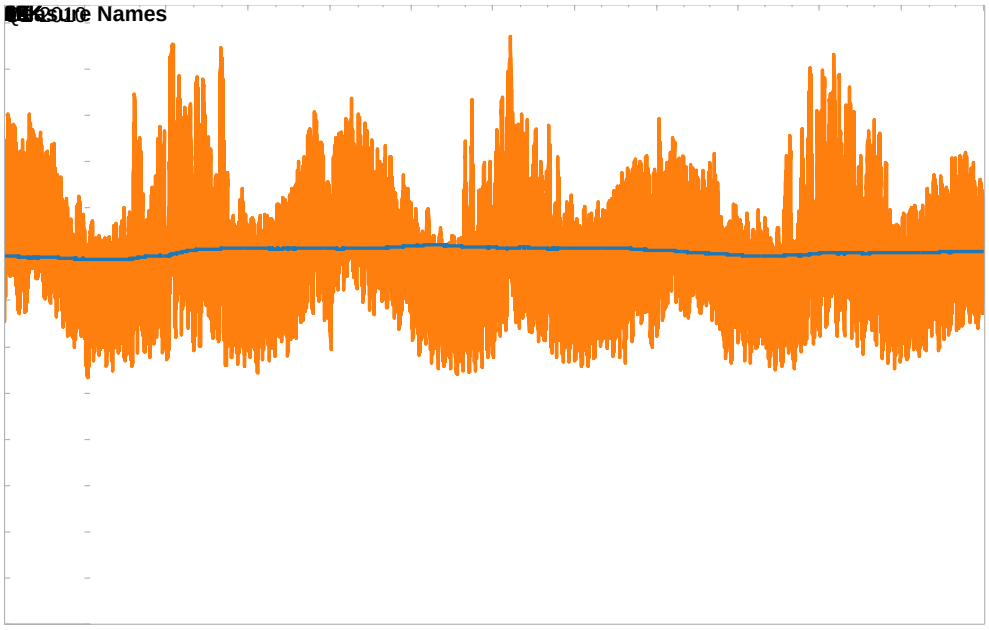

Figure 7.13 Electricity demand in Ontario and its one-year moving average for 2010-2012

At decision point D2, the electrolyzer dispatch is also modified to be triggered by deviation from electricity demand instead of by deviation from electricity market prices (Figure 1.14). At D3 and D4, the logic directing the bypassing of hydrogen and the blending of hydrogen with natural gas, respectively, has remained unchanged. The maximum limit of the quantity of hydrogen and natural gas stored is set by the injectability limit, with priority for hydrogen (Figure 1.9 and Figure 1.10).

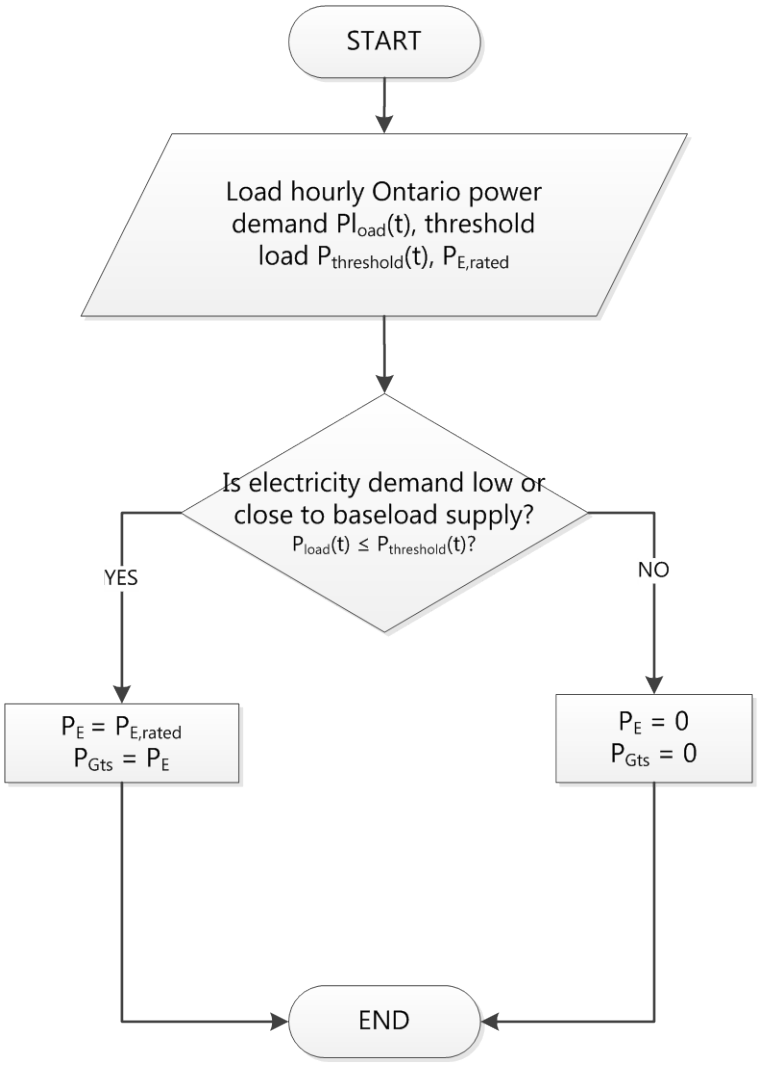

Figure 7.14 Electrolyzer power supply decision block (D2) for the SBG reduction scenario

Finally, once the stored mixture is withdrawn following signals of higher demand, it is necessary to determine its dispatch to different product delivery pathways. The hydrogen-enriched natural gas can be delivered as is through natural gas pipelines and then consumed off-site, or it can be consumed on-site to fuel the CCGT plant. Since the fuel intake of the CCGT plant is much smaller than the average deliverability of the reservoir, the nominal need of the gas turbine is met first, and the remainder of the mixture retrieved is routed toward the gas distribution network (Figure 1.15).

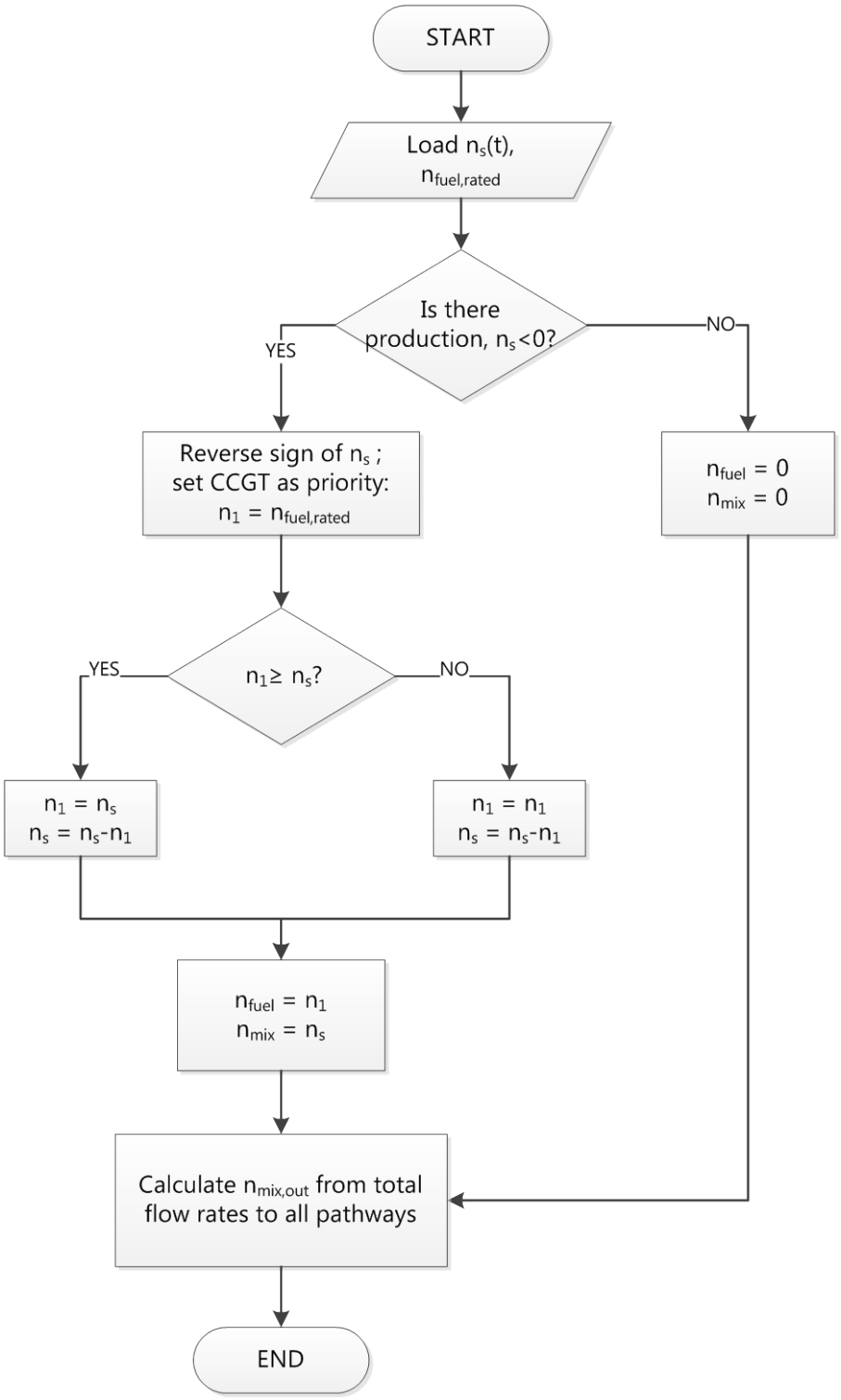

Figure 7.15 Mixture dispatch decision block (D5) for the SBG reduction scenarioLong-Term Scenario: Integration of Wind Power

In this second long-term scenario, on-site or near-by wind turbines are added to the energy hub components present in the previous scenario. The wind turbines are included within the boundary of the energy hub, because it is assumed that they have the same proprietaries and operators as the rest of the energy hub. In keeping with the previous scenarios, the rated capacity of the electrolyzer is maintained at the same level (Table 1.7), and the wind turbines have been sized to match.

7.3.3 Summary

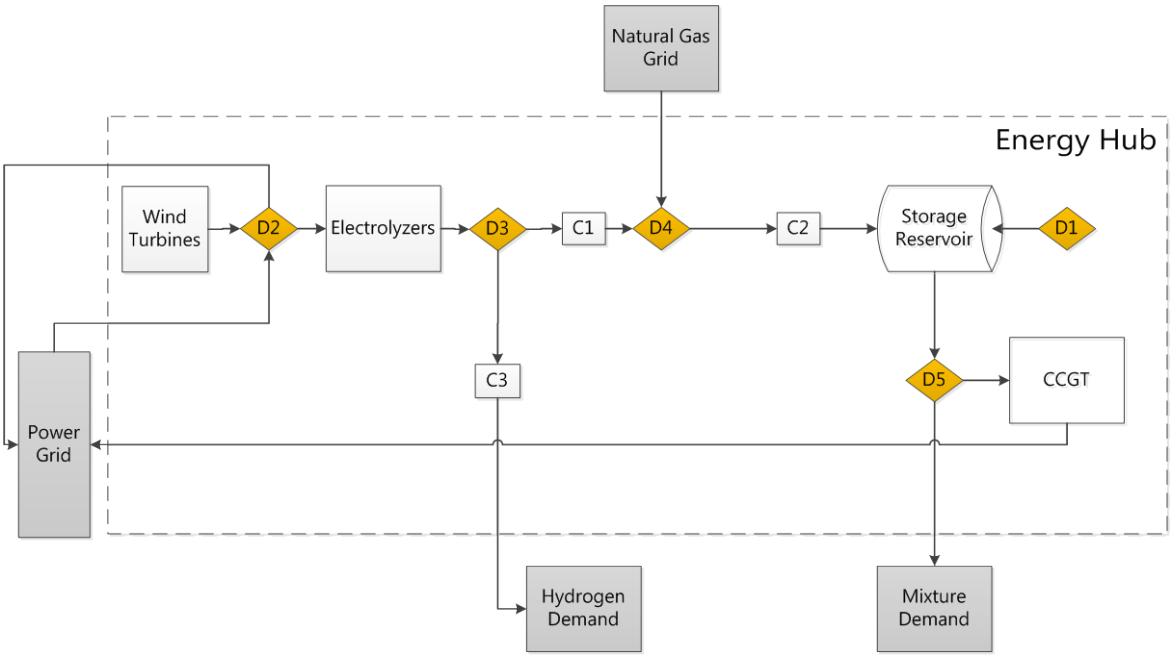

Figure 7.16 Model scope for the wind power integration scenario

Table 7.7 Configuration and capacity of energy hub components for the wind power integration scenario

Component	Status	Rated Capacity
Reservoir	*ON*	6.1-7.6 MMscf
Electrolyzers	*ON*	8.7 MW or 30 units
Wind Turbines	*ON*	10 MW or 5 units
CCGT	*ON*	40 MW
Separator	*OFF*	N/A

The active decision points involved in the wind power integration scenario is the same as in the SBG reduction scenario. D3, D4, D5 remained identical in content, whereas D1 and D2 contain altered logic.

Table 7.8 Summary of decision point logic for the wind power integration scenario

	Description	Action
D1	Reservoir operation regime	Inject when the demand for wind power is low; withdrawal when the demand for wind power is high
D2	Electrolyzer power supply	Produce H_2 when the demand for wind power is low; stay in stand-by when the demand for wind power is high; if wind is not enough for electrolyzers to produce at rated capacity, purchase power from the grid
D3	Hydrogen bypass	Bypass if the reservoir is withdrawing or H_2 produced exceeds the injectability limit
D4	NG/H_2 blending	Prioritize H_2 storage; complete with NG so that mixture storage meets injectability limit
D5	Mixture dispatch	Set mixture produced to deliverability limit; prioritize supplying CCGT before sending the mixture to the NG distribution pipelines
D6	Separator recycle	N/A

7.3.4 Decision Point Modeling Logic

At the first decision point (D1), reservoir is dispatched to inject when the demand for wind power is low, and to withdrawal when the demand for wind power is high. The indicator used to gauge the demand for power form the wind turbines is the time-differentiated FIT contract price, which differentiates between peak and off-peak hours in a week (Figure 1.17)

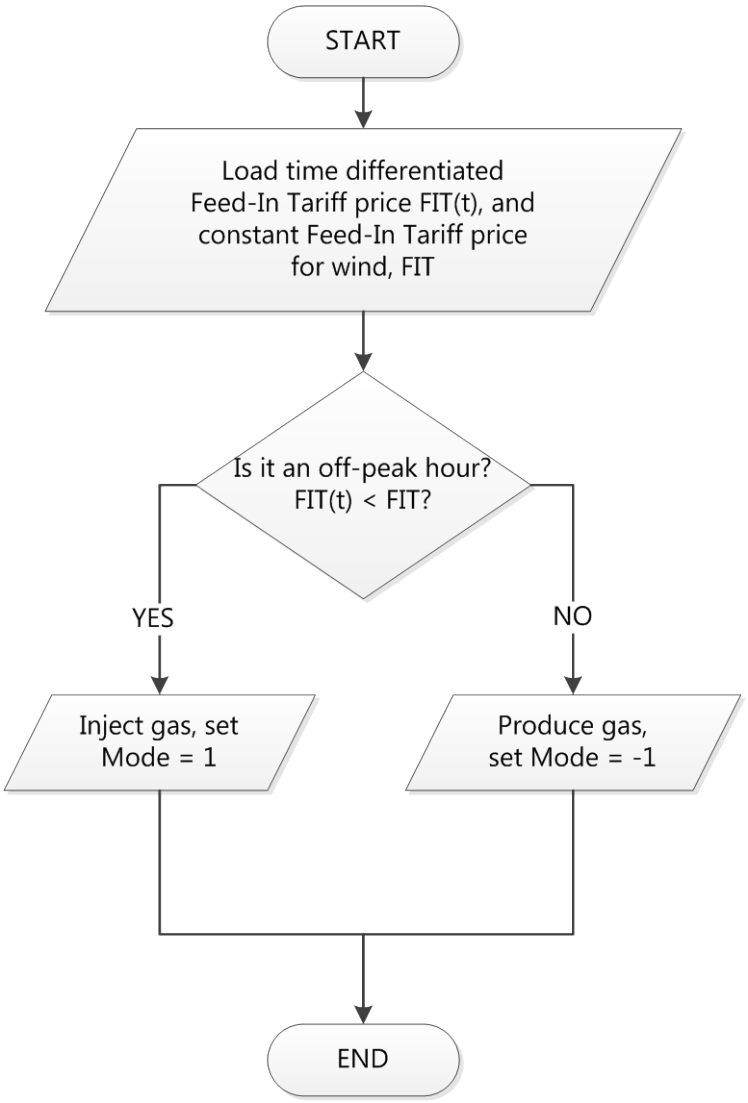

Figure 7.17 Reservoir operation decision point (D1) for the wind power integration scenario

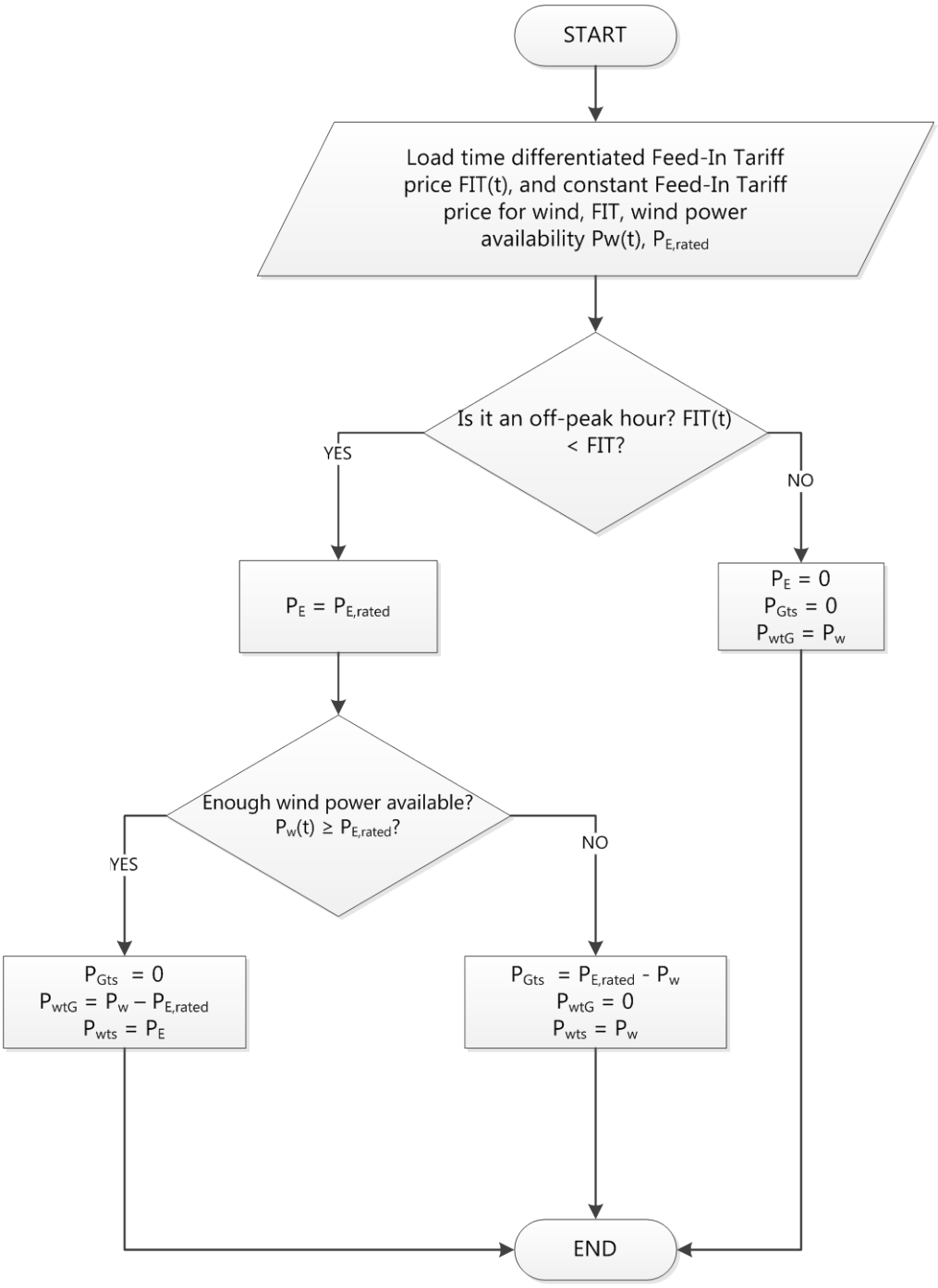

Figure 7.18 Electrolyzer power supply decision point (D2) for the wind power integration scenario

As for D2, the decision to operate the electrolyzers or not is also driven by the perceived demand for wind power. The variability of wind also needs to be addressed here: depending on the local wind

speed, the wind power produced by the turbines may be insufficient to support the electrolyzers to run at their rated capacity, or the wind power available may exceed the rated capacity of the electrolyzers. In such cases, decisions are made to supplement the power supply with electricity purchased from the grid, or to sell wind power exceeding the capacity of electrolyzers to the grid, respectively.

Decision points D3, D4 and D5 have the same logic as in the previous scenario: hydrogen storage is prioritized when injection is possible, injection and withdrawal flow rates area always set to the value of injectability/deliverability limits, and CCGT operation is prioritized when withdrawal is possible.

7.4 Long-Term Scenario: Meeting Large Hydrogen Demand

In the last of the three long-term scenarios, it is assumed that energy is mainly used for hydrogen production, and that the storage reservoir is transitioning toward a pure hydrogen storage facility. In this case, only hydrogen is injected to the reservoir. Assuming that natural gas with relatively high percentages of hydrogen is produced from the reservoir, the main pathway for energy recovery is the purification of produced gas through a PSA separator. The natural gas rich "waste stream" from the separator contains little hydrogen; it is subsequently distributed through the natural gas distribution system.

7.4.1 Summary

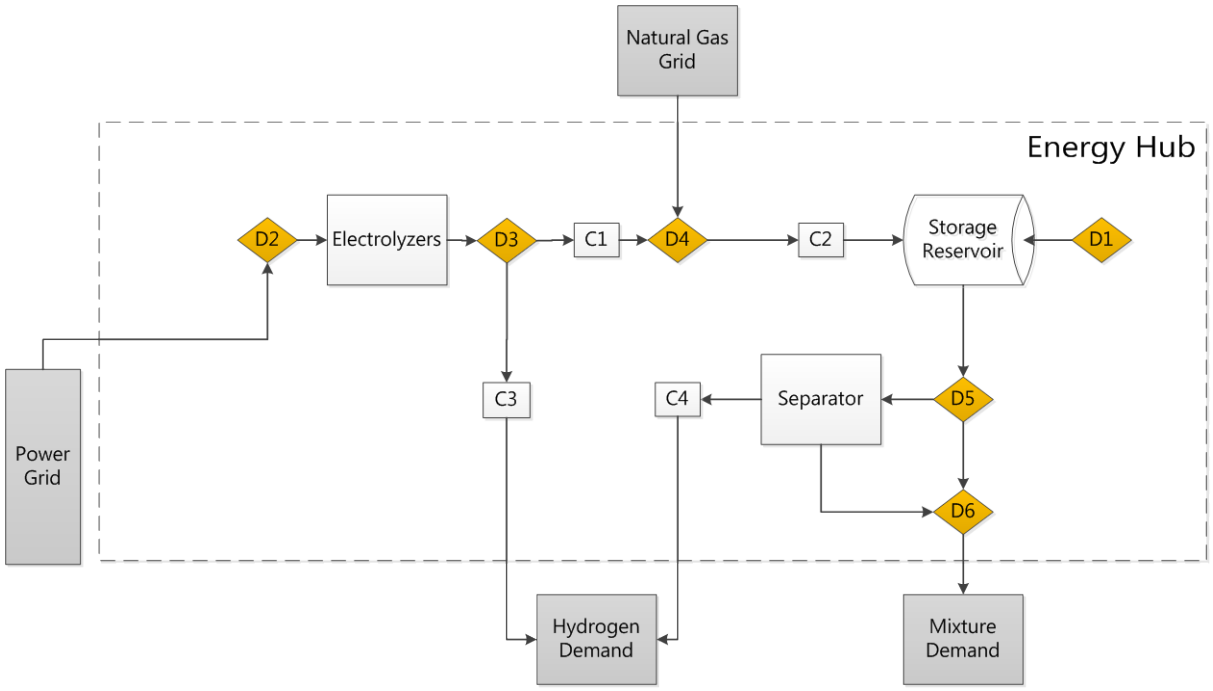

Figure 7.19 Model scope for the large hydrogen demand scenario

Table 7.9 Configuration and capacity of energy hub components for the large hydrogen demand scenario

Component	Status	Rated Capacity
Reservoir	*ON*	6.1-7.6 MMscf
Electrolyzers	*ON*	26.1 MW or 90 units
Wind Turbines	*OFF*	N/A
CCGT	*OFF*	N/A
Separator	*ON*	40,000 Nm^3 feed

The rated capacity of the separator is expressed in terms of feed, for the rated output is dependent on the concentration of hydrogen in the feed stream, which is currently unknown.

Table 7.10 Summary of decision point logic for the large hydrogen demand scenario

	Description	Action
D1	Reservoir operation regime	Inject when there is no hydrogen demand and hydrogen is produced; withdrawal when there is hydrogen demand but no production; standby for other situations
D2	Electrolyzer power supply	Produce hydrogen when market price of electricity is low, remain in standby when price of power is high (same as D2.2)
D3	Hydrogen bypass	Bypass hydrogen if there is hydrogen demand
D4	NG/H_2 blending	Prioritize H_2 storage; **no natural gas injected**
D5	Mixture dispatch	Set mixture produced to rated feed capacity of the separator if there is production; separation is the exclusive pathway
D6	Separator recycle	Waste stream from separator supplied as mixture

7.4.2 Decision Point Modeling Logic

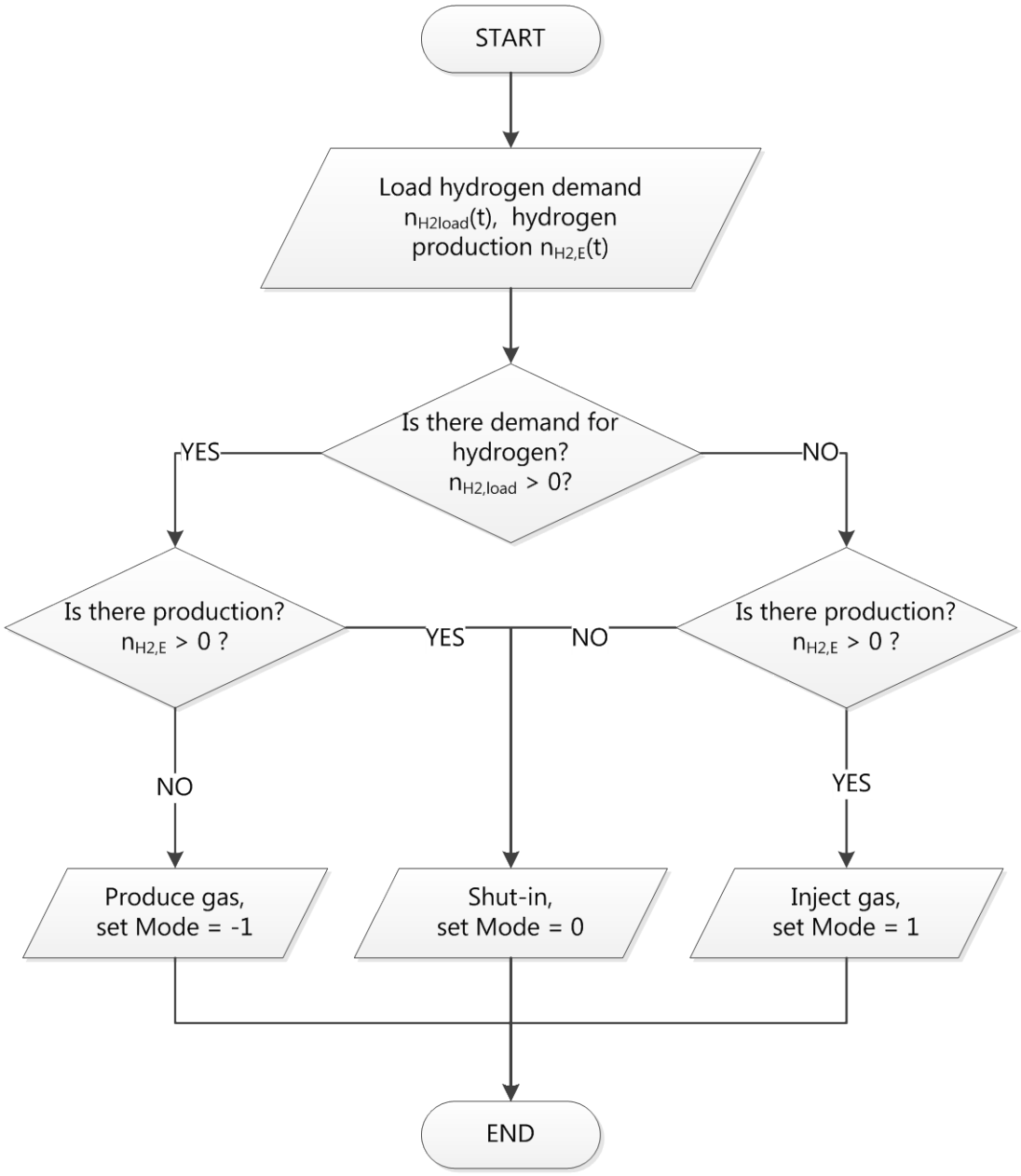

Figure 7.20 Reservoir operation decision point (D1) for the large hydrogen demand scenario

A key difference of the large hydrogen demand scenario compared to the others is that the demand for hydrogen is considered to be fixed in time (hydrogen delivered during some hours are purchased, instead of being fully flexible (hydrogen delivered at all hours are purchased). Here, the main purpose

of the storage reservoir is to provide a source of hydrogen supply when it is not being produced from the electrolyzer, as the demand for hydrogen arises (Figure 1.20). If hydrogen has been produced while there is no demand for hydrogen, the reservoir is activated for injection so the production can be stored. The bypass decision block reflects the priority given to meeting hydrogen demand (Figure 1.21).

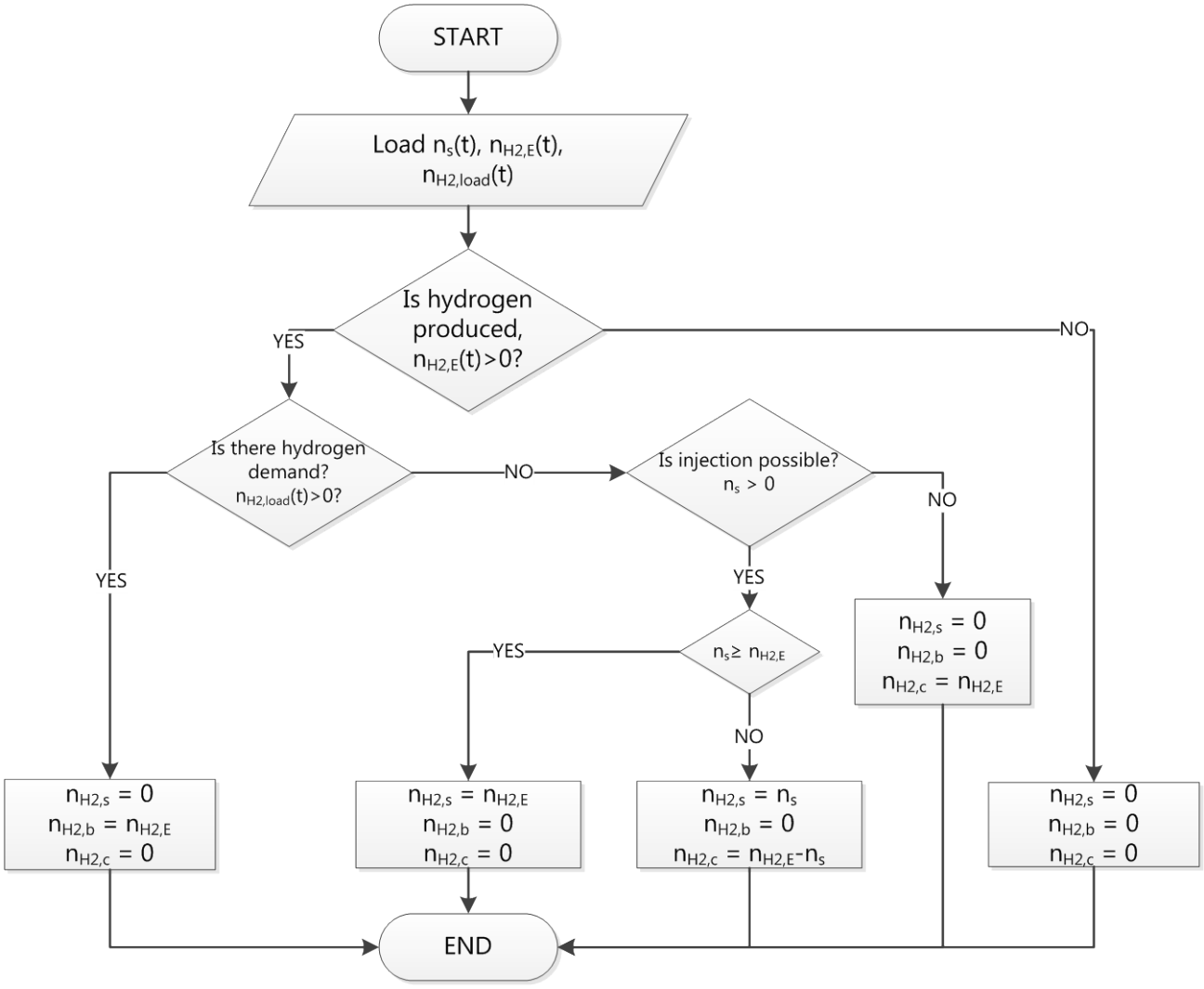

Figure 7.21 Hydrogen bypass decision point (D3) for the large hydrogen demand scenario

This scenario explores the possibility of only injecting hydrogen into an existing natural gas storage reservoir:

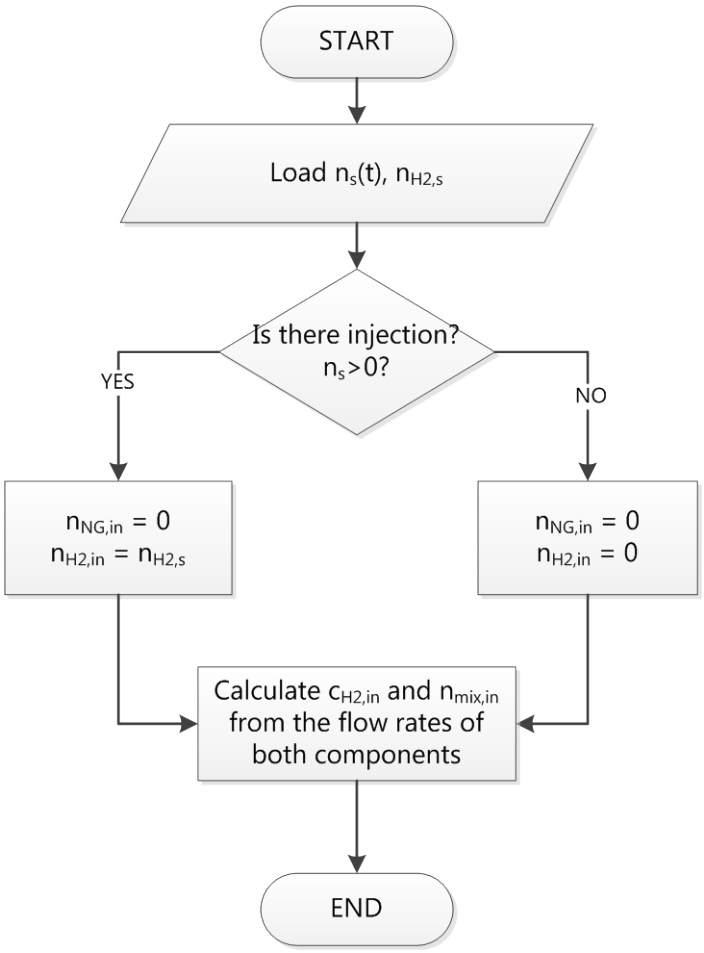

Figure 7.22 Gas blending decision point (D4) for large hydrogen demand scenario

Since no natural gas is injected into the reservoir for this scenario, the concentration of hydrogen with the reservoir is expected to be quite high. Thus, separator is considered as the only energy recovery pathway (Figure 1.23). But, it is assumed that the relatively natural-gas rich waste stream from the separation process can be disposed of via sales through the natural gas pipelines, under terms identical to the sales of hydrogen-enriched natural gas. Given that part of hydrogen has been removed from this stream, it will have a hydrogen concentration lower than that prevalent in the storage reservoir.

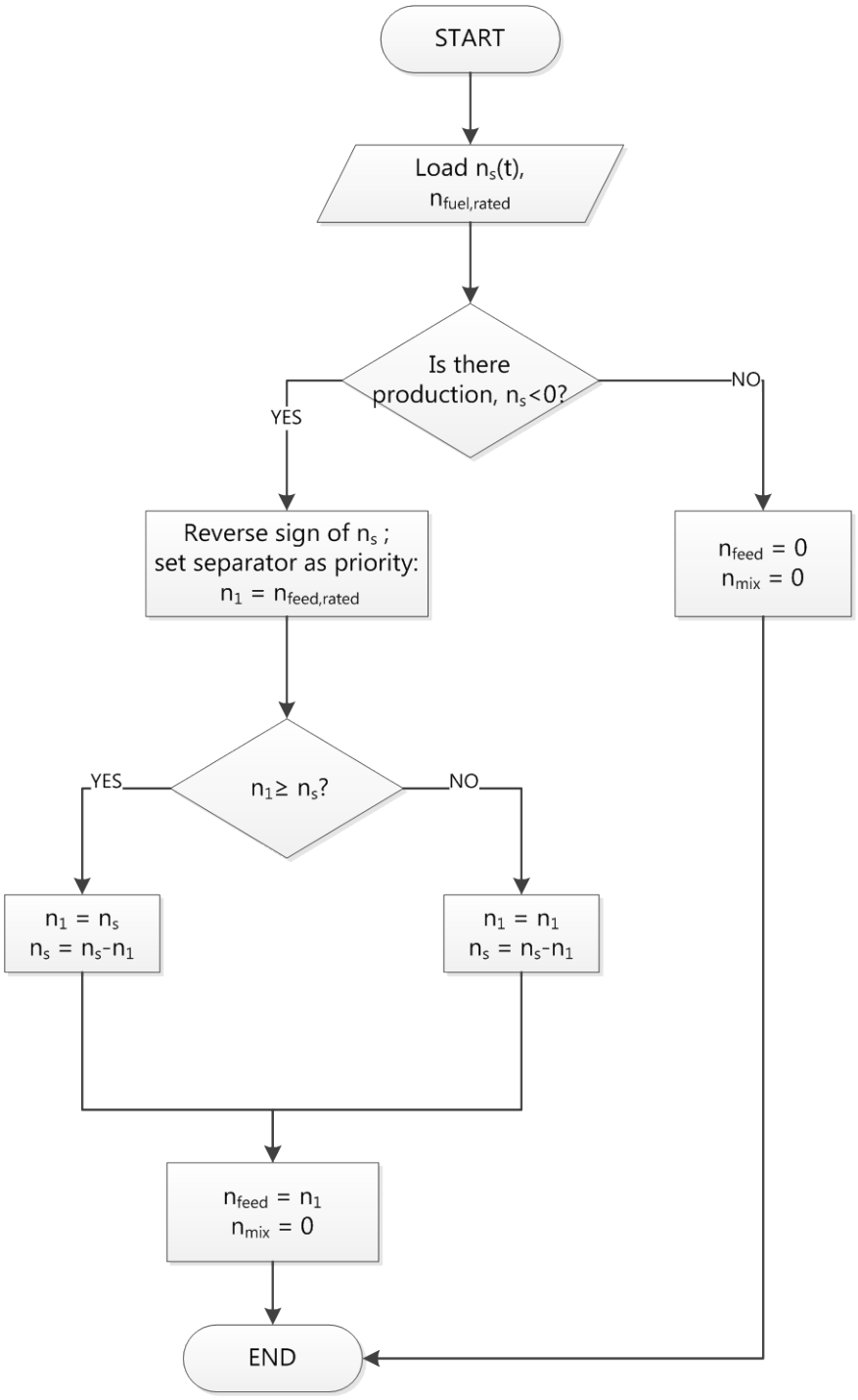

Figure 7.23 Mixture dispatch decision block (D5) for the large hydrogen demand scenario

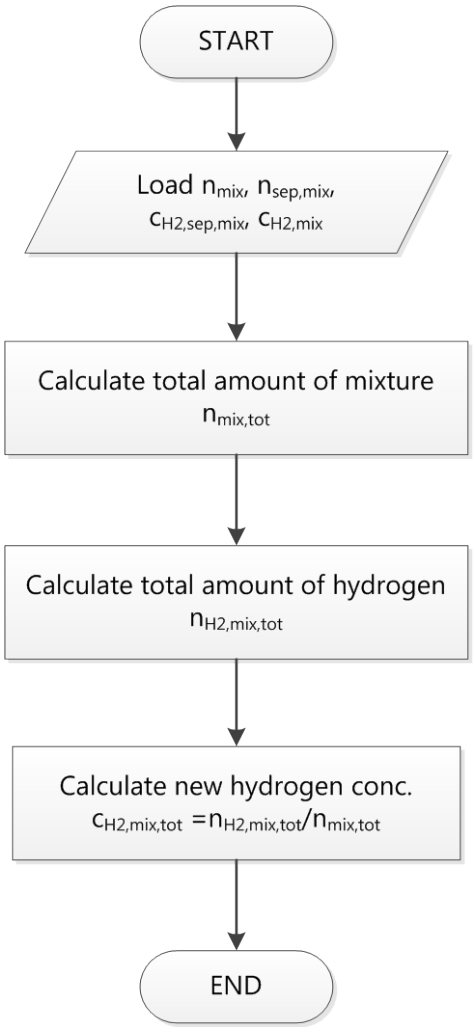

Figure 7.24 Separator recycle decision point (D6) for the large hydrogen demand scenario

Chapter 8
Simulation Results

In this section, the simulation results are presented for each scenario. The physical performance indicators are displayed both as figures and in tabulated forms, while financial and the emission indicators are summarized in tables. All outputs in the form of time series are available at hourly resolution, but they are sometimes averaged by day or week to facilitate display. The label of the time axis identified the resolution of each graph displayed: Hour of time (hourly), day of time (averaged by day), or week of time (averaged by week).

8.1 Base Case Scenario: Underground Gas Storage

In this scenario, no hydrogen is present at the energy hub, which consists only of a typical gas storage reservoir and the accompanying compressors.

The following figure illustrates the dispatch order placed on the reservoir and its injectability /deliverability during the period simulated. The dispatch order to the reservoir alternate semi-regularly, injection and withdrawal periods are of unequal duration. There are times when the actual injectability/deliverability of the reservoir cannot meet the demand placed by the dispatch: the reservoir is full and cannot accept further injection, while the reservoir mode still specifies injection (ex: first and second quarter of 2012), and vice versa (third and fourth quarter of 2012).

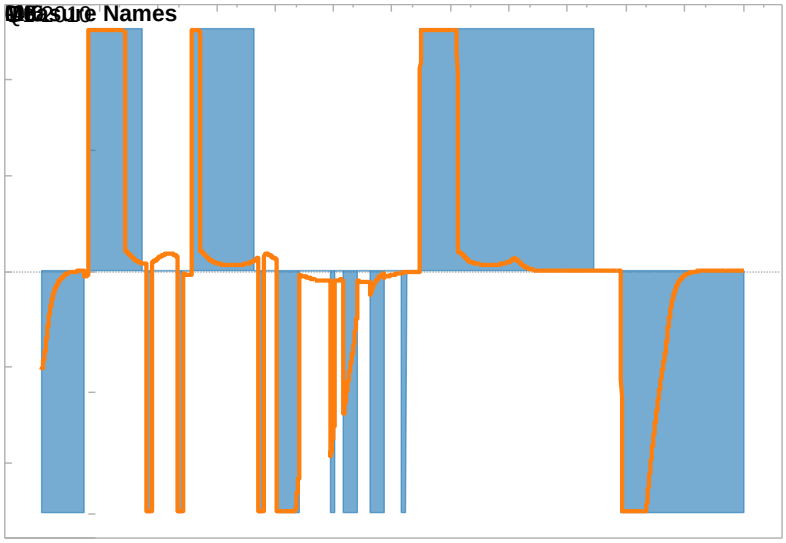

Figure 8.1 Dispatch to reservoir for the base case scenario

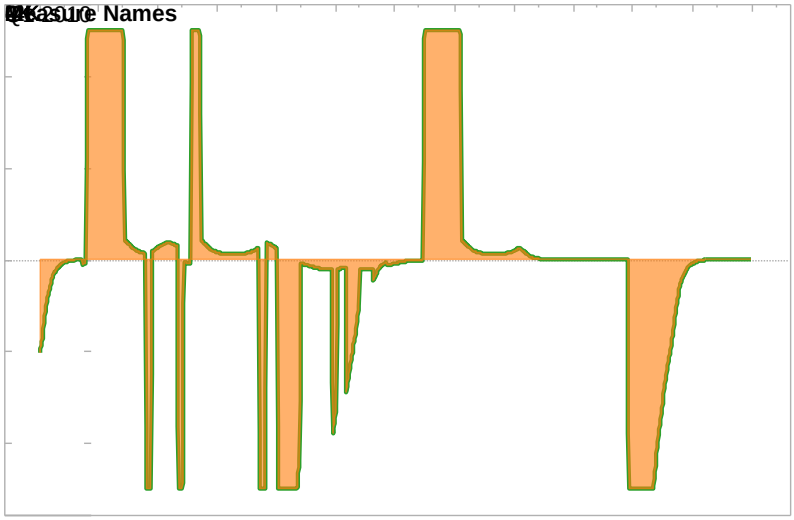

Figure 8.2 Injectability/deliverability and actual reservoir flow rates for the base case scenario

Due to the model logic specified at decision points D4 and D5, the actual flow rate of gas injected and withdrawn is equal to the injectability or deliverability of that given hour (Figure 2.3). This is also true for most scenarios except for the last long term scenario (Figure 2.9, Figure 2.19 and Figure 2.29), the one which is geared to supplying a large demand for hydrogen (Figure 2.40)

Due to the absence of hydrogen within the energy hub for the base case scenario, the concentration of hydrogen in the reservoir gas, as expected, is 0% for all times. Reservoir pressure follows roughly the shape of inventory level, and the wellhead pressure exhibits sharp increases and falls, especially during the year 2010-2011.

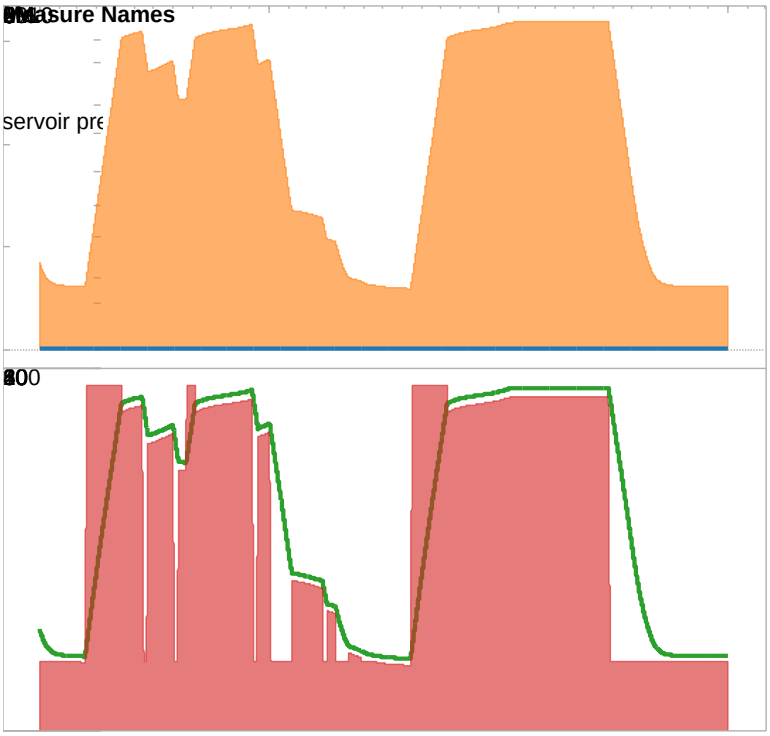

Figure 8.3 Reservoir conditions for the base case scenario

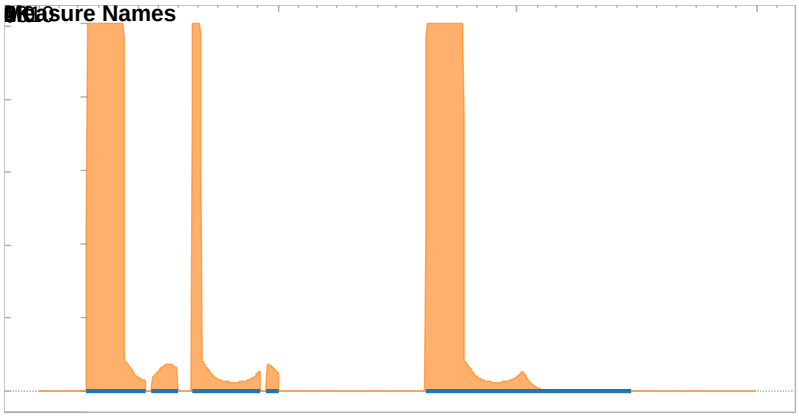

Figure 8.4 Flow rates of injected streams for the base case scenario

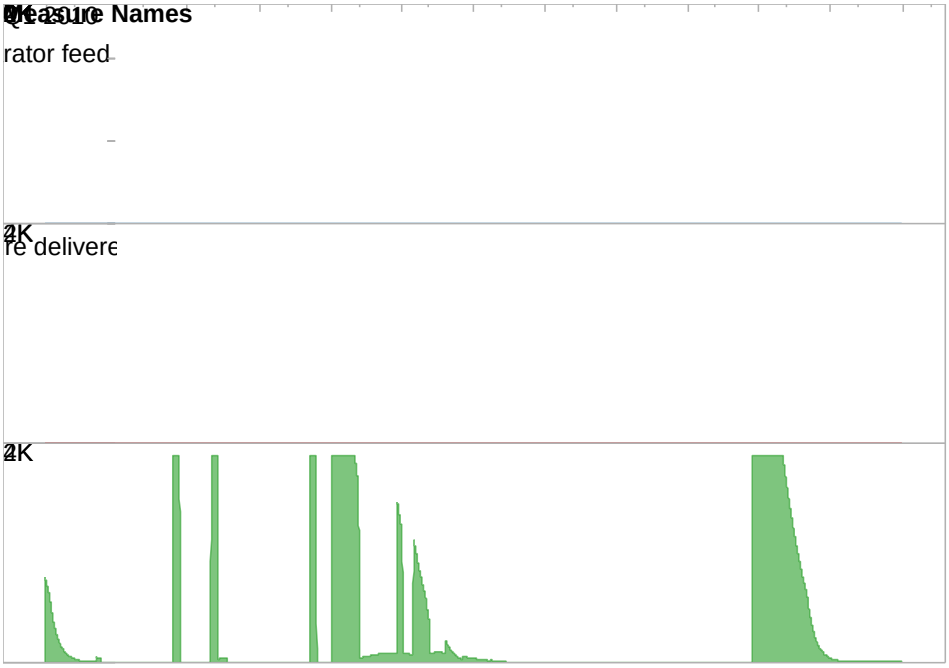

Figure 8.5 Dispatch of the produced mixture for the base case scenario

As described in Section 5.3, the value inventory is taken at the beginning and end of each year to evaluate the inventoriable cost of purchase. The grey lines in Figure 2.5, along with the first and last data point for inventory value, are the values used in the financial analysis.

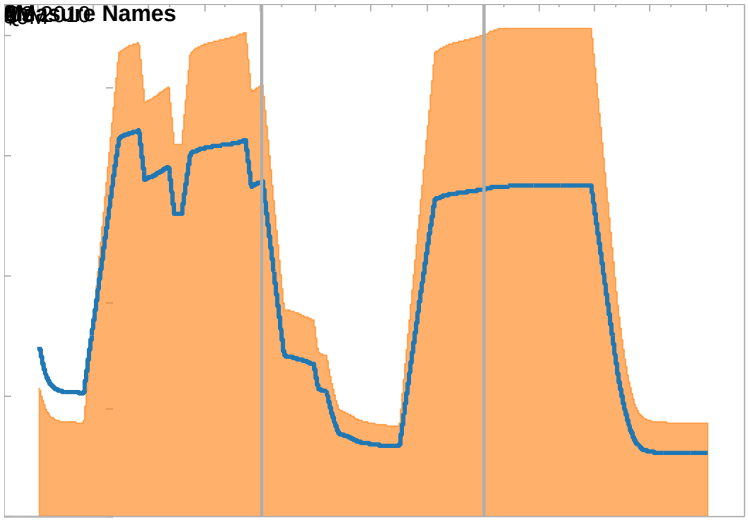

Figure 8.6 Value of inventory for the base case scenario

Table 8.1 Summary of physical performance for the base case scenario

Component	Variable	2010	2011	2012	Average	Unit
D1	Dispatch order to the reservoir	0.26	0.13	-0.16	0.08	N/A
Storage reservoir	Inventory	6.6E+06	4.7E+06	5.9E+06	5.7E+06	kmol
	H_2 conc.					mol %
	Reservoir pressure	77	56	69	67	bar
	Wellhead pressure	76	55	59	63	bar
	Max. inventory change	5.6E+06	9.4E+05	-7.2E+06	2.2E+05	kmol/year
	Actual inventory change	5.6E+06	9.4E+05	-7.2E+06	2.2E+05	kmol/year
Wind turbines	Wind power produced					MWh/year
	Utilization factor					
D2	Wind power stored					MWh/year
	Wind power sold to grid					MWh/year
	Grid power stored					MWh/year
Electrolyzers	H_2 produced					kmol/year
	Utilization factor					
D3	H_2 stored					kmol/year
	H_2 bypassed					kmol/year
	H_2 curtailed					kmol/year
D4	NG stored	9.6E+06	7.3E+06	1.2E+05	5.7E+06	kmol/year
	H_2 conc. of mixture injected					mol %
D5	Feed to separator					kmol/year
	Mixture delivered	4.0E+06	6.4E+06	7.4E+06	5.9E+06	kmol/year
	Fuel to CCGT					kmol/year
CCGT	Power delivered to grid					MWh/year
	Utilization factor					
Separator	H_2 delivered					kmol/year
	Utilization factor					
D6	Revised mixture delivery	4.0E+06	6.4E+06	7.4E+06	5.9E+06	kmol/year
	H_2 conc. of mixture delivered					mol %
Compressors	Work required	3.8E+06	2.9E+06	4.8E+04	2.2E+06	kWh/year

Table 8.2 Summary of financial performance for the base case scenario

Financial Performance	2010	2011	2012	Average
Capital Cost Breakdown				
Compressors				$ 2,843,963
Electrolyzers				$ -
Gas turbine				$ -
Separator				$ -
Wind turbines				$ -
Total Capital Cost				$ 2,843,963
Amortized Capital Cost				**$ 289,664**
O&M Cost Breakdown				
Compression cost	$ 151,066	$ 110,790	$ 1,285	$ 87,714
Fixed O&M	$ 11,587	$ 11,587	$ 11,587	$ 11,587
Total O&M Cost	$ 162,653	$ 122,377	$ 12,872	$ 99,300
Purchase Breakdown				
Natural gas from grid	$ 29,474,361	$ 21,398,243	$ 256,319	$ 17,042,974
Power from grid	$ -	$ -	$ -	$ -
Total Purchase	$ 29,474,361	$ 21,398,243	$ 256,319	$ 17,042,974
Sales Breakdown				
Mixture to grid	$ 14,880,960	$ 21,532,502	$ 16,274,124	$ 17,562,529
Wind power to grid	$ -	$ -	$ -	$ -
CCGT power to grid	$ -	$ -	$ -	$ -
Hydrogen	$ -	$ -	$ -	$ -
Total Sales	$ 14,880,960	$ 21,532,502	$ 16,274,124	$ 17,562,529
Inventory Cost Calculation				
Beginning inventory value	$ 14,112,000	$ 29,474,361	$ 21,398,243	$ 21,661,535
Purchase of material	$ 29,474,361	$ 21,398,243	$ 256,319	$ 17,042,974
Cost of total mixture available	$ 43,586,361	$ 50,872,604	$ 21,654,563	$ 38,704,509
Ending inventory value	$ 27,794,145	$ 27,170,364	$ 5,243,738	$ 20,069,416
Cost of mixture delivered	$ 15,792,216	$ 23,702,240	$ 16,410,824	$ 18,635,094
Inventoried purchase	$ 13,682,145	$ (2,303,997)	$ (16,154,505)	$ (1,592,119)

Table 8.3 Net annual cash flow for the base case scenario

Annual Cash Flow	2010	2011	2012	Average
1. Capital costs	$ (289,664)	$ (289,664)	$ (289,664)	$ (289,664)
2. OM costs	$ (99,300)	$ (99,300)	$ (99,300)	$ (99,300)
3. Cost of sales	$ (15,792,216)	$ (23,702,240)	$ (16,410,824)	$ (18,635,094)
4. Sales	$ 14,880,960	$ 21,532,502	$ 16,274,124	$ 17,562,529
5. Annual net	$ (1,300,221)	$ (2,558,703)	$ (525,665)	**$(1,461,529)**

Table 8.4 Summary of environmental performance for the base case scenario

Environmental Performance	2010	2011	2012	Average
Emission Incurred (kg CO_2/year)				
Compression of natural gas	2.18E+06	1.67E+06	2.75E+04	1.29E+06
Grid power generation for H_2				
Mixture use at CCGT				
Wind power generation for H_2				
Off-site mixture use	1.76E+08	2.81E+08	3.24E+08	2.60E+08
Emission Mitigated (kg CO_2/year)				
Displacement of SMR H_2				
Off-site NG use	1.76E+08	2.81E+08	3.24E+08	2.60E+08
NG use at CCGT				
Net Emission Calculation (kg CO_2/year)				1.29E+06

8.2 Mid-Term Scenario: Hydrogen Injection

In this scenario, the operations of the energy hub are identical to those in the base case, with the exception that hydrogen is being injected into the reservoir during periods of low electricity prices. Since the dispatch order to the reservoir is the same as the one for the base case scenario, Figure 2.8 appears to be quasi-identical to Figure 2.2.

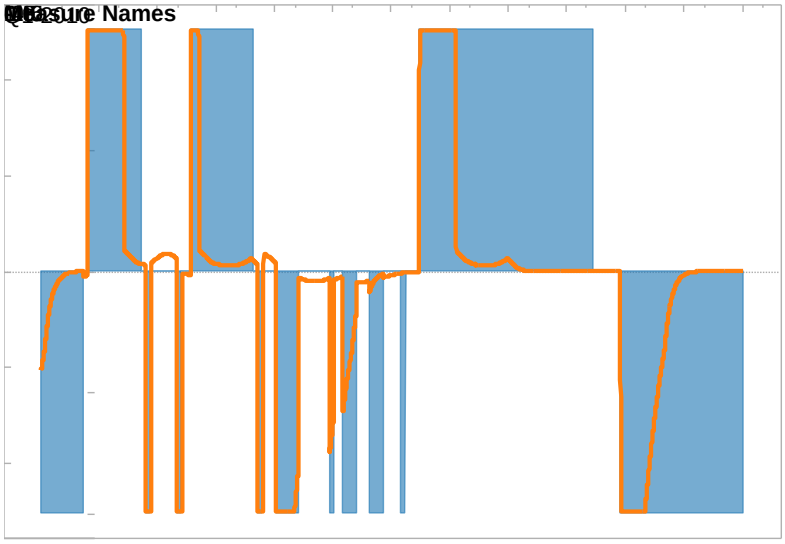

Figure 8.7 Dispatch to reservoir for the hydrogen injection scenario

The actual hourly flow rates into and out of the reservoir is the same as the deliverability/injectability values set by the reservoir model, as specified at decision points D4 and D5 (Figure 2.9).

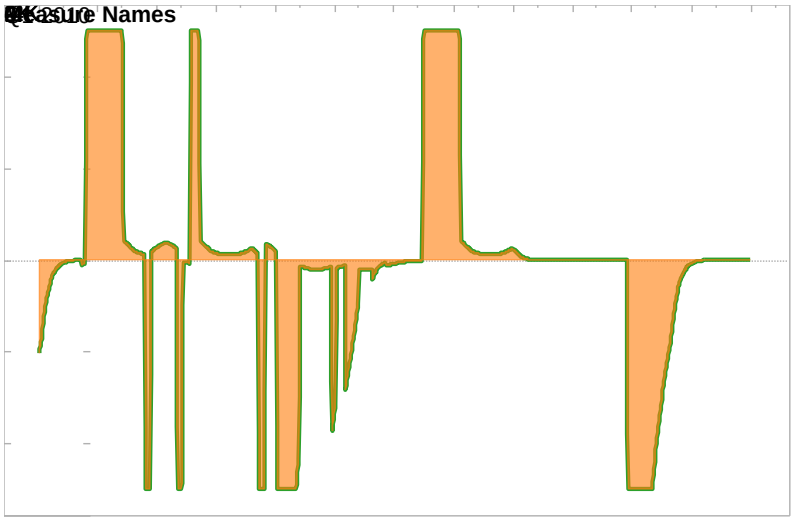

Figure 8.8 Injectability/deliverability and actual reservoir flow rates for the hydrogen injection scenario

The conditions in the reservoir for the hydrogen injection scenario are essentially identical to those in the base case scenario (compare Figure 2.10 to Figure 2.4). The only significant difference is that the concentration of hydrogen of the stored gas is now non-zero: the three year average of the reservoir hydrogen concentration is about 2% (Table 2.5). The hydrogen injected is produced using grid power, when the market price of electricity is relatively low. The amount of grid power consumed by the electrolyzer to produce hydrogen is shown in Figure 2.11.

The electrolyzers used for the production of hydrogen show an average utilization factor of ~50% (Figure 2.12). Over the three years, only 36.5% of the hydrogen produced is stored, the rest needs to be absorbed by client demand at the time of production (Figure 2.13).

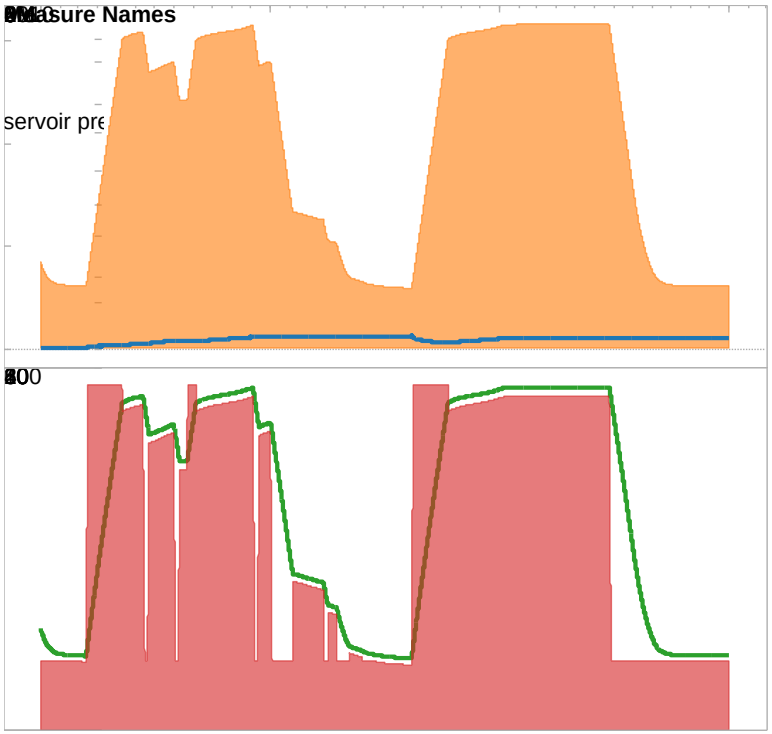

Figure 8.9 Reservoir conditions for the hydrogen injection scenario

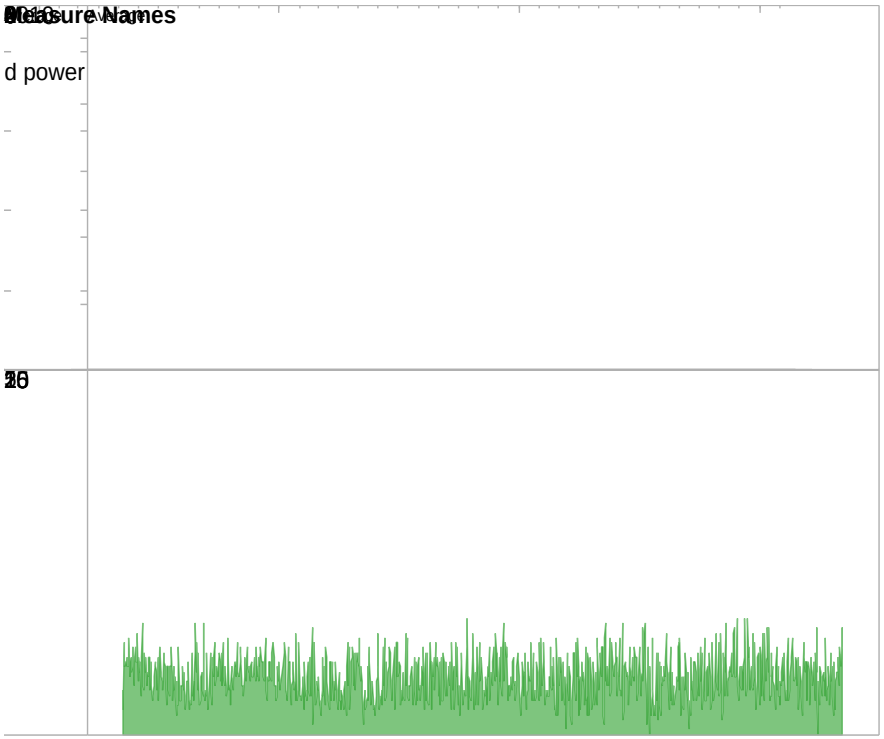

Figure 8.10 Power supply to the electrolyzers in the hydrogen injection scenario

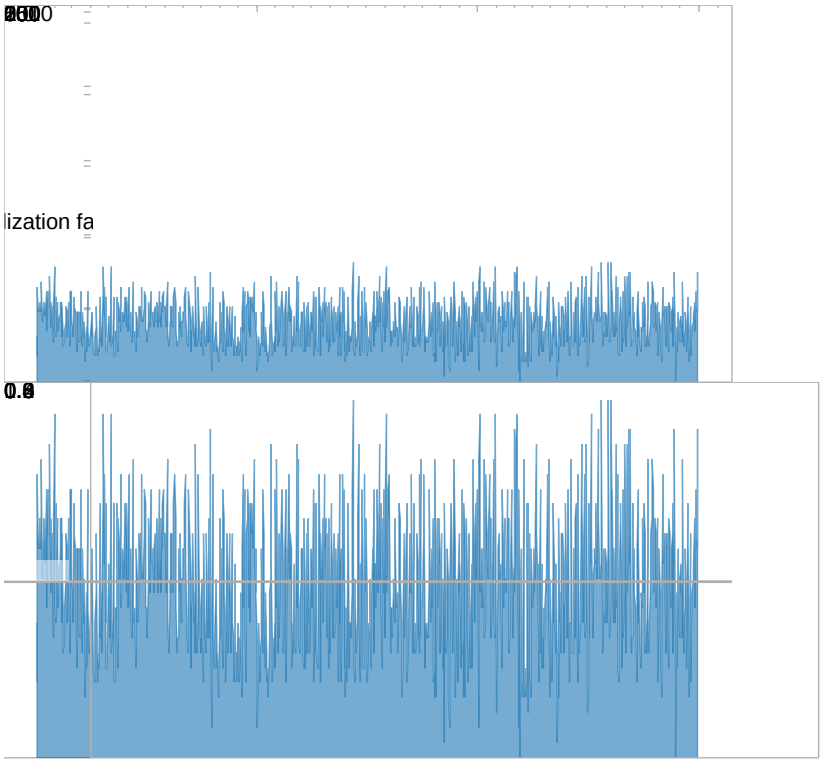

Figure 8.11 Electrolyzer utilization for the hydrogen injection scenario

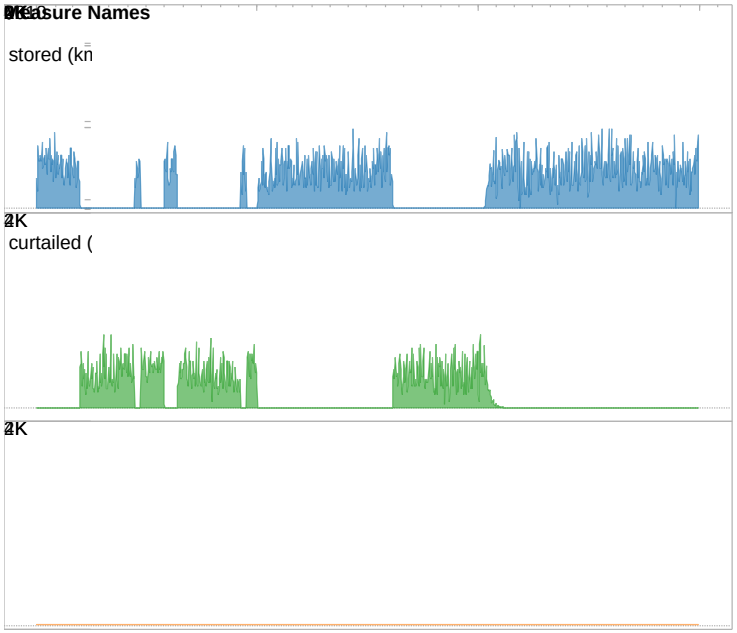

Figure 8.12 Outcome of electrolytic hydrogen produced for the hydrogen injection scenario

The concentration of the mixture stream injected into the reservoir varies widely, from negligible to 100%. Especially high concentrations of hydrogen can occur when the flow rate of natural gas injected is low (first half of 2012).

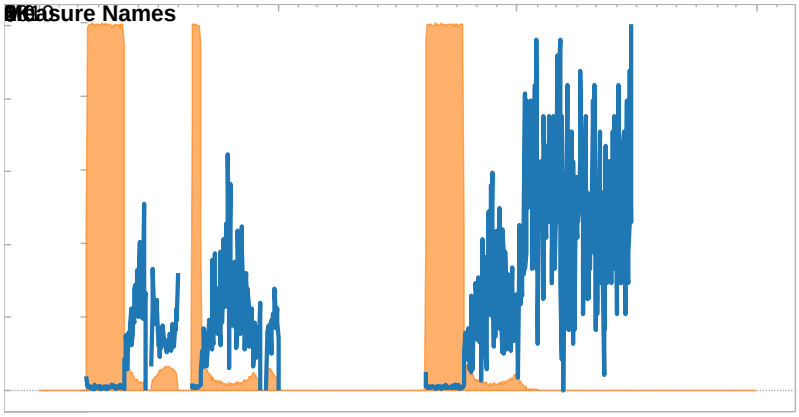

Figure 8.13 Flow rates of injected streams for the hydrogen injection scenario

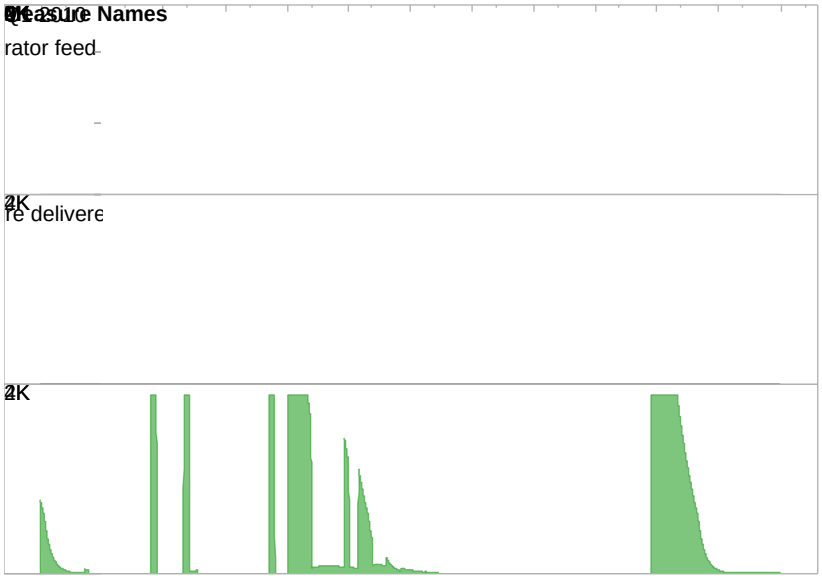

Figure 8.14 Dispatch of the produced mixture for the hydrogen injection scenario

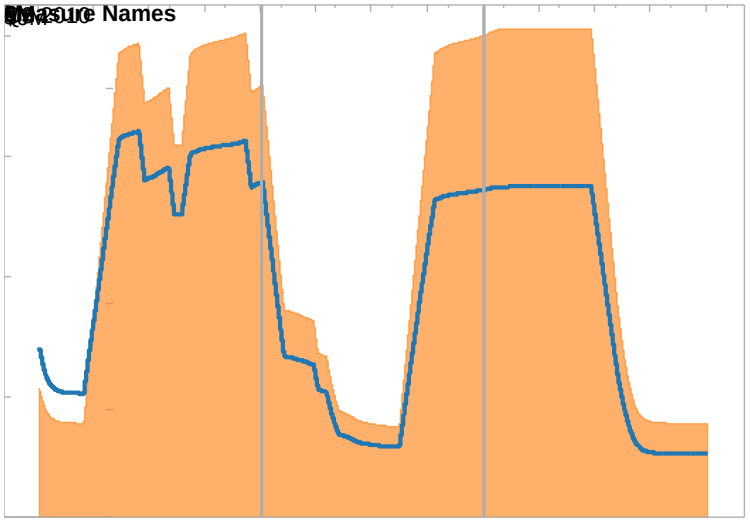

Figure 8.15 Value of inventory for the hydrogen injection scenario

Table 8.5 Summary of physical performance for the hydrogen injection scenario

Component	Variable	2010	2011	2012	Average	Unit
D1	Dispatch order to the reservoir	0.26	0.13	-0.16	0.08	N/A
Storage reservoir	Inventory	6.5E+06	4.7E+06	5.9E+06	5.7E+06	kmol
	H2 conc.	1%	2%	2%	2%	mol %
	Reservoir pressure	77	56	69	67	bar
	Wellhead pressure	76	55	59	63	bar
	Max. inventory change	5.6E+06	9.8E+05	-7.2E+06	-2.2E+05	kmol/year
	Actual inventory change	5.6E+06	9.8E+05	-7.2E+06	-2.2E+05	kmol/year
Wind turbines	Wind power produced					MWh/year
	Utilization factor					
D2	Wind power stored					MWh/year
	Wind power sold to grid					MWh/year
	Grid power stored	3.8E+04	3.6E+04	3.9E+04	3.8E+04	MWh/year
Electrolyzers	H2 produced	3.5E+05	3.4E+05	3.6E+05	3.5E+05	kmol/year
	Utilization factor	50%	47%	51%	49%	
D3	H2 stored	2.4E+05	1.3E+05	2.0E+04	1.3E+05	kmol/year
	H2 bypassed	1.2E+05	2.1E+05	3.4E+05	2.2E+05	kmol/year
	H2 curtailed					kmol/year
D4	NG stored	9.3E+06	7.2E+06	3.7E+04	5.5E+06	kmol/year
	H2 conc. of mixture injected	14%	14%	47%	25%	mol %
D5	Feed to separator					kmol/year
	Mixture delivered	4.0E+06	6.3E+06	7.3E+06	5.9E+06	kmol/year
	Fuel to CCGT					kmol/year
CCGT	Power delivered to grid					MWh/year
	Utilization factor					
Separator	H2 delivered					kmol/year
	Utilization factor					
D6	Revised mixture delivery	4.0E+06	6.3E+06	7.3E+06	5.9E+06	kmol/year
	H_2 conc. of mixture delivered	1%	2%	2%	2%	mol %
Compressors	Work required	4.4E+06	3.6E+06	1.0E+06	3.0E+06	kWh/year

Table 8.6 Summary of financial performance for the hydrogen injection scenario

Financial Performance	2010	2011	2012	Average
Capital Cost Breakdown				
Compressors				$ 3,784,995
Electrolyzers				$ 25,463,526
Gas turbine				$ -
Separator				$ -
Wind turbines				$ -
Total Capital Cost				$ 29,248,521
Amortized Capital Cost				**$ 2,979,026**
O&M Cost Breakdown				
Compression cost	$ 180,479	$ 141,812	$ 27,898	$ 116,730
Fixed O&M	$ 119,161	$ 119,161	$ 119,161	$ 119,161
Total O&M Cost	$ 299,640	$ 260,973	$ 147,059	$ 235,891
Purchase Breakdown				
Natural gas from grid	$ 28,530,669	$ 20,984,313	$ 80,742	$ 16,531,908
Power from grid	$ 1,121,031	$ 815,788	$ 669,578	$ 868,799
Total Purchase	$ 29,651,700	$ 21,800,101	$ 750,320	$ 17,400,707
Sales Breakdown				
Mixture to grid	$ 14,755,856	$ 20,968,870	$ 15,844,113	$ 17,189,613
Wind power to grid	$ -	$ -	$ -	$ -
CCGT power to grid	$ -	$ -	$ -	$ -
Hydrogen	$ 1,178,990	$ 2,086,901	$ 3,400,559	$ 2,222,150
Total Sales	$ 15,934,846	$ 23,055,771	$ 19,244,672	$ 19,411,763
Inventory Cost Calculation				
Beginning inventory value	$ 14,112,000	$ 27,565,298	$ 27,028,642	$ 22,901,980
Purchase of material	$ 29,651,700	$ 21,800,101	$ 750,320	$ 17,400,707
Cost of total mixture available	$ 43,763,700	$ 49,365,399	$ 27,778,962	$ 40,302,687
Ending inventory value	$ 27,565,298	$ 27,028,642	$ 5,234,682	$ 19,942,874
Cost of mixture delivered	$ 16,198,402	$ 22,336,757	$ 22,544,280	$ 20,359,813
Inventoried purchase	$ 13,453,298	$ (536,656)	$ (21,793,960)	$ (2,959,106)

Table 8.7 Net annual cash flow for the hydrogen injection scenario

Annual Cash Flow	2010	2011	2012	Average
1. Capital costs	$ (2,979,026)	$ (2,979,026)	$ (2,979,026)	$ (2,979,026)
2. OM costs	$ (235,891)	$ (235,891)	$ (235,891)	$ (235,891)
3. Cost of sales	$ (16,198,402)	$ (22,336,757)	$ (22,544,280)	$ (20,359,813)
4. Sales	$ 15,934,846	$ 23,055,771	$ 19,244,672	$ 19,411,763
5. Annual net	$ (3,478,473)	$ (2,495,903)	$ (6,514,525)	**$(4,162,967)**
Difference from Base Case ($/year)				**$ (2,701,438)**

Table 8.8 Summary of environmental performance for the hydrogen injection scenario

Environmental Performance	2010	2011	2012	Average
Emission Incurred (kg CO2/year)				
Compression of natural gas	2.55E+06	2.10E+06	5.81E+05	1.74E+06
Grid power generation for H2	5.88E+06	3.90E+06	4.18E+06	4.66E+06
Mixture use at CCGT				
Wind power generation for H2				
Off-site mixture use	1.73E+08	2.71E+08	3.14E+08	2.53E+08
Emission Mitigated (kg CO2/year)				
Displacement of SMR H2	2.50E+06	4.43E+06	7.22E+06	4.72E+06
Off-site NG use	1.76E+08	2.78E+08	3.20E+08	2.58E+08
NG use at CCGT				
Net Emission Calculation (kg CO2/year)				-3.41E+06
Difference from Base Case (kg CO2/year)				**-4.71E+06**

8.3 Long-Term Scenario: Surplus Baseload Generation (SBG) Reduction

In this scenario, the energy hub is equipped to produce hydrogen for energy storage and to deliver stored energy to the power grid via the use of an on-site CCGT plant. The dispatch issued to the reservoir is based on the deviation of Ontario power demand from its annual moving average.

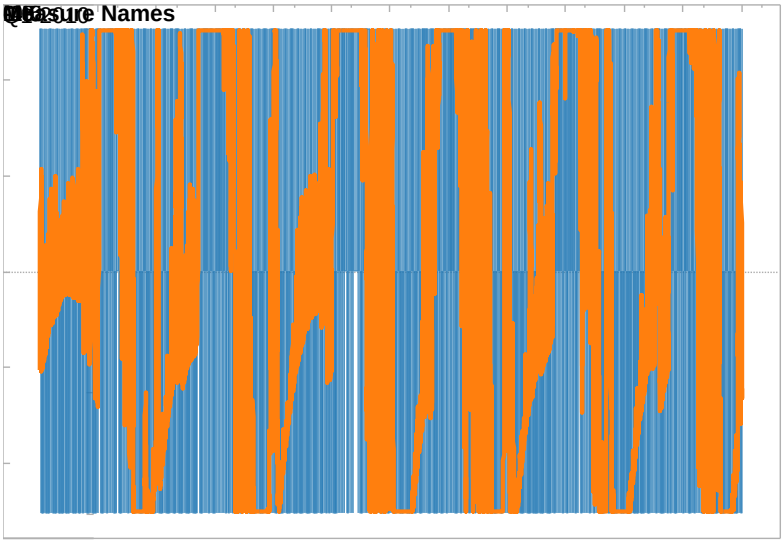

Figure 8.16 Dispatch to reservoir for the SBG reduction scenario

It can be seen that the dispatch order shifts rather violently, from hour to hour, making the figure indecipherable at hourly resolution. The same information is plotted, averaged by day (i.e. the dispatch order is averaged for distinct groups of 24 hours) in Figure 2.18. Once averaged by day, which reduces the visibility of hourly fluctuations, it can be seen that the dispatch order to the reservoir is largely organized by season. Spring and autumn represent periods of injection (positive dispatch order); summer and winter represent periods of withdrawal (negative dispatch order).

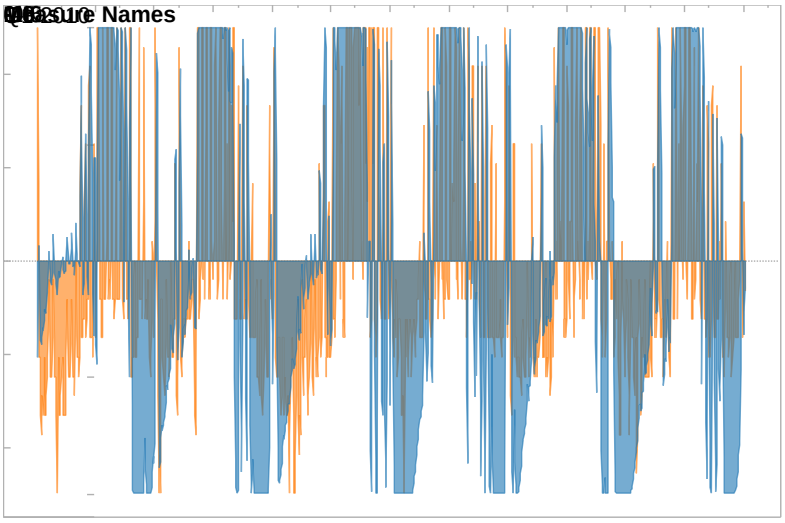

Figure 8.17 Daily average of dispatch to reservoir for the SBG reduction scenario

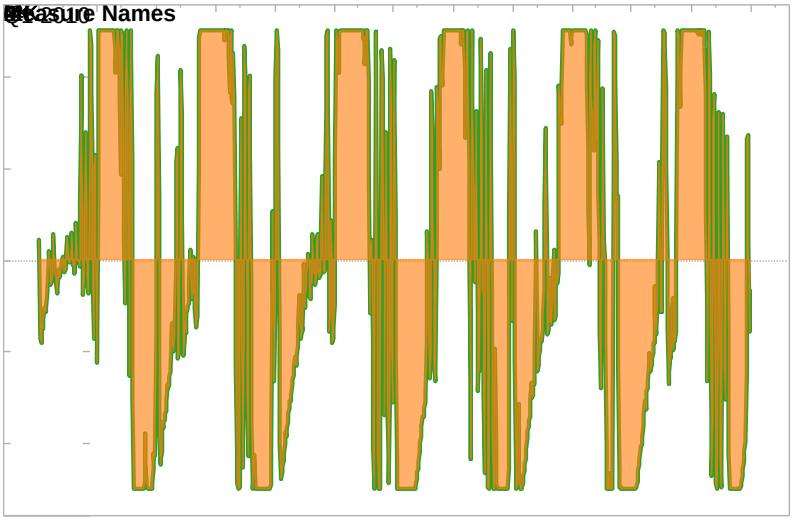

Figure 8.18 Injectability/deliverability and actual reservoir flow rates for the SBG reduction scenario

The inventory level for this simulated scenario follows the seasonal pattern dictated by its dispatch order, with peaks during spring and autumn and troughs during summer and winter. The 3-year average for hydrogen concentration inside of the reservoir is 1% (Table 2.9). Its profile is relatively flat, except for the first two months during which hydrogen is initially introduced into the reservoir. In Figure 2.4, it can be seen that wellhead pressure undergoes many high frequency low-magnitude changes.

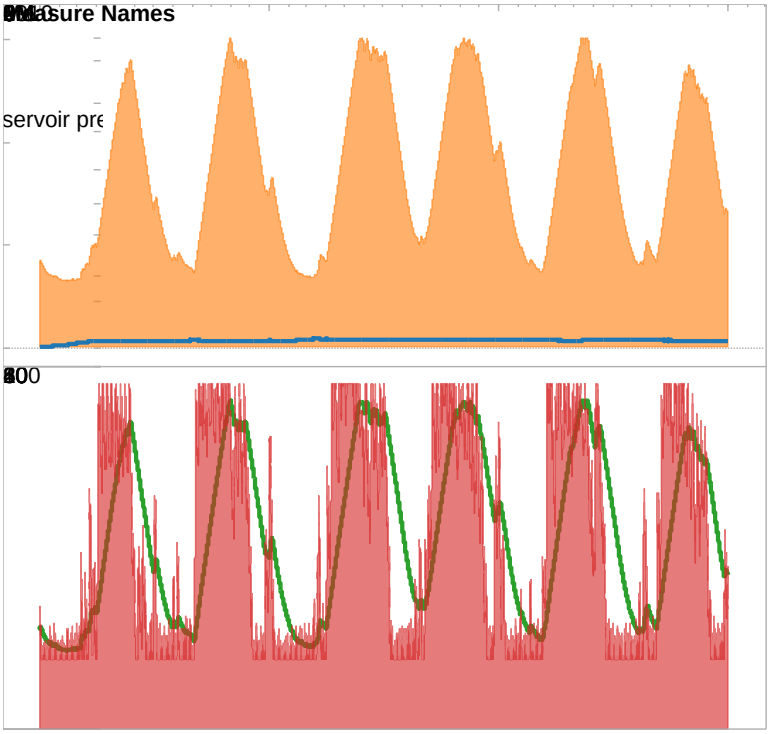

Figure 8.19 Reservoir conditions for the SBG reduction scenario

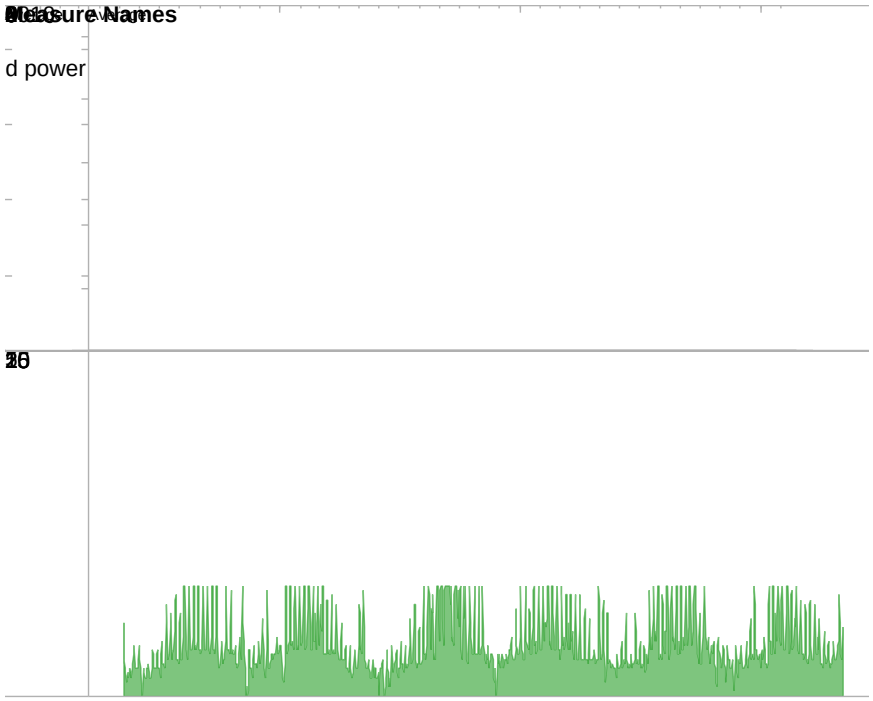

Figure 8.20 Power supply to the electrolyzers in the SBG reduction scenario

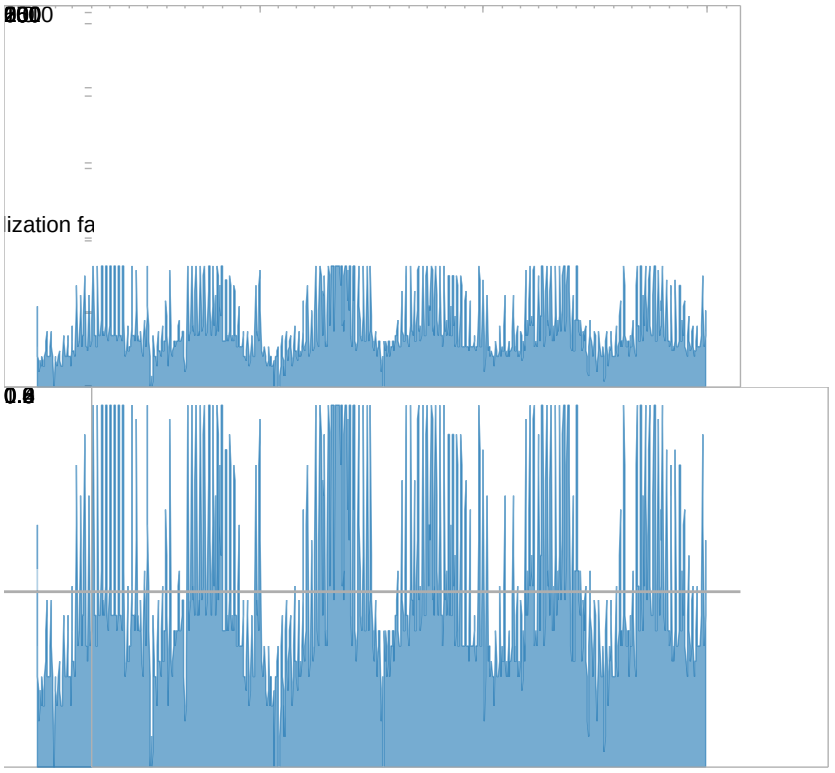

Figure 8.21 Electrolyzer utilization for the SBG reduction scenario

From Figure 2.21, a clearly visible seasonal trend can be detected: during periods of low demand, the electrolyzers operate nearly every hour, consuming a daily average of ~8MW (close to 100% utilization) , whereas during periods of high electricity demand in Ontario, that value drops to 2-3 MW (about 30% utilization).

Figure 2.23 shows that not all hydrogen produced by the electrolyzers is stored via injection. Actually, of all the hydrogen produced by the electrolyzer, 60% has been injected into the reservoir. The rest needed to be absorbed by local hydrogen demand at the time of production (Table 2.9).

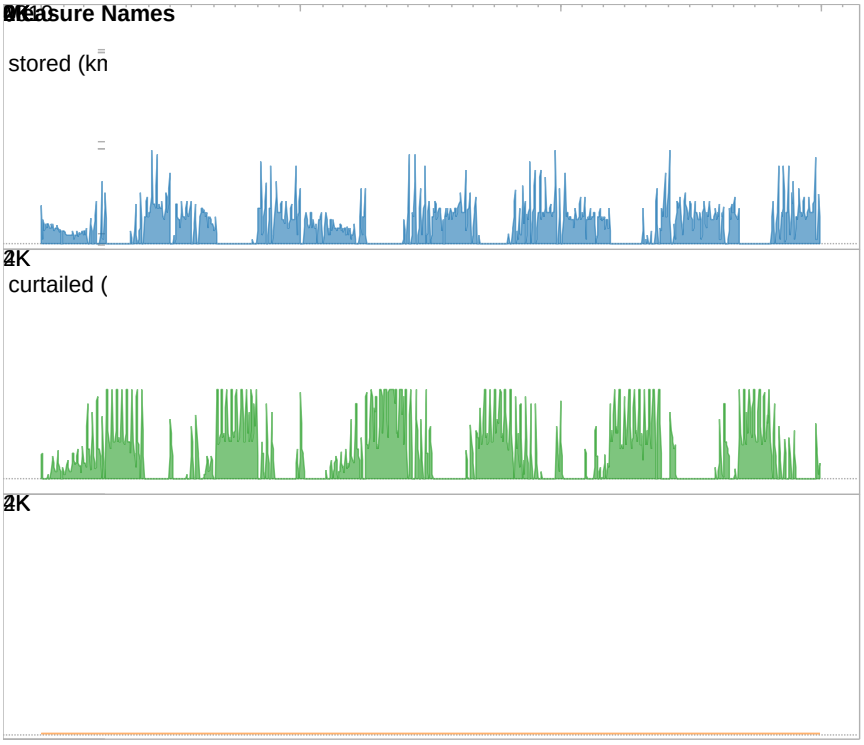

Figure 8.22 Outcome of electrolytic hydrogen produced for the SBG reduction scenario

Compared to the hydrogen concentration in the injected mixture for the previous scenario (Figure 2.14), the concentration in this scenario is much more stable, limited to 0% to 30%. The overall average of hydrogen concentration in the injected stream is 3%.

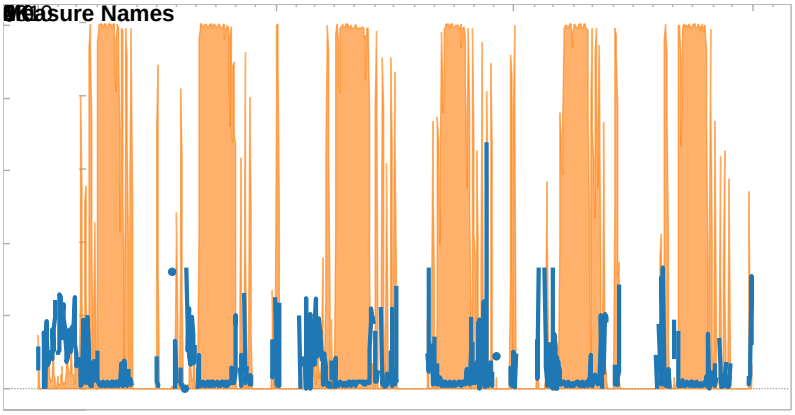

Figure 8.23 Flow rates of injected streams for the SBG reduction scenario

As expected, the CCGT plant is operated whenever there is production of stored gas from the reservoir. The quantity of mixture consumed by the on-site CCGT is less than 10% of that delivered to off-site customers via the distribution pipelines. The utilization of the CCGT plant is about 50% (Figure 2.26), about the same as the electrolyzers.

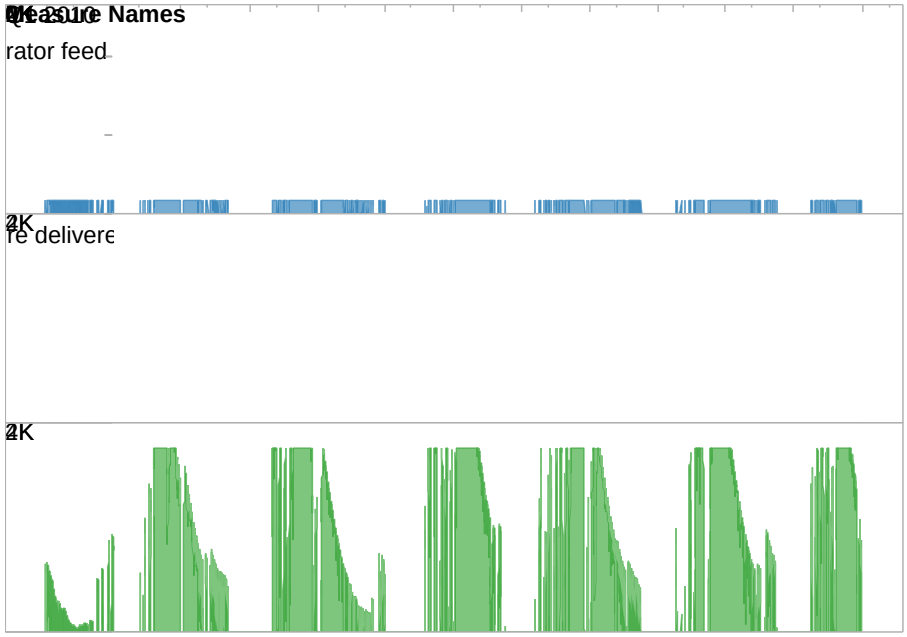

,

Figure 8.24 Dispatch of the produced mixture for the SBG reduction scenario

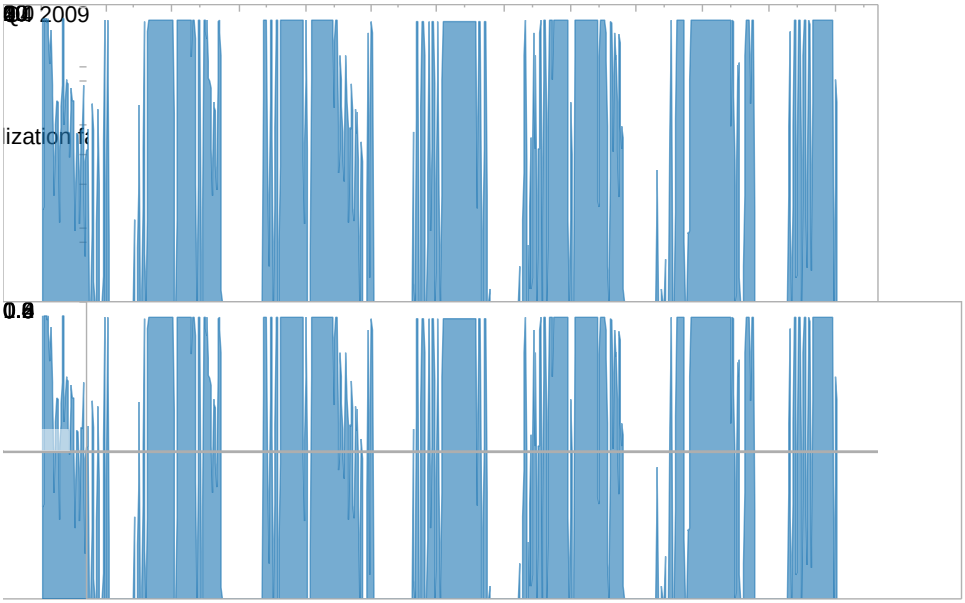

Figure 8.25 CCGT utilization for the SBG reduction scenario

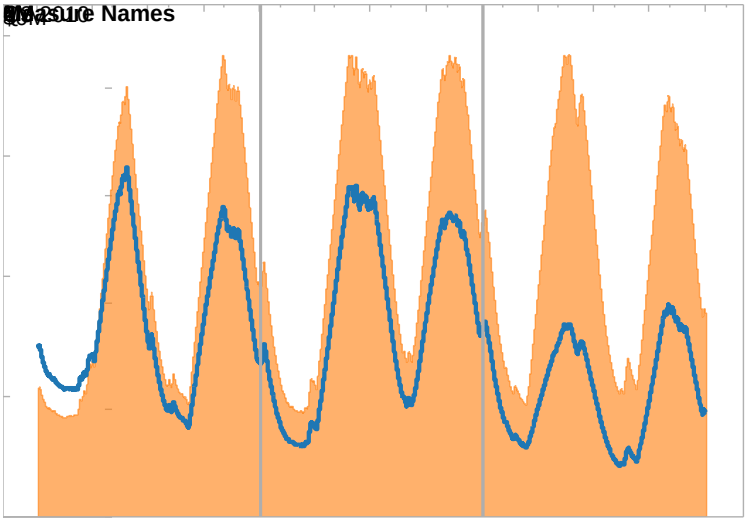

Figure 8.26 Value of inventory for the SBG reduction scenario

Table 8.9 Summary of physical performance for the SBG reduction scenario

Component	Variable	2010	2011	2012	Average	Unit
D1	Dispatch order to the reservoir	-0.09	0.02	-0.04	-0.03	N/A
Storage reservoir	Inventory	4.4E+06	5.4E+06	5.0E+06	4.9E+06	kmol
	H2 conc.	1%	1%	1%	1%	mol %
	Reservoir pressure	54	64	60	59	bar
	Wellhead pressure	53	61	57	57	bar
	Max. inventory change	1.8E+06	1.2E+06	-1.7E+06	4.6E+05	kmol/year
	Actual inventory change	1.8E+06	1.2E+06	-1.7E+06	4.6E+05	kmol/year
Wind turbines	Wind power produced					MWh/year
	Utilization factor					
D2	Wind power stored					MWh/year
	Wind power sold to grid					MWh/year
	Grid power stored	3.5E+04	3.9E+04	3.7E+04	3.7E+04	MWh/year
Electrolyzers	H2 produced	3.2E+05	3.6E+05	3.4E+05	3.4E+05	kmol/year
	Utilization factor	46%	51%	48%	48%	
D3	H2 stored	2.0E+05	2.3E+05	1.9E+05	2.1E+05	kmol/year
	H2 bypassed	1.3E+05	1.3E+05	1.5E+05	1.4E+05	kmol/year
	H2 curtailed					kmol/year
D4	NG stored	1.5E+07	1.6E+07	1.5E+07	1.5E+07	kmol/year
	H2 conc. of mixture injected	4%	3%	3%	3%	mol %
D5	Feed to separator					kmol/year
	Mixture delivered	1.2E+07	1.4E+07	1.5E+07	1.6E+07	kmol/year
	Fuel to CCGT	1.5E+06	1.5E+06	1.7E+06	1.6E+06	kmol/year
CCGT	Power delivered to grid	1.7E+05	1.7E+05	1.9E+05	1.8E+05	MWh/year
	Utilization factor	49%	48%	53%	50%	
Separator	H2 delivered					kmol/year
	Utilization factor					
D6	Revised mixture delivery	1.2E+07	1.4E+07	1.5E+07	4.0E+07	kmol/year
	H2 conc. of mixture delivered	1%	1%	1%	1%	mol %
Compressors	Work required	5.0E+06	5.7E+06	5.2E+06	1.6E+07	kWh/year

Table 8.10 Summary of financial performance for the SBG reduction scenario

Financial Performance	2010	2011	2012	Average
Capital Cost Breakdown				
Compressors				$ 3,784,995
Electrolyzers				$ 25,463,526
Gas turbine				$ 29,944,756
Separator				$ -
Wind turbines				$ -
Total Capital Cost				$ 59,193,277
Amortized Capital Cost				**$ 6,028,966**
O&M Cost Breakdown				
Compression cost	$ 195,709	$ 226,861	$ 136,056	$ 186,209
Fixed O&M	$ 241,159	$ 241,159	$ 241,159	$ 241,159
Total O&M Cost	$ 436,868	$ 468,020	$ 377,215	$ 427,368
Purchase Breakdown				
Natural gas from grid	$ 44,473,714	$ 48,802,563	$ 29,725,676	$ 41,000,651
Power from grid	$ 1,024,681	$ 959,970	$ 626,722	$ 870,458
Total Purchase	$ 45,498,396	$ 49,762,533	$ 30,352,399	$ 41,871,109
Sales Breakdown				
Mixture to grid	$ 38,998,303	$ 41,175,297	$ 33,093,634	$ 37,755,745
Wind power to grid	$ -	$ -	$ -	$ -
CCGT power to grid	$ 6,888,079	$ 5,559,530	$ 4,728,503	$ 5,725,371
Hydrogen	$ 1,272,798	$ 1,322,498	$ 1,475,605	$ 1,356,967
Total Sales	$ 47,159,179	$ 48,057,326	$ 39,297,742	$ 44,838,082
Inventory Cost Calculation				
Beginning inventory value	$ 14,112,000	$ 12,629,359	$ 15,527,837	$ 14,089,732
Purchase of material	$ 45,498,396	$ 49,762,533	$ 30,352,399	$ 41,871,109
Cost of total mixture available	$ 59,610,396	$ 62,391,892	$ 45,880,236	$ 55,960,841
Ending inventory value	$ 12,629,359	$ 15,527,837	$ 8,609,279	$ 12,255,491
Cost of mixture delivered	$ 46,981,037	$ 46,864,055	$ 37,270,957	$ 43,705,350
Inventoried purchase	$ (1,482,641)	$ 2,898,478	$ (6,918,558)	$ (1,834,240)

Table 8.11 Net annual cash flow for the SBG reduction scenario

Annual Cash Flow	2010	2011	2012	Average
1. Capital costs	$ (6,028,966)	$ (6,028,966)	$ (6,028,966)	$ (6,028,966)
2. OM costs	$ (427,368)	$ (427,368)	$ (427,368)	$ (427,368)
3. Cost of sales	$ (46,981,037)	$ (46,864,055)	$ (37,270,957)	$ (43,705,350)
4. Sales	$ 47,159,179	$ 48,057,326	$ 39,297,742	$ 44,838,082
5. Annual net	$ (6,278,191)	$ (5,263,063)	$ (4,429,548)	**$(5,323,601)**
Difference from Base Case ($/year)				**$ (3,862,071)**

Table 8.12 Summary of environmental performance for the SBG reduction scenario

Environmental Performance	2010	2011	2012	Average
Emission Incurred (kg CO2/year)				
Compression of natural gas	2.90E+06	3.29E+06	3.01E+06	3.07E+06
Grid power generation for H2	4.07E+06	3.12E+06	2.87E+06	3.35E+06
Mixture use at CCGT	6.64E+07	6.55E+07	7.15E+07	6.78E+07
Wind power generation for H2				
Off-site mixture use	5.06E+08	5.89E+08	6.59E+08	5.85E+08
Indirect Emission Mitigated (kg CO2/year)				
Displacement of SMR H2	2.70E+06	2.81E+06	3.13E+06	2.88E+06
Off-site NG use	5.12E+08	5.98E+08	6.68E+08	5.92E+08
NG use at CCGT	6.64E+07	6.55E+07	7.15E+07	6.78E+07
Net Emission Calculation (kg CO2/year)				-4.04E+06
Difference from Base Case (kg CO2/year)				**-5.34E+06**

8.4 Long-Term Scenario: Integration of Wind Power

In this scenario, in additional to the electrolyzer and the CCGT, components which allow for the storage and recovery of electrical energy via hydrogen, a small scale wind farm is set-up on-site at the energy hub. The operations of the reservoir, in this case, are directed from the perspective of wind power generation: wind power generated during off-peak periods is stored for delivery during peak periods.

From Figure 2.28, it is observed that the dispatch order received by the reservoir is predominantly for injection (Note that the following figure has been averaged by day to facilitate interpretation).

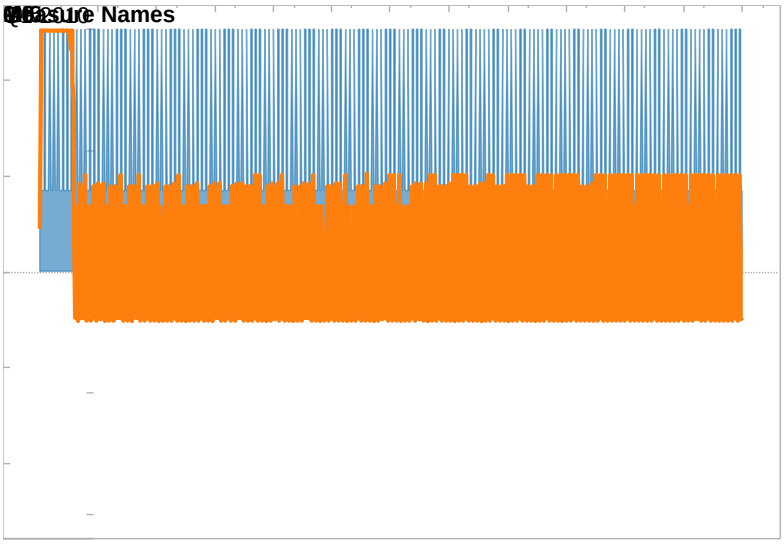

Figure 8.27 Daily average of dispatch to reservoir for the wind power integration scenario

The injectability/deliverability curve of this scenario displays some unique features. Compared to the band of dense oscillations which last for most of the simulation, there is a singular increase during the first few months of storage operation. Also, the maximum deliverability (negative region of the injectability/deliverability curve) is lower than the maximum injectability.

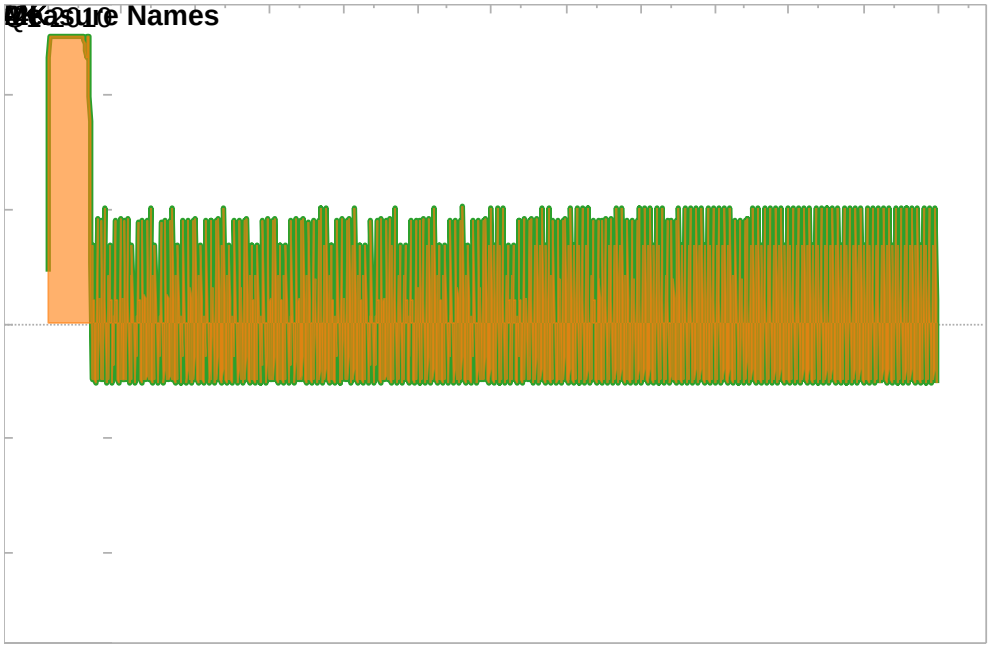

Figure 8.28 Injectability/deliverability and actual reservoir flow rates for the wind power integration scenario

The most striking observation about the reservoir inventory for this scenario is that it does not exhibit any cycles. In Figure 2.30, the reservoir is shown to be almost always full, except for the first few months during which it is filled, which is starting with low inventory at the beginning of 2010. Although the reservoir inventory remains relatively stable for much of the three years under simulation, the concentration of hydrogen in the reservoir steadily climbs from year to year (2%, 5% and 6%, respectively).

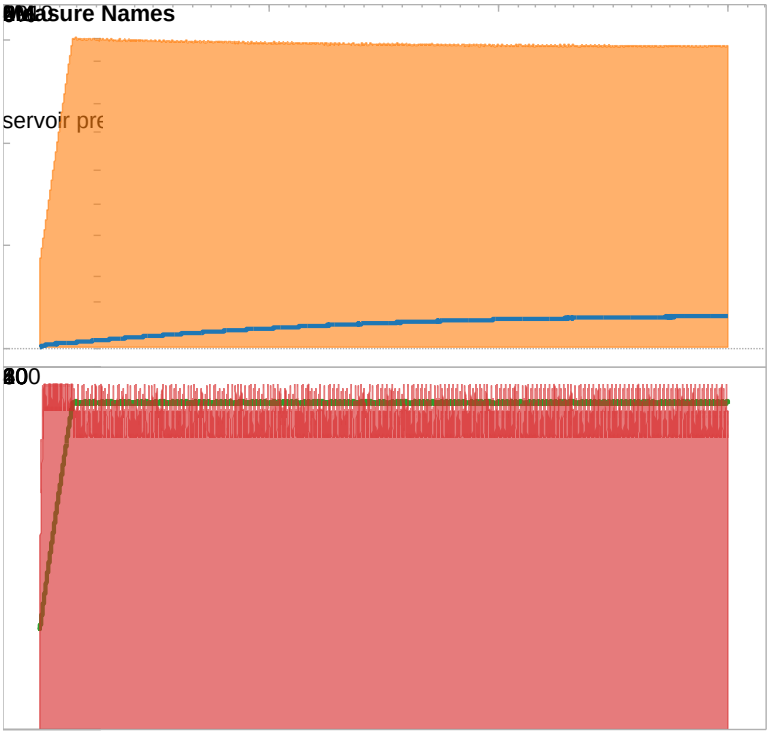

Figure 8.29 Reservoir conditions for the wind power integration scenario

Studying the trend in wellhead pressure in Figure 2.30, it is seen that it is maintained within a very narrow range: between 103 and 87 bar. Other than that, the wellhead pressure does not exhibit any clear trend over the time scale chosen. Observing the relationship between the reservoir pressure and the wellhead pressure over the course of a month, instead of three years, it is observed that the changes in wellhead pressure are frequent but shallow. Rarely does the wellhead pressure exceed the reservoir pressure.

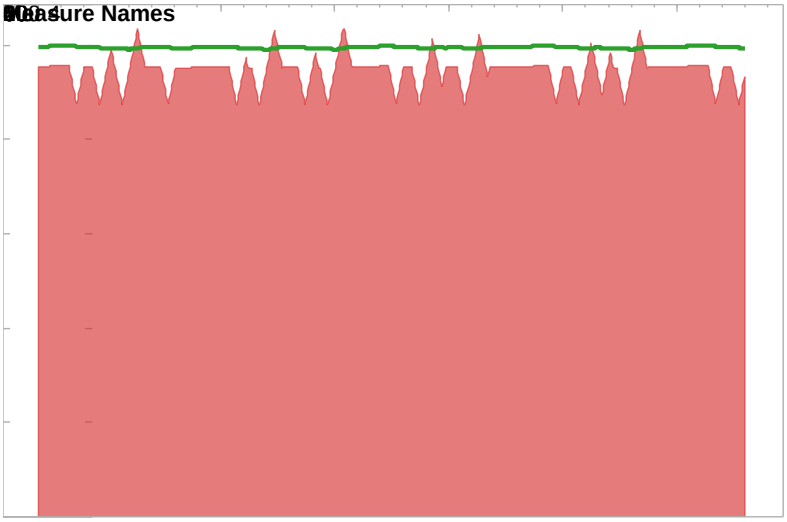

Figure 8.30 Wellhead pressure and reservoir pressure during March 2010 for the wind power integration scenario

The overall average capacity utilization factor of wind turbines at the site of the energy hub (Sarnia, Lambton County, Ontario) is calculated to be 25%, in line with 29.5% the average value for Ontario wind farms [107]. About 70% of all wind power generated has been used to produce hydrogen; all the wind power supplied to the electrolyzer, in its turn, represents about 25% of the total electricity consumption of the electrolyzer, for the time period simulated. The capacity utilization factor of the electrolyzers is much higher compared to previous scenarios (80% as opposed to 50%) and experiences no year-to-year variation. More than 75% of the hydrogen produced by the electrolyzer has been stored.

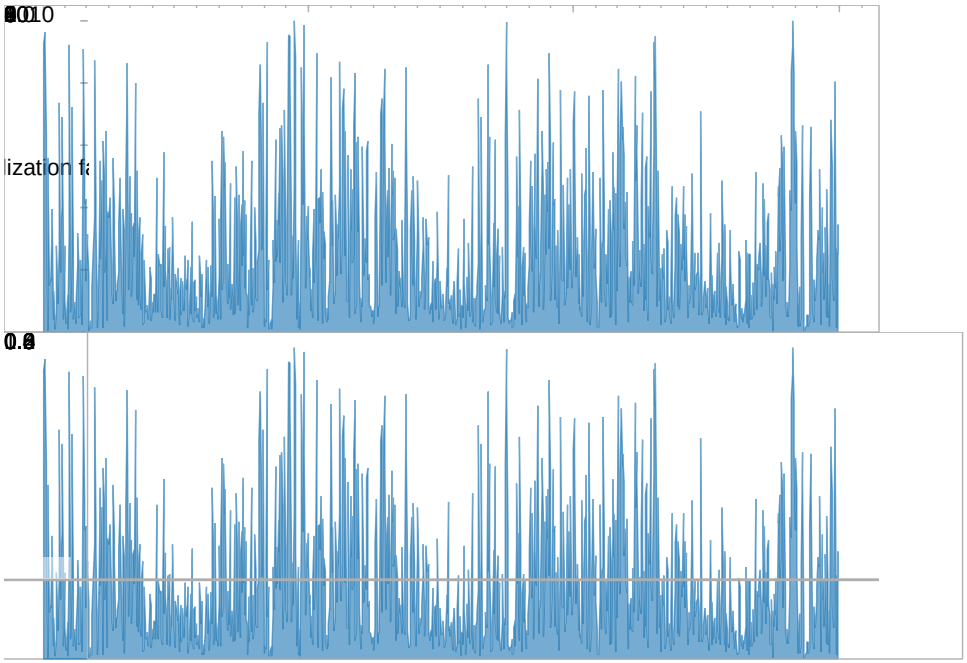

Figure 8.31 Wind turbines utilization for the wind power integration scenario

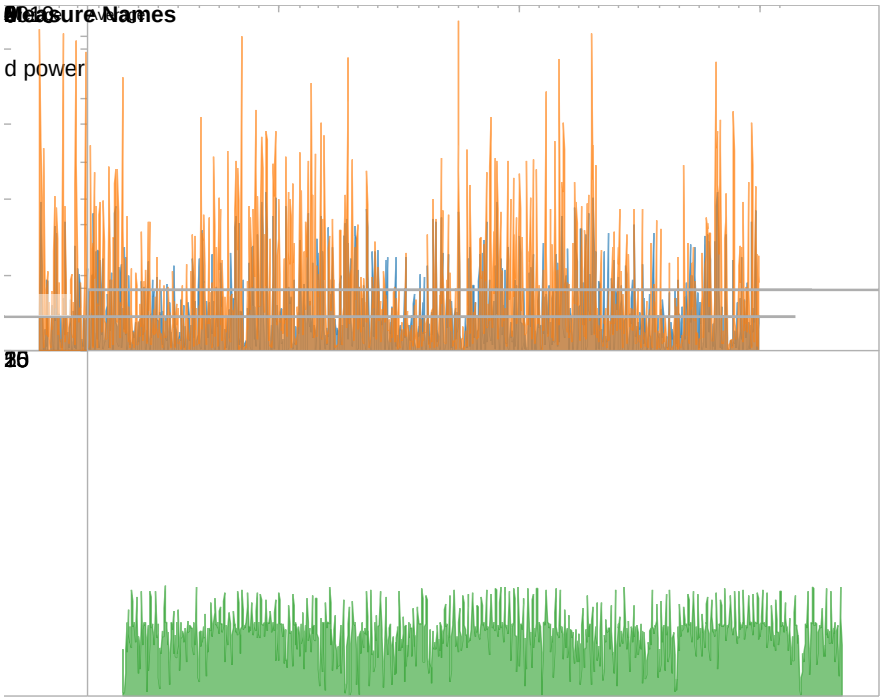

Figure 8.32 Power supply to the electrolyzers in the wind power integration scenario

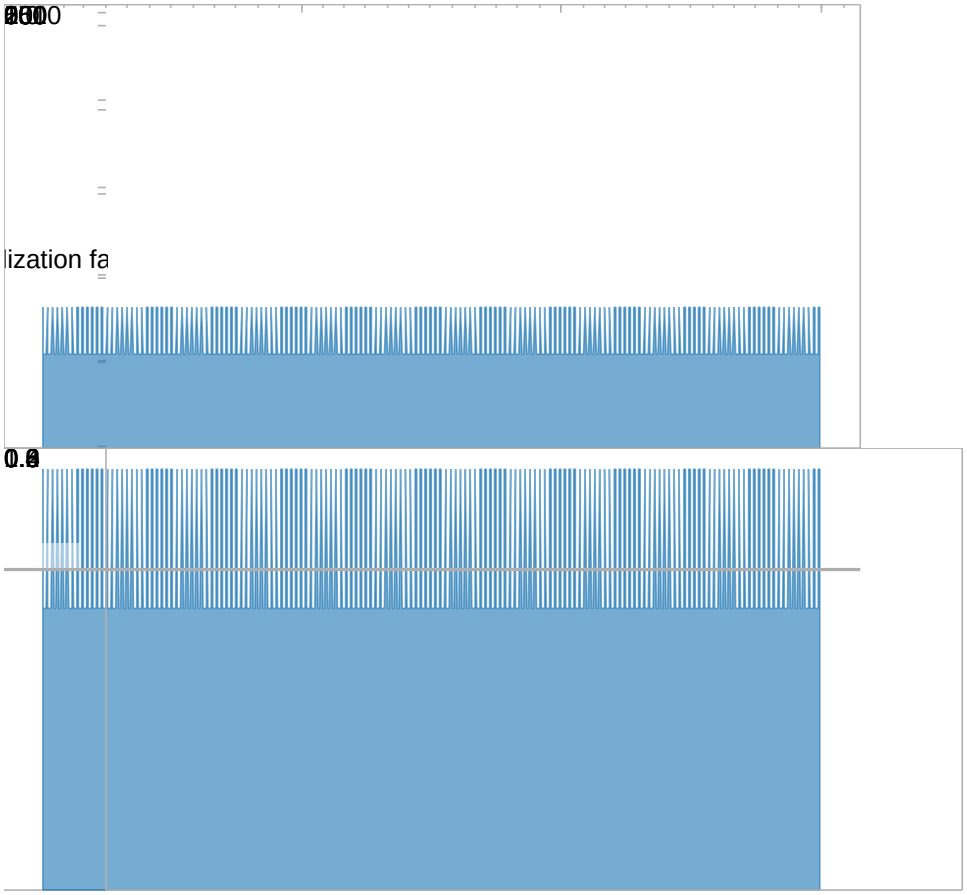

Figure 8.33 Electrolyzer utilization for the wind power integration scenario

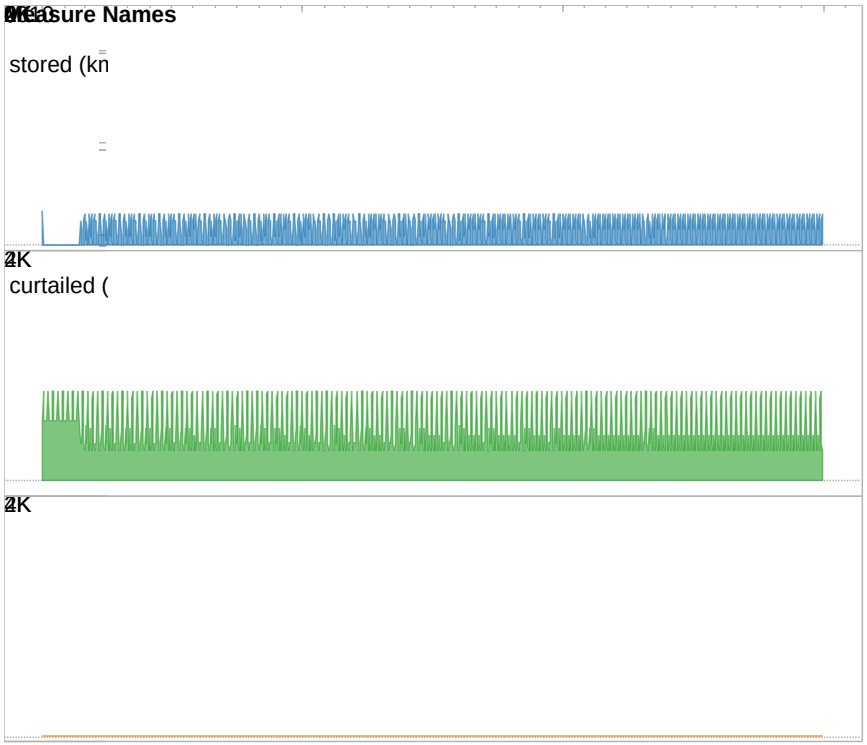

Figure 8.34 Outcome of electrolytic hydrogen produced for the wind power integration scenario

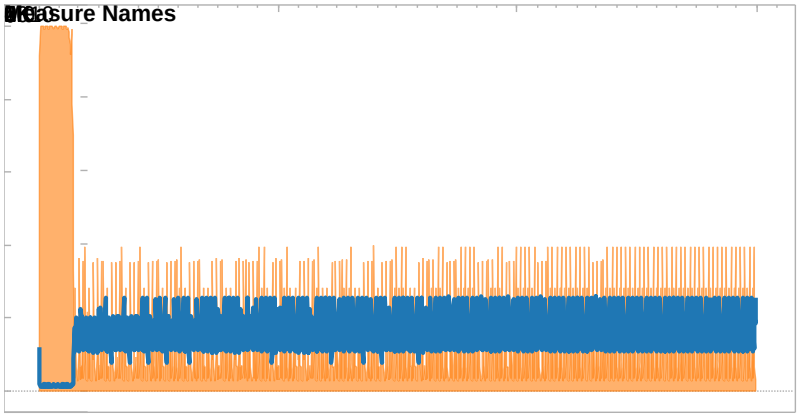

Figure 8.35 Flow rates of injected streams for the wind integration scenario

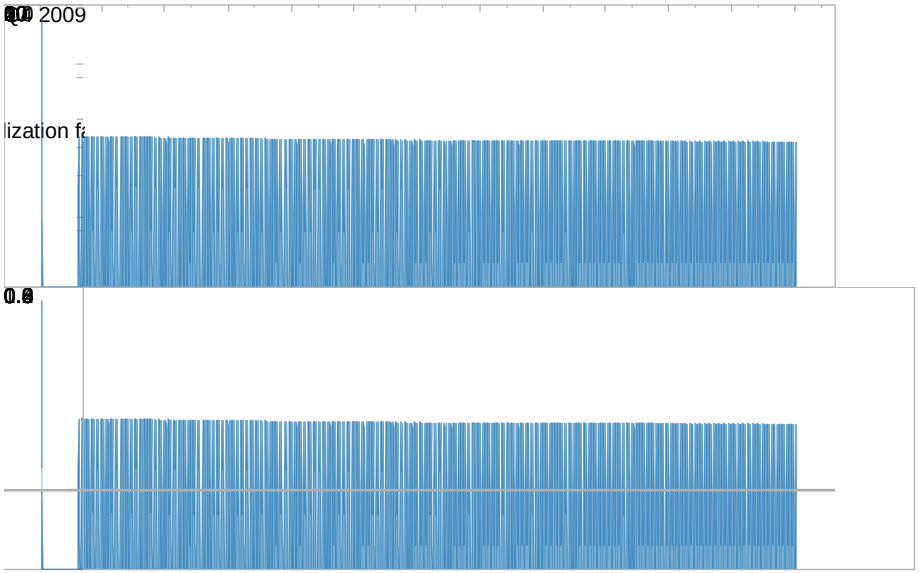

Figure 8.36 CCGT utilization for the wind power integration scenario

Although the level of the physical inventory of the reservoir seems to stagnate at its maximum capacity, the value of the gas stored in the reservoir is gradually decreasing.

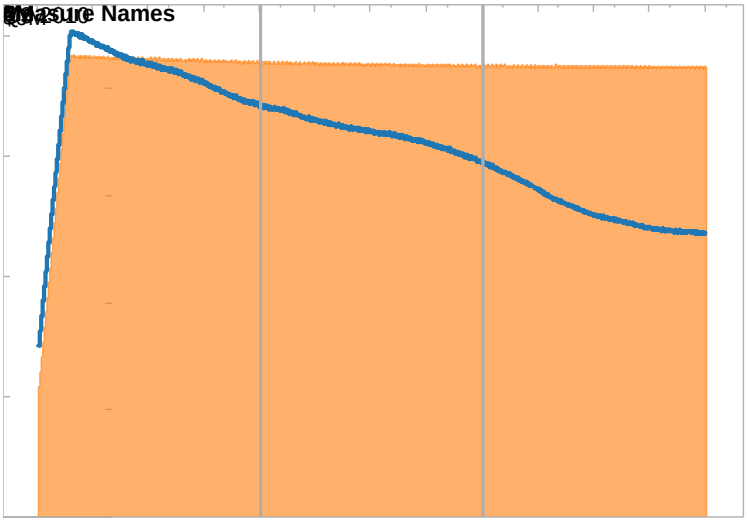

Figure 8.37 Value of inventory for the wind power integration scenario

Table 8.13 Summary of physical performance for the wind power integration scenario

Component	Variable	2010	2011	2012	Average	Unit
D1	Dispatch order to the reservoir	0.53	0.53	0.52	0.52	N/A
Storage reservoir	Inventory	8.1E+06	8.4E+06	8.4E+06	8.3E+06	kmol
	H2 conc.	2%	5%	6%	4%	mol %
	Reservoir pressure	94	99	99	98	bar
	Wellhead pressure	95	94	94	95	bar
	Max. inventory change	6.1E+06	-4.5E+04	-7.4E+04	2.0E+06	kmol/year
	Actual inventory change	6.1E+06	-4.5E+04	-7.4E+04	2.0E+06	kmol/year
Wind turbines	Wind power produced	2.3E+04	2.2E+04	2.2E+04	2.2E+04	MWh/year
	Utilization factor	26%	25%	25%	25%	
D2	Wind power stored	1.5E+04	1.4E+04	1.4E+04	1.4E+04	MWh/year
	Wind power sold to grid	7.7E+03	7.9E+03	8.1E+03	7.9E+03	MWh/year
	Grid power stored	4.3E+04	4.4E+04	4.5E+04	4.4E+04	MWh/year
Electrolyzers	H2 produced	5.4E+05	5.4E+05	5.4E+05	5.4E+05	kmol/year
	Utilization factor	76%	76%	76%	76%	
D3	H2 stored	4.3E+05	4.1E+05	4.0E+05	4.1E+05	kmol/year
	H2 bypassed	1.1E+05	1.3E+05	1.4E+05	1.3E+05	kmol/year
	H2 curtailed					kmol/year
D4	NG stored	1.0E+07	5.2E+06	5.6E+06	7.1E+06	kmol/year
	H2 conc. of mixture injected	14%	17%	16%	16%	mol %
D5	Feed to separator					kmol/year
	Mixture delivered	4.0E+06	4.7E+06	5.1E+06	4.6E+06	kmol/year
	Fuel to CCGT	7.8E+05	9.3E+05	9.9E+05	9.0E+05	kmol/year
CCGT	Power delivered to grid	8.7E+04	1.0E+05	1.1E+05	9.9E+04	MWh/year
	Utilization factor					
Separator	H2 delivered					kmol/year
	Utilization factor					
D6	Revised mixture delivery	4.0E+06	4.7E+06	5.1E+06	4.6E+06	kmol/year
	H2 conc. of mixture delivered	2%	5%	6%	4%	mol %
Compressors	Work required	5.0E+06	3.0E+06	3.2E+06	3.8E+06	kWh/year

Table 8.14 Summary of financial performance for the wind power integration scenario

Financial Performance	2010	2011	2012	Average
Capital Cost Breakdown				
Compressors				$ 3,784,995
Electrolyzers				$ 25,463,526
Gas turbine				$ 29,944,756
Separator				$ -
Wind turbines				$ 21,882,706
Total Capital Cost				$ 81,075,983
Amortized Capital Cost				**$ 8,257,768**
O&M Cost Breakdown				
Compression cost	$ 242,546	$ 121,513	$ 88,609	$ 150,889
Fixed O&M	$ 330,311	$ 330,311	$ 330,311	$ 330,311
Total O&M Cost	$ 572,857	$ 451,823	$ 418,920	$ 481,200
Purchase Breakdown				
Natural gas from grid	$ 39,546,411	$ 15,765,439	$ 11,703,904	$ 22,338,585
Power from grid	$ 1,498,881	$ 1,292,831	$ 997,797	$ 1,263,169
Total Purchase	$ 41,045,291	$ 17,058,270	$ 12,701,701	$ 23,601,754
Sales Breakdown				
Mixture to grid	$ 12,339,439	$ 13,846,121	$ 10,202,400	$ 12,129,320
Wind power to grid	$ 1,164,431	$ 1,201,745	$ 1,238,542	$ 1,201,573
CCGT power to grid	$ 3,566,614	$ 3,501,045	$ 2,795,764	$ 3,287,808
Hydrogen	$ 1,111,656	$ 1,316,249	$ 1,406,016	$ 1,277,974
Total Sales	$ 18,182,139	$ 19,865,160	$ 15,642,722	$ 17,896,674
Inventory Cost Calculation				
Beginning inventory value	$ 14,112,000	$ 34,175,457	$ 29,491,302	$ 25,926,253
Purchase of material	$ 41,045,291	$ 17,058,270	$ 12,701,701	$ 23,601,754
Cost of total mixture available	$ 55,157,291	$ 51,233,726	$ 42,193,003	$ 49,528,007
Ending inventory value	$ 34,175,457	$ 29,491,302	$ 23,441,869	$ 29,036,209
Cost of mixture delivered	$ 20,981,835	$ 21,742,424	$ 18,751,134	$ 20,491,798
Inventoried purchase	$ 20,063,457	$ (4,684,154)	$ (6,049,433)	$ 3,109,956

Table 8.15 Net annual cash flow for the wind power integration scenario

Annual Cash Flow	2010	2011	2012	Average
1. Capital costs	$ (8,257,768)	$ (8,257,768)	$ (8,257,768)	$ (8,257,768)
2. OM costs	$ (481,200)	$ (481,200)	$ (481,200)	$ (481,200)
3. Cost of sales	$ (20,981,835)	$(21,742,424)	$ (18,751,134)	$ (20,491,798)
4. Sales	$ 18,182,139	$ 19,865,160	$ 15,642,722	$ 17,896,674
5. Annual net	$ (11,538,663)	$(10,616,233)	$ (11,847,380)	**$ (11,334,092)**
Difference from Base Case ($/year)				**$ (9,872,563)**

Table 8.16 Summary of environmental performance for the wind integration scenario

Environmental Performance	2010	2011	2012	Average
Emission Incurred (kg CO_2/year)				
Compression of natural gas	2.89E+06	1.76E+06	1.86E+06	2.17E+06
Grid power generation for H2	7.07E+06	5.17E+06	5.18E+06	5.81E+06
Mixture use at CCGT	3.34E+07	3.89E+07	4.11E+07	3.78E+07
Wind power generation for H_2	4.29E+05	4.20E+05	4.17E+05	4.22E+05
Off-site mixture use	1.70E+08	1.98E+08	2.09E+08	1.92E+08
Indirect Emission Mitigated (kg CO_2/year)				
Displacement of SMR H_2	2.36E+06	2.79E+06	2.99E+06	2.71E+06
Off-site NG use	1.74E+08	2.08E+08	2.22E+08	2.01E+08
NG use at CCGT	3.34E+07	3.89E+07	4.11E+07	3.78E+07
Net Emission Calculation (kg CO_2/year)				-3.28E+06
Difference from Base Case (kg CO_2/year)				**-4.57E+06**

8.5 Long-Term Scenario: Meeting Large Hydrogen Demand

In this scenario, hydrogen is injected into a natural gas storage reservoir, with a pre-existing amount of natural gas present as cushion gas. No natural gas is injected into the reservoir with hydrogen, and the signals on which reservoir operations is based are the schedule of hydrogen demand and the varying production of hydrogen.

In Figure 2.39 (displaying daily averages), it is seen that the reservoir is subjected to injection most of the time, given that the dispatch (reservoir mode) is mostly above zero. Consequently, the injectability/deliverability of the reservoir is also mostly positive, indicative of high injection potential, but low withdrawal potential.

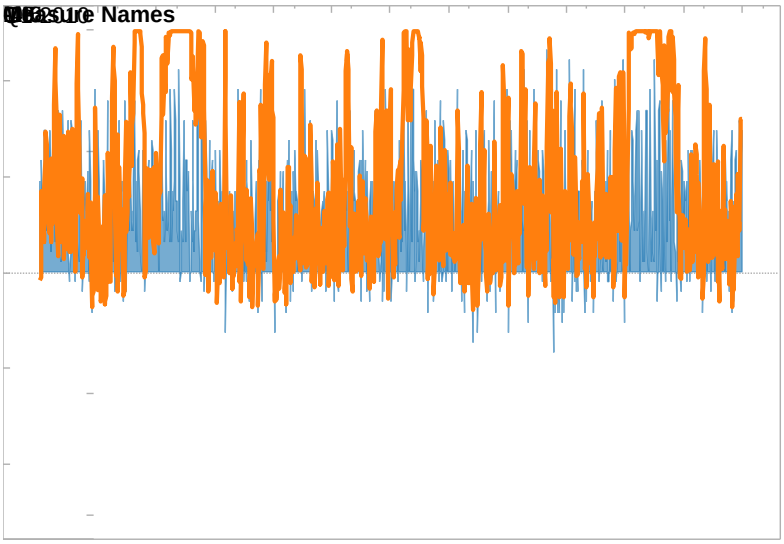

Figure 8.38 Daily average of dispatch to reservoir for the large hydrogen demand scenario

Because only hydrogen is injected into the reservoir in this scenario, and the scale of hydrogen production is moderate (26.1 MW or 242 kmol/h), the actual flow rate for injection is much smaller than the injectability allowed by the reservoir conditions. At the same time, the flow rates withdrawn from the reservoir is largely limited by the deliverability (Figure 2.40).

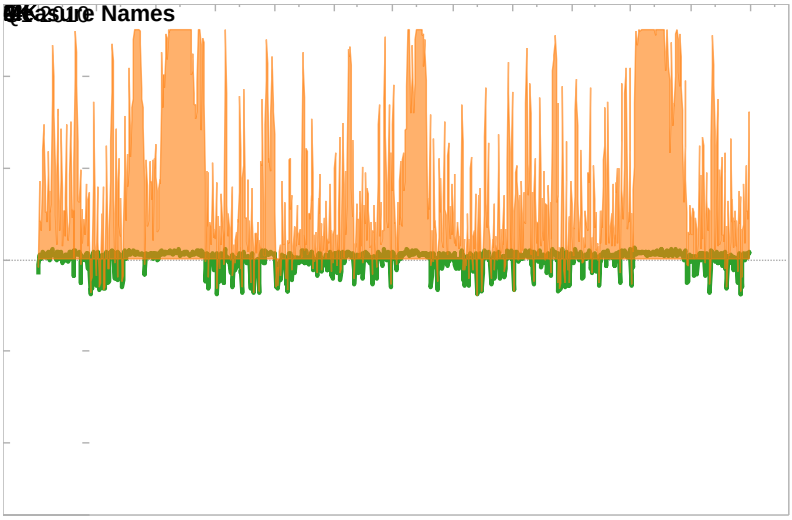

Figure 8.39 Injectability/deliverability and actual reservoir flow rates for the large hydrogen demand scenario

Compared to the previous scenario, the inventory level in this last scenario is also flat, devoid of characteristics of storage cycles. But, it remains in the lower end of the spectrum instead (Figure 2.41). Due to the absence of natural gas injection, the concentration of hydrogen in the stored gas rises much more rapidly than in any of the other scenarios: annual averages are 15%, 38% and 56%, for 2010-2012 respectively (Table 2.17). In this case, the wellhead pressure appears highly volatile and does not exhibit any clear trend over the time scale chosen (Figure 2.41).

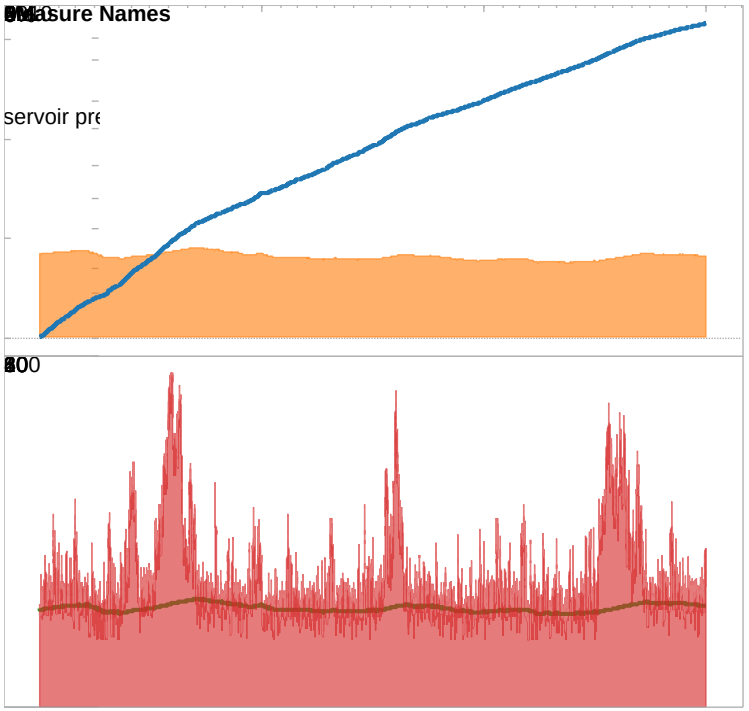

Figure 8.40 Reservoir conditions for the large hydrogen demand scenario

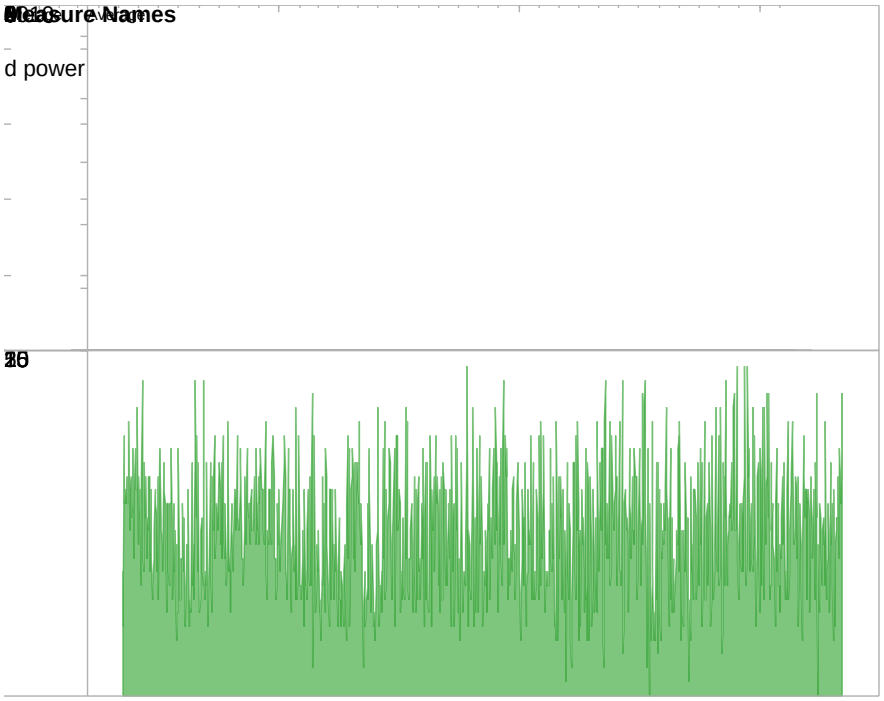

Figure 8.41 Power supply to the electrolyzers in the large hydrogen demand scenario

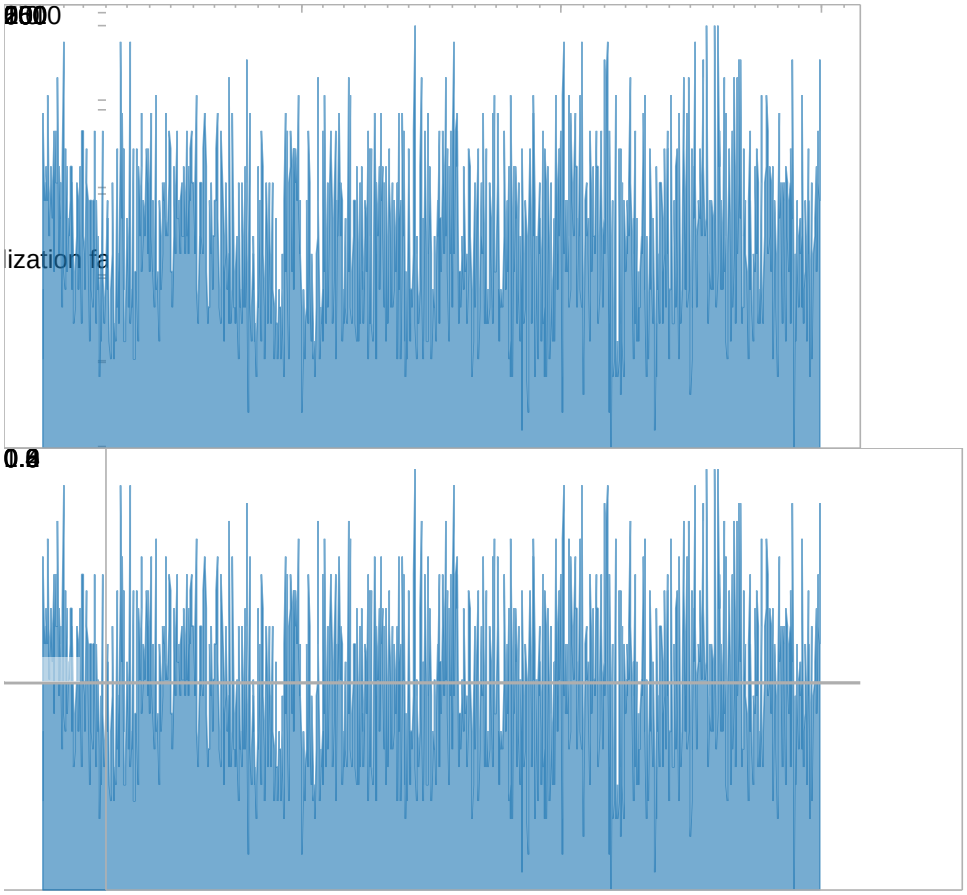

Figure 8.42 Electrolyzer utilization for the large hydrogen demand scenario

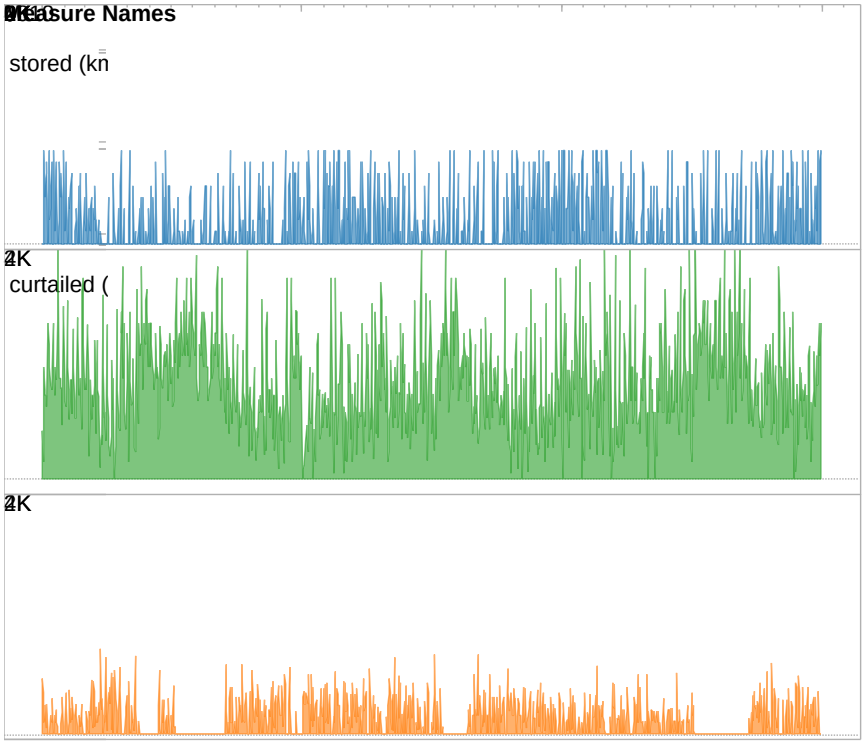

Figure 8.43 Power supply to the electrolyzers in the large hydrogen demand scenario

The key factor differentiating this scenario from the others is the inflexibility of hydrogen demand: in other scenarios, it is assumed that all hydrogen produced that cannot be stored is bought immediately. In this last scenario, this assumption no longer holds. Instead, once hydrogen is produced, it can only be sold to customer if pre-scheduled hydrogen demand is present in the form of a pre-arranged pick-up. If there is no hydrogen demand, and the reservoir cannot accommodate the injection of hydrogen produced, then the amount of hydrogen in question is considered to be lost, or curtailed. Of all the hydrogen produced from the electrolyzer in this scenario, 77% is stored, 10% is curtailed and 13% is delivered to pre-scheduled hydrogen demand.

All of the mixture produced from the reservoir is sent to the separator to recovery pure hydrogen; this flow rate is largely limited by the deliverability of the reservoir (Figure 2.40). The relatively low injection and withdrawal flow rates that alternate lead to a relatively static level of inventory (Figure 2.41).

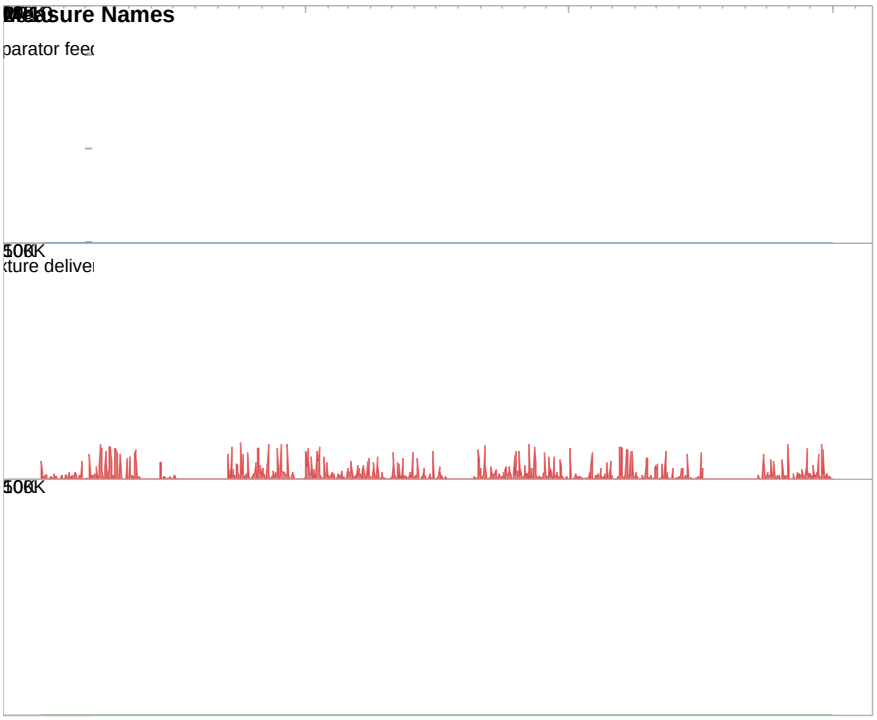

Figure 8.44 Dispatch of the produced mixture for the large hydrogen demand scenario

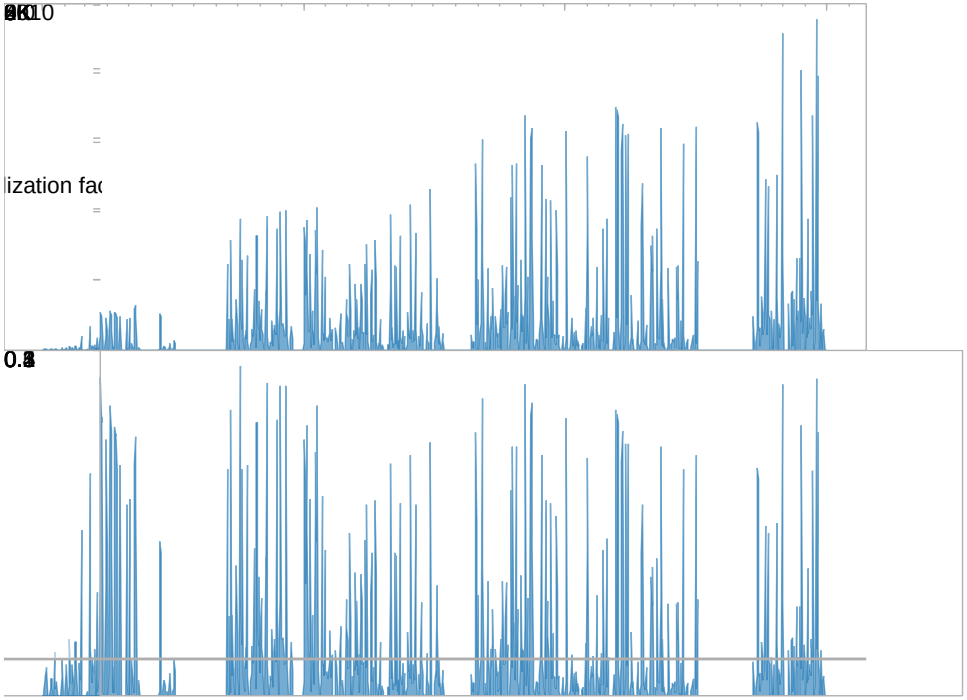

Figure 8.45 Separator utilization for the large hydrogen demand scenario

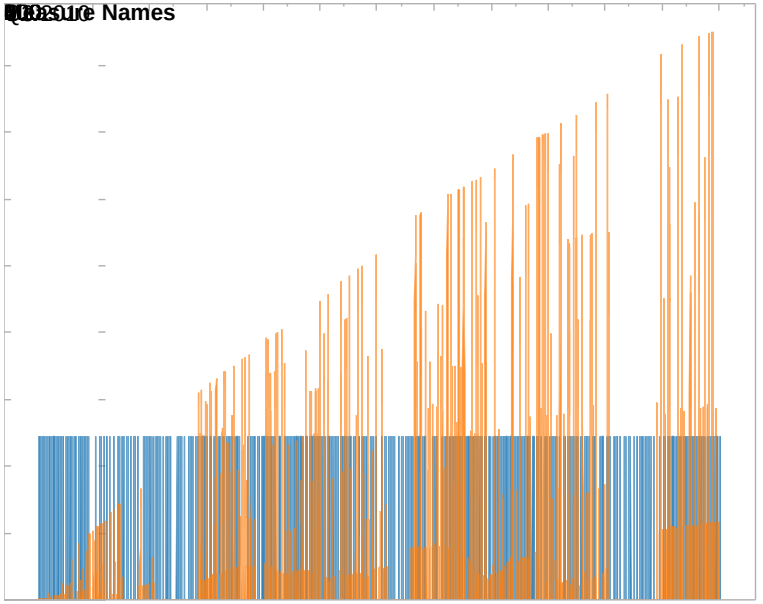

Figure 8.46 Hydrogen delivered to customers for the large hydrogen demand scenario

The limited amount of feed dispatched to the separator leads to an especially low capacity utilization factor: 5% (Figure 2.46). Even during the days with the highest utilization, the daily average capacity utilization factor does not exceed 50%.

Unlike previous scenarios, in which the hydrogen from bypass is the only source of pure hydrogen, this last scenario also allows pure hydrogen to be recovered from a natural gas/hydrogen mixture via the use of the PSA separator. The hourly flow rate of hydrogen that can be recovered through separation gradually increases, because the feed to the separator is becoming richer in hydrogen (Figure 2.47). And, the separator is responsible for supplying most of the hydrogen delivered to customers: about 73%.

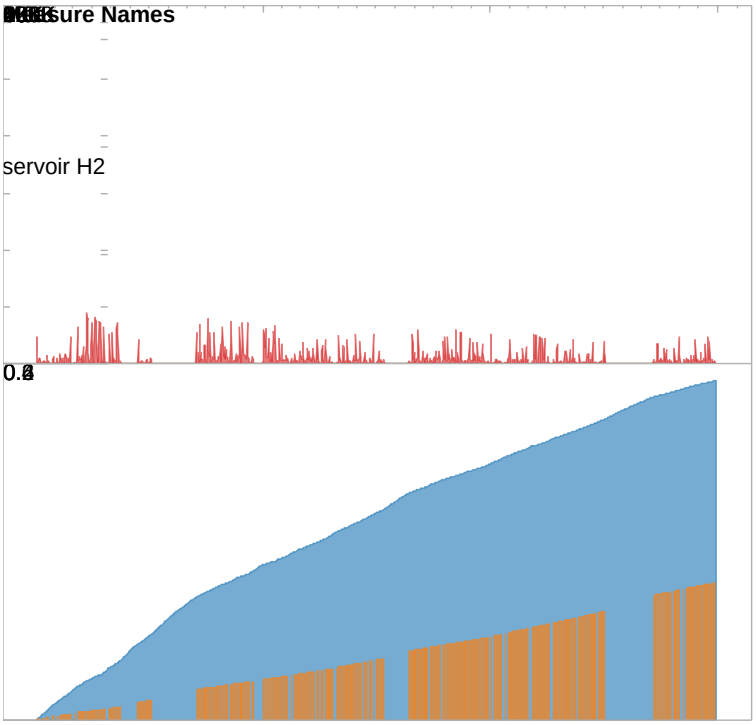

Figure 8.47 Hydrogen concentration of mixture delivered for the large hydrogen demand scenario

It is assumed that the natural gas-rich adsorbate from the separator is marketed as hydrogen-enriched natural gas. Compared to mixture produced directly from storage, the concentration of hydrogen in this stream has been lowered by undergoing separation of hydrogen from natural gas. When reservoir concentration of hydrogen has reached 60%, the concentration of the separator “effluent” is about 20% (Figure 2.48).

The gas in storage inside the reservoir experiences a gradual decline in value over the course of three years. But it occurs at a rate much slower than the decrease in inventory value for the previous scenarios.

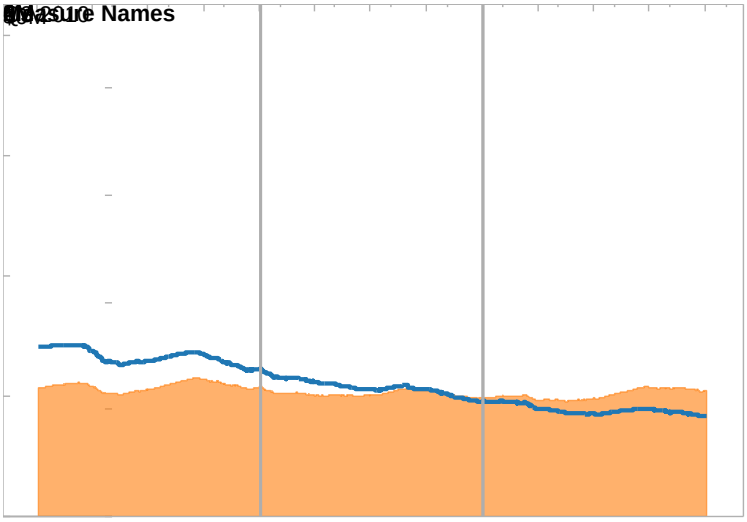

Figure 8.48 Value of inventory for the large hydrogen demand scenario

Table 8.17 Summary of physical performance for the large hydrogen demand scenario

Component	Variable	2010	2011	2012	Average	Unit
D1	Dispatch order to the reservoir	0.26	0.24	0.27	0.26	N/A
Storage reservoir	Inventory	2.4E+06	2.3E+06	2.3E+06	2.3E+06	kmol
	H2 conc.	15%	38%	56%	37%	mol %
	Reservoir pressure	32	31	31	31	bar
	Wellhead pressure	42	35	40	39	bar
	Max. inventory change	1.8E+07	1.1E+07	1.7E+07	1.5E+07	kmol/year
	Actual inventory change	1.2E+04	-2.0E+05	1.3E+05	-2.1E+04	kmol/year
Wind turbines	Wind power produced					MWh/year
	Utilization factor					
D2	Wind power stored					MWh/year
	Wind power sold to grid					MWh/year
	Grid power stored	1.1E+05	1.1E+05	1.2E+05	1.1E+05	MWh/year
Electrolyzers	H2 produced	1.1E+06	1.0E+06	1.1E+06	1.0E+06	kmol/year
	Utilization factor	50%	47%	51%	49%	
D3	H2 stored	8.2E+05	7.0E+05	8.0E+05	7.7E+05	kmol/year
	H2 bypassed	1.4E+05	1.7E+05	1.9E+05	1.6E+05	kmol/year
	H2 curtailed	1.0E+05	1.4E+05	9.3E+04	1.1E+05	kmol/year
D4	NG stored					kmol/year
	H2 conc. of mixture injected	100%	100%	100%	100%	mol %
D5	Feed to separator	8.1E+05	9.0E+05	6.7E+05	7.9E+05	kmol/year
	Mixture delivered					kmol/year
	Fuel to CCGT					kmol/year
CCGT	Power delivered to grid					MWh/year
	Utilization factor					
Separator	H2 delivered	1.0E+05	2.7E+05	3.0E+05	2.2E+05	kmol/year
	Utilization factor	5%	6%	5%	5%	
D6	Revised mixture delivery	7.1E+05	6.2E+05	3.7E+05	5.7E+05	kmol/year
	H2 conc. of mixture delivered	4%	11%	20%	12%	mol %
Compressors	Work required	1.7E+06	2.0E+06	2.3E+06	2.0E+06	kWh/year

Table 8.18 Summary of financial performance for the large hydrogen demand scenario

Financial Performance	2010	2011	2012	Average
Capital Cost Breakdown				
Compressors				$ 5,303,626
Electrolyzers				$ 76,390,578
Gas turbine				$ -
Separator				$ 3,453,446
Wind turbines				$ -
Total Capital Cost				$ 85,147,649
Amortized Capital Cost				**$ 8,672,476**
O&M Cost Breakdown				
Compression cost	$ 74,408	$ 80,746	$ 63,555	$ 72,903
Fixed O&M	$ 346,899	$ 346,899	$ 346,899	$ 346,899
Total O&M Cost	$ 421,307	$ 427,645	$ 410,454	$ 419,802
Purchase Breakdown				
Natural gas from grid	$ -	$ -	$ -	$ -
Power from grid	$ 3,363,093	$ 2,447,365	$ 2,008,734	$ 2,606,397
Total Purchase	$ 3,363,093	$ 2,447,365	$ 2,008,734	$ 2,606,397
Sales Breakdown				
Mixture to grid	$ 2,159,736	$ 1,763,610	$ 652,935	$ 1,525,427
Wind power to grid	$ -	$ -	$ -	$ -
CCGT power to grid	$ -	$ -	$ -	$ -
Hydrogen	$ 2,370,634	$ 4,466,426	$ 4,853,506	$ 3,896,856
Total Sales	$ 4,530,371	$ 6,230,036	$ 5,506,441	$ 5,422,283
Inventory Cost Calculation				
Beginning inventory value	$ 14,112,000	$ 12,233,591	$ 9,531,972	$ 11,959,188
Purchase of material	$ 3,363,093	$ 2,447,365	$ 2,008,734	$ 2,606,397
Cost of total mixture available	$ 17,475,093	$ 14,680,956	$11,540,705	$ 14,565,585
Ending inventory value	$ 12,233,591	$ 9,531,972	$ 8,282,121	$ 10,015,895
Cost of mixture delivered	$ 5,241,502	$ 5,148,985	$ 3,258,584	$ 4,549,690
Inventoried purchase	$ (1,878,409)	$ (2,701,619)	$ (1,249,851)	$ (1,943,293)

Table 8.19 Net annual cash flow for the large hydrogen demand scenario

Annual Cash Flow	2010	2011	2012	Average
1. Capital costs	$ (8,672,476)	$ (8,672,476)	$ (8,672,476)	$ (8,672,476)
2. OM costs	$ (419,802)	$ -	$ -	$ (139,934)
3. Cost of sales	$ (5,241,502)	$ (5,148,985)	$ (3,258,584)	$ (4,549,690)
4. Sales	$ 4,530,371	$ 6,230,036	$ 5,506,441	$ 5,422,283
5. Annual net	$ (9,803,409)	$ (7,591,425)	$ (6,424,619)	**$ (7,939,818)**
Difference from Base Case ($/year)				**$ (3,776,851)**

Table 8.20 Summary of environmental performance for the large hydrogen demand scenario

Environmental Performance	2010	2011	2012	Average
Emission Incurred (kg CO2/year)				
Compression of natural gas	9.81E+05	1.18E+06	1.32E+06	1.16E+06
Grid power generation for H2	1.76E+07	1.17E+07	1.25E+07	1.40E+07
Mixture use at CCGT				
Wind power generation for H2				
Off-site mixture use	3.01E+07	2.45E+07	1.31E+07	2.26E+07
Indirect Emission Mitigated (kg CO2/year)				
Displacement of SMR H2	5.03E+06	9.48E+06	1.03E+07	8.27E+06
Off-site NG use	3.12E+07	2.75E+07	1.64E+07	2.51E+07
NG use at CCGT				
Net Emission Calculation (kg CO2/year)				4.38E+06
Difference from Base Case (kg CO2/year)				**3.09E+06**

8.6 Energy Storage Benchmark Parameters

8.6.1 Roundtrip Efficiency

Because of the definition of the roundtrip efficiency (AC-to-AC), of the three energy storage pathways – Power to Gas, Power to Power and Power to Hydrogen – only roundtrip efficiency of the second pathway can be calculated.

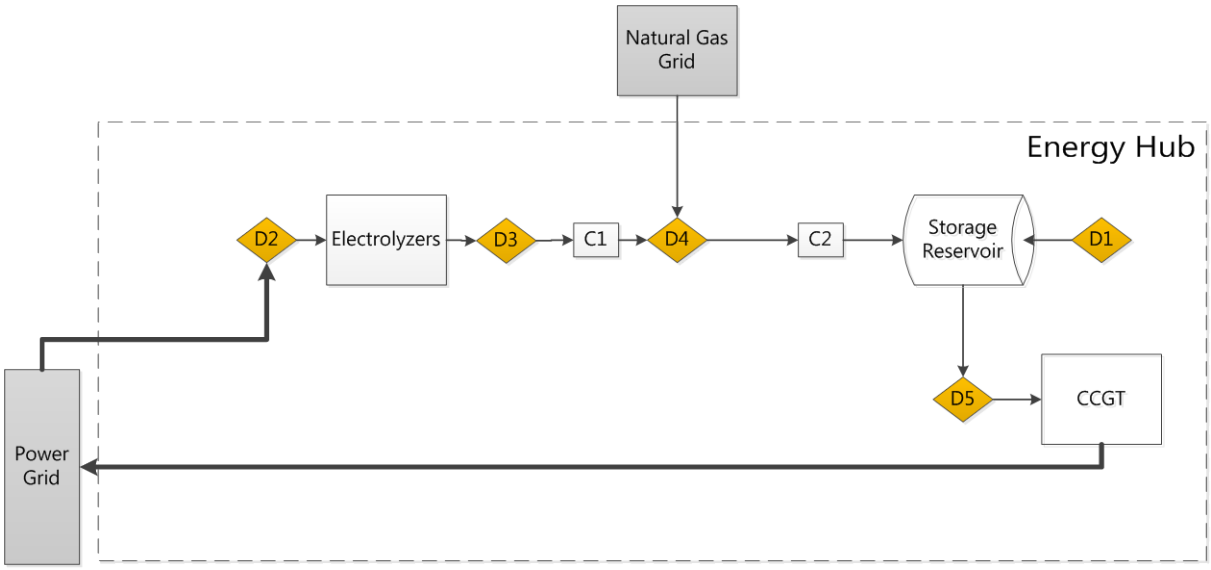

Figure 8.49 The Power to Power pathway for the energy hub

Assuming lossless storage, the overall efficiency or the pathway can be calculated as follows:

$$\eta_{RT} = \eta_{E,rated}\eta_{CC,rated} \tag{1.1}$$

The rated efficiency of the electrolyzer and the combined cycle gas turbine modeled are 73% and 53% respectively. Therefore, the maximum roundtrip efficiency for the UHNG technology is 39%.

8.6.2 Rated Capacity

The rated storage capacity of the UHNG technology is limited by the storage capacity of the underground reservoir. Given a specific reservoir pore volume, which is the result of the local geology, the amount of gas that can be stored varies depending on its temperature, pressure and

composition. It can be derived that the rated storage capacity for underground reservoirs is a function of the reservoir hydrogen concentration.

$$n_{total} = \frac{p_{res} V_{\max}}{zRT_{res}} \; n_{total} = \frac{p_{res} V_{\max}}{zRT_{res}} \tag{1.2}$$

$$n_{H_2,res} = c_{H_2,res} n_{total} \tag{1.3}$$

$$E_{H_2,res} = E_{HHV} n_{H_2,res} \tag{1.4}$$

$$E_{H_2,res} = \frac{c_{H_2,res}}{z} \frac{E_{HHV} p_{res} V_{\max}}{RT_{res}} \tag{1.5}$$

Given the reservoir parameters in Table 4.5 and a reservoir pressure of 105 bar (maximum limit), the possible storage capacity using hydrogen storage ranges from 25,000 MWh (2% hydrogen) to 582,000 MWh (100% hydrogen).

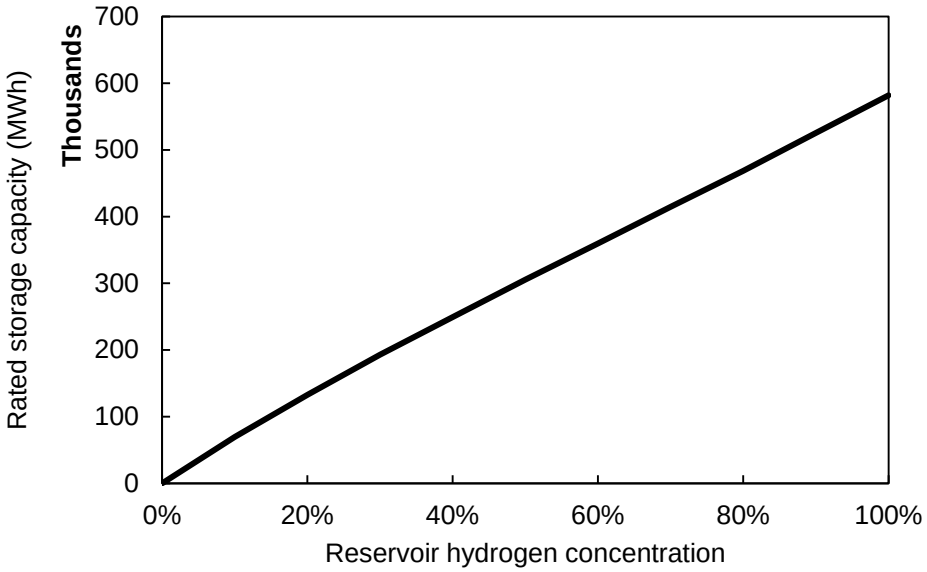

Figure 8.50 Rated storage capacity of UHNG as a function of the reservoir hydrogen concentration

8.6.3 Rated Power

The rated power of the UHNG technology is limited by the component with the lowest power in the energy storage and recovery pathway. The rated power of the components is first examined.

For the storage reservoir, the maximum rate at which it can store or discharge energy in the form of hydrogen is limited by its injectability and deliverability. For the reservoir simulated in this project, the maximum injectability and deliverability are both capped at 5000 kmol/h (Section Injectability and Deliverability). This molar flow rate is then converted into energy units. Analogous to the storage capacity, the rated power is also a function of hydrogen concentration of the mixture being stored or produced. It can vary from 8 MW (2% hydrogen) to 390 MW (100% hydrogen).

$$P_{H_2,\max} = c_{H_2} \dot{n}_{s,\max} E_{HHV} \tag{1.6}$$

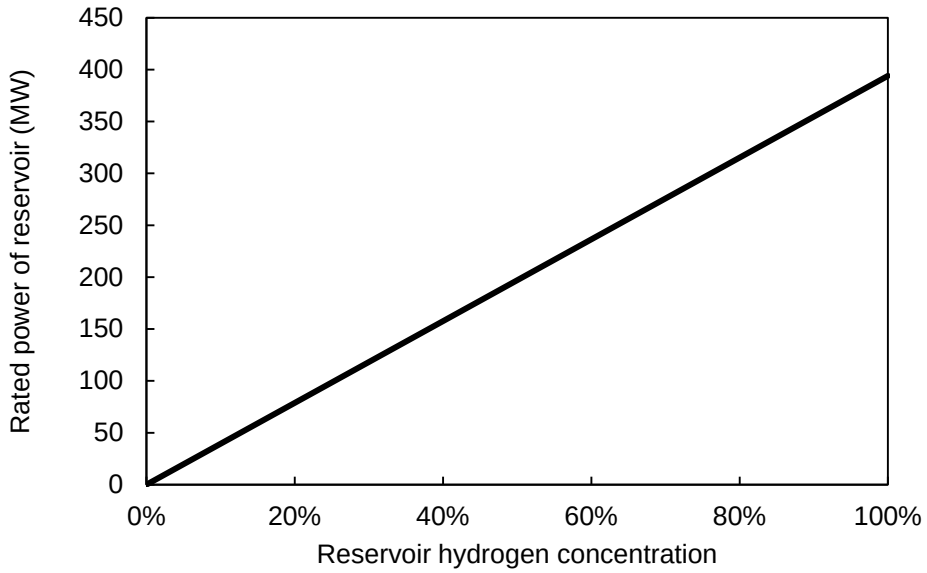

Figure 8.51 Rated power of reservoir for UHNG as a function of the stored/discharged mixture hydrogen concentration

For all other components, the rated power of each component is dependent on decisions made by the energy hub operators with regard to procurement. The rated power of the electrolyzers and the CCGT

plant is already known in terms of electrical energy units (MW). However for the CCGT, only the portion of power that is generated via the combustion of hydrogen is counted; the contribution of the natural gas present in the mixed fuel is not included:

$$\dot{W}_{CC,H_2,rated} = c_{H_2,fuel}\dot{W}_{CC,rated} \tag{1.7}$$

Finally, the rated power of the separator is also found to be a function of the hydrogen concentration of the feed being processed:

$$\dot{n}_{H_2,sep,rated} = c_{H_2,feed}\dot{n}_{feed,rated}\eta_{sep} \tag{1.8}$$

$$\dot{W}_{sep,H_2,rated} = \dot{n}_{H_2,sep,rated}E_{HHV} \tag{1.9}$$

$$\dot{W}_{sep,H_2,rated} = c_{H_2,feed}\left(\dot{n}_{feed,rated}\eta_{sep}E_{HHV}\right) \tag{1.10}$$

From the table below, it can be observed that, for all simulation scenarios studied, the reservoir has always had a rated power that is higher than all other components (8-390MW). In other words, the rated power of the energy hub, in all scenarios, is limited by the scale of electrolyzers, CCGT or separator selected, not by the properties of the chosen reservoir. This applies for all scenarios.

Table 8.21Rated power of energy hub components for all scenarios

Scenario	Pathway	Charging		Discharging	
1. Base Case	N/A				
2. Hydrogen Injection	Power to Gas	Electrolyzers	8.7 MW		
3. SBG Reduction	Power to Power	Electrolyzers	8.7 MW	CCGT	0.8-40 MW*
4. Wind Power Integration	Power to Power	Electrolyzers	8.7 MW	CCGT	0.8-40 MW*
5. Large H_2 Demand	Power to H_2	Electrolyzers	26.1 MW	Separator	2- 107 MW*

*The range of rated power is determined with hydrogen concentration of 2% and 100%.

8.6.4 Self-Discharge rate

In this model of the UHNG technology, it has been assumed that the loss from the storage reservoir is negligible. However, this may need to be re-evaluated in more detailed models.

A list of potential point of losses has been compiled by Carden and Paterson. They conclude that once-only losses, associated with the preparation and abandonment of the storage reservoir, are is more significant than the operating losses (Table 2.22).

The most important once-only loss is the cushion gas that has to remain within the reservoir for the entire lifetime of the energy storage operations. Other once-only losses are the saturation of connate water (water trapped inside the pore volume) by the gas in storage and the diffusion of the stored gas into the ground water surrounding the reservoir. The most important source of operating loss is the pumping loss, which is, as defined by Carden and Paterson, not a loss of stored material but an energy loss (i.e. drop in pressure when gas is produced from the reservoir). Given that the storage capacity of the reservoir selected is 25,000 to 582,000 MWh (variable because of changing hydrogen concentration); the magnitudes corresponding to the percentages provided can be estimated.

Table 8.22 Summary of sources of losses for underground hydrogen storage [108]

Source	% of reservoir capacity	Energy loss (MWh)
Cushion gas	~33	8250– 192,000
Solution via connate water	~2	5000 – 116,400
Diffusion	~2	5000 – 116,400
Pumping	~1 per cycle	2500 – 58,200

8.6.5 Durability

The durability of the UHNG technology, like its rated power, is dependent on the durability of individual components. The durability can be either expressed in terms of years (physical lifetime) or in terms of cycles. Note that only the reservoir is subjected to the storage cycle; all other components only experience charging or discharging. Therefore, the durability (cycles) measure is not applicable to them. The durability of the physical reservoir for UHNG is estimated to be of similar scale as that for CAES, which also involves the use of an underground reservoir.

Table 8.23 Expected lifetime of UHNG technology components [43, 109]

Component	Durability (years)	Durability (cycles)
Reservoir	20-100	30,000 +
Electrolyzer	5-15	N/A
CCGT	30	N/A
Separator	20+ (columns) 10 (adsorbent)	N/A

8.6.6 Cost of Storage

The cost of storage includes only the capital costs for equipment. The total capital costs is then normalized using the storage capacity ($/MWh) or the rated power ($/MW). As Table 2.24 demonstrates, the cost of storage is much lower on a capacity basis (less than $4) than on a power basis (hundreds to tens of thousands of dollars).

Table 8.24 Estimated cost of storage for UHNG based on simulation scenarios

Scenario	Total Capital Costs ($)	Storage capacity (MWh)	Rated Power (MW)		Cost ($/kWh)	Cost ($/kWh)	
			Charging	Discharging		Charging	Discharging
1. Base Case							
2. Hydrogen Injection	29,248,521	25,000-582,000	8.7		0.05-1.2	3362	
3. SBG Reduction	59,193,277	25,000-582,000	8.7	0.8-40	0.10-2.4	6804	1480-73,992
4. Wind Power Integration	81,075,983	25,000-582,000	8.7	0.8-40	0.14-3.2	9319	2027-101,345
5. Large H_2 Demand	85,147,649	25,000-582,000	26.1	2-107	0.15-3.4	3262	796-42,574
OVERALL					**0.05-3.4**	**800-74,000**	

Chapter 9
Results Discussion

In this chapter, the results presented in the previous chapter for each of the five scenarios studied are compared for analysis, so that the impact of various types of decision variables – energy hub configuration, scale and decision point logic – can be evaluated.

9.1 Base Case Scenario Validation

The base case scenario is the scenario in which the configuration of the energy hub and the scale of components do not influence the performance indicators. It is used as the baseline for cross-scenario comparison. Before the comparison of various scenario results, the validity of base case scenario as modeled is assessed by comparing simulation results from the base case scenario to historical data available. More specifically, the reservoir inventory for the base case scenario is compared to the historical inventory level for natural gas storage in Eastern United States (weekly data published by the EIA, [110]). An energy hub model which has captured the key characteristics of existing UGS facility operations is expected to generate inventory profile that is similar to the historical one.

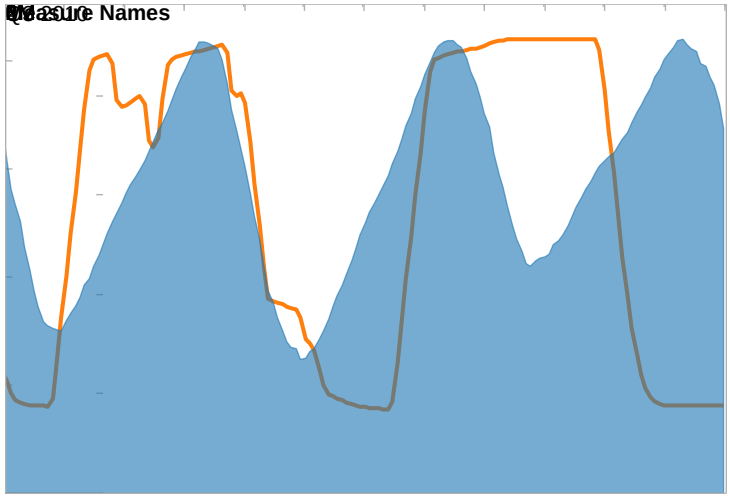

Figure 9.1 Comparison of simulated and actual 2010-2012 inventory level for UGS facilities

Figure 9.1shows that the simulated base case partially conforms to the historical trend of storage levels. The key similarities and discrepancies are described below:

1. Both set of data exhibit long-term storage cycles: the period for the simulated base case is 7 quarters (21 months), while the period of the historical inventory level is shorter at 4 quarters (12 months);
2. The rate at which the simulated reservoir is charged and discharged is equal (symmetrical injectability and deliverability is assumed, reservoir is filled/emptied in the same amount of time), while the injection rate and withdrawal rate for the historical data set is unequal, lending to its tilted shape (the charging rate is slower than the discharging rate, the time it takes to fill the reservoir is longer). Also, at the end of 2012, the injection rate is visibly different from the two previous years;
3. The inventory of the simulated reservoir always oscillates between the reservoir capacity maximum and minimum, while the historical inventory shows variable minimum inventory, i.e. the gas in storage at the end of the heating (producing) season changes from year to year.

It is understood that the key driving force for natural gas storage is the seasonal variation in natural gas demand. In the base case scenario, at decision point D1, it has been assumed that the price of natural gas can be used as a proxy indicating the level of demand. Therefore, the market price of natural gas is used as the main signal that triggers different reservoir operating modes. It is therefore expected that the reservoir inventory is correlated to the variation in natural gas demand and to the price of natural gas. This expectation is verified by scatter plots of simulated and historical inventory levels with respect to demand variation and to price.

The correlation coefficients for the four plots displayed in Figure 9.2 indicate that the historical inventory level is highly correlated to change in natural gas demand ($R = 0.82$), whereas the simulated reservoir inventory is more highly correlated to the price of natural gas ($R = 0.45$). This finding suggests that when simulating UGS operations as they have been conducted in the recent past (2010-2012). A more realistic model logic should be based on the changes in demand for natural gas, instead of being based on the price of natural gas.

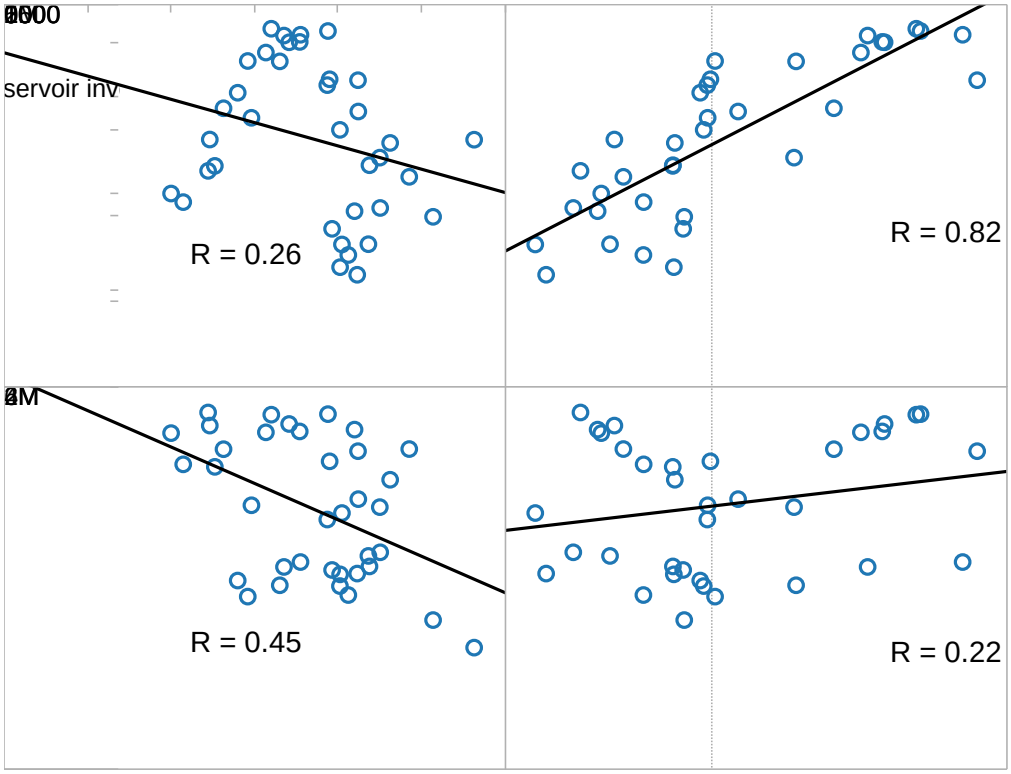

Figure 9.2 Correlation of simulated and historical gas storage inventory with respect to A) natural gas price and B) variation in natural gas demand

Given the constraint for time, the simulated base case is presented and discussed as shown, without further adjustment of the decision point model logic for better fitting with the historical trend. But, the discrepancies outlined above are basis over which the model logic for the base case scenario can be improved upon, for future simulation trials using the same modeling framework.

9.2 Effect of Decision Variables on Financial Performance Indicators

In this section, the financial performance indicators of all scenarios are compared to the performance of the base case scenario, and the key differences are explored and discussed. It is important to remember that, given the limited opportunity for model validation, the comparison presented below is only meant as sketches of actual possibilities.

9.2.1 Financial Performance Baseline

To begin, it has been found that, the UGS facility at the heart of the UHNG technology, operated as specified in the base case scenario, leads to an average annual loss of more than $1,400,000. This loss is mainly caused by the imbalanced cost of sales and revenues from the sales (Figure 9.3). In other words, the natural gas that is stored, on average, costs more than the price at which they are later sold. Given that the sales of stored natural gas is the only source of revenue for the base case scenario, it is impossible to have a positive cash flow, if the revenues from natural gas sales are not enough to cover the cost of the stored gas.

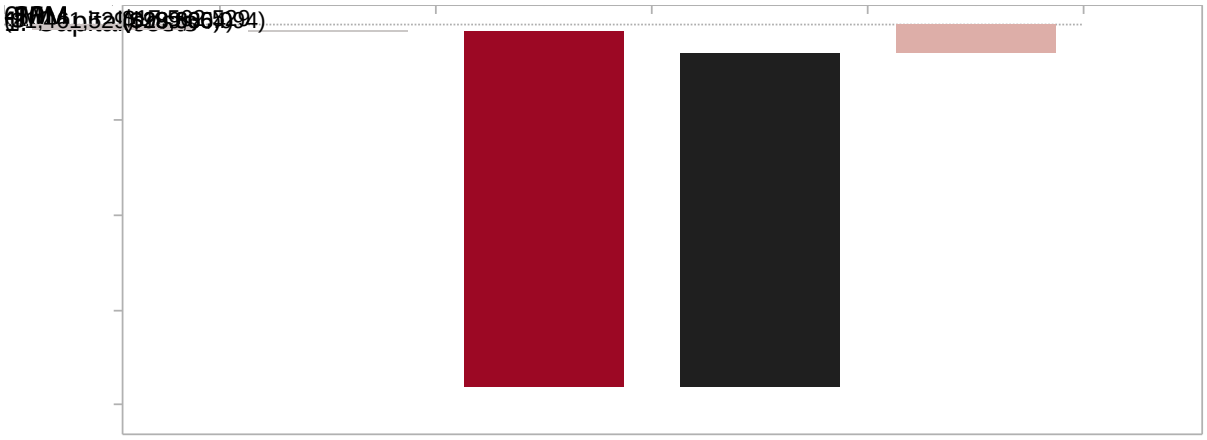

Figure 9.3 Waterfall chart for the expected annual cash flow of the base case scenario

The cause of this cost imbalance is traced to the overall downward trend in the price of natural gas, over the period simulated (2010-2012). The profitability of UGS operations is reliant upon the inter-

seasonal difference in natural gas price, expected because of the seasonal changes in demand. But, as Figure 9.4 shows, the seasonal term changes expected are suppressed by the larger market force depressing the price of natural gas over the course of several years, starting from late 2008.

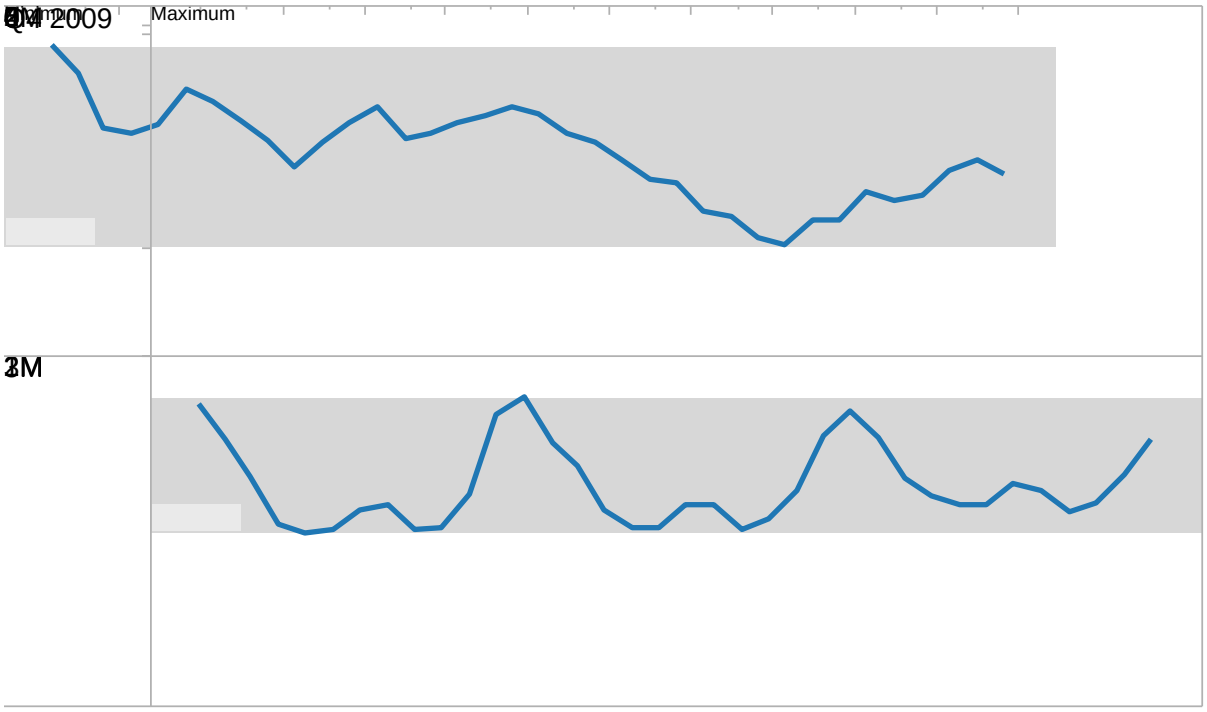

Figure 9.4 Seasonal and annual trend in natural gas price and demand for 2010-2012

The inter-year trend in the price of natural gas is found to be a key factor influencing the operating profits of UGS facilities. The current approach involves determining project value based on average annual cash flow from a much shorter simulation period. This rests upon the underlying assumption that identical cash flow pattern can be expected for all future years of operation. This is an untenable position if the price of natural gas were to change significantly beyond the period of simulation. Therefore, when evaluating such a facility over its physical lifetime spanning more than 20 years, it would be preferable to forecast the long-term price of natural gas over the course of its lifetime, and to extend the period simulation to be identical to the expected lifetime of the project. For the same reason, it is decided to not calculate the net present value of the energy hub using the short-term

average cash flow, because it is not representative of the long-term average annual cash flow which is used in NPV calculations.

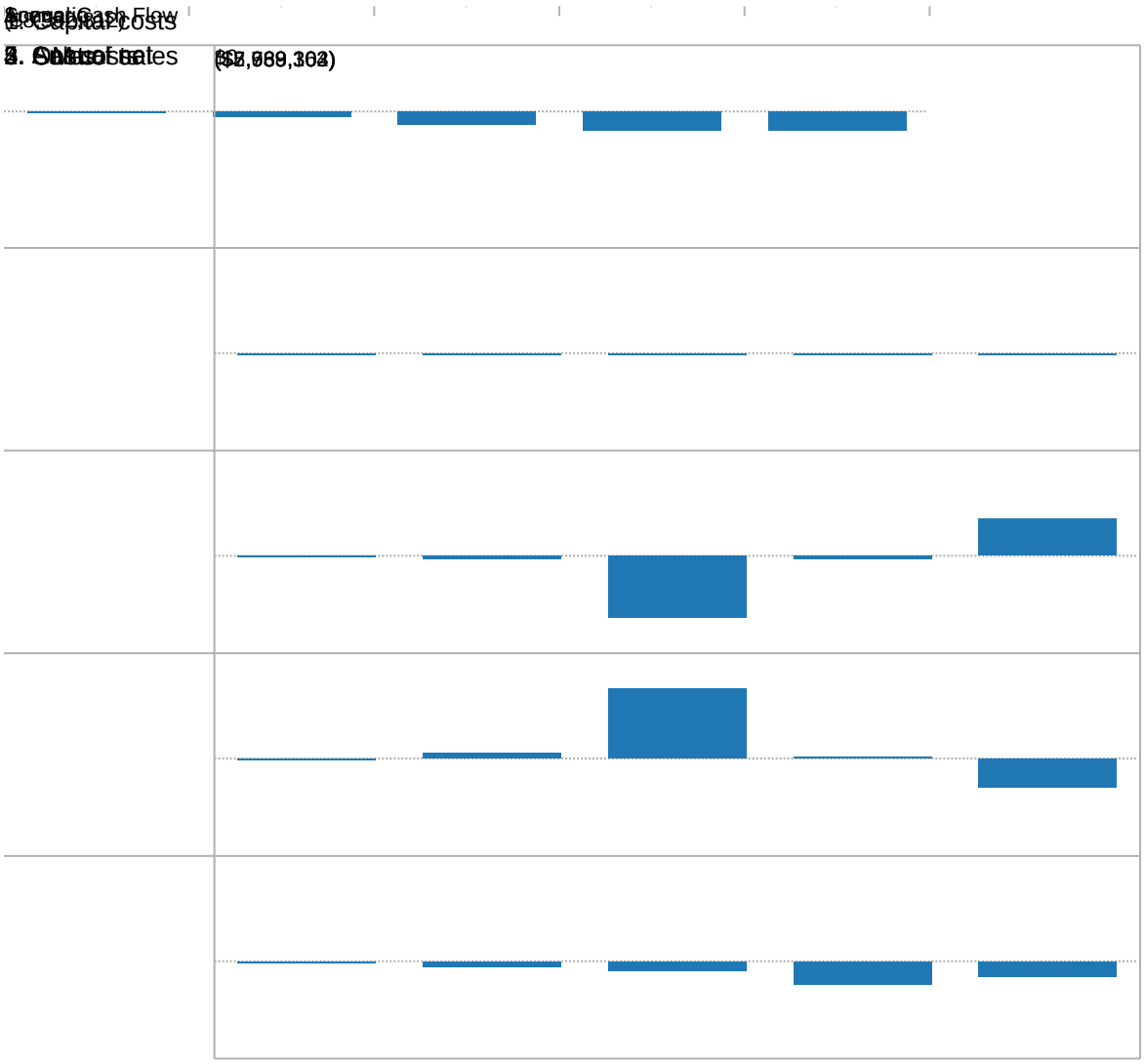

Figure 9.5 Comparison of financial performance of all scenarios, all values are displayed relative to the base case value

Compared to the base case scenario, the expected net cash flow of all future scenarios decreased further (Figure 9.5). Here, all costs items (1,2, and 3) are shown as negative values, so that the annual net cash flow is the sum of all five items.

Because, other than the change in capital cost, the differences between scenarios are mainly driven by the changes in the operating profits, the sales and cost of sales are further broken down to be compared (Figure 9.6).

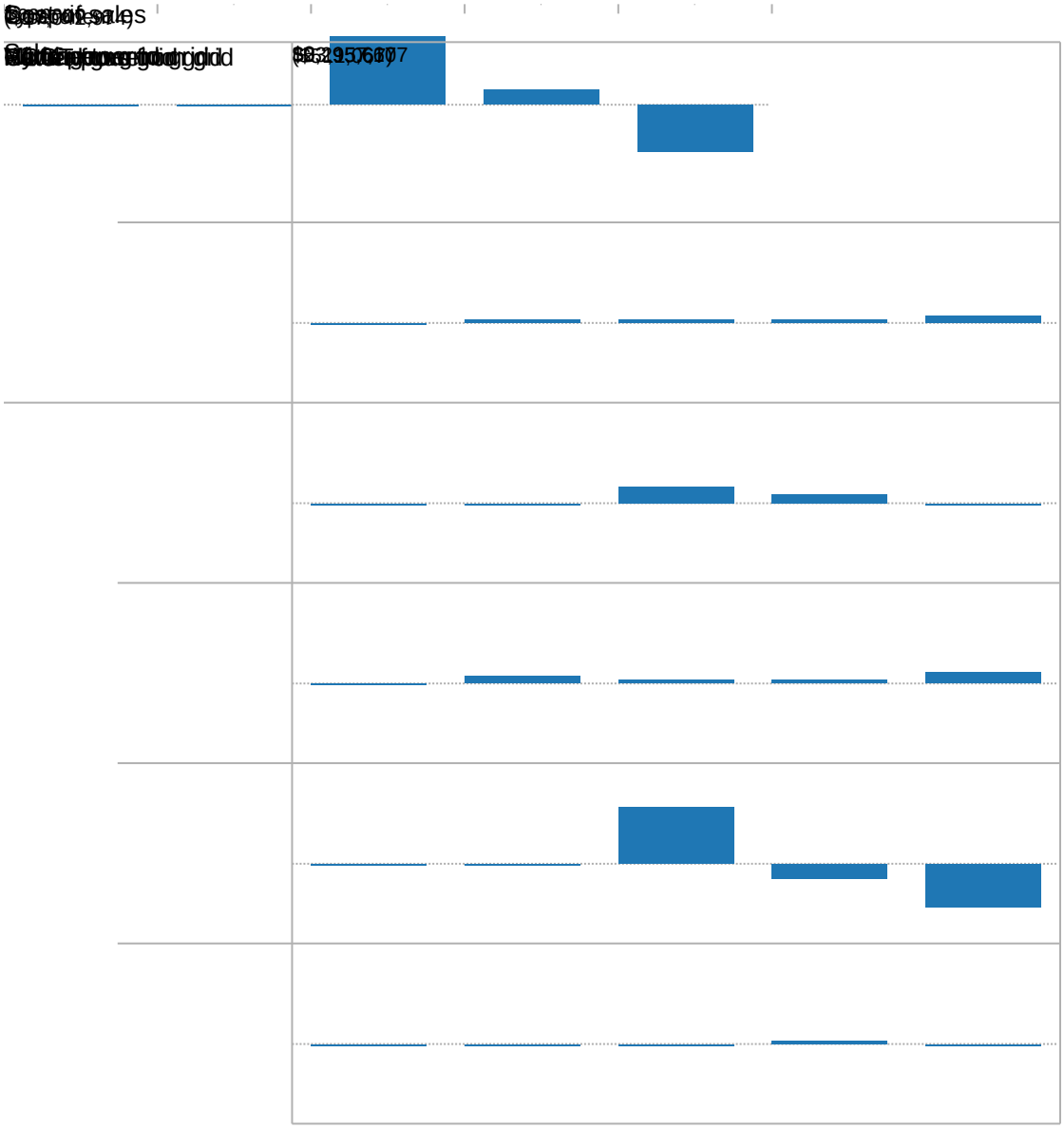

Figure 9.6 Comparison of operating profits for all scenarios, all values are displayed relative to the base case value

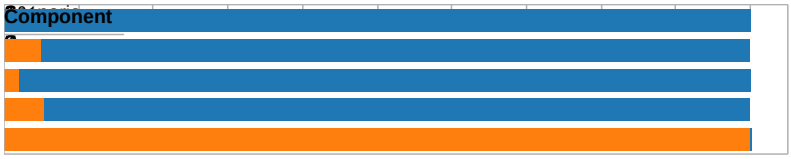

Figure 9.7 Shares of purchase by components for all scenarios

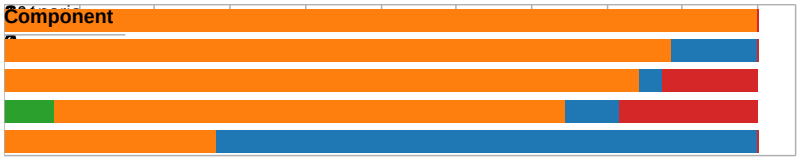

Figure 9.8 Shares of sales by components for all scenarios

9.2.2 On Hydrogen Injection

In scenario 2, the additional loss is almost completely attributable to the additional capital cost requirement: the purchase of the electrolyzer units. There has been a modest increase in operating profits (Δ Sales +Δ Cost of sales = $124,515), but it barely covers the increase from annual O&M costs. This increase is mostly from the sales of bypassed hydrogen: the hydrogen that is not stored, but sold directly to meet local demand.

Because the largest share of revenues for scenario is from the sales of hydrogen-enriched natural gas (Figure 9.8), the most likely course of action to increase revenues to break even with expenses is to increase the price of mixture sold. Given that the average amount of mixture delivered per year is 5.9×10^{6} 5.9×10^{6} kmol and the average concentration of hydrogen in the reservoir is 2% (0.75MMBtu/kmol), the annual output of mixture in terms of energy is 4.4×10^{6} MMBtu (Table 8.5). Supposing everything else remaining equal (same configuration, scale and decision point logic), to cover the additional cost incurred by the electrolyzer, the increase in price per MMBtu delivered need to be $0.60, 16% of the 2010-2012 natural gas price average of $3.77.

If the price of mixture delivered cannot be increased, then another option to increase the operating profit to offset the cost of the electrolyzers is to increase the quantity of hydrogen directly delivered to meet local demand. However, the assumption that the all hydrogen not stored can be absorbed by local demand at the moment of its production may no longer hold true as the quantity that needs to be absorbed increases.

9.2.3 On SBG Reduction

In scenario 3, the volume of sales and its corresponding cost have both increased significantly. This large change in throughput of the energy storage reservoir is caused by the change in the reservoir dispatch model logic at decision point D1, reducing the period of a storage cycle from 21 months (base case) to six months (Figure 8.19), mirroring the peak and off-peak periods for power. This decrease in periods of storage cycles is also associated with a heightened throughput through the reservoir. Such a change can be realized practically only if the downstream gas distribution system can accommodate the increased throughput.

Furthermore, the change in operating profit is positive (Δ Sales +Δ Cost of sales = $2,205,298). It partially offsets the additional cost of capital (electrolyzers and CCGT), but not completely. The sales of pure hydrogen and power generated by the on-site CCGT have both contributed to this increase in operating profit. It is believed that, increasing the utilization factor of the electrolyzer and of the CCGT should further increase the operating profit. More of the capital cost incurred will be offset, for the profit margin for hydrogen delivery and power delivery is higher than for mixture delivery ($44/MMBtu H_2 and $4.4/MMBtu mixture versus $3.77/MMBtu mixture, respectively). But, the capacity utilization factors are limited by the decision points specified for this scenario: the electrolyzers, responsible for producing hydrogen to charge the reservoir, is only run when demand is low (D2), and, the CCGT, responsible for discharging the reservoir by producing electricity, is only run when demand is high (D5). It is assumed that the reservoir cannot charge and discharge at the same time, therefore the utilization factor of each of those components cannot exceed 50%. Unless the revenues from the sales of hydrogen-enriched natural gas can be increased, an operating loss seems inevitable because of the high capital cost required by the electrolyzers and the CCGT.

At its current scale of energy storage and release, the effect of the energy hub on short-term SGB is minimal. It is possible for the storage reservoir to accommodate all of the surplus energy available shown in Figure 9.9 (~370,800 MWh for 10 days), for its rated storage capacity is 25,000 to 582,000 MWh. However, the majority of SBG is available for short periods, with power ranging from hundreds to thousands of MW. The rate at which energy can be stored delivered by the energy hub varies between 3-8 MW and 30-40 MW, respectively (Figure 8.20 and Figure 8.25), much too low to absorb any sizeable portion of the SBG immediately during time of needs.

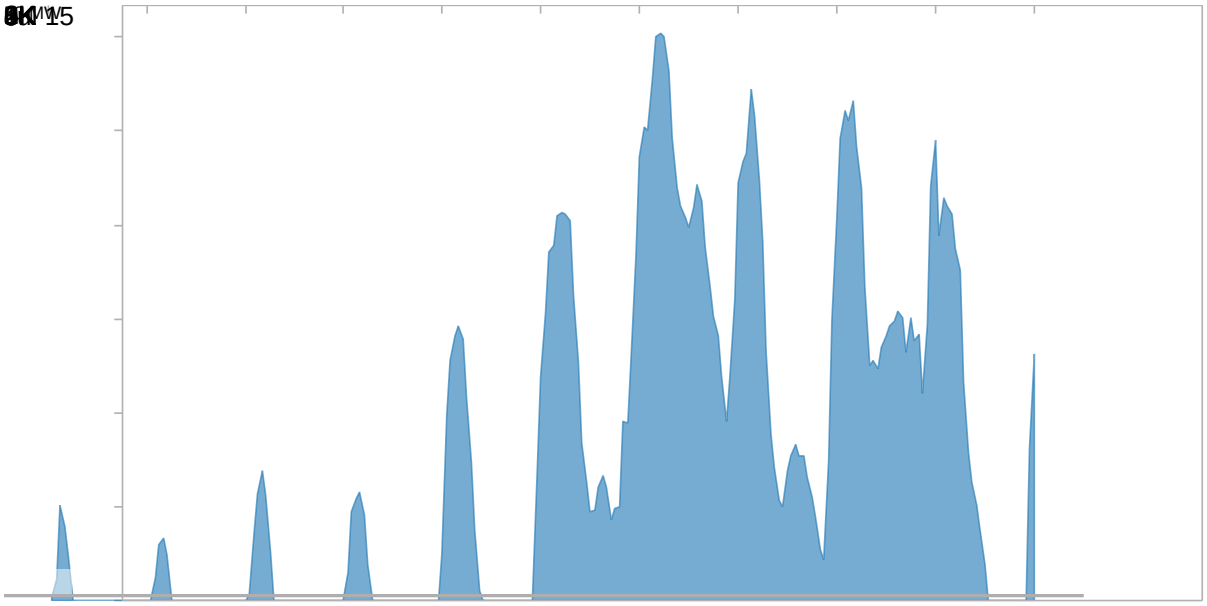

Figure 9.9 Forecast surplus baseload generation report for July 2013 from the IESO

9.2.4 On Wind Power Integration

In scenario 4 the change in operating profit is negative by much (Δ Sales +Δ Cost of sales = -$1,552,559), so that the annual loss is even higher than the additional capital investment required. By examining Figure 9.6, it is found that although the cost of natural gas purchased from the gas grid increased, the sales of mixture to the grid decreased. This is believed to be caused by the overall increase in inventory level occurring in this scenario (Figure 8.29), which is in turn cause by the short duration of the withdrawal window. The FIT schedule with time differentiation as defined by the

Ontario Power Authority is used as the signal on which reservoir operations are based (D1): the off-peak hours (128 hours in a week), which incent energy storage, by far outnumber the peak hours (40 hours in a week), which incent energy production.

This scenario is very capital-intensive, since on-site wind turbines are included as part of the energy hub. It appears that the inclusion of wind turbine did not improve the net cash flow of the energy hub. Actually, in terms of operating profit, the direct sales of wind power is the most profitable when compared to all other options: recovering wind power as bypassed hydrogen, recovering wind power as power generated by the CCGT, or recovering wind power as energy contained in the hydrogen/natural gas mixture (Table 9.1). Therefore, unless special consideration is given to these other pathways, for example: special premium prices are provided for hydrogen produced using wind power or CCGT power partially fuelled by hydrogen produced from wind power, there is no financial incentive for the energy hub operators to store wind power during off-peak hours. Selling all wind power disregarding its time of production seems to be the most profitable use of wind turbines.

9.2.5 On Large Hydrogen Demand

In scenario 5, in contrast with scenario 3, in which the volumes of sales and cost of sales both increased, the two indicators decreased. This is because the scale of injection and withdrawal occurring is much smaller, since only hydrogen is injected and the mixture is only dispatched to the separator so that hydrogen can be recovered in its pure form. The resulting change in operating profit is positive, (Δ Sales +Δ Cost of sales = $1,945,157) mostly from the increased sales of pure hydrogen.

However, this increase is not enough to offset the increase in capital cost required by the electrolyzers scaled up for this scenario. For this particular scenario, the rated capacity of the electrolyzer has been increased (26.1 MW as opposed to 8.7 MW for all previous cases), which increased the capital cost significantly. On the other hand, the separator, although underutilized (Figure 2.45) has relatively low capital cost (4% of total capital cost).

In three years, the concentration of hydrogen in the reservoir increased steadily to reach 60%. If the operations were to be maintained, in 2-3 more years, the hydrogen concentration will reach levels above 90%. As the hydrogen concentration increases, the output of hydrogen by the separator also

increases (Figure 8.46). It might be necessary to adjust the mixture withdrawn for separation if the hydrogen demand cannot accommodate this increase.

Table 9.1 Comparison of average profit per energy unit recovered for different storage pathways

Input	Value	Unit	$/unit	Conversion required	Efficiency	Output		Unit	$/unit	Profit per unit
Wind power	1	MWh	0	NO	100%	Wind Power	1.00	MWh	115	115.00
Wind power	1	MWh	0	Electrolyzer	70%	Bypassed H2	17.77	kg H2	5	88.83
Grid power	1	MWh	30	Electrolyzer	70%	Bypassed H2	17.77	kg H2	5	58.83
Grid power	1	MWh	30	Electrolyzer + separator	56%	Separated H2	14.21	kg H2	5	41.07
Wind power	1	MWh	0	Electrolyzer + CCGT	35%	CCGT Power	0.35	MWh	30	10.50
Wind power	1	MWh	0	Electrolyzer	70%	Mixture	2.39	MMBtu	3.7	8.84
Natural gas	1	MMBtu	3.7	CCGT	50%	CCGT Power	0.15	MWh	30	0.69
Natural gas	1	MMBtu	3.7	NO	100%	Mixture	1.00	MMBtu	3.7	0.00
Grid power	1	MWh	30	Electrolyzer + CCGT	35%	CCGT Power	0.35	MWh	30	-19.50
Grid power	1	MWh	30	Electrolyzer	70%	Mixture	2.39	MMBtu	3.7	-21.16

Conversion factors: 1 MWh = 3.413 MMBtu, 1 MWh = 25.38 kg H_2 (based on HHV), 1 MMBtu = 0.29 MWh

9.3 Effect of Decision Variables on Environmental Performance Indicators

Analogous to the financial performance, the emission indicators derived from all five scenarios are compared, using the base case scenario as the base line.

Given that in the base case, no hydrogen is produced or stored, the so-called mixture produced from the reservoir is actually pure natural gas. Therefore, it matches the expected emissions from off-site use of natural gas by end-users. In other words, there is no emission mitigated by using hydrogen-free natural gas delivered by the energy hub. Then, the net emission from the energy hub is positive and equivalent to the emissions from compressors used for gas injection.

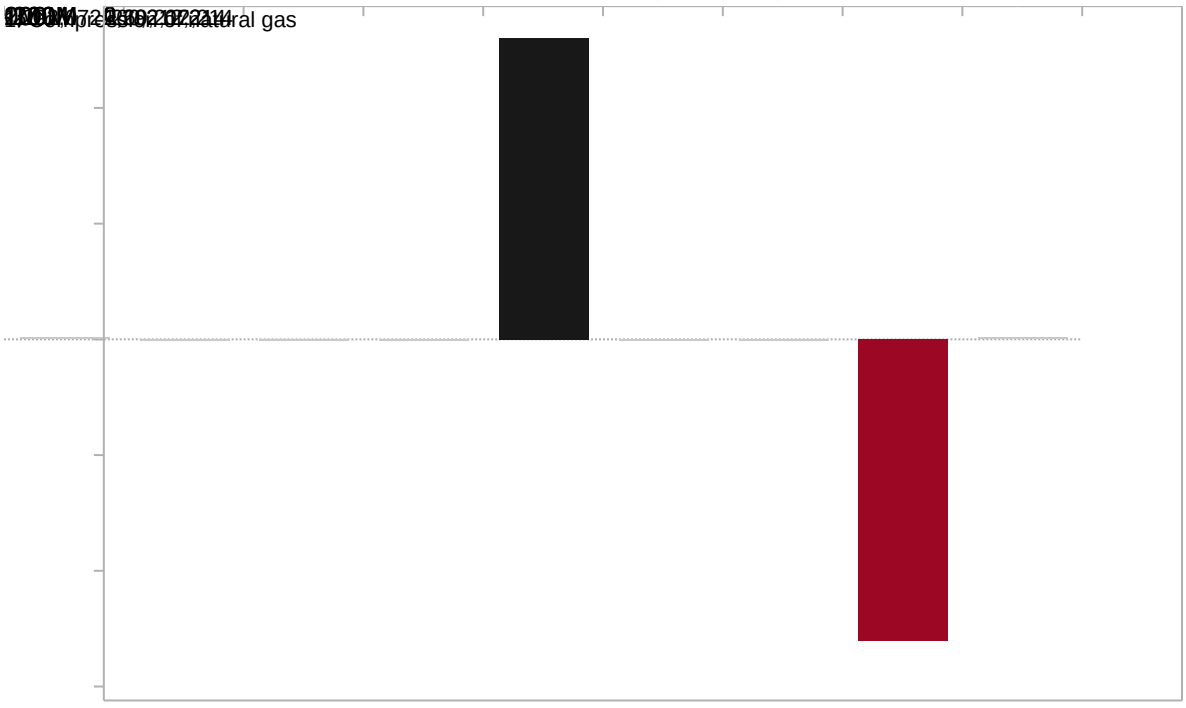

Figure 9.10 Waterfall chart for the expected annual emission of the base case scenario

The four other scenarios are all compared to the emission profile of the base case, the amount of emissions incurred by the energy hub and potential emissions mitigated varied widely from one

scenario to another. However, their relative difference, the net emission, remained relatively constant for scenarios 2, 3, and 4: net reductions in emission in the order of 5000 tons per year are observed. Only scenario 5 deviates from this trend: a net increase in of 3000 tons per year is observed (Figure 9.11).

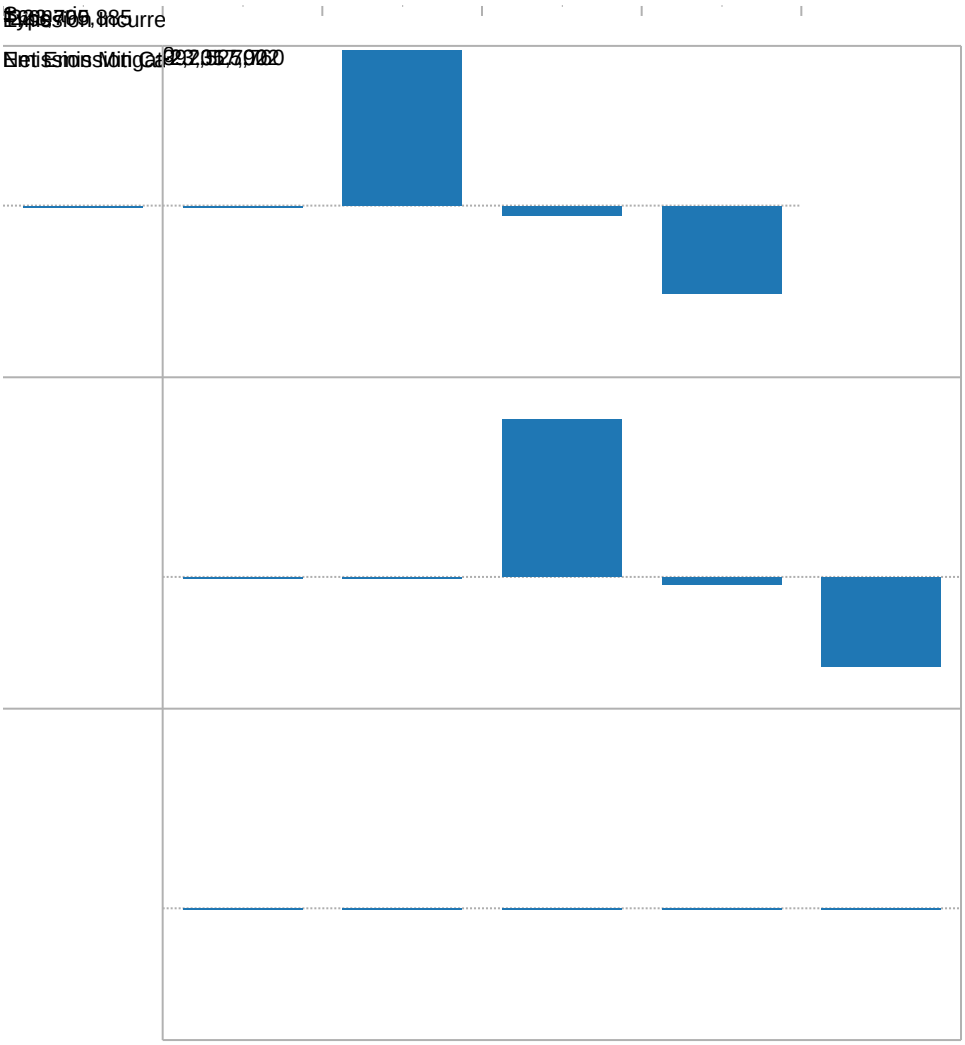

Figure 9.11 Comparison of environmental performance of all scenarios, all values are displayed relative to the base case value

Although the production and storage of hydrogen reduces potential carbon dioxide emission in most application scenarios, it is found that when the production of hydrogen becomes important and consumes a relatively important amount of energy from the grid, there is an increase in net emission.

Given the current supply mix in Ontario, the amount of carbon dioxide emitted by grid-connected generators exceeds the potential savings from the displacement of hydrogen produced via SMR.

Chapter 10
Conclusion

Within the scope of this project, the composite technology of underground storage of hydrogen with natural gas (UHNG) is proposed and studied using a scenario-based modeling approach. The work completed to achieve the six research objectives is summarized and presented below. Then, additional research than can be completed to improve the existing body of work is also suggested.

10.1 Key Decision Variables

Through the formulation of the model of the energy hub, a physical facility embodying the principle of UHNG, where electric power, natural gas and hydrogen can be conditioned and inter-converted, three types of key decision variables have been identified:

1. Variables which describe the configuration of energy hub components;
2. Variables which describe the rated capacity of energy hub component; and,
3. Model logics which describe the relationships between exogenous and endogenous process variables, and the relationship between endogenous process variables.

The first type of variables is binary, indicating the inclusion or exclusion of a given component in the design of the energy hub. The technological components which can be designated ON/OFF are the electrolyzers, the CCGT, the separator and the on-site wind turbines. The storage reservoir is a component by default and should not be excluded. The second type of variables is quantitative, defining the rated input/output of a given component which is included in the design of the energy hub. The range of values that these two types of variables can take on can be found in Table 3.1 List of system configuration and capacity variables.

At six locations within the energy hub model, additional relationships between process variables are required to completely specify the system of equations that is the model. They are named decision points and the variables that they need to relate are shown in Table 3.2 List of decision point inputs and outputs.

Other than the three types of decision variables outlined above, another category of variables is found to exert great influence over the simulation. They are simplified representations of the external environment with which the energy hub interacts with: the exogenous environmental variables. They are different from the decision variables in that they cannot be manipulated by the modeler to alter simulation outcome. Examples include that market price of electricity, the market price of natural gas, the hourly demand for power in Ontario, etc. The complete list is shown in Table 3.3 List of exogenous environmental variables.

10.2 Physical Constraints

Three types of constraints have been identified as the most important to model the physical components of the energy hub: the constraints relating physical output to input, the constraints limiting the maximum/minimum allowable input or output, and the constraints limiting the difference between consecutive input/output points. Due to differences in availability of information and level of complexity, for the six types of components available, the level of detail at which each type of constraint is captured differs. In the table below, the constraints of every component are briefly described, and major assumptions or simplifications are stated.

Table 10.1 Summary of physical constraints used for component models

Components	Constraints on input/output relationship	Constraints on min/max allowable input/output	Constraints on difference in consecutive input/output
Storage reservoir	Basic mass balance and many simplifying assumptions: negligible loss from storage, no water influx, constant volume reservoir, CSTR type mixing.	Calculated assuming that the empirical backpressure equation constants are applicable to production and injection, and that injectability /deliverability is independent of H_2 concentration.	Assumed rate of change of wellhead pressure is 1 bar/hour; Assume rate of change of average reservoir pressure (and associated pressure profile) negligible.
Wind turbines	Power curve from manufacturer specifications.	Modular system, rated power depending on number of units.	Estimated to be negligible at hourly timescale.
Electrolyzers	Efficiency rating from manufacturer specifications.	Modular system, rated power depending on number of units.	Estimated to be negligible at hourly timescale.
CCGT	Calculated from first principles, with some simplification (cold-air standard analysis, 100% combustion efficiency) and use of empirical relationships to relate efficiency of gas turbine cycle to combined cycle efficiency.	Assumed that the same design (same rated efficiency) can be scaled-up or down.	Simplified to be negligible at hourly timescale while it is known that start-up time from standby state requires a few hours.
Separator	Assumed based on values from separation experiments/simulations with much higher concentration of H_2 in feed.	Range obtained from manufacturer specifications.	Assumed to be negligible at hourly timescale.
Compressors	Calculated from first principles + use of empirical efficiency, neglected intercooling required.	No constraint set, units sized based on maximum power requirement.	Estimated to be negligible at hourly timescale.

10.3 Benchmark Parameters

The following benchmark parameters have been evaluated based on the physical model established. They are first estimates which can be used in the comparison of the UHNG concept against other alternatives for energy storage. The summary of Section 8.6 Energy Storage Benchmark Parameters is below:

Table 10.2 List of energy storage benchmark parameters for UHNG concept

Parameter	Value
Roundtrip efficiency	39%
Rated capacity	25,000 MWh (2% H_2) to 582,000 MWh (100% H_2), reservoir specific
Rated power*	Charging: 8.7-26.1 MW; Discharging: 0.8-107 MW
Self-discharge rate	1% per cycle (energy, not material loss)
Durability	20 years, provided that electrolyzers are replaced
Cost of storage	0.05-3.4 $/kWh; 800-74,000 $/kW

*These values are not the only range of rated power allowed; they are the range of rated power evaluated in the project, and can be increased/decreased.

10.4 Performance Indicators

Three types of performance indicators have been identified: physical, financial and environmental. The financial and environmental indicators are derived from the physical performance indicators available. Therefore, the scope of the physical model and its outputs, the physical performance indicators, limit the scope of financial and environmental analysis that can be conducted. The most important physical performance indicators used in this model is the physical inventory of gas in storage, the concentration of hydrogen in the stored gas, and the flow rate of material/energy stream from and to the energy hub. For a complete list, please see Table 3.4 List of physical performance indicators.

The most important financial performance indicators are the capital costs of technological components included in the energy hub, determined by the configuration and rated input/output of components, the operating and maintenance costs, the revenues from sales of products delivered by

the energy hub, and the cost of the products delivered. The key environmental performance indicators used are the emissions incurred by the operations of the energy hub and the emissions which have been displaced by the same operations. For a complete breakdown of components of the financial and environmental performance model, please refer to Figure 3.17 Scope for financial model and Figure 3.18.

Currently, the simulation is conducted for a period of three years with hourly time step; this departs from typical timescale of one year. The current timescale is preferred over that of only one year, because, during preliminary simulation trials, inter-year variations in exogenous environmental variables, such as the market price of natural gas, are found to have significant influence over the performance of the energy hub. Therefore, the financial and environmental performance of each of the three years simulated are compiled and averaged to yield an average annual value used in reporting. Previously, the determination of the project Net Present Value, an overall financial performance indicator, was planned; however, since it has been recognized that the inter-year variability is too great for the extrapolation of life time annual averages (20 years +) from the short-term simulation results (3 years), the NPV is not calculated.

10.5 Simulation Scenarios

A total of five scenarios have been developed for this simulation study. Each of the scenarios target a particular use of energy storage through UHNG, with the exception of the base case scenario, in which a basic UGS facility is simulated, without on-site production and storage of hydrogen. All scenarios are subjected to the same exogenous environmental variables (market prices of natural gas and electricity, etc.), but the design and operating philosophy of the energy hub is altered for each case: a different set of decision variables, judged to be most pertinent to the proposed purpose of the energy hub, is used as inputs for each scenario. A complete description of the configuration of energy hub components, rated capacity of components and decision point logic can be found in Chapter 7.

While assembling sets of decision variables for scenarios, it is found that there is most confidence that the choice of energy hub configuration befits the proposed function (hydrogen injection, SBG reduction, wind power integration, etc.). The selection of rated capacity for the energy hub components is based on likelihood of investment: they are sized to be on the small side of the

spectrum. It is highly recommended that sensitivity analysis be conducted with respect to the rated capacity of each energy hub component. Finally, there is a large amount of uncertainty associated with the choice of model logic at decision points for each scenario. The current choices are at best educated guesses. In future optimizing studies for the energy hub, the decision points present the most opportunity for optimization.

10.6 Assessment of Scenarios

Given the uncertainty associated with model components and scenario inputs, as explained by the sections above, the outputs of the scenario are only meant as sketches and cannot be taken to be exact.

Of all five scenarios, the base case scenario, which only involves basic UGS operations, is the only one which can be fully compared against actual data for model validation. It is found that existing natural gas storage practices are more driven by variations in the demand for natural gas than by the price of natural gas, especially in recent years. If the energy hub were to operate using the decision point logic as specified by the base case scenario, the energy hub is expected to incur financial losses for the simulation period chosen. Such losses are mainly caused by the downward trend in market natural gas prices, which diminish or even eliminate the profitability of temporal arbitrage, the only source of revenues for the basic UGS facility modeled.

The second scenario involves the injection of hydrogen into the reservoir along with natural gas. Only one pathway for energy recovery exists for this scenario: the distribution and used of hydrogen-enriched natural gas by off-site users. This scenario can also be known as the Power to Gas pathway. It is found that, if operated as the decision points have specified, at the end of three years, the concentration of hydrogen in the reservoir is expected to increase to 2%. It is not advised to extrapolate future concentration using the existing simulation results; the preferred course of action is to extend the simulation for the entire duration of the projects' lifetime. Then, the long-term hydrogen concentration can be determined with more certainty. Also, it is found that it is not profitable to sell the hydrogen-enriched natural gas at the same price as regular natural gas; in order to break even with the additional costs required by the electrolyzer, a 16% premium is needed for the mixture (basis is the 2010-2012 average natural gas price of $3.7/MMBtu).

The results for the third scenario aimed at reducing Surplus Baseload Generation (SBG) in Ontario is set up in absence of information of the actual variable level of SBG, the difference between the hourly Ontario demand and the annual average is used as a proxy signal. It is seen that the estimated level of SGB shows variation at both short-term and long-term level. Because of the limited rated input/output of the energy hub compared to its capacity, it is preferable to target long-term trend in SGB instead of the hourly variations. If hydrogen is still to be stored together with natural gas, then operating it to store/discharge long-term SGB will alter the pattern of natural gas flow into and out of the storage reservoir, increasing the throughput of gas through the reservoir and the frequency of storage cycles.

In the fourth and the last scenario, focused on wind power integration and meeting large supply of hydrogen, respectively, the level of inventory remained relatively flat throughout the periods of simulation, without exhibiting clearly visible storage cycles. It is unlikely for the wind power storage scenario to financially sustainable, if the energy recovered from wind power in the form of hydrogen, mixture or power is not recognized and given a price different from the market one. As for the large hydrogen demand scenario, if the energy hub is operated as the scenario specifies, the concentration of hydrogen inside the reservoir will increase to 60% after three years of storage. The signal used to trigger energy storage for both scenarios need to be improved. The current signals used to indicate a need for storage/withdrawal is the time differentiated FIT schedule and a hydrogen pick-up schedule centered around working hours. Both of them are unbalanced, having more off-peak hours than peak hours, implying the storage reservoir is more often charged than discharged.

Overall, compared to the base case scenario, the other four scenarios all incurred average annual losses. In terms of emission, scenario 2, 3, and 4 had limited effect on emission: reductions in the order of 5000 tons per year are observed. More notable is scenario 5, in which there is relatively larger scale for production and storage of hydrogen. The emissions incurred by hydrogen production using grid power actually exceed the potential emissions that can be mitigated through the corresponding displacement of SMR hydrogen.

10.7 Recommendations for Future Research

Given the same modeling frame work, the simulation results that can be obtained will gain in credibility and accuracy if the following tasks can be carried out:

With respect to exogenous environmental variables used to represent the wider environment in which the energy hub operates, it would be necessary to extend some of the historical time series currently used into the future, in order to extend the simulation period to cover the expected physical lifetime of the project. The exogenous variables that need to be forecasted are: the market price of electricity in Ontario, the North American market price of natural gas, the demand of electricity in Ontario. To evaluate the long-term impact of the project, it is preferred to extend the period covered by the simulation from three historical years (2010-2012) to the actual span of the project's expected lifetime (2015 – 2035, possibly). This would require better future projections of natural gas and electricity pricing, which uses a stochastic approach. The rest of the other exogenous variables need to be continuously reviewed and replaced better information if available. For example, the market price for hydrogen-enriched natural gas can be altered to become a function of H_2 concentration instead of being equaled to the price of natural gas), the schedule for hydrogen pick-up at the energy hub, and the expected level of baseload generators in operation (changes in levels related to retirement and refurbishment of nuclear power plants).

With respect to physical constraints used in this model, the assumptions and simplifying estimations listed in Table 10.1 need to be verified experimentally or validated using historical data. Priority is given to the assumptions associated with the storage reservoir, which is at the heart of the UHNG concept.

With respect to the performance indicators, it is important to periodically review the indicators chosen and decide whether additional measures are required to support the decision making process for the research and development of the UHNG concept. Changes in the performance indicators are likely to lead to corresponding change in the scope of the physical model. For examples, if local air pollution is considered to be an important environmental performance indicator, than the current physical model needs to be modified so that the effect of inputs on local air pollution is captured. A financial performance indicator omitted from this project is the levelized cost of different energy products delivered by the energy hub, calculated using accounting cost allocation principles. If included, it

should provide more insights on the relative profitability of different energy recovery pathways, especially when they are available within the same scenario.

With respect to the simulation process itself, it is hoped that sensitivity analysis can be conducted for the rated capacity of all energy hub components. Following subsequent modeling efforts should make use of optimization methods to determine the optimal model logic to deploy at the six decision points identified.

Finally, for this project, the scope of the model, as shown in Figure 3.1 Detailed view of the energy hub, has been limited to the components contained by the energy hub and simplified representation of the environment that it interacts with (exogenous environmental variables). This limits the scope of analysis that can be conducted: all costs and benefits are assessed from the point of the energy storage facility operator. Therefore, the results from this model are only pertinent to energy storage facility operators, even when improved along the recommendations given above.

In the case that the performance of UHNG (or any other energy storage technology) needs to be analyzed from the perspective other than the energy storage facility operators, it is advisable to gradually expand the scope of model to include other participants in the electricity supply chain. This is so that system-wide benefits and costs, not directly harvested or born by the operators of energy storage facilities, can also be assessed. To do this, the elements which have been simplified to be represented by the exogenous environmental variables (power supply and demand, natural gas supply and demand, hydrogen supply and demand, etc.) need to be expanded. Their geographic disaggregation is an essential factor that needs to be explicitly represented in assessing the overall benefits of storage.

The proposed changes to the scope of the model are illustrated by Figure 10.1. The scope of the model for this project is approximated by the elements enclosed within Zone C. Elements that are disaggregated components of the power grid are coloured in yellow; elements which are part of the disaggregated natural gas grid are coloured in red. The physical constraints of the network lines connecting the various zones are an integral part of the new model. Using input-output relationships from the existing modeling framework, a surrogate model can be developed to represent the energy hub in this expanded study.

To understand the full impact of energy storage and whether it should be implemented, it is necessary to assess the economic costs and benefits from the perspective of the whole system (zone A, B, C and D, altogether); to understand how individual participant (Baseload generator, NG supplier, NG consumers, power consumers, etc.) would gain or lose from energy storage and how it can be implemented, it is necessary to analyze the financial costs and benefits from the perspective of each participant. The two perspectives complement each other. A system wide simulation with multiple nodes producing hydrogen, then the nodes injecting and withdrawing mixed natural gas and hydrogen at different times of the day and year needs to be conducted.

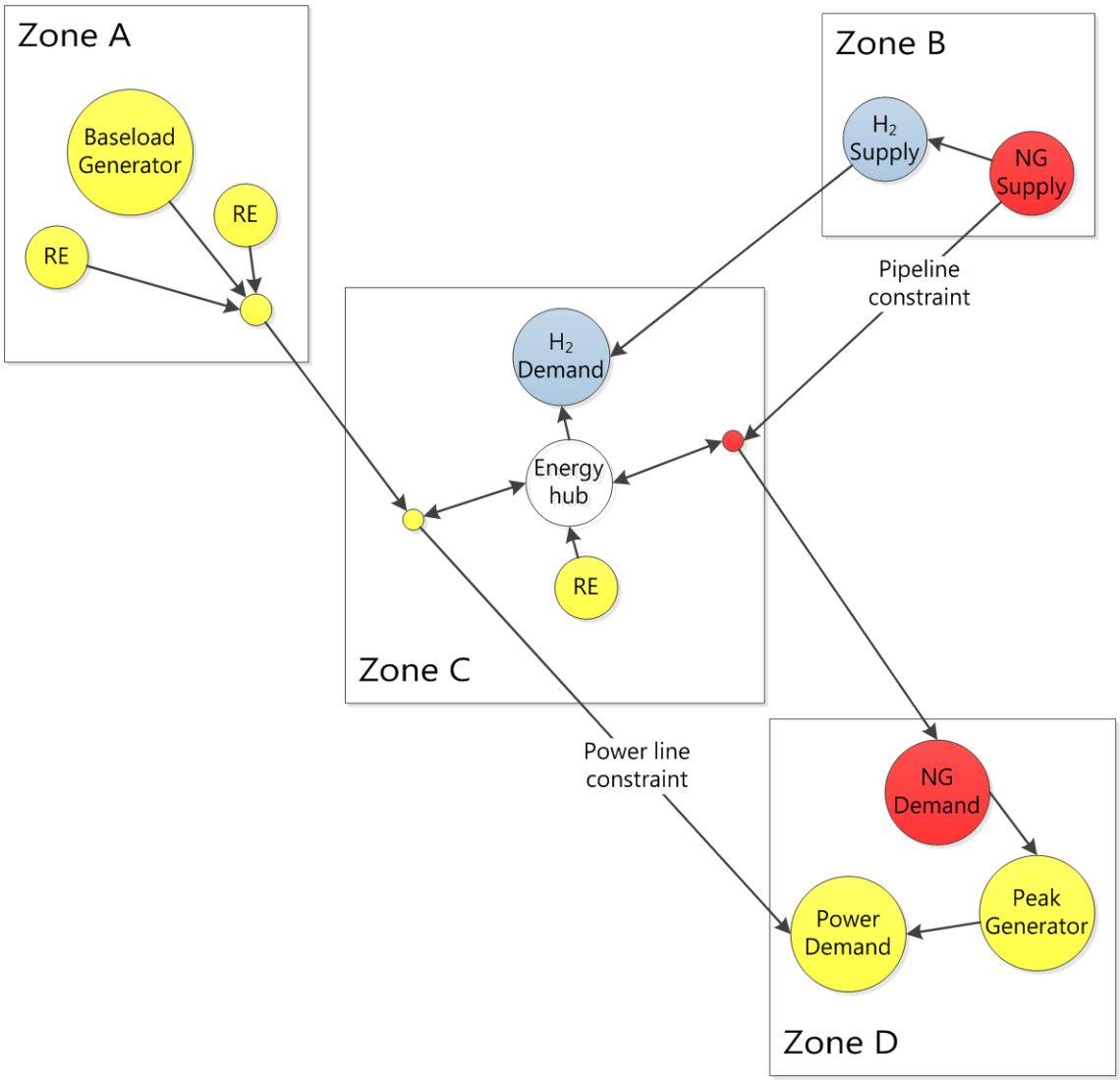

Figure 10.1 Expanded scope for future models assessing the benefits of energy storage via the energy hub

References

1. Baxter, R., *Energy Storage: a Nontechnical Guide*. 2006: PennWell Books.
2. IESO. *Composition of Ontario's Electricity Mix Continues to Change: Consumer Response Supports Reliability*. 2012 [cited 2012 August 8th]; Available from: http://www.ieso.ca/imoweb/media/md_newsitem.asp?newsID=5930.
3. IESO, *Surplus Baseload Generation (SBG)*. 2012, IESO.
4. IESO, *Forecast Weekly Minimum Demand and Baseload Generation*, 18MonthOutlookTables_2013may, Editor. 2013.
5. Ontario Ministry of Energy, *Ontario's Feed-in Tariff Program Two-Year Review Report*. 2012, Ontario Ministry of Energy: Toronto.
6. Ribeiro, P.F., et al., *Energy storage systems for advanced power applications.* Proceedings of the IEEE, 2001. **89**(12): p. 1744-1756.
7. Schaber, C., P. Mazza, and R. Hammerschlag, *Utility-Scale Storage of Renewable Energy.* The Electricity Journal, 2004. **17**(6): p. 21-29.
8. Hadjipaschalis, I., A. Poullikkas, and V. Efthimiou, *Overview of current and future energy storage technologies for electric power applications.* Renewable and Sustainable Energy Reviews, 2008. **13**(6-7): p. 1513-1522.
9. Oudalov, A., T. Buehler, and D. Chartouni. *Utility Scale Applications of Energy Storage*. in *Energy 2030 Conference, 2008. ENERGY 2008. IEEE*. 2008.
10. Electric Power Research Institute, *Electricity Energy Storage Technology Options*. 2010, Electric Power Research Institute: Palo Alto, CA.
11. Vazquez, S., et al., *Energy Storage Systems for Transport and Grid Applications.* Industrial Electronics, IEEE Transactions on, 2010. **57**(12): p. 3881-3895.
12. International Energy Agency, *2011 Key World Energy Statistics*. 2011, International Energy Agency, .
13. Cullen, J.M., Allwood, Julian M., *The efficient use of energy: Tracing the global flow of energy from fuel to service.* Energy Policy, 2010. **38**(1).
14. IESO, *Historical Market Data*, IESO, Editor. 2012, IESO: Toronto.
15. Duguid, B., *Supply Mix Directive*, Ministry of Energy, Editor. 2011, Ontario Power Authority: Canada.
16. Sioshansi, R., *Some Policy and Research Questions Related to Energy Storage*, in *EUI Working Papers*, E.U. Institute, Editor. 2010, Robert Schuman Centre for Advanced Studies: Fiesole, Italy.
17. Sovacool, B.K. and R.F. Hirsh, *Beyond batteries: An examination of the benefits and barriers to plug-in hybrid electric vehicles (PHEVs) and a vehicle-to-grid (V2G) transition.* Energy Policy, 2009. **37**(3): p. 1095-1103.
18. Ibrahim, H., A. Ilinca, and J. Perron, *Energy storage systems—Characteristics and comparisons.* Renewable and Sustainable Energy Reviews, 2008. **12**(5): p. 1221-1250.
19. Divya, K.C. and J. Østergaard, *Battery energy storage technology for power systems—An overview*. Electric Power Systems Research, 2009. **79**(4): p. 511-520.
20. Nomura, S., et al., *Technical and Cost Evaluation on SMES for Electric Power Compensation.* Applied Superconductivity, IEEE Transactions on, 2010. **20**(3): p. 1373-1378.

21. Nielsen, L. and R. Leithner, *Dynamic Simulation of an Innovative Compressed Air Energy Storage Plant - Detailed Modelling of the Storage Cavern*. WSEA Transactions on Power Systems, 2009. **4**(8): p. 253-263.
22. IESO. *Supply Overview*. 2012 [cited 2012 August 8th]; Available from: http://www.ieso.ca/imoweb/media/md_supply.asp.
23. Reuters. *Ontario to shut Pickering B nuclear plant in 2020*. 2010 [cited 2013 July 19th]; Available from: http://ca.reuters.com/article/domesticNews/idCATRE61F5SP20100216.
24. Krause, T., et al., *Multiple-Energy Carriers: Modeling of Production, Delivery, and Consumption.* Proceedings of the IEEE, 2011. **99**(1): p. 15-27.
25. Geidl, M., *Integrated Modeling and Optimization of Multi-Carrier Energy Systems*. 2007, ETH Zurich: Zurich.
26. Geidl, M. and G. Andersson, *Optimal Power Flow of Multiple Energy Carriers.* Power Systems, IEEE Transactions on, 2007. **22**(1): p. 145-155.
27. Geidl, M. and G. Andersson. *Optimal coupling of energy infrastructures*. in *PowerTech Conference*. 2007. Lausanne, Switzerland.
28. Geidl, M. and G. Andersson. *A Modeling and optimization approach for multiple energy carrier power flow*. in *IEEE PES PowerTech*. 2005. St. Petersburg, Russia.
29. Koeppel, G., *Reliability considerations of future energy systems: Multi-carrier systems and the effect of energy storage*. 2007, Swiss Federal Institute of Technology Zurich: Zurich, Switzerland.
30. Koeppel, G. and G. Andersson. *The influence of combined power, gas, and thermal networks on the reliability of supply*. in *6th International World Energy System Conference*. 2006. Torino, Italy.
31. Koeppel, G. and G. Andersson, *Reliability modeling of multi-carrier energy systems.* Energy, 2009. **34**(3): p. 235-244.
32. Arnold, M., et al. *Distributed control applied to combined electricity and natural gas infrastructures*. in *International Conference on Infastructure Systems and Services*. 2008. Rotterdam, The Netherlands.
33. Arnold, M., et al. *Model-based predictive control applied to multi-carrier energy systems*. in *IEEE Power ENergy Society General Meeting*. 2009. Calgary, Canada.
34. Kienzle, F., et al., *Valuing Investments in Multi-Energy Conversion, Storage, and Demand-Side Management Systems Under Uncertainty.* Sustainable Energy, IEEE Transactions on, 2011. **2**(2): p. 194-202.
35. Kienzle, F. and G. Andersson, *Valuing investments in multienergy generation plants under uncertainty: A real options analysis*, in *IAEE European Conference*. 2009: Vienna.
36. Kienzle, F. and G. Andersson. *Location-dependent valuation of energy hubs with storage in multi-carrier energy systems*. in *Energy Market (EEM), 2010 7th International Conference on the European*. 2010.
37. Kienzle, F. and G. Andersson. *Efficient multi-energy generation portfolios for the future*. in *4th Annual Carnegie Mellon Conference on Electricity Industry*. 2008. Pittsburgh, PA.
38. Kienzle, F. and G. Andersson. *Comprehensive performance and incertitude analysis of multi-energy portfolio*. in *IEEE PowerTech*. 2009. Bucharest, Romania.
39. Kienzle, F. and G. Andersson. *A greenfield approach to the future supply of multiple energy carriers*. in *Power & Energy Society General Meeting, 2009. PES '09. IEEE*. 2009.
40. Cumalioglu, I., et al., *State of the Art: Hydrogen storage.* Journal of Fuel Cell Science and Technology, 2008. **5**(3): p. 034001-10.
41. Holladay, J.D., et al., *An overview of hydrogen production technologies.* Catalysis Today, 2009. **139**(4): p. 244-260.

42. Schmid, R. *Electrolysis for grid balancing*. in *International Water Electrolysis Symposium*. 2012. Copenhagen, Denmark.
43. Ivy, J., *Summary of Electrolytic Hydrogen Production*. 2004, National Renewable Energy Laboratory: Golden, Colorado.
44. International Energy Agency, *Hydrogen Production and Storage*. 2006, International Energy Agency,: Paris.
45. Briguglio, N., et al., *Development of a Compact PEM Electrolyzer System for Applications with Microdistributed Renewable Sources.* ECS Transactions, 2012. **42**(1): p. 95-100.
46. Turner, J.A., *Sustainable Hydrogen Production.* Science, 2004. **305**(5686): p. 972-974.
47. León, A., *Hydrogen technology: mobile and portable applications*. 2008, Berlin: Springer.
48. International Gas Union. *2006-2009 Triennium Work Report Working Committee 2: Storage*. 2009 [cited 2011 December 15th]; SG 2.1 UGS Database]. Available from: http://www.igu.org/html/wgc2009/committee/WOC2/WOC2.pdf.
49. Foh, S., et al., *Underground Hydrogen Storage Final Report*. 1979, Institute of Gas Technology: Chicago.
50. Katz, D.L. and M.R. Tek, *Overview on Underground Storage of Natural Gas.* Journal of Petroleum Technology, 1981. **33**(6).
51. Plaat, H., *Underground gas storage: Why and how.* Geological Society, London, Special Publications, 2009. **313**(1): p. 25-37.
52. Bary, A., et al., *Storing Natural Gas Underground*, in *Oilfield Reviews*. 2002, Schlumberger.
53. Miyazaki, B., *Well integrity: An overlooked source of risk and liability for underground natural gas storage. Lessons learned from incidents in the USA*, in *Underground Gas Storage: Worldwide Experiences and Future Development in the UK and Europe*, E.J. Evans and R.A. Chadwick, Editors. 2009, The Geological Society: London.
54. Laier, T. and H. Øbro, *Environmental and safety monitoring of the natural gas underground storage at Stenlille, Denmark,* in *Underground Gas Storage: Worldwide Experiences and Future Development in the UK and Europe*
E.J. Evans and R.A. Chadwick, Editors. 2009: London.
55. Ontario Petroleum Institute. *Industry Fast Facts: Ontario*. 2003 [cited 2012 July 17th]; Available from: http://www.ontpet.com/documents/ont_fast_facts.pdf.
56. Breeze, P., *Gas Turbines and Combined Cycle Power Plants*, in *Power Generation Technologies*. 2005, Elsevier.
57. Molière, M., *Stationary gas turbines and primary energies: A review of fuel influence on energy and combustion performances.* International Journal of Thermal Sciences, 2000. **39**(2): p. 141-172.
58. Kehlhofer, R., et al., *Combined-Cycle Gas and Steam Turbine Power Plants (3rd Edition)*. 2009: PennWell.
59. Haeseldonckx, D. and W. D'haeseleer, *The use of the natural-gas pipeline infrastructure for hydrogen transport in a changing market structure.* International Journal of Hydrogen Energy, 2007. **32**(10–11): p. 1381-1386.
60. De Simio, L.G., M; Iannaccone, S. *Use of Hydrogen-Methane Mixtures for Heavy Duty Engines*. in *12th World IANGV Conference and Exhibition*. 2010. Rome.
61. Rahm, S.G., Jeffery; Molière, Michel; Eranki, Aditya, *Addressing Gas Turbine Fuel Flexibility*, G. Energy, Editor. 2009.
62. Barnicki, S.D. and J.R. Fair, *Separation system synthesis: a knowledge-based approach. 2. Gas/vapor mixtures.* Industrial & Engineering Chemistry Research, 1992. **31**(7): p. 1679-1694.

63. Peramanu, S., B.G. Cox, and B.B. Pruden, *Economics of hydrogen recovery processes for the purification of hydroprocessor purge and off-gases.* International Journal of Hydrogen Energy, 1999. **24**(5): p. 405-424.
64. Agarwal, A., *Advanced Strategies for Optimal Design and Operation of Pressure Swing Adsorption Processes*, in *Chemical Engineering*. 2010, Carnegie Mellon University: Pittsburgh.
65. NaturalHy, *Using the Existing Natural Gas System for Hydrogen*. 2009, European Commission's Sixth Framework Programme.
66. National Grid, A.H.I., *Hydrogen-Enriched Natural Gas*, in *World Energy Council*. 2009.
67. Clarke, J., *Correspondence with senior geologist from Union Gas*, Dan Peng, Editor. 2012.
68. Hydrogenics, *Technical Specifications for HySTAT-60 Fueling Station*. 2011.
69. Vestas, *V90-1.8/2.0 MW Maximum output at medium-wind and low-wind sites*. 2009.
70. The Linde Group, *Hydrogen Recovery by Pressure Swing Adsorption*. 2012.
71. Ontario Power Authority. *FIT Program Pricing > FIT Price Schedule*. 2011 [cited 2011 December 2nd]; Available from: http://fit.powerauthority.on.ca/fit-price-schedule.
72. Energy Information Administration, *Henry Hub Gulf Coast Natural Gas Spot Price*. 2013, U.S. Energy Information Administration.
73. Hajimiragha, A., M.W. Fowler, and C.A. Cañizares, *Hydrogen economy transition in Ontario – Canada considering the electricity grid constraints.* International Journal of Hydrogen Energy, 2009. **34**(13): p. 5275-5293.
74. Canadian Centre for Energy Information. *Energy Facts & Statistics - Ontario*. [Webpage Table] 2011 2009 December 30th [cited 2011 December 20th]; Available from: http://www.centreforenergy.com/FactsStats/Statistics.asp?Template=5,5.
75. Ontario Energy Board, *Natural Gas Regulation in Ontario: A Renewed Policy Framework*, in *Natural Gas Forum*. 2005.
76. Natural Resources Canada, *The Atlas of Canada > Pipeline Infrastructure Map*. 2009.
77. Statistics Canada, *Sales of Natural Gas*, Statistics Canada, Editor. 2013.
78. Sustainable Development Technology Canada, *Renewable Fuel -- Hydrogen, SD Business Case*. 2006.
79. Cicha, W.V.G., Alan. *Hydrogen Production Trends, Canadian Prospects within a Global Perspective*. in *World Hydrogen Energy Conference 2012*. 2012. Toronto, Canada.
80. Horngren, C.T.D., Srikant M.; Rajan, Madhav, *Cost accounting : a managerial emphasis* 14th ed. 2012, Upper Saddle River, New Jersey: Pearson.
81. Lemus, R.G. and J.M. Martínez Duart, *Updated hydrogen production costs and parities for conventional and renewable technologies.* International Journal of Hydrogen Energy, 2010. **35**(9): p. 3929-3936.
82. Read, C.J., *DOE Hydrogen Program Overview*. 2008, International Energy Agency Hydrogen Implementing Agreement.
83. Ikoku, C.U., *Natural Gas Engineering: A system Approach*. 1980, Tulsa: PennWell Books. 788.
84. Enbridge. *Components of Natural Gas*. 2011 [cited 2012 April 11th]; Available from: https://www.enbridgegas.com/gas-safety/about-natural-gas/components-natural-gas.aspx.
85. Hagoort, J., *Fundamentals of Gas Reservoir Engineering*. Developments in Petroleum Science. 1988, Amsterdam: Elsevier.
86. Flanigan, O., *Underground Gas Storage Facilities: Design and Implementation*. 1995, Houston: Gulf Professional Publishing.

87. Environment Canada. *National Climate Data and Information Archive.* 2011 May 14th 2013 [cited 2013 May 15th]; Available from: http://www.climate.weatheroffice.gc.ca/climateData/canada_e.html.
88. Cargnelli, J., *Bridging Power and Gas Grids*. 2011, International Partnership for Hydrogen and Fuel Cells in the Economy.
89. Gandía, L.M., et al., *Renewable Hydrogen Production: Performance of an Alkaline Water Electrolyzer Working under Emulated Wind Conditions.* Energy & Fuels, 2007. **21**(3): p. 1699-1706.
90. Bruynooghe, C., A. Eriksson, and G. Fulli, *Load-following operating mode at Nuclear Power Plants and incidence on Operation and Maintenance costs*. 2010, European Commission Joint Research Centre.
91. Moran, M.J.S., Howard N., *Fundamentals of engineering thermodynamics*. 2004, Hoboken: Wiley.
92. Sircar, S. and T.C. Golden, *Purification of Hydrogen by Pressure Swing Adsorption.* Separation Science and Technology, 2000. **35**(5): p. 667-687.
93. Yang, R.T. and S.J. Doong, *Gas Separation by Pressure Swing Adsorption: A Pore-Diffusion Model for Bulk Separation.* AICHE Journal, 1985. **31**(11).
94. Waldron, W.E. and S. Sircar, *Parametric Study of a Pressure Swing Adsorption Process.* Adsorption, 2000. **6**(2): p. 179-188.
95. Brown, R.N., *Compressors: Selection and Sizing*. 1997: Elsevier Gulf.
96. Walas, S.M., *Chemical Process Equipment - Selection and Design*. 1990, Elsevier.
97. Weil, S., *Hydrogen Delivery: Session Introduction*. 2012, U.S. Department of Energy.
98. International Renewable Energy Agency, *Wind Power*, in *Renewable Energy Technologies: Cost Analysis Series*. 2012, International Renewable Energy Agency
99. Prince-Richard, S., *A Techno-Economic Analysis of Decentralized Electrolytic Hydrogen Production fo Fuel Cell Vehicles*, in *Mechanical Engineering*. 2004, University of Victoria: Victoria.
100. Hammerli, M., *When will electrolytic hydrogen become competitive?* International Journal of Hydrogen Energy, 1984. **9**(1–2): p. 25-51.
101. Stucki, S., *The cost of electrolytic hydrogen from off-peak power.* International Journal of Hydrogen Energy, 1991. **16**(7): p. 461-467.
102. Agrawal, R., L. Biegler, and A. Westerberg. *Pressure Swing Adsorption Sizing/Costing*. Introduction to Air Separation 1999 [cited 2013 April 1st]; a Process Design Case Study distributed by CACHE Corporation]. Available from: http://www.cheme.cmu.edu/course/06302/airsep2/PSADesign.html.
103. McCollum, D.O., J, *Techno-Economic Models for Carbon Dioxide Compression, Transport, and Storage & Correlations for Estimating Carbon Dioxide Density and Viscosity*. 2006, Institute of Transporatation Studies UC Davis.
104. Amos, W.A., *Costs of Storing and Transporting Hydrogen*. 1998, National Renewable Energy Laboratory: Golden, Colorado.
105. Spath, P.L. and M.K. Mann, *Life Cycle Assessment of Hydrogen Production via Natural Gas Steam Reforming*. 2001, National Renewable Energy Laboratory: Golden.
106. Weisser, D., *A guide to life-cycle greenhouse gas (GHG) emissions from electric supply technologies.* Energy, 2007. **32**(9): p. 1543-1559.
107. Dewees, D.N., *The Economics of Renewable Electricity Policy in Ontario*. 2013, University of Toronto.

108. Carden, P.O. and L. Paterson, *Physical, chemical and energy aspects of underground hydrogen storage*. International Journal of Hydrogen Energy, 1979. **4**(6): p. 559-569.
109. Spath, P.L. and M.K. Mann, *Life Cycle Assessment of a Natural Gas Combined-Cycle Power Generation System*. 2000, National Renewable Energy Laboratory.
110. Energy Information Administration, *Weekly Natural Gas Storage Report*, Energy Information Administration, Editor. 2011, Energy Information Administration,

.